Integrated Filtering Antennas for Wireless Communications

By

Chunxu Mao

A Thesis Submitted to the University of Kent
For the Degree of Doctor of Philosophy
In Electronic Engineering

September 2017

Abstract

In traditional radio frequency (RF) front-end subsystems, the passive components, such as antennas, filters, power dividers and duplexers, are separately designed and cascaded via the 50 Ω interfaces. This traditional approach results in a bulky and heavy RF front-end subsystem, and suffers from compromised efficiency due to the losses in the interconnections and the mismatching problems between different components. The frequency responses of the antennas such as the frequency selectivity and bandwidth are usually degraded, especially for microstrip antennas. To improve the frequency responses and reduce the size of RF front ends, it is important to investigate novel highly integrated antennas which exhibit multiple functions such as radiation, filtering, power dividing and combining or duplexing, simultaneously.

In this thesis, several innovative designs of compact, multi-functional integrated antennas/arrays are proposed for wireless communication applications. First, new methods of designing integrated filtering antenna elements with broadband or dual-band performance are investigated. These antennas also feature high frequency selectivity and wideband harmonic suppression. Based on these studies, several integrated filtering array antennas with improved gains and frequency responses are developed for the first time. Compared with traditional array antennas, these proposed antennas exhibit improved bandwidths, out-of-band rejection and wideband harmonic suppression. The application of the filtering antennas in millimeter-wave (mm-Wave) frequency band is also investigated as it can potentially reduce the cost of the mm-Wave front-end subsystems significantly while providing the improved impedance bandwidth. The integrated design techniques are further developed to design novel dual-port highly integrated antennas with filtering and duplexing functions integrated. Such a new concept and the prototypes could find potential applications in wireless communication systems and intelligent transportation system (ITS).

In this thesis, comprehensive design methodologies and synthesis methods are provided to guide the design of the integrated filtering antennas. The performance is evaluated with the help of full-wave electromagnetics (EM) simulations. All of the prototypes are fabricated and tested for validating the design concepts. Good agreement between the simulation and measurement results is achieved, demonstrating the integrated antennas have the advantages of compact size, flat gain performance, low losses and excellent harmonic suppression performance. These researches are important for modern wireless communication systems.

Acknowledgement

I am very grateful for the guidance, support and encouragement from my supervisor, Professor Steven Gao. In the past three and half years, he has provided me with very good research atmosphere, excellent hardware and software for my research. Most importantly, he has given lots of useful and insightful instructions and comments, which help me enormously during my research in University of Kent. He has also been taught me other useful things in communication affairs which will benefit my future research career and personal life.

I would also like to express my gratitude to my two co-supervisors, Dr. Yi Wang from University of Greenwich and Dr. Benito Sanz-Izquierdo from University of Kent. They helped me a lot during my PhD program. Especially, Dr. Wang provided me a lot of technique supports and comments in the research and writing of the papers.

I also thank the academic staff, technicians and colleagues in the EDA, University of Kent for their kind help throughout my PhD program.

Finally, I would like to thank my parents, my other family members and all my friends for their kind support and accompany in the past several years. There encouragement helped me overcome all kinds of difficulties and finally complete my dissertation.

Contents

Abbreviation

3D	Three-Dimensional
5G	5th Generation Mobile Networks
AR	Axial Ratio
AFA	Antenna-Filter-Antenna
BW	Bandwidth
CPW	Coplanar Waveguide
DBF	Digital Beamforming
DBDP	Dual-Band Dual-Polarized
DRA	Dielectric resonator antenna
FBW	Fractional Bandwidth
FSS	Frequency Selective Surfaces
FDD	Frequency Division Duplex
HFSS	High Frequency Structural Simulator
ITS	Intelligent Transportation System
MIMO	Multiple Input, Multiple Output
mmWave	millimetre wave
RF	Radio Frequency
RFID	Radio Frequency Identification
SLL	Side Lobe Level
SLR	Stub-Loaded Resonator

Tx/Rx	Transmitting/Receiving
WLAN	Wireless Local Area Networks
XPD	Cross Polarization Discrimination

List of Figures

List of Tables

Chapter 1. Introduction

1.1 Motivation

The rapid development of wireless communications increasingly demands RF front-end subsystems of devices with the properties of compact size, light weight, low cost and multiple functions. Traditionally, passive components with different functions such as filtering, power dividing/combining and radiation, are designed separately and then cascaded into a system through 50 Ω interfaces and the corresponding matching networks. Such a cascaded scheme inevitably leads to a bulky and complex system at the front-end. Other problems such as mismatching between the passive components and resultant insertion losses could deteriorate of the frequency responses of the RF frontend subsystems [1]-[3]. All these problems should be taken into consideration in the modern RF front-end subsystem designs.

To solve the dilemmas in the modern wireless communication systems, a novel integrated design scheme was proposed that passive components such as filters, power dividers and antennas are integrated in a single device. In this way, not only the volume and weight of the system can be reduced but also the frequency performance of the systems could be significantly improved. It is very important to investigate the integration of these passive components and use them in modern wireless communication systems. The integration of passband filters and various types of antennas, the so called 'filtering antenna', has attracted significant research interests in the past few years. Compared with traditional antennas, the integrated filtering antenna has many advantages such as:

- Enhancement of antenna's impedance bandwidth;
- Filter-like frequency selectivity;
- Wideband harmonic suppression;
- Improved out-of-band rejection and therefore reduced interference.

In view of these noticeable advantages, this thesis focuses on the research of the integrated filtering antennas. Microstrip antenna, as one of the most widely used antenna types, has a lot of merits such as low profile, light weight and low cost. This thesis mainly concentrates on the integrated microstrip filtering antennas. Several filtering antennas/arrays based on microstrip patch antenna are proposed concerning impedance bandwidth improvement, high-order frequency selectivity, dual-band operation, and dual-band dual-polarization applications. In addition, the filtering antennas/arrays in mm-Wave applications and the filtering antenna/array with duplexing functions are investigated.

1.2 Main Contributions

In this thesis, the novel methods of designing integrated filtering antennas are first investigated. Based on these novel techniques, several highly integrated filtering arrays with improved frequency responses are proposed and demonstrated for different applications. A new concept of dual-port high-integration filtering antenna/array with duplexing functions is then investigated for the first time based on the proposed filtering antenna techniques. The major novelty and contributions of this thesis are listed as follows:

1. Broadband filtering microstrip antenna/array with a low profile.
    - Integrating the resonator-based power dividing network in array antenna design, realizing high-order filtering and broad bandwidth;
    - Using dual-mode stub-loaded resonator (SLR) as the feed to couple with patch antenna to form a multi-resonance broadband patch antenna;
    - Employing SLR in dual-band dual-polarized filtering antenna array for simplifying the feed networks;
    - Integrating slot resonator in the ground to achieve the strong coupling so as to broaden the bandwidth of the antenna.
2. Frequency selectivity improved microstrip antenna/array
    - Using the SLR as the feed to generate radiation nulls to improve the filtering performance;
    - Employing the cross-coupling at the feed networks to produce transmission zeros to improve the out-of-band rejection;
    - Higher order filtering channels are adopted to increase the frequency selectivity and isolation.
3. Filtering antennas with harmonic suppression
    - By purposely using different types of resonators to cancel out the higher order harmonics of the antenna;
    - Employing resonant structures on the feed of the filtering antenna to eliminate the harmonics at the designated frequencies;
    - Using the resonators with different harmonics to detune the high-order harmonics of the antenna.
4. Investigation of dual-band filtering antenna and its applications in dual-polarization antenna array

- Employing dual-mode SLR to feed a U-slot inserted patch antenna to implement dual-band filtering antenna;
- The SLR is further developed to feed two microstrip patches simultaneously to achieve dual-band dual polarization array antenna with a low frequency ratio;
- The integrated dual-band dual-polarized filtering antenna is further employed as the feed of reflector antennas to reduce the complexity.

5. Investigation of dual-port filtering antenna/array with duplexing functions
   - Dual-port dual-band filtering antenna with duplexing functions are achieved with the same polarization for the first time;
   - Strong coupling between the hairpin resonator and patch antenna is employed to produce two closely located frequency bands for uplink and downlink applications;
   - High-order filtering channels are adopted to improve the impedance bandwidth as well as the isolation between the two channels.

1.3 Publication List

Journals (related to the subject of this thesis)

1. **Chunxu Mao**, Steven Gao, and Yi Wang, "Highly Integrated Full-Duplex Tx/Rx Antennas for Vehicular Communications," ***IEEE Transactions on Vehicular Technology***, accepted, 2017.
2. **Chunxu Mao**, Steven Gao, Yi Wang, "Broadband High-Gain Beam-Scanning Antenna Array for Millimeter-Wave Applications," ***IEEE Transactions on Antenna and Propagation***, vol. 65, no. 9, pp. 4864 - 4868, Sep. 2017.
3. **Chunxu Mao**, Steven Gao, Yi Wang, Qi Luo, Qing-Xin Chu, "A Shared-Aperture Dual-Band Dual-Polarized Filtering-Antenna-Array With Improved Frequency Response," ***IEEE Transactions on Antenna and Propagation***, vol. 65, no. 4, pp. 1836-1844, Apr. 2017.
4. **Chunxu Mao**, Steven Gao, Yi Wang, Benito Sanz-Izquierdo, Zhengpeng Wang et al., "Dual-Band Patch Antenna with Filtering Performance and Harmonic Suppression," ***IEEE Transactions on Antenna and Propagation***, vol. 64, no. 9, pp. 4074-4077, Sep. 2016.
5. **Chunxu Mao**, Steven Gao, Yi Wang, Fan Qin, Qing-Xin Chu, "Compact Highly Integrated Planar Duplex Antenna for Wireless Communications," ***IEEE Transactions on Microwave Theory and Techniques,*** vol. 64, no. 7, pp. 2006-2013, Jul. 2016.
6. **Chunxu Mao**, Steven Gao, Yi Wang, Zhengpeng Wang, Fan Qin, Benito Sanz-Izquierdo, Qing-Xin Chu, "An Integrated Filtering Antenna Array With High Selectivity and Harmonics Suppression," ***IEEE Transactions on Microwave Theory and Techniques,*** vol. 64, no. 6, pp. 1798-1805, Jun. 2016.

7. **Chunxu Mao**, Steven Gao, Yi Wang, Fan Qin, Qing-Xin Chu, "Multimode Resonator-Fed Dual-Polarized Antenna Array With Enhanced Bandwidth and Selectivity," ***IEEE Transactions on Antenna and Propagation***, vol. 63, no. 12, pp. 5492-5499, Dec. 2015.
8. **Chunxu Mao**, Steven Gao, Yi Wang, Zhiqun Cheng, "Filtering Antenna With Two-Octave Harmonic Suppression," ***IEEE Antennas and Propagation letters***, vol. 16, pp. 1361-1364, 2017.

Journals (not related)

1. **Chunxu Mao**, Steven Gao, and Yi Wang, Sri Sumantyo, Josaphat, "Compact Dual-Sense Broadband Circularly-Polarized Microstrip Antenna/Array with Enhanced Isolation," ***IEEE Transactions on Antenna and Propagation***, vol. 65, no. 12, pp. 7073-7082, Dec. 2017.
2. **Chunxu Mao**, Steven Gao, Yi Wang, Qing-Xin Chu, Xue-Xia Yang, "Dual-Band Circularly-Polarized Shared-Aperture Array for C/X-Band Satellite Communications," ***IEEE Transactions on Antenna and Propagation***, vol. 65, no. 10, pp. 5171-5178, Oct. 2017.
3. **Chunxu Mao**, Steven Gao, Carolina Tienda, Tobias Rommel, Anton Patyuchenko et al., "X/Ka-Band Dual-Polarized Digital Beamforming Synthetic Aperture Radar," ***IEEE Transactions on Microwave Theory and Techniques***, vol. 65, no. 11, pp. 4400-4407, Nov. 2017.
4. **Chunxu Mao**, Steven Gao, Qi Luo, Tobias Rommel, Qing-Xin Chu, "Low-Cost X/Ku/Ka-Band Dual-Polarized Array with Shared-Aperture," ***IEEE Transactions on Antenna and Propagation***, vol. 65, no. 7, pp. 3520 - 3527, Jul. 2017.
5. **Chunxu Mao**, Steven Gao, Yi Wang, Benito Sanz-Izquierdo, "A Novel Multiband Directional Antenna for Wireless Communications," ***IEEE Antennas and Propagation letters***, vol. 16, pp. 1217-1220, 2017.

Conferences (related to the subject of this thesis)

1. **Chunxu Mao**, S. Gao, Z. P. Wang, Y. Wang, F. Qin, B. Sanz-Izquierdo, Q. X. Chu, "Integrated filtering-antenna with controllable frequency bandwidth," ***2015 9th European Conference on Antennas and Propagation (EuCAP***), pp. 1-4, 2015.
2. **Chunxu Mao**, Steven Gao, Yi Wang, "Stub-loaded resonator-fed filtering patch antenna with improved bandwidth," ***46th European Microwave Conference (EuMC)***, pp. 317-320, 2016.

Conferences (not related)

3. **Chunxu Mao**, Steven Gao, Tobias Rommel, "Low Profile Shared-Aperture Dual Band Dual Polarized Antenna for SAR Applications," in ***Proceedings of 2017 International Workshop on Antenna Technology: Small Antennas, Innovative Structures, and Applications (iWAT)***, 104-107, 2017. (This paper was selected as the shortlist of the best paper award)
4. S. Gao, **Chunxu Mao**, F. Qin, A. Patyuchenko, Carolina Tienda et al, "Dual-band digital beamforming synthetic aperture radar for earth observation," ***2015 Asia-Pacific Microwave Conference (APMC),*** pp. 1-3, 2015.

1.4 Outline of the Thesis

This thesis is organized as follows.

Chapter 1 briefly introduces the motivation for leading the research and the technical contributions of this thesis. In addition, the research achievements and the publication in the past three years are summarized.

Chapter 2 firstly discusses the background and the significance of the filtering antenna research. Then, the synthesis methodology and the basic theory of the integrated filtering antenna are introduced. Finally, the state-of-the-art research progress on filtering antennas are summarized. The filtering antennas can be classified into three categories, including cascaded filter-antennas, broadband antennas with embedded bandstop filters, and the integrated filtering antennas. Specifically, the integrated filtering antennas based on different types of antennas are studied and discussed in details.

Chapter 3 presents the design methods for achieving the integrated filtering antennas with broad bandwidth, wideband harmonic suppression and dual-band operations based on three proposed antenna prototypes, respectively. The designing methods, optimizations and validation based on the prototype measurements are discussed in details.

Chapter 4 demonstrates four microstrip antenna arrays with integrated filtering performances. The first one is a low profile broadband dual-polarized microstrip antenna, which is achieved by integrating SLR in the feeds of the array. The second one presents a highly integrated microstrip array antenna with the filtering and power dividing functions integrated seamlessly. In the third work, the techniques of filtering antenna are developed to overcome the difficulty in the design of a dual-band dual-polarized aperture-shared array antenna with a low frequency ratio. In the last prototype, a broadband, high gain microstrip antenna array for millimeter wave applications is investigated. The achieved broadband and the filtering features are realized by adopting an embedded slot resonator in the ground and stacked coupled structure in the design.

Chapter 5 explores a novel dual-port antenna with integrated filtering and duplexing functions. The dual-band capability and the bandwidth enhancement as well as the isolation between the two ports/channels are investigated. Such a compact device can be used as the uplink and downlink channels of the wireless communication systems simultaneously.

Chapter 6 is the conclusion of the thesis with the research achievements highlighted. Moreover, future work is discussed.

Chapter 2. Overview of State-of-the-Art Filtering Antenna Techniques

2.1 Background

Wireless communication systems have experienced unprecedented development in the past decades. Modern wireless communication demands the RF front-end subsystems with compact size, low cost, high integration and multiple functions. In traditional RF frontend subsystems, the passive components such as antennas, filters, power dividers and duplexers/diplexers are designed separately and then cascaded through 50 Ω interfaces and transmission lines. This results in the division of 'antenna designers', 'filter designers' and other designers specialized in specific microwave components. This division is useful in reducing the complexity of the work in each 'component' group, but the good performance of each component cannot guarantee the performance of the whole RF frontend system. The other important issue to be concerned with is that the mismatching between the components often occurs when they are connected together. This problem will deteriorate the frequency response and therefore the system performance, especially when the cascaded components have different impedance bandwidths [1]-[3].

To overcome these problems, a co-design concept that the filter, antenna or other passive components are seamlessly integrated in a single inseparable device has been developed in the past few years. Compared with traditional cascaded components, the integrated co-design method has the following advantages:

- Reduced component count in the RF frontend subsystem;
- Improved frequency responses;
- Low weight, compact size;
- Low cost;
- Low loss and high efficiency;
- Structural and functional integration.

All these advantages make the integrated co-design scenario much more preferable in modern wireless communication systems. In the integrated scenario, several passive components such as filters and antennas can be merged into a single module, resulting in a simplified RF frontend systems. In addition, the frequency responses such as frequency selectivity, bandwidth and out-of-band rejection could be improved significantly. This integrated design scenario could also lead to the reduction of weight, size and cost of the RF frontend system,

especially when the system works in millimeter-wave frequency bands. Owing to the removal of the interfaces and matching networks between the components, the integrated design has a higher efficiency and the insertion losses in the transmission/receiving paths can be reduced. Furthermore, the integrated multiple functions make the device more versatile in meeting different application requirements.

Since Pues *et al*. first proposed an impedance matching technique to increase the bandwidth of microstrip antennas [1] in 1989, the merits of integrated design concept have been gradually recognized and developed. Towards the end of the last century, the concept of filter/antenna integration was proposed based on multilayer substrate techniques [2]-[3]. Since then, various techniques have been adopted to design the devices with integrated functions of filtering and radiation. The integrated design of filters/antennas have been used to enhance the impedance bandwidth, frequency selectivity, and suppress the harmonics out of the band.

2.2 Filter-Antenna Integration Methodology

The integration of filter and antenna is usually achieved by replacing the last order resonator of a band-pass filter with a resonant radiating element. To realize such a filtering antenna with the frequency responses as the corresponding band pass filter, it is essential to conceive the radiating element with the consistent coupling coefficient M between the resonator and the radiator as well as consistent external quality factor Q_{ext}. To exemplify it, a generic synthesis approach is provided in this section to guide the designing procedure of the filtering antennas in the following chapters.

Due to the filtering antenna is derived from a normal band-pass filter, the first and foremost step is to design a band-pass filter which is to serve as the reference to the filtering antenna. As a common case, a band pass filter with Chebyshev responses is exemplified. The steps for designing a filtering antenna can be summarized as following [4],

(1) The specifications, including the order of the resonators N, center frequency f_0, ripple level in the band L_A, and the fractional bandwidth Δf of the band pass filter (filtering antenna) are given first;

(2) According to the specifications, the required external quality factor Q_{ext} and the coupling coefficients between the resonators m_{ij} can be achieved by utilizing the bandpass filter synthesis technology.

(3) Using a full-wave simulation, the required Q_{ext} and m_{ij} can be realized and the corresponding parameters such as thickness and spaces between the resonators can be obtained.

(4) The desired filtering antenna with the frequency responses as the counterpart bandpass filter is then achieved.

Assuming that we have the information of the order of the resonators N, center frequency f_0, ripple level L_A, and the bandwidth Δf of the required filtering antenna, the external quality factor Q_{ext} and the coupling coefficients m_{ij} can be calculated using the bandpass filter synthesis technology in [5],

$$Q_{ext} = \frac{g_0 g_1}{\Delta f} \quad \text{(Eq. 2.1)}$$

$$m_{ij} = \frac{\Delta f}{g_i g_j} \quad \text{(Eq. 2.2)}$$

where $g_0, g_1 \ldots g_i, g_j$ are the normalized Chebyshev low-pass filter prototype element values, which are functions of the ripple level L_A. By looking up the table in the literature [4], the normalized Chebyshev low-pass filter prototype element values can be found and the required Q_{ext} and m_{ij} can be obtained by applying the equations above.

For a filtering antenna, the external quality factor Q_{ext} can be expressed by using the loaded quality factor Q_L, and the unloaded quality factor Q_U [6],

$$\frac{1}{Q_{ext}} = \frac{1}{Q_L} - \frac{1}{Q_U} \quad \text{(Eq. 2.3)}$$

Assuming the radiator of the antenna to be lossless, namely $Q_U = \infty$, the equation above can be simplified as,

$$\frac{1}{Q_{ext}} = \frac{1}{Q_L} \quad \text{(Eq. 2.4)}$$

Consequently, the Q_{ext} of the antenna can be obtained by assuming the dielectric loss is zero and extracting the value of the Q_L. Using the method presented in [6], Q_L can be extracted from the reflection coefficients,

$$Q_L = (1 + m)\frac{f_0}{f_2 - f_1} \quad \text{(Eq. 2.5)}$$

where m is the coupling coefficient between the excitation port and the last resonator of the filtering antenna, f_1 and f_2 are corresponding frequencies when $S_{11} = S_{11}^{\Phi}$, S_{11}^{Φ} is defined as

$$S_{11}^{\Phi} = \sqrt{\frac{1 + \left|S_{11}^{\min}\right|^2}{2}} \qquad \text{(Eq. 2.6)}$$

where $S_{11}^{\min}$ is the minimum reflection coefficient occurring at the resonant frequency f_0. The coupling coefficient m can be found using the equations,

$$m = \frac{1 - S_{11}^{\min}}{1 + S_{11}^{\min}}, \text{ when the resonator is under coupled,} \qquad \text{(Eq. 2.7)}$$

$$m = \frac{1 + S_{11}^{\min}}{1 - S_{11}^{\min}}, \text{ when the resonator is over coupled,} \qquad \text{(Eq. 2.8)}$$

Using full-wave simulation, the required loaded quality factor Q_L and therefore the external quality factor Q_{ext} can be obtained.

2.3 State-of-the-Art Filter/Antenna Integration Techniques

Various techniques have been investigated to integrate filters and antennas in a single module in the past decades. Filtering Antennas can be divided into three categories, as shown in Figure 2.1. The first category is the cascaded approach that a filter is cascaded with an antenna at the feed of the antenna [7]-[10]. The second category is to integrate band-stop filters in the wideband antennas for suppressing the signals/interferences in the given frequency bands [11]-[18]. The last category is the integrated filtering antenna, which combines

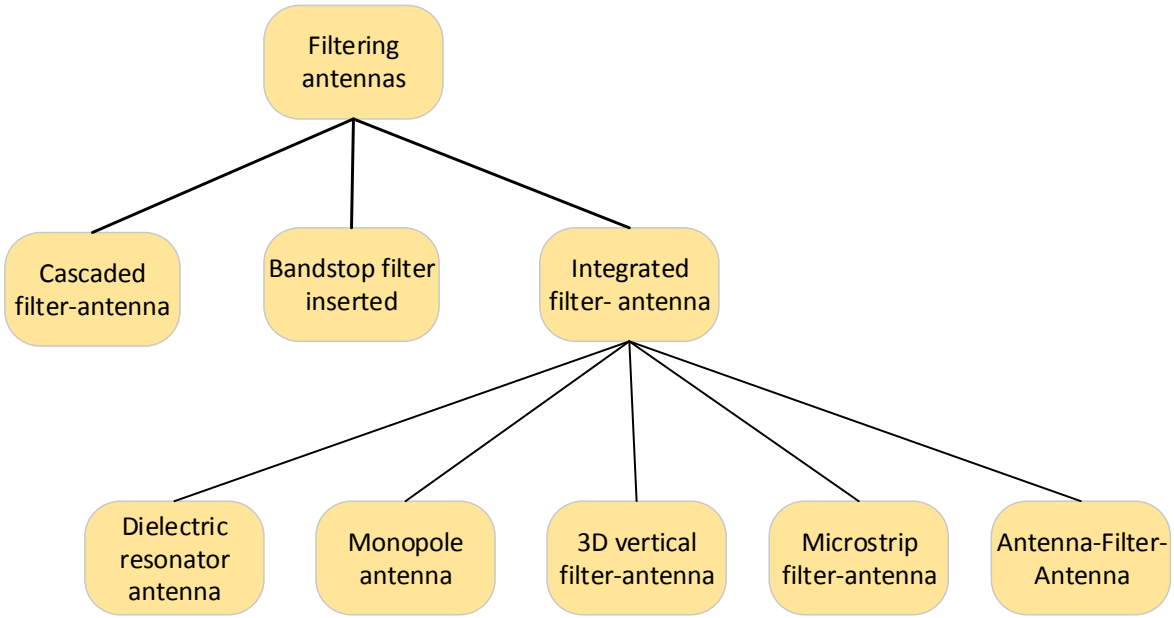

Figure 2.1 Classification of the Filtering Antennas

the functions of filtering and radiation in a single device [19]-[28]. This thesis mainly focuses on the third category of filtering antenna. For the first two categories, a brief introduction is given below.

2.3.1 Cascaded Filter-Antenna

To achieve a cascaded filter-antenna, the filter part and antenna part are designed separately and connected using the 50 Ω interfaces. There are two cases for this kind filtering antennas. The first case is that the filter and the antenna are designed to have the same bandwidths and connected through 50 Ω ports [7]-[8]. The other case is that the antenna has a wider bandwidth than the bandpass filter. When they are cascaded as a module, the operation band of the module is determined by the narrow-band bandpass filter, and therefore the signals in specific frequency band are selected out. This design scheme has been reported and discussed in [10].

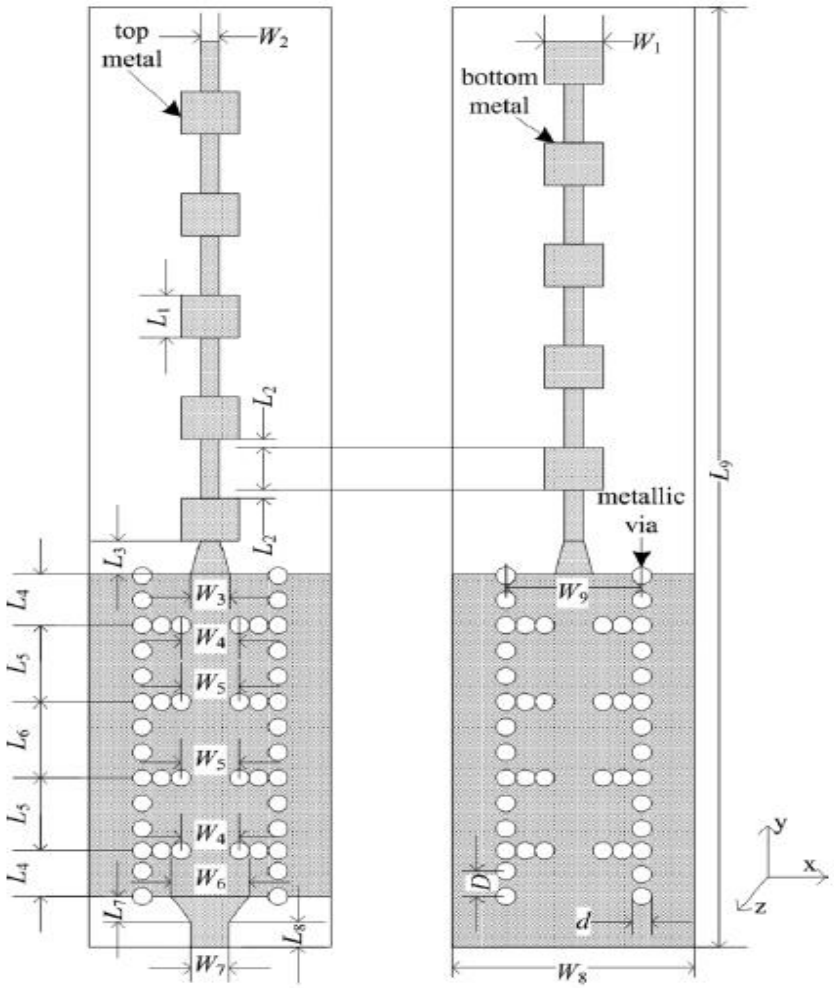

(a) **(b)**

Figure 2.2 Configuration of the cascaded filtering antenna in [10]: (a) front-view, (b) back-view.

Figure 2.2 shows the front- and back-view of the cascaded filtering antenna configuration in [10]. The antenna is composed of a planar coaxial co-linear radiation array on the top and a 3rd-order substrate integrated waveguide (SIW) band-pass filter at the bottom. The coaxial co-linear radiating element has a wide impedance bandwidth, while the bandwidth of the SIW filter is comparably narrower. Because the radiation part has a broad bandwidth, the antenna is prone to unexpected channel interference outside of the operation band, which deteriorates the performance of the system. The SIW bandpass filter is therefore used as a window filter, which provides a good frequency selectivity at the given frequency and excellent rejection characteristics out of the band. When the SIW filter and the radiating elements are cascaded, only the signals located in the bandwidth of the filter can pass through and the signals out of the band are rejected, producing the antenna with the expected filtering characteristics.

When the SIW filter works at its TE_{101}-mode, the size of the cavity can be determined by the expression below [29],

$$f_{101} = \frac{c}{2\sqrt{\varepsilon_r \mu_r}} \sqrt{\left(\frac{1}{W_{eff}}\right)^2 + \left(\frac{1}{L_{eff}}\right)^2} \qquad \text{(Eq. 2.9)}$$

where ε_r and μ_r are the relative permittivity and permeability of the substrate, c is the velocity of the light in free space, W_{eff} and L_{eff} are the equivalent width and length of the resonant SIW cavity, which can be evaluated by [30],

$$W_{eff} = W - \frac{d^2}{0.95\ D} \qquad \text{(Eq. 2.10)}$$

$$L_{eff} = L - \frac{d^2}{0.95\ D} \qquad \text{(Eq. 2.11)}$$

where W is the width of the SIW, L is the length of the SIW cavities, d and D are the diameter of the metallic via and the distance between two adjacent via, respectively.

For the cascaded filtering antenna, it should be noted that the bandwidth of the radiating element ought to be wider than the bandwidth of the corresponding band-pass filter. If the radiating element is a narrow-band antennas such as a microstrip antenna, it is usually challenging to design a bandpass filter with a narrower bandwidth. On the other hand, due to the antenna part and the filter part being designed separately, this kind of filtering antenna cannot be considered as an integrated design.

2.3.2 Antenna with Embedded Band-stop Filter

The other category of filtering antenna is the antenna with mismatching frequency bands, also called band-notched antenna which has been widely used in ultra-wideband (UWB) applications. For the UWB antenna, which has a very wide bandwidth from 3.1 to above 10 GHz, it is critical to avoid the interference between the UWB applications with other narrow-band wireless applications located inside the band. For example, the wireless local area network (WLAN) occupies the frequency bands of 3.6, 5.2 and 5.8 GHz. They should be masked in the UWB antenna designs. Usually, the notched bands in the UWB are achieved by inserting resonant structures in the radiating element or on the feed line, producing the band-notched UWB antenna with band stop filtering features at the given frequency bands [14].

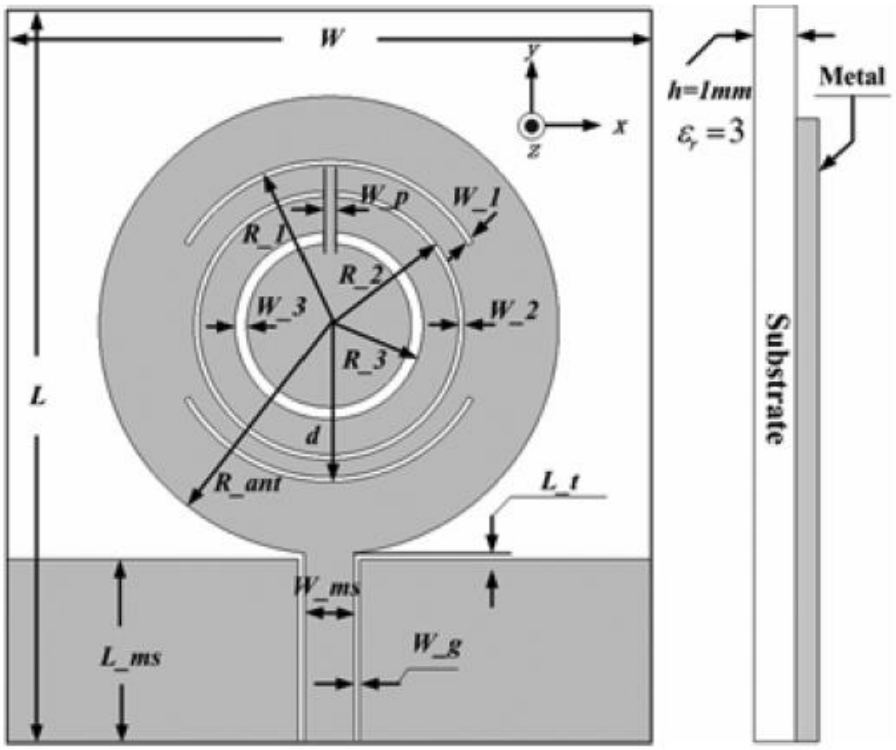

Figure 2.3 Configuration of the band-notched UWB antenna with filtering/resonant structures in the radiating element [14].

To illustrate this kind of filtering antenna, the UWB antennas with multiple notched bands in [14] are discussed here. Figure 2.3 shows the configuration of the band-notch UWB antenna with filtering structures in the radiating element. The UWB antenna itself is a monopole antenna, and the radiating element is a circular patch. On the patch, two split ring slots

and two arc slots are etched for generating triple stop bands in the UWB. The resonant frequencies of these slot resonators can be controlled by adjusting the physical dimensions of the slots. A coplanar waveguide (CPW) on the same plane is used to excite the antenna. The parameters of the ring slots can be approximately calculated by

$$f_r \approx \frac{c}{\lambda_g \sqrt{\varepsilon_{eff}}} \approx \frac{c}{2 \cdot l_{ring}} \quad \text{(Eq. 2.12)}$$

$$l_{ring} \approx 2 \cdot \pi \cdot R_{ring} \quad \text{(Eq. 2.13)}$$

$$\varepsilon_{eff} \approx \frac{\varepsilon_r + 1}{2} \quad \text{(Eq. 2.14)}$$

where f_r is the resonant frequencies of the split ring slots; c and ε_{eff} are the speed of light in the free space and the approximated effective dielectric constant, respectively; R_{ring} and l_{ring} are the radius and the length of the split ring slots. The resonant frequencies of the slots can be controlled by changing the radius of the ring slots. Provided the dimensions of the slots are properly optimized, these resonant structures will resonate at the given frequency bands, resulting in the band-notch UWB antenna with the band-stop filtering characteristics at the given bands.

2.3.3 Integrated Filtering Antennas

Although the cascaded and the band-stop inserted filtering antennas mentioned above have been used in practical applications, they are not considered as integrated filtering antennas. This is mainly because the filtering section and the radiating section of the antenna are designed separately and a considerable large area is needed to arrange the filtering module and radiation module. In this section, a high integration filtering antenna concept is introduced. For the integrated filtering antenna, the radiating element of the antenna is also served as one of the resonators of a band pass filter, resulting a device with the combined radiation and filtering capacities. Such an integrated module is beneficial in reducing the size of the RF frontend systems and the losses associated with the interfaces. Moreover, the frequency responses, such as the bandwidth, frequency selectivity and high-order harmonic suppression could be improved significantly. Due to the radiating element is regarded as the last order resonator of the bandpass filter, this integrated design is more suitable for narrow-band antennas, such as microstrip antennas.

In this section, a variety of state-of-the-art integrated filtering antennas, including dielectric resonator antennas, monopole antennas and microstrip antennas, are discussed in detail. The designing process and methodologies of these filtering antenna are also presented as the guidance for the filtering antennas in the following chapters.

(1) Integrated Filtering Monopole Antenna

To design a filtering antenna, the first and foremost step is to choose a suitable type of antenna, which should exhibits resonant characteristics with a relatively high quality factor. One type of feasible antennas is the monopole antenna, which has a compact size and exhibits the omni-directional radiation. In some circumstances when omni-directional radiation is required, a monopole antenna is suitable for filtering antenna integration. The filtering antennas based on monopole antennas have been investigated in the past and several types of filtering integrated monopole antennas have been reported [4], [31]-[38]. To illustrate the typical configuration of this kind of filtering antenna, the prototype in [4] is shown in Figure 2.4.

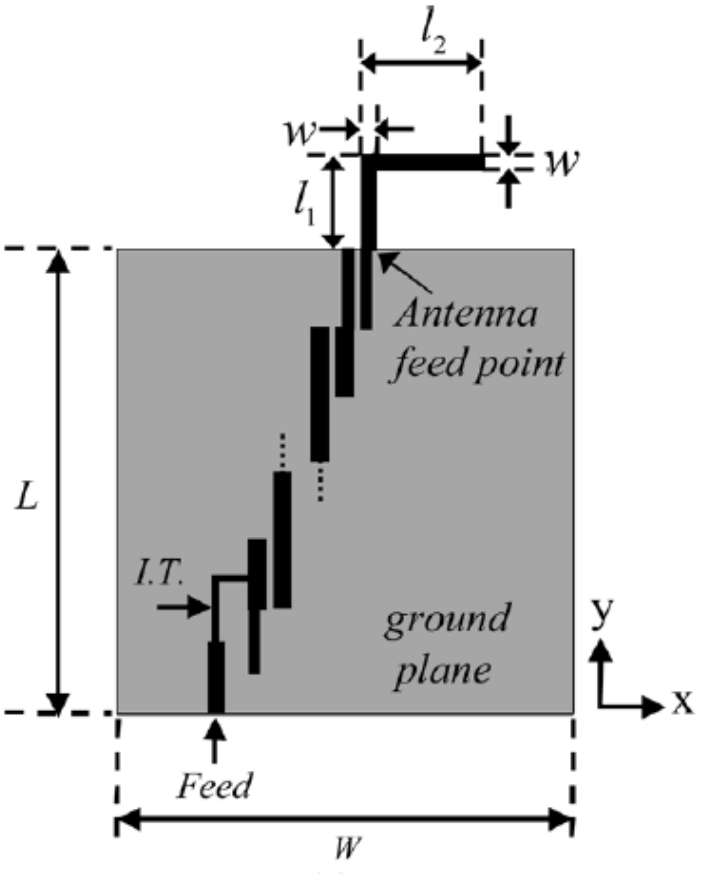

Figure 2.4 Configuration of the monopole filtering antenna in [4].

The antenna consists of an inverted-L antenna and *N*-1 parallel coupling half-wavelength microstrip resonators. To increase the fabrication tolerance, a quarter wavelength admittance inverter with characteristic impedance of 30 Ω is introduced in the synthesis process. The required parameters of the counterpart filter are: center frequency f_0 = 2.53 GHz, the fractional bandwidth FBW = 3.0%, and the order of the filter N = 3 in this work.

In order to serve as the last order of the filtering antenna, the inverted-L monopole antenna is used as the radiator. The equivalent circuit of the inverted-L antenna is shown in Figure 2.5. L_A and C_A represent the resonant inductance and resonant capacitance of the antenna, respectively. R_A corresponds to the radiation resistance of the antenna.

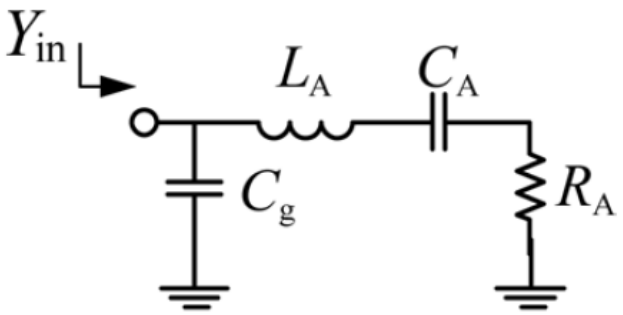

Figure 2.5 The equivalent circuit of the antenna in [4].

As the antenna is connected to an *N*-1th coupled line, the filtering antenna can be synthesized based on an *N*-th order Chebyshev bandpass filter and replacing the last resonator with the inverted-L monopole antenna. Figure 2.6 shows the equivalent circuit of the proposed filtering antenna. The *N*-1-th parallel coupled lines of the filtering antenna is modeled by the shunt *LC* resonators. The couplings between the resonators are represented using the admittance inverters $J_1 \ldots J_N$.

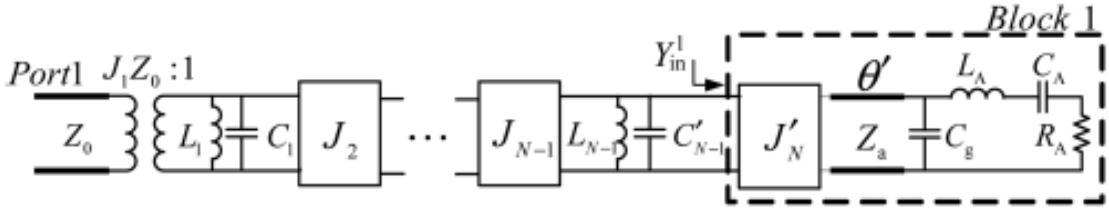

Figure 2.6 The equivalent circuit of the filtering antenna.

According to the equivalent circuit, the quality factor of the antenna Q_A and the inverter constant $J'_N Z_0$ can be calculated by,

$$Q_A = \frac{2\pi f_0 L_A}{R_A} = \frac{\pi}{2(Z_0 J_{N+1})^2} \quad \text{(Eq. 2.15)}$$

$$J_N' Z_0 = \frac{J_N Z_0}{Z_a}\left(\frac{2Q_A R_A Z_0}{\pi}\right)^{1/2} \quad \text{(Eq. 2.16)}$$

By calculating the antenna quality factor Q_A and the choosing a suitable characteristic impedance Z_a, the parameters of the antenna and the inverter constant $J_N' Z_0$ are obtained. Then, all the dimensions of the coupled lines of the filtering antenna can be determined.

(2) Cavity-Backed Slot Filtering Antenna

Although the filtering antenna based on monopole antenna is easy for implementation, it suffers from the problems of low gain due to the omnidirectional radiation. In many cases, the antenna with a high gain and unidirectional radiation is required. To achieve a high gain filtering antenna, especially in millimeter wave applications, the integration of cavity-backed slot antenna and substrate integrated waveguide (SIW) is believed to a good candidate. The filtering antennas based on cavity-backed slot antennas have been reported in the past few years [39]-[60]. Compared with other types of antennas, the cavity-backed slot filtering antenna has the advantages of low loss, low cost, high power handling capacity and ease of integration with other circuits. In addition, the integration of the slot antenna and SIW could provide a high quality factor Q, which could reduce the out-of-band noise and insertion loss.

The cavity-backed slot filtering antenna can be usually achieved by etching a slot in the upper ground of the last cavity resonator of the SIW-based cavity passband filter. The slot leads to the leakage of the electromagnetic wave, forming the radiating element of the antenna. In this way, the radiating element and the resonators of the filter are seamlessly integrated without adding any extra circuits and volume. Using the SIW technologies, the resonant cavities are formed by adding a circle of shorted via between the two copper planes of the substrate. The resonant frequency of the cavity is determined by the dimension of the cavity while the antenna's resonant frequency mainly depends on the size of the slot. It should be noted that the resonant frequency of the last cavity/slot antenna is different from the other cavities due to the loading effect of the radiation. To achieve the cavity-backed slot filtering antenna, a counterpart passband filter is usually designed first as a reference with

the required coupling coefficients and external quality factor obtained. Then the last resonator is replaced by a slot antenna, which is designed to have a consistent external quality factor. To illustrate the design method, the antenna in [44] is introduced in Figure 2.7.

As can be seen, the sidewalls of each cavity resonator are formed by closely placing metallic vias. The two cavities are stacked vertically, forming a second order resonant device within a compact size. The coupling between them are realized by etching a coupling slot in the ground between the two cavities. On the top, a radiating slot is inserted to produce the slot antenna. On the bottom layer, a coplanar-cavity transition is adopted for enabling the connection with the SMA connector.

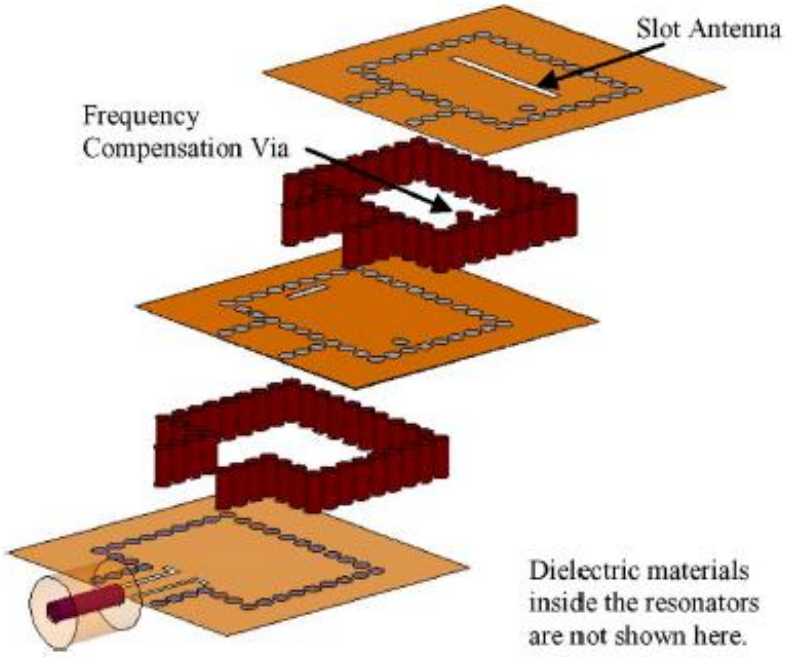

Figure 2.7 Configuration of the cavity-backed filtering antenna in [44].

In this work, the center frequency of the antenna is 10.18 GHz and the required fractional bandwidth is 2.9%. According to Eq. 2.1 and 2.2, the internal coupling coefficient m_{ij} and the external quality factor Q_{ext} can be found to be 0.021 and 54.4, respectively. The synthesis process can be referred to the methods presented in Chapter 2.2. Thanks to the near-zero transmission loss between the filter and antenna, this type filtering antenna shows the improved efficiency with the dielectric and metallic losses reduced.

Due to the coupling slot is placed close to the sidewall, magnetic coupling is predominant between the resonators. This can be verified by the simulated magnetic distribution of the cavity, as shown in Figure 2.8(a). When a slot is inserted in the ground of the cavity, the magnetic distribution is changed, as can be observed in Figure 2.8(b). The position of the

slot antenna, denoted as X_a, is used to control the coupling between the upper resonator and slot antenna. The coupling increases as the X_a decreases. By adjusting the location of the slot, the external quality factor Q_{ext}, and therefore the bandwidth of the antenna can be controlled accordingly. Similarly, the internal coupling coefficient m_{12} between the two resonators can be changed by adjusting the location and the dimension of the coupling slot. In this way, the filtering antenna could realize the required frequency responses as the reference passband filter.

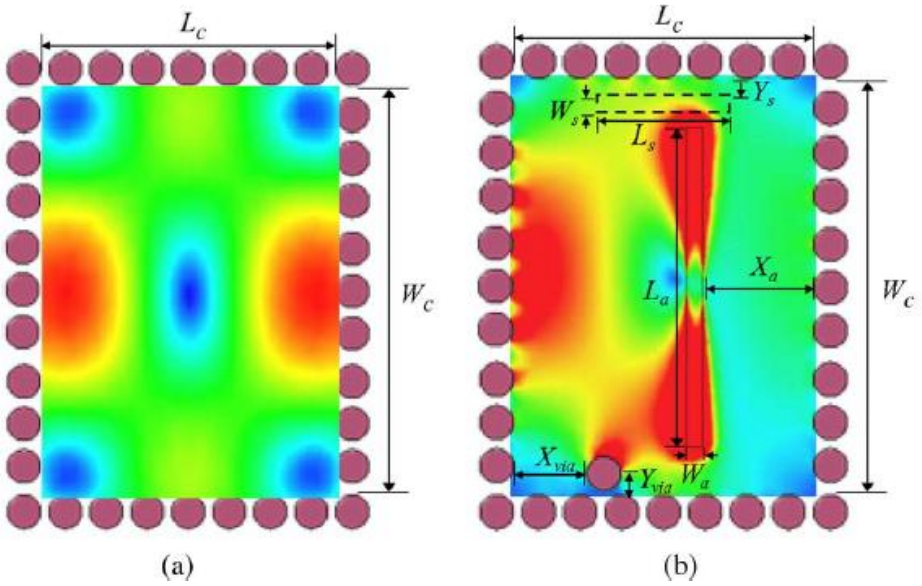

Figure 2.8 Simulated magnetic distribution of the top cavity: (a) unperturbed cavity, (b) slot inserted [44].

(3) Filtering Dielectric Resonator Antenna (DRA)

Dielectric resonator antenna (DRA) has been widely investigated and applied in microwave or millimeter wave applications. The dielectric resonator, which mounted on a ground plane, can be fed flexibly by microstrip, coupling slot or coplanar waveguide. The radio waves introduced into the resonator material bounce back and forth between the resonator walls, forming the standing waves and radiating into space [61]. One of important advantages of the DRA is the high radiation efficiency due to the removal of the conductor loss [62]. The dimension of the DRA is associated with the dielectric constant of the resonant material, $\sim \lambda_0 / \sqrt{\varepsilon_r}$, where λ_0 is the wavelength in free space, ε_r is the dielectric constant of the material. Thus, the size of the DRA can be reduced by selecting the high value of ε_r. The other virtue is the bandwidth of DRA can be achieved over a wide range by properly choosing the dielectric constant of the resonator and shapes of the resonator material.

Due to the advantages mentioned above, DRA can be used to design filtering antenna, also called filtering DRA [62]-[67]. To achieve the filtering DRA, some filtering or band-stop structures are embedded into the antenna radiator and feeding circuit of a DRA to stop the pass at designated frequency bands. As a result, a passband like S-parameters as well as gain responses can be produced, generating the filtering antenna. Using this fusion method, the size and loss of the antenna can be reduced. Take the antenna presented in [63] as an example, the design methodology and the process of a filtering DRA is investigated in this section.

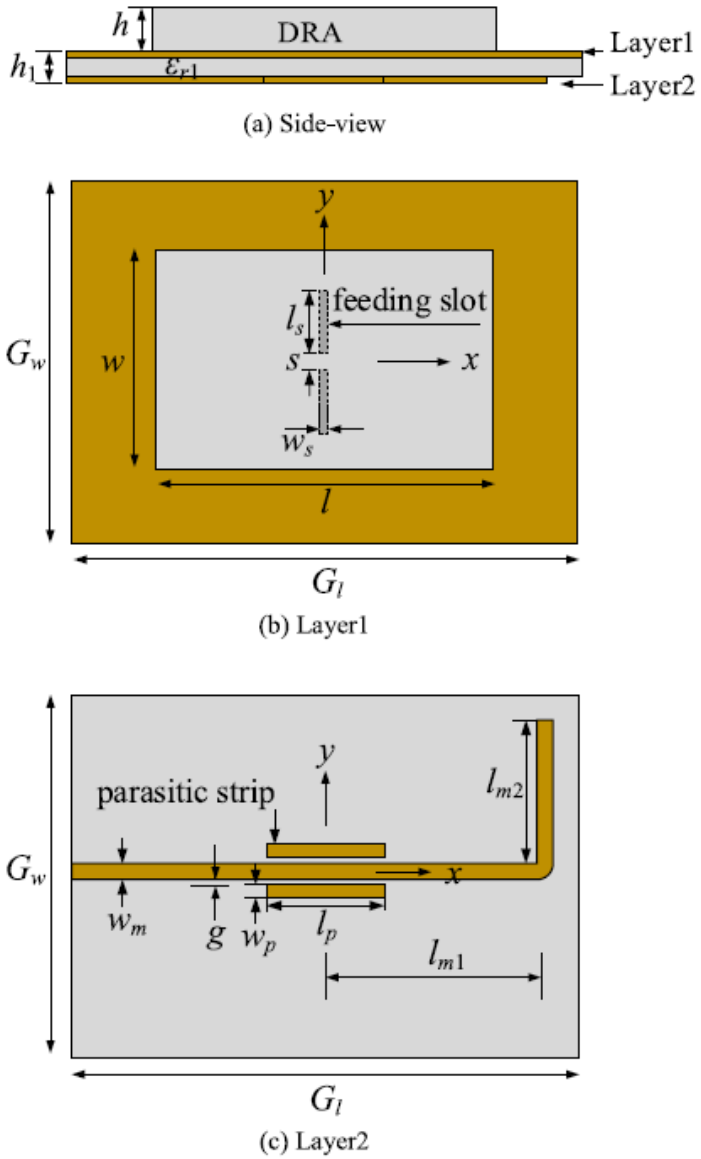

Figure 2.9 Configuration of the filtering DRA in [64]. (a) side view of the whole antenna, (b) ground plane with two separated slots, (c) microstrip feed line on bottom layer [63].

Figure 2.9 shows the configuration of the reported filtering DRA in [63]. The antenna is composed of rectangular DRA and a feeding networks on the bottom layer. The DRA has a length of l = 40 mm, width of w = 26 mm and height of h = 5.2 mm. The dielectric constant of the DRA ε_r = 10. The length and width of the two identical coupling slots are l_s and w_s, respectively. On the bottom, an L-shaped microstrip line, which is accompanied by two parasitic strips, is utilized to feed the slots. The total length from the opened end to the coupling point is $l_m = l_{m1} + l_{m2}$, which is used to generate the two radiation nulls at the both edges of the passband. The design process of such a filtering DRA can be summarized as follows:

a. A DRA is firstly designed. The two radiation nulls are designed at the both edges of the designated band by adjusting the length of the open stub.
b. Then, two identical slots instead of one single slot, are etched in the ground plane for suppressing the radiation in the lower band.
c. Finally, two parasitic strips are added and in parallel with the microstrip line, which serve as a bandstop filter, to further eliminate the radiation in the higher band.

Following the steps above, a filtering DRA with improved frequency selectivity and out-of-band rejection can be achieved without resorting to extra filtering circuits.

(4) Filtering Microstrip Antenna/Array

Microstrip antenna is one of the most popular candidates in the design of directive antennas. Compared with other types of antennas, a microstrip antenna has the advantages of low profile, light weight, low cost and ease of fabrication. In addition, microstrip antenna is more suitable to extend into a large array for enhancing the antenna gain. Therefore, it is worthwhile to investigate the integration of the microstrip antenna/array with the passband filters. The filtering microstrip antenna has attracted wide research interests in the past years and many filtering microstrip antennas have been reported [68]-[104]. There are two main methods that have been widely employed in achieving the filtering microstrip antennas. One is to use a synthesis method and replace the last resonator of the passband filter with a radiation patch. The other is to use a fusion method, which designs a filtering antenna by introducing band-notched structures out of the passband, shaping a filter like frequency response. In this section, both methods will be illustrated. It should be noted that to realize a filtering array antenna, the filtering power dividing networks or the filtering baluns based on coupled resonators could also be integrated so that the feeding networks have the functions of power dividing and frequency selectivity.

Figure 2.10 shows the configuration of the 2 × 2 filtering antenna array in literature [83], which consists of four radiating elements, two vertical half wavelength resonators, one inverted E-shaped resonator and one 50 Ω feeding microstrip with the interdigital coupler. In this work, the radiating elements function the last resonator of the passband filter. The feeding network contributes the first and second stages of the filter. As a result, the entire filtering antenna array can exhibit the third-order Chebyshev filtering responses.

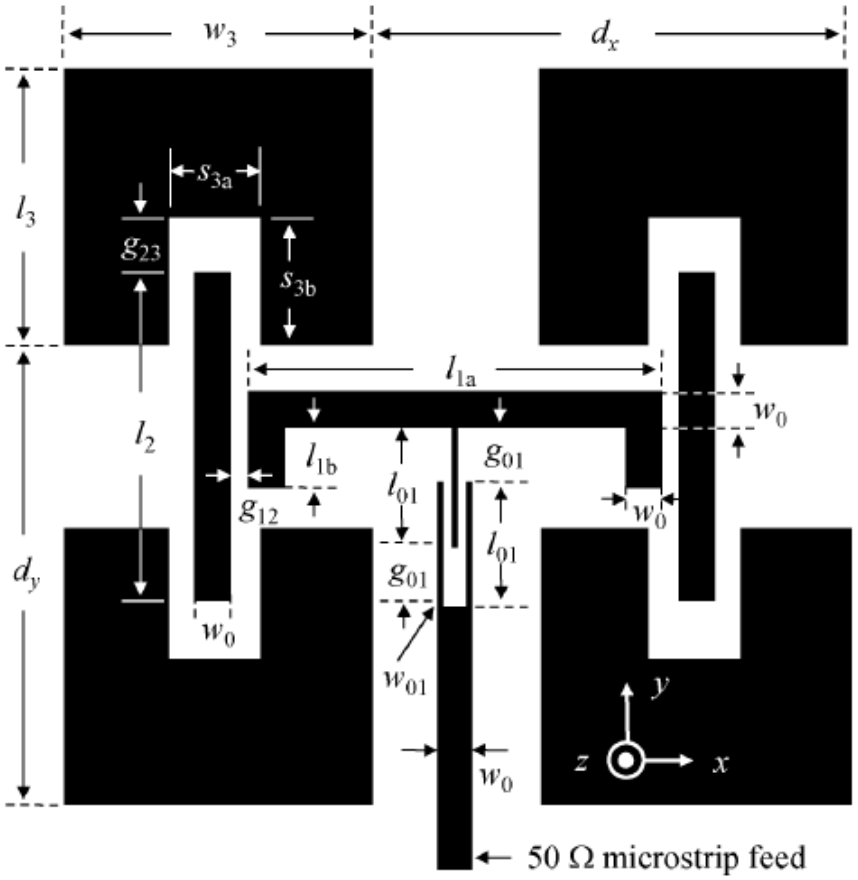

Figure 2.10 Configuration of the filtering microstrip antenna array in [83].

As can be observed, the microstrip line is coupled with the E-shaped resonator via an interdigital coupler at the one end, forming the first stage. The E-shaped resonator is essentially a half-wavelength resonator at the designated frequency. At the both sides, the E-shaped resonator is coupled with two identical vertical half-wavelength resonators, which act as the second stage of the resonators. Since the symmetry of the geometry, the couplings of these two resonators are equal. Therefore, the first and the second stages can be treated as an equal power equal phase power divider. Observing the transition between the vertical resonator and the patch, there exists a 90 degree phase difference between the second and

the third resonators. Since both radiation patch and the second stage resonator are half wavelength resonator and they have the same resonant frequency, the current on the patch has the consistent magnitude and phase characteristics. Using the synthesis method presented in Chapter 2.2, the coupling coefficients m_{ij} and external quality factor Q_{ext} can be calculated. In this design, Q_{ext} = 45.7 and m_{12} = m_{23} = 0.024 is obtained. According to these values, the physical dimensions of the antenna can be achieved by using the full-wave simulations.

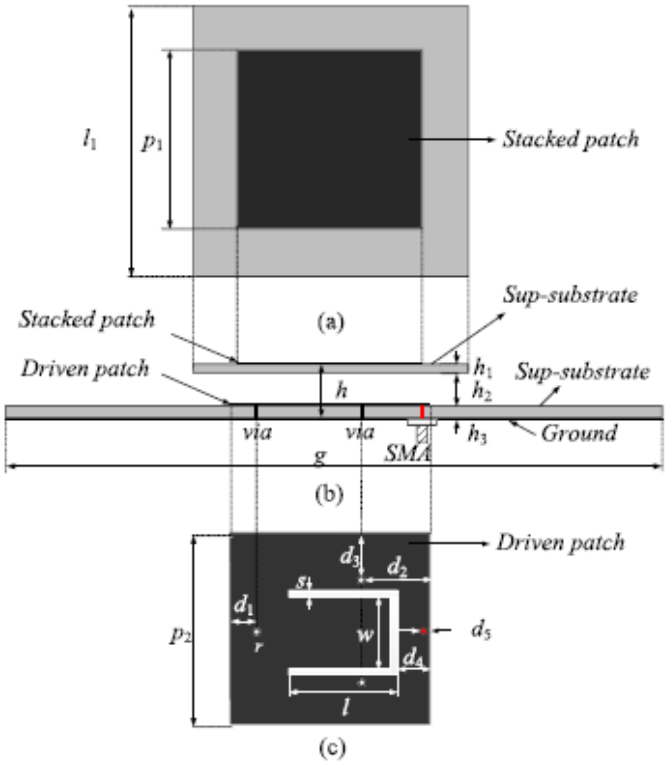

Figure 2.11 Configuration of the filtering microstrip antenna in [89]: (a) upper stacked patch, (b) side view of the antenna, (c) driven patch with a U-slot and three shorting pins.

The other method of designing a filtering microstrip antenna is to integrate the resonant structures in the feed or the radiating element of the antenna to shape the frequency response, called fusion method. Figure 2.11 shows the configuration of the filtering microstrip antenna in [89]. It consists of two layers of stacked patch and a ground plane. Compared with traditional patch antenna, three shorting pins and a U-shaped slot are embedded in the driven patch. To integrate the filtering features into the antenna, a stacked patch is used to enhance the impedance bandwidth and antenna gain and to introduce a radiation null near the upper band edge. Then, the three shorting pins and the U-slot in the driven patch are optimized to provide two radiation nulls in the lower stopband. The three shorting pins are organized to produce the out-of-phase current distribution on the driven and parasitic patches. The U-

slot, which operates as an additional resonator, introducing an extra radiation null in the lower band for further improving the roll-off rate at the lower band edge.

(5) Integrated Antenna-Filter-Antenna for Frequency Selective Surface (FSS)

The last type of integrated filtering antenna is called "Antenna-Filter-Antenna (AFA)", which is composed of a receiving antenna, a non-radiative resonant structure and a transmitting antenna [104]. The AFA is usually used in the uniform arrays to achieve the frequency selective surfaces (FSS) and operated between the input and output radiation ports. The high-order FSS can be achieved by combining several stacked FSS layers with a thick spacer (0.2-0.3 λ) between them. Although the single antenna element has a limited bandwidth, the AFA can realize the filtering frequency responses as a module.

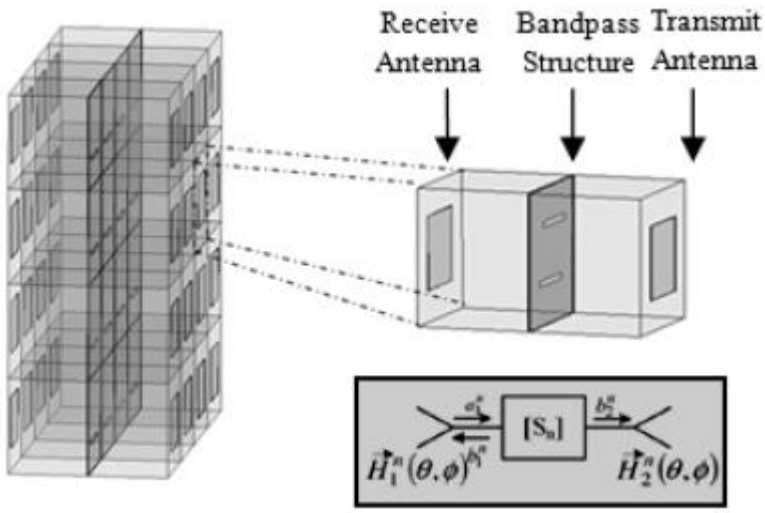

Figure 2.12 Configuration of an AFA array composed of receive antennas, bandpass structures, and transmit antennas [104].

Figure 2.12 shows the configuration of an AFA array, which composed of stacked receive antennas, bandpass structures and transmit antennas. The middle non-radiative structure is used to control the coupling between the receiving and transmitting antennas and form a two-pole bandpass filter. The elementary cell consists of a single ground plane, two substrate layers and two coupled patch antennas at both sides of the ground plane. The element is designed at 42 GHz, with the size of 3.6 × 3.6 mm. The cell can be used in uniform array for Q-band FSS applications.

2.4 Summary and Objectives of the Thesis

In this chapter, the background and advantages of the integrated filtering antenna are introduced at first. The advantages include simplified and compact RF frontend, reduced insertion losses, and improved frequency responses. Then, the methodology of filtering antenna synthesis is presented, providing the guidance for the filtering antennas design in the later parts of this dissertation. Finally, the state-of-the-art filtering antennas are introduced, including three main categories: cascaded filter-antenna, bandstop filter inserted antenna and integrated filtering antenna. This thesis focuses on the integrated filtering antenna.

Based on the outcomes of researches in recent years, the integrated filtering antennas achieved on different types of antennas are summarized. To date, there are five types of integrated filtering antennas reported, they are:

- Filtering monopole antenna;
- Cavity-backed filtering slot antenna;
- Filtering dielectric resonator antenna;
- Filtering microstrip antenna/array;
- Antenna-Filter-Antenna for FSS applications.

In this thesis, the research mainly focuses on the microstrip filtering antenna and array. The objective of the research is to investigate different methods for integrating various filtering features into the patch antennas. In the following chapters, the filtering antennas/arrays with the following filtering characteristics and the corresponding implementation methods will be discussed in detail. Based on the proposed methods, the filtering antenna with integrated duplexing function is also presented. The objectives of this thesis include the researches of:

1. Broadband filtering antenna/array;
2. Filtering antenna/array with high frequency selectivity;
3. Filtering antenna with wideband harmonic suppression;
4. Dual-band filtering antenna;
5. Dual-band dual-polarized filtering array antenna;
6. Filtering antenna/array for mm-Wave applications;
7. Duplexing filtering antenna/array.

Chapter 3. Highly Integrated Filtering Antenna Elements with Improved Performance

3.1 Introduction

In traditional wireless communication systems, the passive components such as filter and antenna are designed separately due to the different theories and implementation methods. These components are then cascaded through 50 Ω interfaces and matching networks. However, owing to the difference in bandwidths between the filters and the antennas, they are usually not well matched, especially at the edges of the operating band, leading to the unwanted insertion losses [83]. This mismatch also degrades the frequency performance of the system. For the traditional cascaded communication systems, the operation bandwidth is determined by the narrowest band of the component. Thus, to design a broadband communication system, the bandwidths of all subsystems should have the broad bandwidths, which usually puts much burden on different component designers. Another critical issue to be concerned in wireless communication systems is the interference caused by harmonics [105]-[106]. These harmonics are usually suppressed or eliminated by the bandpass filters, which inevitably increases the weight and complexity of the systems [105]. The integration of passive components provides an easy and flexible way to solve these problems and challenges.

On the other hand, the development of wireless systems such as mobile communications, wireless local area networks and satellite communications always demand the RF front-end systems to be compact, lightweight, low cost and multi-functional. These increasingly stringent requirements stimulate the emergence of the high-integration device: filtering antenna. Filtering antenna can not only overcome the aforementioned problems but also maintain a compact size of the front-ends. The integration of filters and antennas has attracted significant research interests during the past decades. By virtue of the antenna's resonant nature, some radiating elements can be served as the last resonators of the filters. As a result, the antennas can contribute to the poles of the filter and therefore the bandwidth and frequency selectivity, which is defined as a ratio of -10 dB bandwidth and -3 dB bandwidth (BW_{-10dB}/BW_{-3dB}).

Microstrip antenna is one of the most widely used types of antennas in wireless systems for its merits of low profile, light weight and low cost [107]-[108]. As we know, the traditional microstrip antennas have the drawback of narrow bandwidth due to their resonant

characteristics and relatively high *Q*-values [109]-[111]. The highly integrated filtering antennas provide a feasible solution to improve the bandwidth of the microtrip antenna without incurring extra footprint. The integrated filtering could also improve the frequency selectivity and out-of-band rejection with the harmonics suppressed over a broad bandwidth. Besides, the dual-band filtering antenna are also developed for the first time for the wireless applications.

3.2 Bandwidth Improved Microstrip Filtering Antenna

In this section, a novel method is explored to improve the bandwidth and frequency selectivity of the traditional microstrip patch antenna. In traditional aperture-coupled microstrip antenna designs, a microstrip line is used to feed the patch through a slot in the ground. Here, the microtrip line is replaced with a dual-mode stub loaded resonator (SLR), which is coupled and tuned with the patch so as to generate multiple resonant modes in the operation band. As a result, the bandwidth can be enhanced greatly.

3.2.1 Configuration

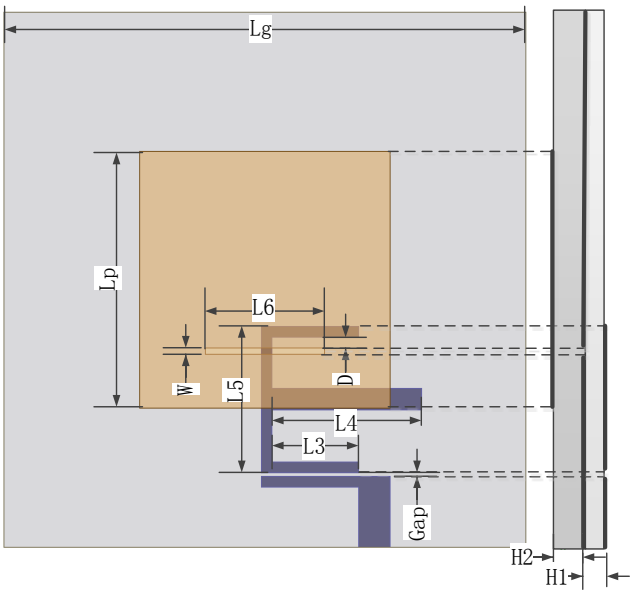

Figure 3.1 Configuration of proposed SLR-fed filtering patch antenna

Table 3.1 Parameters of the Proposed Antenna: (mm)

Lg	Lp	L3	L4	L5	L6
30	14.2	5.6	8.6	7	6.8
W	Gap	D	H1	H2	
0.35	0.25	0.6	0.8	1.6	

Figure 3.1 shows the configuration of the proposed SLR-fed filtering antenna. The antenna is composed two stacked substrates. The SLR and the feeding network are printed on the bottom layer of the lower substrate, whereas, the square patch is printed on the top layer of the upper substrate. The SLR and the patch share the common ground plane in the middle, which is printed on the top layer of the bottom substrate. In the ground plane, a slot line is etched to enable the electromagnetic energy transmits from the SLR to the patch for radiating out. The dimension of the patch is approximate a half wave-length and the resonant modes of the SLR can be analyzed using odd- and even-mode. The stacked configuration employed here could not only make the design compact, but also reduce the interference between the feeding networks and radiation patch. Rogers 4003 substrates with a dielectric constant of 3.55 and loss tangent of 0.009 are used in the design. The thicknesses of the lower and upper substrates are 0.8 mm and 1.6 mm, respectively. The design and optimization were performed using High Frequency Simulation Software (HFSS 15) and the optimized parameters are shown in Table 3.1.

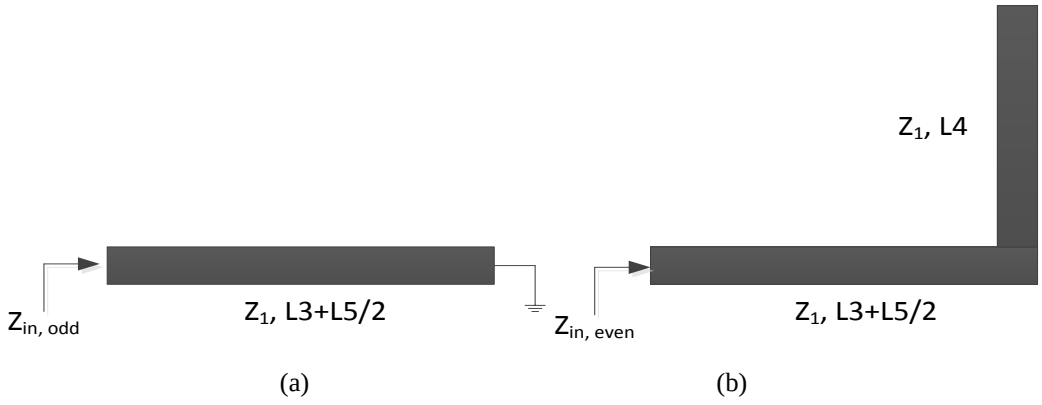

Figure 3.2 The equivalent circuits of the SLR: (a) odd-mode, (b) even-mode.

3.2.2 Methodology

The design principles of the proposed antenna can be explained using the filter designs methods. Figure 3.2 shows the equivalent circuits of the SLR in Figure 3.1. Due to the symmetry of the SLR, it can be analyzed using odd- and even-mode [112]-[113]. When the odd-mode is excited, the voltage at the middle of the SLR is close to 0. Thus, the middle plane of the SLR can be treated as ground plane, as shown in Figure 3.2(a). However, when the even-mode is excited, the symmetrical plane is regarded as the magnetic wall, which can be equivalent as open end, as depicted in Figure 3.2(b). The input impedance for the odd-mode and even-mode can be derived as

$$Z_{in,odd} = jZ_1 \tan\beta(L3 + L5/2) \quad \text{(Eq.3.1)}$$

$$Z_{in,even} = -\frac{Z_1}{j\tan\beta(L3 + L5/2 + L4)} \quad \text{(Eq.3.2)}$$

where Z_1 is the characteristic impedance of the microstrip and β is the transmission constant. When the Z_{in} is infinite, the SLR resonates and the odd-mode and even-mode resonant frequencies can be derived,

$$L3 + L5/2 = \frac{\lambda}{4}(2n-1) \quad \text{(Eq.3.3)}$$

$$L3 + L4 + L5/2 = \frac{n\lambda}{2} \quad \text{(Eq.3.4)}$$

where n = 1, 2, 3…. In this work, the n = 1 is chosen. According to Eq. 3.3 and Eq. 3.4, the odd-mode and even-mode resonant frequencies can be controlled by tuning the *L3* and *L4*. Figure 3.3 shows odd- and even-mode of the SLR with different *L3*. It is observed that the odd-mode and even-mode move towards lower band simultaneously as *L3* increases, but the odd-mode is much more significant than the even-mode. The even-mode can be controlled independently from equation Eq.3.4, as shown in Figure 3.4. The even-mode frequency shifts to lower band when *L4* increases, however, the odd-mode maintains unchanged.

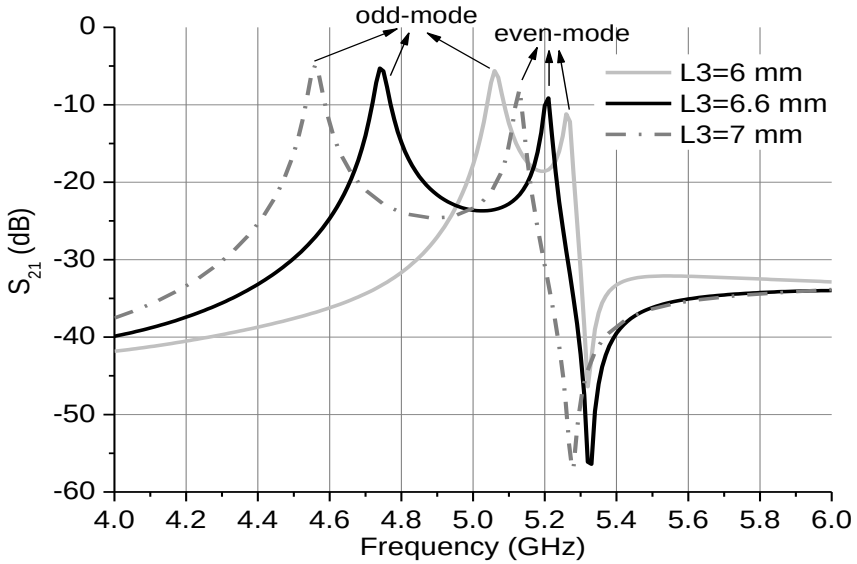

Figure 3.3 The odd- and even-mode of the SLR with different *L3*.

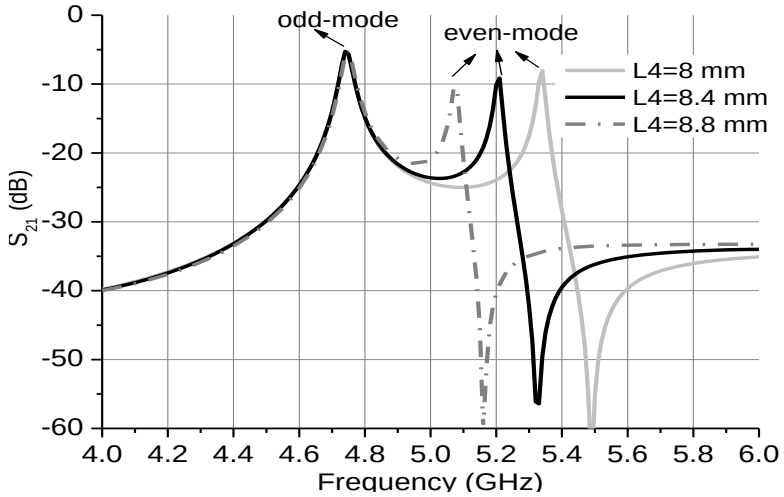

Figure 3.4 The odd- and even-mode of the SLR with different *L4*.

As the microstrip patch antenna can be regarded as a single-mode half wavelength resonator, the bandwidth of the patch itself is limited. To enhance the bandwidth of the microstrip patch antenna, the resonant frequencies of the SLR and patch are combined together, forming a broad impedance bandwidth. To shape the band, the resonant modes of the SLR are adjusted and located on the both sides of the patch's resonant mode, as shown in Figure 3.5. Figure 3.6 compares the bandwidth of the proposed SLR-fed patch antenna with a traditional microstrip-fed patch antenna. As can be seen, the traditional patch antenna has only one reflection zero in the band, showing a narrow bandwidth about 140 MHz. In contrast, the proposed antenna exhibits a broad bandwidth around 400 MHz with three reflection zeros in the band identified. Moreover, owing to the resonant characteristics of the SLR, the SLR-fed patch antenna exhibits the filter-like frequency selectivity with a sharp skirt at the both edges of the operation band.

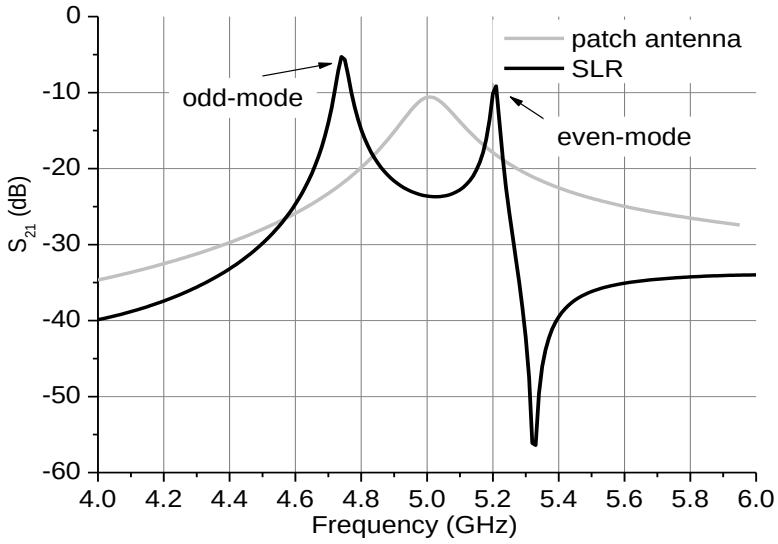

Figure 3.5 The resonant modes of SLR and patch.

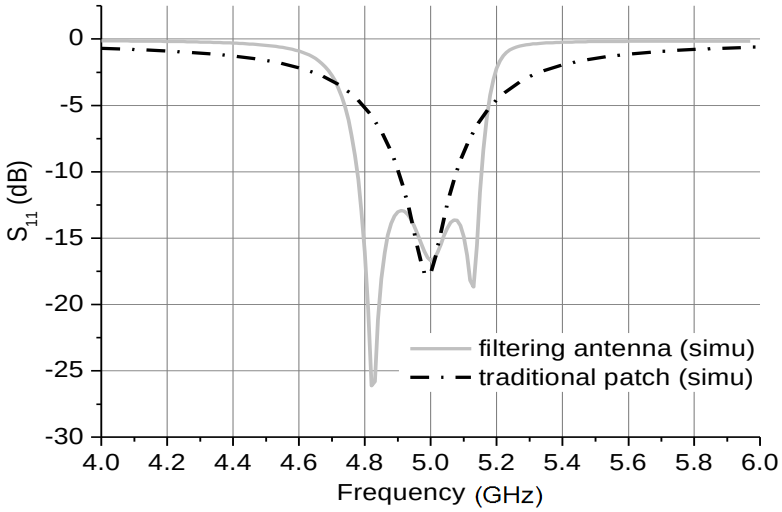

Figure 3.6 The bandwidth comparison between SLR-fed and microstrip-fed patch antennas.

3.2.3 Results and Discussion

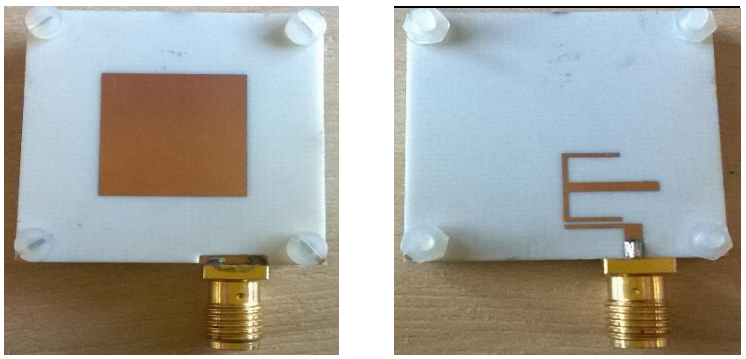

(a) **(b)**

Figure 3.7 Prototype of the proposed SLR-feed microstrip antenna: (a) front view, (b) back view.

The SLR-fed microstrip filtering antenna was fabricated and the prototype is shown in Figure 3.7. Figure 3.8 shows the simulated and measured S_{11} and antenna gain. For comparison, the simulated S_{11} of a patch antenna with the same parameters but fed by a microstrip line was added. As can be observed, the measured S_{11} of the SLR-feed antenna agrees well with the simulation with the three reflection zeros at 4.8, 5 and 5.2 GHz, respectively. The measured fractional bandwidth (FBW) is over 8 %. Compared with the microstrip-fed patch antenna, the bandwidth is significantly improved. In addition, the proposed antenna exhibits the excellent filtering features with a good frequency selectivity (BW_{-10dB}/BW_{-3dB} = 0.78) and good out-of-band rejection (close to 0 dB). Seeing the antenna gain curve, we can see the proposed antenna has a flat gain response around 6 dBi from 4.8 to 5.2 GHz. Out of band, the gain rapidly decreases to below -15 dBi, demonstrating an excellent filtering performance in terms of frequency selectivity and out-of-band rejection.

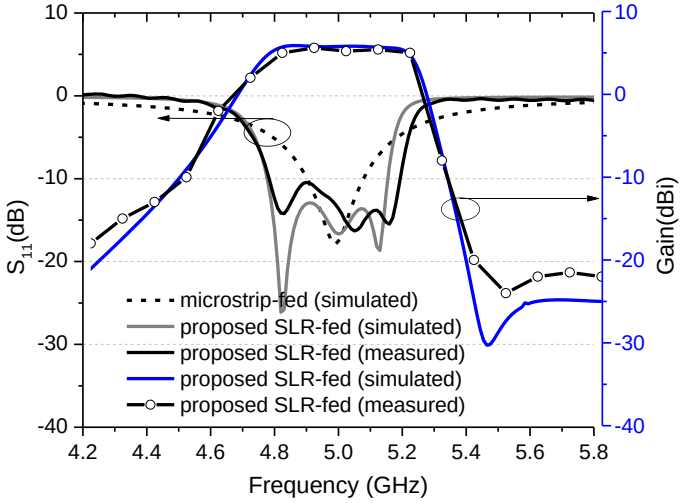

Figure 3.8 Simulated and measured S_{11} and gain of the proposed antenna.

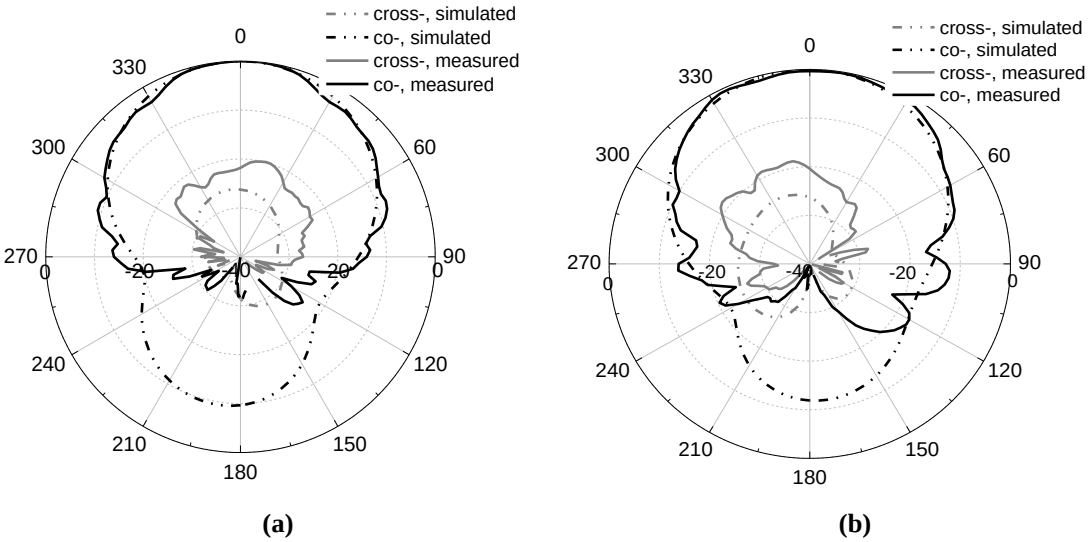

Figure 3.9 Simulated and measured normalized radiation patterns of the proposed microstrip antenna at 5 GHz: (a) E-plane, (b) H-plane.

Figure 3.9 shows the simulated and measured E- and H-plane normalized radiation patterns of the proposed SLR-feed microstrip antenna at 5 GHz. The antenna exhibits the broadside radiation with the cross polarization discrimination is better than 20 dB. The measured results agree well with the simulations. The main mismatching in the backward radiation is caused by the blockage of the measure instruments for mounting the antenna.

3.3 Wideband Harmonic Suppression Filtering Antenna

The other important function of the integrated filtering antenna is the wideband harmonic suppression performance. It is well-known that higher-order modes are widely existing in

distributed microwave components, such as antenna and filters. These harmonics will lead to the unwanted interferences and deterioration of the system. Therefore, it is worthwhile to eliminate these harmonics. To date, various methods have been used to suppress the harmonics. In [114]-[117], slots or shorted pins are inserted in the radiating element to produce mismatching at the given bands. In [118]-[123], periodic structures such as defected ground structures (DGS) are used to reduce the effects of the harmonics. Harmonics can also be reduced by placing a notch resonator close to the feed [124]. However, most of the techniques presented are dealing with the 2nd-order harmonics, the higher-order harmonics are rarely looked at. The other limitation of these works is the narrow bandwidth in-band. It is usually a challenge to achieve a multi-octave harmonic suppression because of the space limitation.

In this section, a highly integrated filtering antenna is proposed, which not only suppresses the harmonics but also improves the bandwidth of the patch antenna. Here, we use a modified planar inverted-F antenna (PIFA) as the feed of a rectangular patch, 2nd-order frequency responses with improved bandwidth and selectivity are achieved. Moreover, the 2nd, 3rd and 4th-order harmonics over a two-octave band are significantly suppressed without incurring any additional circuits.

3.3.1 Configuration

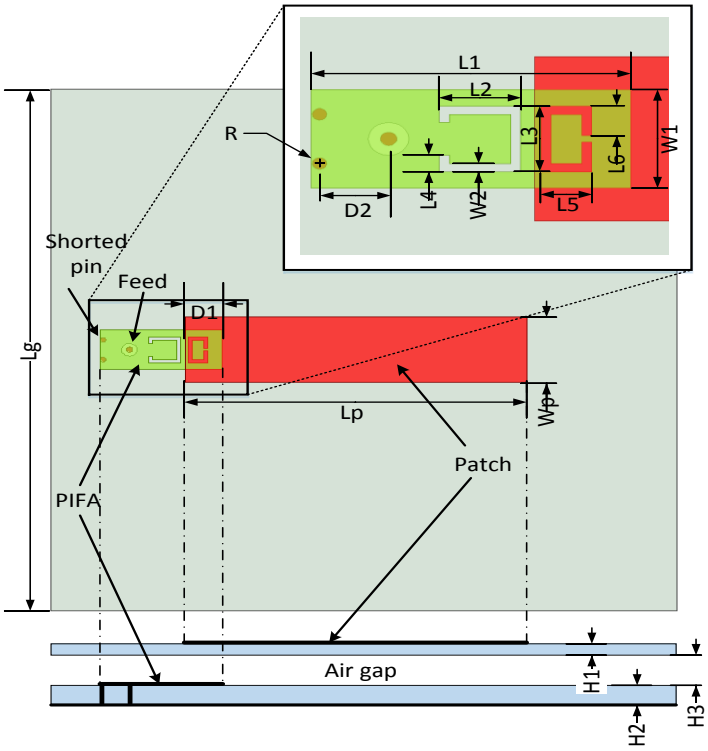

Figure 3.10 Configuration of the proposed PIFA-fed patch antenna.

Table 3.2 Parameters of the Proposed Antenna: (mm)

Lg	Lp	Wp	H1	H2	H3	R	L1	L2
80	43.6	10	0.813	1.525	4	0.35	15.7	4
L3	L4	L5	L6	W1	W2	D1	D2	
4	1	2.5	1.8	6	0.5	5.2	3.4	

Figure 3.10 shows the configuration of the proposed PIFA-fed patch antenna. The patch is rectangular printed on the upper layer of the top substrate and the PIFA is printed on the upper layer of the bottom substrate while the ground plane is printed on the lower layer of the bottom substrate. Between the two substrates, an air gap is inserted for improving the impedance matching. The PIFA is shorted to the ground through two pins at the one end. The PIFA and the patch have the same resonant frequency of 2.4 GHz and they are coupled to generate a 2nd-order filtering antenna through electromagnetic coupling. This results in the improved bandwidth and frequency selectivity when compared with the traditional patch antenna. Moreover, two complementary split-ring resonators are embedded in the PIFA so as to suppress its 3rd-order harmonics. RO4003C substrate with a relative permittivity of 3.55 and loss tangent of 0.0027 @ 10GHz is used in the design. The thicknesses of the top and the bottom substrates are 0.813 mm and 1.525 mm. All the simulations are performed using High Frequency Structure Simulator (HFSS 15) and the optimized parameters are listed in Table 3.2.

3.3.2 Equivalent circuit and methodology

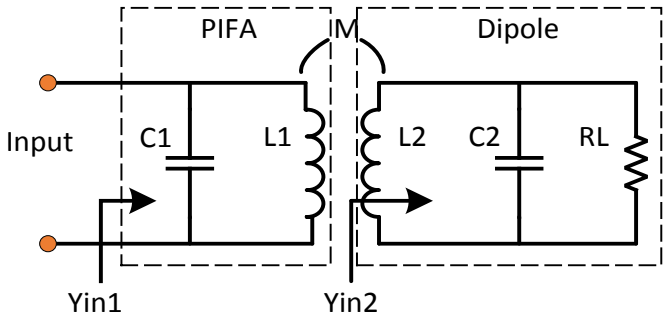

Figure 3.11 Schematic equivalent circuit of the coupled PIFA-patch structure.

Because the PIFA works at odd modes (f_0, $3f_0$, $5f_0$…), it can be regarded as a quarter wavelength resonator. The patch antenna, however, works at its integral multiples of fundamental frequency (f_0, $2f_0$, $3f_0$…) and can be equivalent to a half wavelength resonator. Thus, the proposed antenna can be modulated to a 2nd-order resonant circuit, as shown in Figure

3.11. The PIFA is represented by a lumped shunt *LC* resonator. The open-end with the length less than a quarter wavelength is equivalent as a capacitance *C* and the short-end is equivalent as an inductance *L*. The patch antenna above the PIFA can be equivalent as an *RLC* resonator, where the R_L indicates the radiation resistance. When the PIFA and the patch are stacked and overlapped, electromagnetic coupling between them occurs, which is indicated using *M* in the figure.

The resonant frequencies of the PIFA and the dipole are determined by adjusting the physical dimension of the PIFA and patch, respectively. The coupling strength is decided by tuning the air gap thickness and the overlap area between the PIFA and the dipole, related to *D1* in Figure 3.10. In this design, the antenna is designed to operate at 2.4 GHz and *Lp* = 44 mm, *L1* = 15.5 mm and *D1* = 5 mm are chosen as the original values.

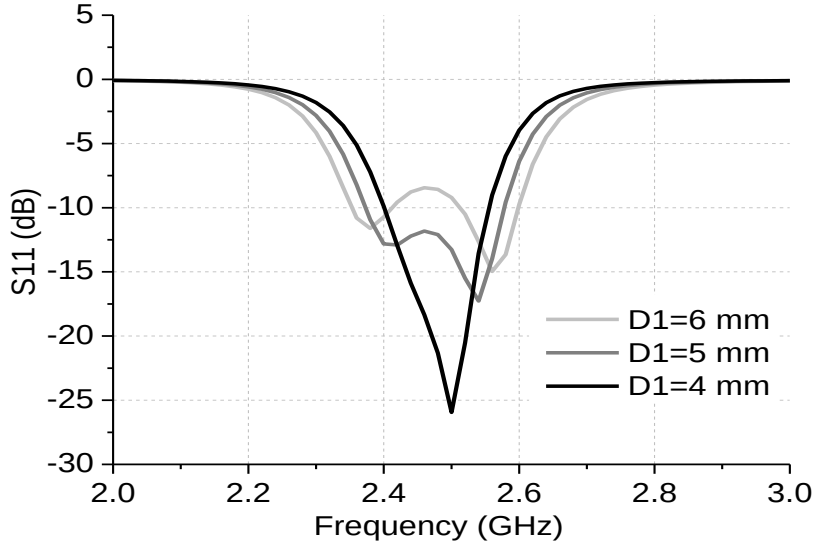

Figure 3.12 The reflection coefficient of the antenna with different *D1*.

According to the equivalent circuit presented in Figure 3.11, 2nd-order frequency responses can be achieved for the proposed PIFA-fed patch antenna. The bandwidth of the antenna can be adjusted by changing the coupling strength between the PIFA and the patch. Figure 3.12 shows the simulated S_{11} with different overlapping size as related to *D1*. As can be seen, a 2nd-order frequency response with two reflection zeros can be observed in the band, which is beneficial to improve bandwidth. The two reflection zeros move close to each other as *D1* decreases, resulting in a narrower band.

3.3.3 Harmonic Suppression

One important function of this integrated antenna is the wideband harmonic suppression by using their intrinsically different harmonic properties. It is known that dipole is a

half wavelength resonator with its harmonics at $2f_0$, $3f_0$, $4f_0$…, f_0 is the fundamental resonant frequency. However, the PIFA can be regarded as a quarter wavelength resonator and its harmonics locate at $3f_0$, $5f_0$…. Thus, when the PIFA and the patch are synchronically tuned at their fundamental frequency, the even-order harmonics of the dipole at $2f_0$, $4f_0$…can be innately eliminated. To verify this, three types of patch antennas with different feeds are investigated, as the configurations shown in Figure 3.13. Figure 3.13(a) is a traditional patch fed by microstrip, denoted as Antenna-I. In Figure 3.13(b), two shorted pins are drilled close to the feed point to form a PIFA, denoted as Antenna-II. Figure 3.13(c) is the proposed antenna, which is conceived by etching two split-ring slots in the PIFA of Antenna-II. The two slots produce resonant notches at 7.5 GHz to suppress the 3rd-order harmonics. The lengths of the slots are approximately half of a wavelength at the resonant frequencies.

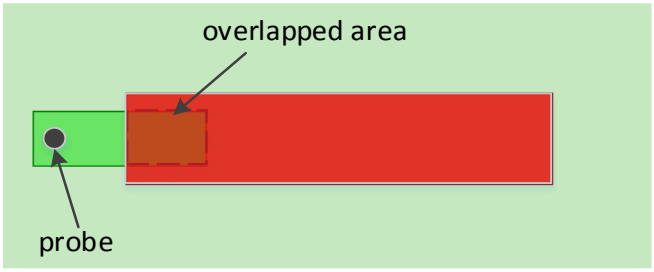

(a)

(b)

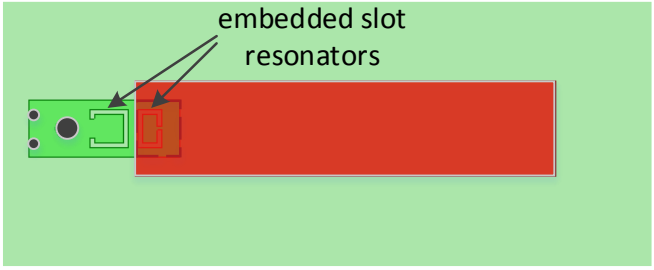

(c)

Figure 3.13 Configurations of three patch antennas: (a) traditional microstrip-fed, Antenna-I; (b) PIFA-fed, Antenna-II; (c) PIFA-fed with embedded split-ring notch resonators, Antenna-III.

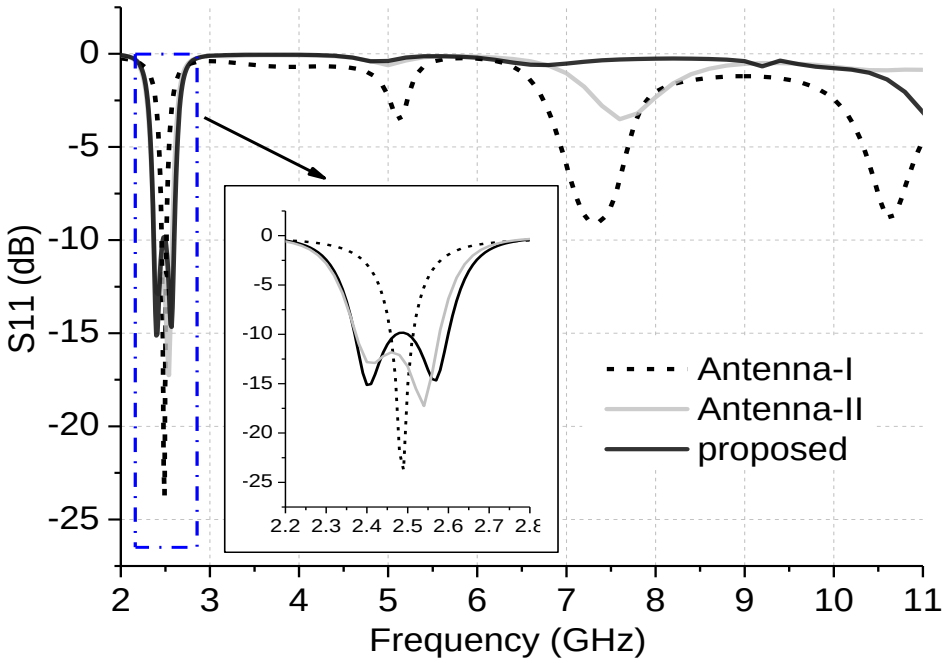

Figure 3.14 Comparison of the S_{11} of the three antennas.

Figure 3.14 compares the simulated reflection coefficients of the Antenna-I, Antenna-II and proposed antenna over a broad frequency range. The three antennas have the same working frequency at 2.5 GHz. However, they show very different higher-order harmonic responses. For Antenna-I, the 2nd, 3rd and 4th-order harmonics at 5, 7.4 and 10.5 GHz can be clearly identified. For the Antenna-II, the 2nd- and the 4th–order harmonics at 5 GHz and 10.5 GHz are significantly suppressed due to the PIFA is used as the feed. However, the 3rd-order harmonic still exists. For the proposed antenna, the 3rd-order harmonic at 7.4 GHz is eliminated because of the split-ring notch resonators integrated into the PIFA. As can be seen, the proposed antenna exhibits a two-octave harmonic-free band up to 11 GHz. Another advantage of the proposed PIFA-fed patch antenna is that the operation bandwidth is significantly improved, as the inset shown in Figure 3.14. It is observed that the two PIFA-fed antennas have two reflection zeros in the bands, contributing to improved bandwidths (220 MHz vs 70 MHz) and frequency selectivity.

The simulated current distribution of the antenna at 2.5, 5, 7.4 and 10.5 GHz is shown in Figure 3.15. As can be observed from Fig. 3.15(a), the current on the antenna exhibits a sinusoidal distribution, indicating a radiation on the patch at 2.5 GHz. However, very weak current on the patch can be observed at other frequencies. At 7.4 GHz, the current mainly concentrates around the slot resonators in the PIFA, causing a strong reflection at the input.

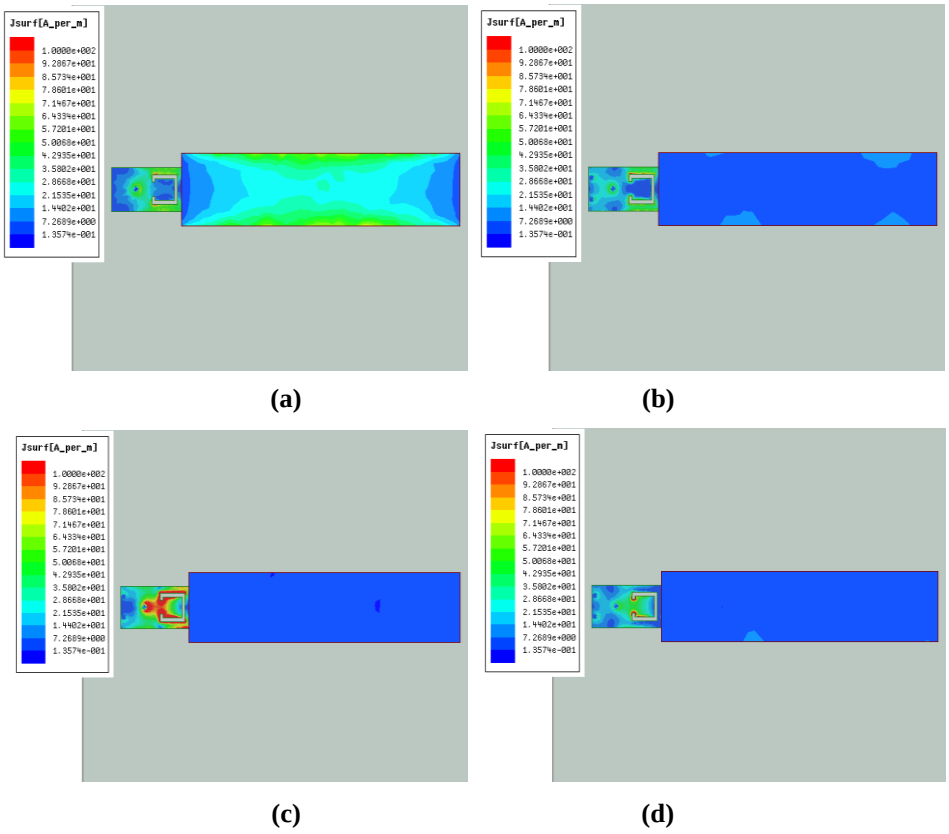

Figure 3.15 Current distribution of the proposed FIFA-fed antenna at different frequencies: (a) 2.5 GHz, (b) 5 GHz, (c) 7.4 GHz, (d) 10. 5 GHz.

Table 3.3 Results Comparison of the Three Antennas

Antenna type	Fractional band-width	Harmonic suppression ($\|S_{11}\|$)		
		2nd-order	3rd-order	4th-order
Antenna-I	2.8%	-3.6 dB	-8.5 dB	-8.5 dB
Antenna-II	8.8%	-0.4 dB	-3.5 dB	-0.8 dB
Antenna-III	9.0%	-0.3 dB	-0.2 dB	-1.2 dB

Table 3.3 summaries and compares the three antennas in terms of the bandwidth and harmonics suppression performance. As can be seen, the proposed antenna has an excellent out-of-band rejection with the 2nd-, 3rd- and 4th-order harmonics significantly suppressed.

The resonant frequencies of the PIFA and the dipole are determined by adjusting the physical dimension of the PIFA and patch, respectively. The coupling strength is decided by tuning the air gap thickness and the overlap area between the PIFA and the dipole, related to *D1* in Figure 3.10. In this design, the antenna is designed to operate at 2.4 GHz and *Lp* = 44 mm, *L1* = 15.5 mm and *D1* = 5 mm are chosen as the original values.

3.3.4 Results and Discussion

Figure 3.16 shows the simulated and measured S-parameters from 2 to 11 GHz. The measured result agrees well with the simulated one, showing an impedance matching bandwidth from 2.32 to 2.57 GHz. Out-of-band, the 2nd, 3rd and 4th harmonics of the patch at around 5, 7.4 and 10.5 GHz are significantly suppressed, contributing to an excellent harmonic suppression performance over a two-octave bandwidth (from 2.7 to 11 GHz).

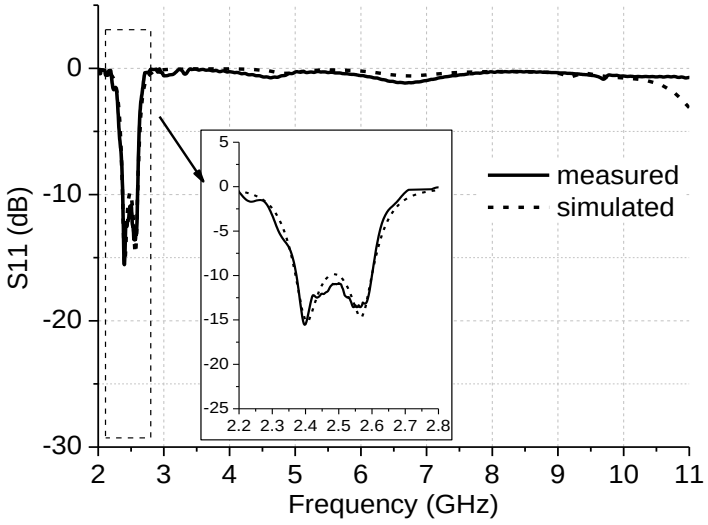

Figure 3.16 Simulated and measured S_{11} of the proposed PIFA-dipole element.

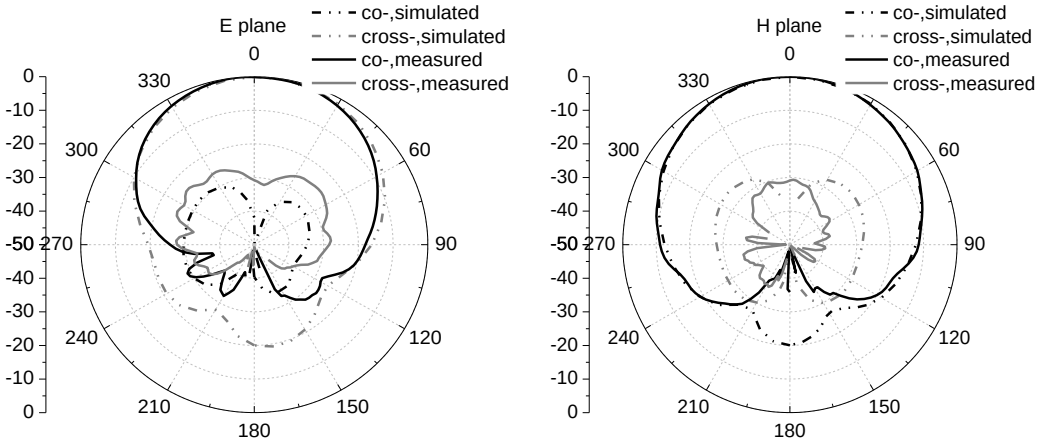

Figure 3.17 Normalized simulated and measured radiation patterns of the antenna at 2.5 GHz: (a) E plane, (b) H plane.

Figure 3.17 shows the simulated and measured normalized radiation patterns of the antenna in E- and H-plane. The measured patterns agree well with the simulations, exhibiting directional radiation pattern in broadside. The cross polarization discrimination (XPD) are better than 30 dB in both the E and H planes. The discrepancy of the backward patterns

between the simulation and the measurement is caused by the absorber material mounted on the back of the antenna under the measurement.

Figure 3.18 shows the simulated and measured gains of the proposed PIFA-fed antenna as a function of frequency. The measured result exhibits a flat gain response of 6.7 dBi at around 2.5 GHz, which is slightly lower than the simulated 7.2 dBi. Out of the band, the measured gain is lower than -7 dBi from 2.8 to 10.5 GHz, demonstrating that the PIFA-fed patch antenna exhibits an excellent harmonic suppression performance over a wideband with the 2nd, 3rd and 4th harmonics of the patch are significantly suppressed.

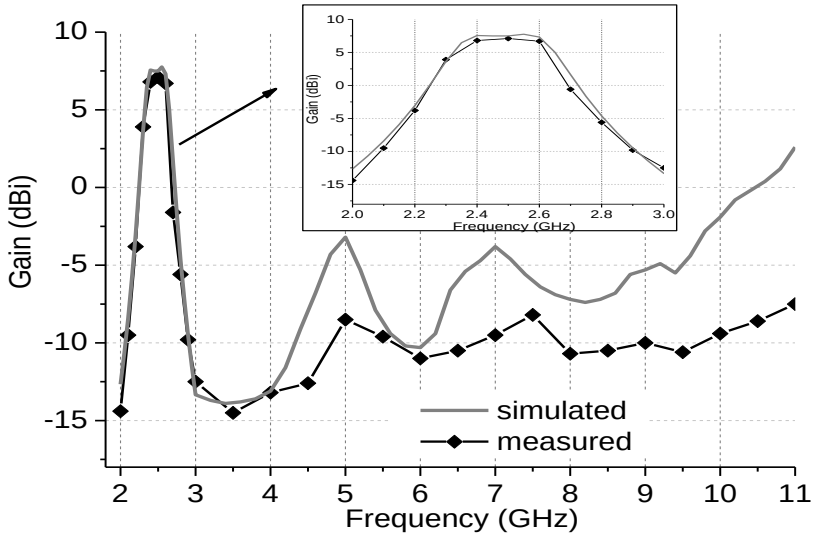

Figure 3.18 Simulated and measured gain of the PIFA-fed patch antenna.

Table 3.4 compares the proposed antenna in this paper with several other reported works with harmonic suppression capabilities in [119]-[122]. The comparison mainly focuses on the orders of in-band responses, the order of harmonics suppressed and suppression performance. From the comparison, we can see the proposed PIFA-fed patch antenna has a higher-order in-band frequency response and a better harmonic suppression performance with 2nd, 3rd and 4th harmonics significantly suppressed.

Table 3.4 Comparison with Other Harmonic Suppression Antennas

Types of antennas	Operation frequency	Poles in the band	harmonics suppressed	Rejection performance
Ref. [122]	0.9 GHz	1	2nd, 3rd	-1.3 dB
Ref. [119]	3.1 GHz	1	2nd, 3rd	-2.5 dB
Ref. [120]	2.45 GHz	1	2nd, 3rd	-3 dB
Ref. [121]	2.2 GHz	1	2nd, 3rd	-4 dB
This work	2.5 GHz	2	2nd, 3rd, 4th	-1 dB

3.4 Dual-Band Filtering Antenna

Unidirectional antenna with dual-band or multi-band operations is becoming more and more important due to the increasing wireless applications. Significant effort has gone into the research of dual-band or multi-band antennas [125]-[128]. Dual-band operations are usually achieved by utilizing the fundamental mode and higher order modes of the patch [129]-[130]. One of the disadvantages of this method is the limited frequency ratio of the two operation bands. It is very challenging to obtain a dual-band microstrip antenna with a low frequency ratio. The other problems include limited bandwidths of both operations, low gain and out-of-band interference.

The integration of filter and antenna provides a feasible method to realize the band-band operation with improved frequency responses. In [131]-[132], dual-band filtering patch antennas were proposed. However, the antenna in [131] works in the two orthogonal modes of a rectangular patch and very complicated matching structures were adopted. Besides, the antenna has a low gain of only -1.8 dBi and 1.1 dBi at the two bands and many unwanted harmonics emerge between the two bands. In [132], the TM_{10} and TM_{30} modes of the patch were employed to achieve the dual-band operation. But, the gain of the antenna is considerable low (-4 dBi) and the feeding network is complicated. In this section, a novel method is presented to achieve a dual-band filtering antenna with improved the bandwidth and wideband harmonic suppression. The two bands are designed at 3.6 and 5.2 GHz for WiMAX and WLAN applications. We use a dual-mode stub loaded resonator (SLR) to feed a dual-mode U-slot patch antenna through electromagnetic coupling, producing a 2^{nd}-order dual-band filtering antenna. Compared with traditional patch, the bandwidth, frequency selectivity and gain are significantly improved. The antenna also exhibits very good harmonics suppression performance over a broadband.

3.4.1 Antenna Configuration

Figure 3.19 shows the configuration of the proposed dual-band microstrip filtering antenna. The antenna is composed of two substrates separated by a thin foam (1 mm). The square patch is printed on the upper layer of the top substrate with a U-shaped slot is etched in it for dual-band operation. The feeding line and the dual-mode E-shaped SLR are printed on the bottom layer of the lower substrate. The patch and the feeding network share a same ground plane in the middle layer with an aperture etched in it. Figure 3.19(b) illustrates the stacked structure of the proposed design. Rogers 4003 substrate with a dielectric constant of

3.55 and a loss tangent of 0.0027 was used. All simulations were performed using High Frequency Structural Simulator (HFSS 15) and the optimized parameters are listed in Table 3.5.

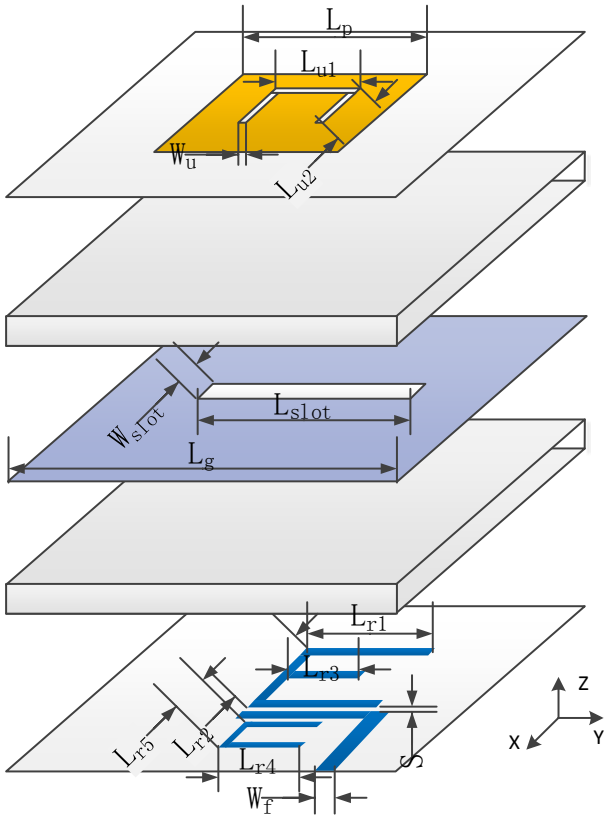

(a)

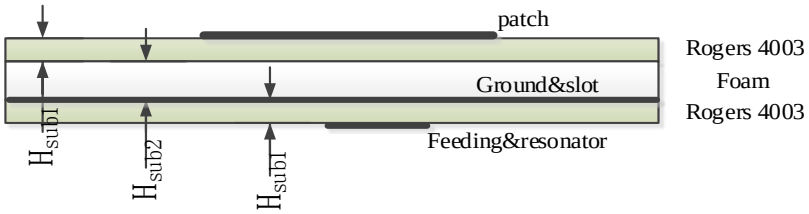

(b)

Figure 3.19 Configuration of the proposed dual-band filtering antenna: (a) exploded perspective view, (b) the stacked structure.

Table 3.5 Parameter of the Proposed Dual-Band Filtering Antenna: (mm)

L_p	L_{u1}	L_{u2}	W_u	L_g	L_{slot}	W_{slot}	L_{r1}
27.2	7.5	8	0.45	60	9.4	0.7	8.2
L_{r2}	L_{r3}	L_{r4}	L_{r5}	S	W_f	H_{sub1}	H_{sub2}
8	6.15	4.2	2.8	0.3	1.8	0.813	1

To achieve the dual-band patch antenna with filtering performance, a dual-mode SLR is employed to couple and synchronically tune with the U-slot patch. In contract with the traditional method of cascading a filter with an antenna [133], the filtering and radiating components are seamlessly integrated in this work. The U-slot patch here serves as the last-order dual-mode resonator of the dual-band passband filter (SLR) as well as the radiating element. This contributes to a higher order filtering performance (2^{nd}-order) while maintaining a compact footprint.

Owing to the high freedom in controlling the resonant frequencies, the E-shaped SLR is widely used as a dual-mode resonator in filter design. The SLR can be analyzed using the odd- and even-mode method. When the odd-mode is excited, the center part of the SLR is equivalent to a shorted end and the resonant frequency can be approximately derived as,

$$f_{odd} = \frac{c}{2\sqrt{\varepsilon_r}(2L_{r1} + L_{r2})} \quad \text{(Eq.3.5)}$$

When the even-mode is excited, the symmetrical plane can be viewed as an opened end and the resonant frequency can be expressed as,

$$f_{even} = \frac{c}{2\sqrt{\varepsilon_r}(L_{r1} + L_{r2}/2 + L_{r3})} \quad \text{(Eq.3.6)}$$

where the f_{odd} and f_{even} are the odd- and even-mode resonant frequencies of the SLR. c is the light velocity in free space and ε_r is the effective permittivity. Thus, the odd-mode and even-mode resonant frequencies can be easily tuned by adjusting the dimensions of the SLR.

3.4.2 Improved Bandwidth

Normally, the bandwidth of the dual-band U-slot patch antenna is limited, especially for the low profile antennas. In this design, a new method for enhancing both bandwidths of the patch antenna by using a dual-mode resonator to feed the U-slot patch is investigated. The U-slot patch and the dual-mode resonator are coupled by electromagnetic, leading to a higher order frequency responses at the two bands without increasing the profile of the antenna. Figure 3.20 compares the simulated S_{11} of standalone U-slot patch, SLR filter and the proposed filtering antenna. It is observed that the traditional U-slot patch only shows one pole in each band and the fractional bandwidths at both bands are only about 1.8%. In contrast, the proposed antenna exhibits the improved bandwidths at both bands with 2^{nd}-order filtering features. At each band, two reflection zeros can be identified, contributing to sharp roll-offs at both bands.

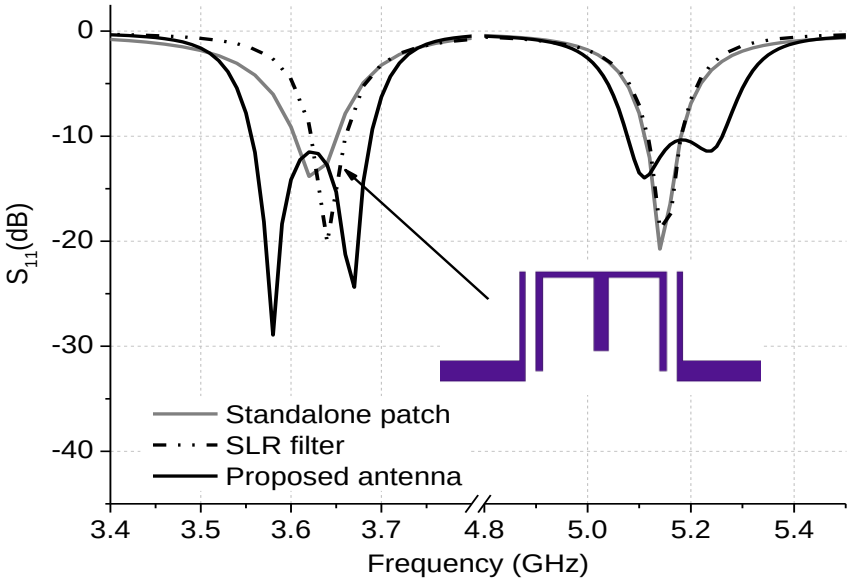

Figure 3.20 S_{11} comparison among standalone U-slot patch, SLR filter and proposed filtering antenna.

The other advantage of the proposed dual-band method is that the bandwidth can be tuned by adjusting the coupling strength between the resonators. Figure 3.21(a)-(b) shows the bandwidths of the two operation bands with different lengths and widths of the aperture. It is observed that when the length of aperture L_{slot} is shorter than 8 mm, the two reflection zeros merge together, leading to a narrow bandwidth of less than 50 MHz (FBW = 1.4%). As L_{slot} increases, indicating that the coupling strength between the SLR and the U-slot patch increases, the two reflection zeros are divided and a wider bandwidth of over 150 MHz (4.2%) is achieved for the low-band. When L_{slot} further increases, the impedance matching performance will deteriorate. The length of the aperture has a similar but less significant

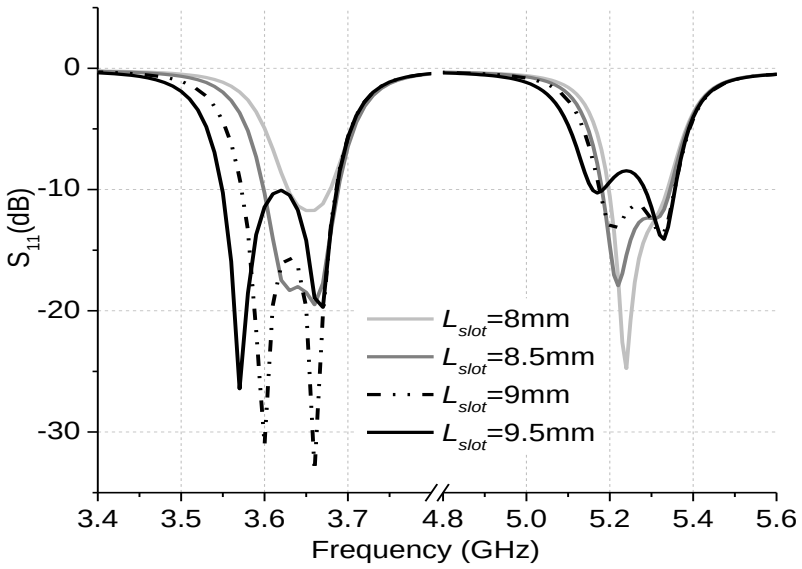

(a)

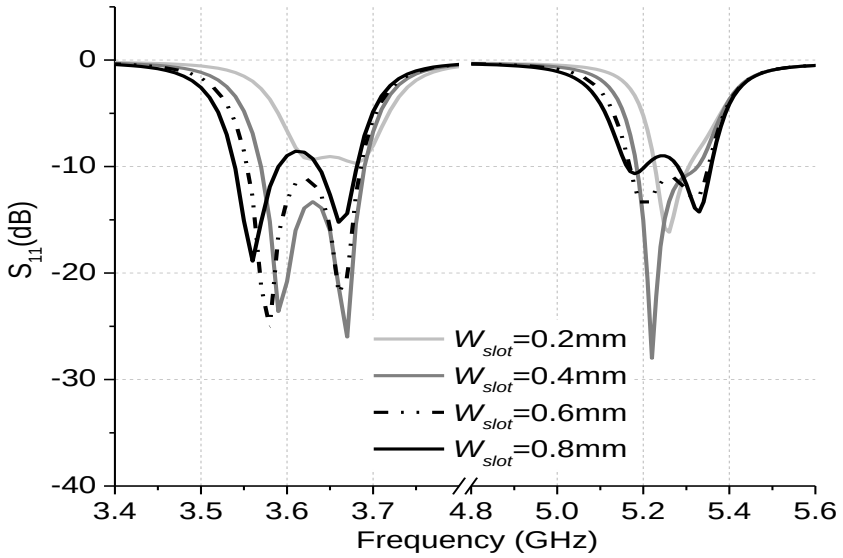

(b)

Figure 3.21 Variation of the bandwidths with different (a) L_{slot}, and (b) W_{slot}.

effect on the high-band operation. The effects of the width of the aperture on the bandwidth are shown in Figure 3.21(b). When the width of the aperture decreases from 0.8 to 0.2 mm, the bandwidths of the low-band and high-band decrease from 4.2% to 1.9% and from 3.8% to 1.2%, respectively. Different from the traditional patch antenna, where the bandwidth is usually tuned by adjusting the profile of the antenna, this work provides a new method to tune the bandwidth of the antenna without changing the thickness of the antenna.

3.4.3 Harmonic Suppression

Harmonics is a serious problem to be concerned in wireless communication systems. Traditionally, harmonics are often eliminated by cascading a filter at the backend [127]. However this increases the complexity and the volume of the RF front-end. In the integrated filtering antenna, harmonics can be significantly suppressed without resorting extra circuits. Figure 3.22 compares the frequency responses of a traditional U-slot patch, a SLR-fed patch without hairpin and the proposed filtering antenna. As can be observed, the traditional patch antenna has two obvious harmonics at 8.75 and 11.7 GHz, respectively. When the U-slot patch is fed by a SLR, the two harmonics are eliminated. This is attributed to the fact that the dual-mode SLR and the dual-band U-slot patch have the same fundamental resonant frequencies but different higher order harmonics. As a result, these two components are de-tuned at the high band and the higher order harmonics are suppressed.

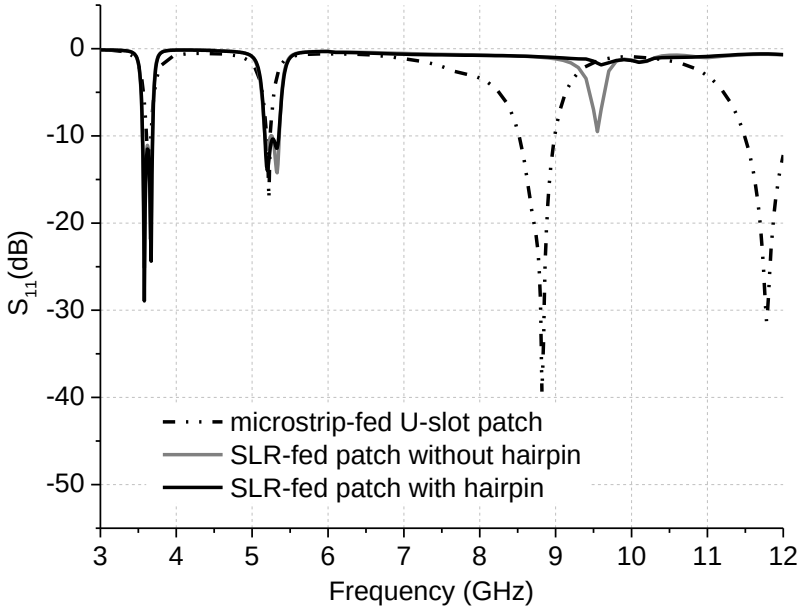

Figure 3.22 Frequency responses of a microstrip-fed U-slot patch, SLR-fed patch without hairpin and proposed filtering antenna over a wideband.

It should also be noted that the SLR itself also introduces an unwanted harmonic at 9.5 GHz. To eliminate this interference, a small hairpin resonator resonates at 9.5 GHz is shunted at the feed line, as presented in the proposed antenna. This hairpin resonator introduces a notch-band at 9.5 GHz to eliminate the interference. For the proposed antenna, excellent out-of-band rejection up to 12 GHz can be achieved. Compared with the traditional method in [133], the harmonics are suppressed without increasing the footprint of the antenna. Moreover, the frequency responses, including the bandwidth and the frequency selectivity, are improved.

3.4.4 Results and Discussion

The simulated and measured S_{11} of the proposed filtering antenna are presented in Figure 3.23. A broad frequency range from 3 to 12 GHz was tested to show the harmonic suppression performance. The measured result agrees very well with the simulation with dual operation bands from 3.5 to 3.65 GHz and 5.1 to 5.3 GHz achieved. The minor discrepancy between the simulation and the measurement is attributed to the fabrication errors. At the both bands, 2^{nd}-order filtering features with two reflection zeros are identifiable. This results in improved bandwidth and frequency selectivity performance. Out of the bands, the antenna exhibits wideband harmonic suppression up to 12 GHz.

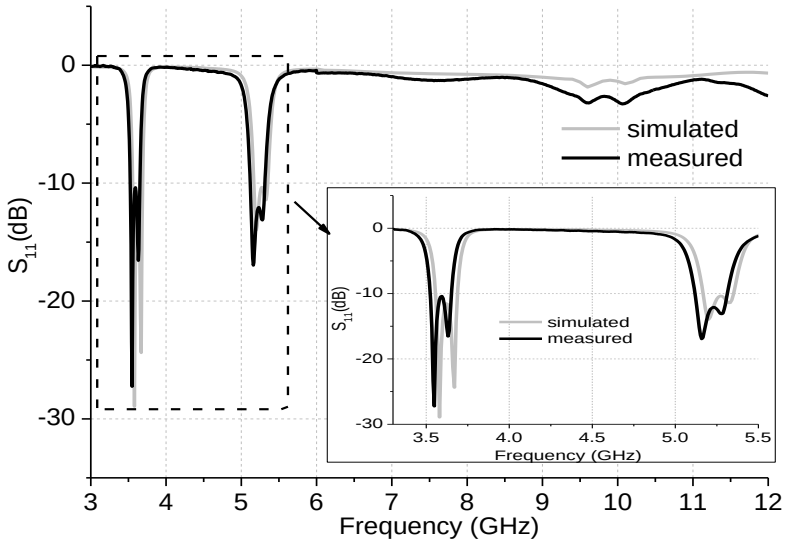

Figure 3.23 Simulated and measured S_{11} of the proposed dual-band filtering patch antenna.

Figure 3.24(a)-(b) shows the normalized simulated and measured co- and cross-polarization radiation patterns at 3.6 GHz in the E plane (XZ) and H plane (YZ), respectively. The antenna exhibits the radiation in broadside direction with a cross polarization discrimination (XPD) of -25 dB in both planes. The E and H plane radiation patterns at 5.2 GHz are presented in Figure 3.25. It is observed that the measured results agree well with simulations. Compared with the microstrip-fed U-slot microstrip antenna, the XPD of this antenna is improved, especially in the directions offset the broadside. The discrepancy between the simulated and measured patterns, especially the nulls in the backward radiation, is mainly attributed to the influence of the printed SLR which also contributes to the backward radiation.

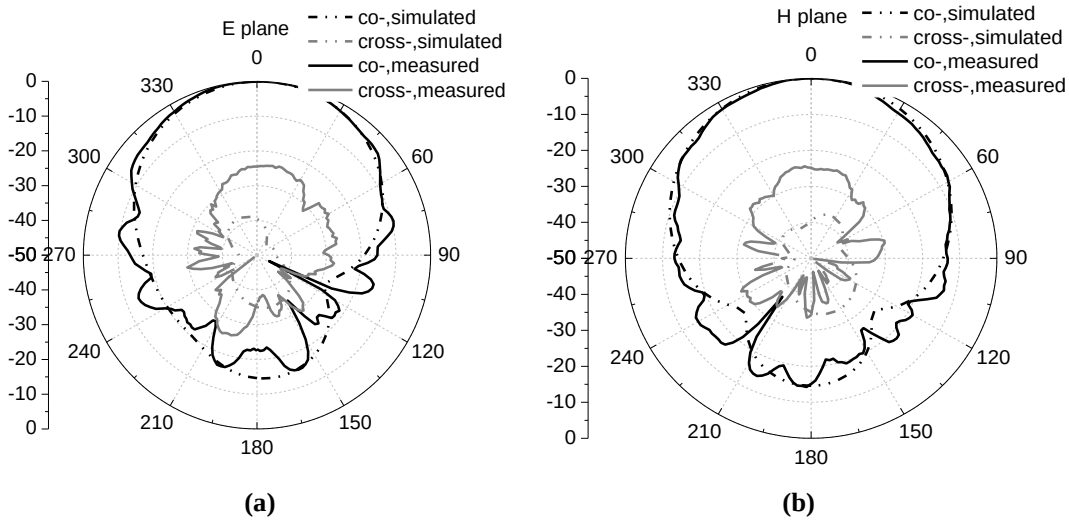

(a) **(b)**

Figure 3.24 Simulated and measured normalized radiation patterns at 3.6 GHz: (a) E plane, (b) H plane.

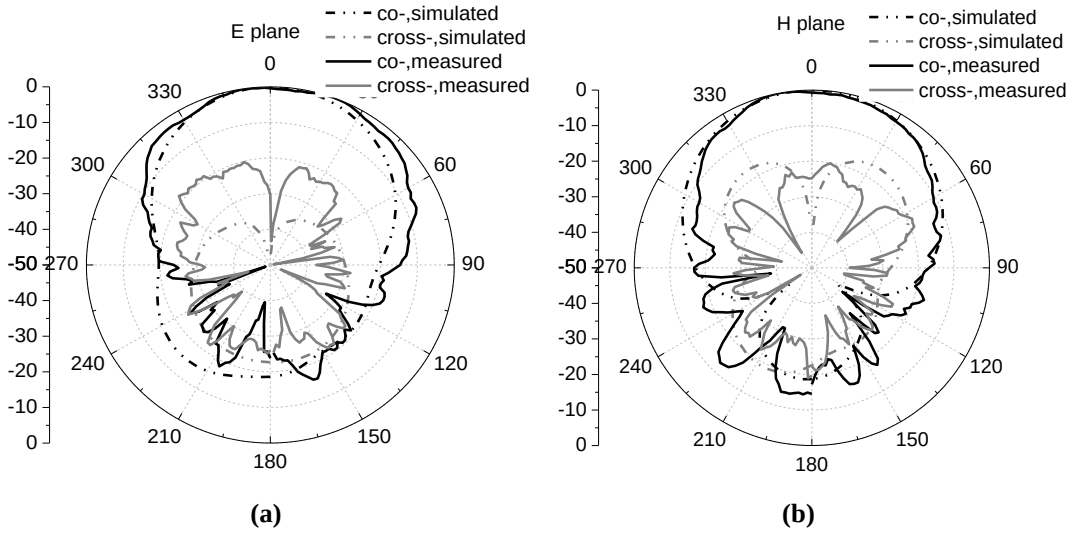

Figure 3.25 Simulated and measured normalized radiation patterns at 5.2 GHz: (a) E plane, (b) H plane.

Figure 3.26 shows the simulated and measured realized gains of the proposed dual-band filtering antenna in a broadband from 3 to 12 GHz. To demonstrate the advantages of the proposed antenna, the simulated gain of the standalone U-slot patch antenna is also included. The proposed antenna has the gains of 6.5 and 7 dBi at the low- and high-band, respectively. At the harmonics (8.5 and 11.7 GHz), the standalone U-slot patch antenna has a high gain of 7.5 dBi. In contrast, the gain drops significantly to below -7.5 dBi for the proposed filtering antenna. These results demonstrate that the proposed antenna has excellent frequency selectivity and out-of-band harmonic suppression over a wideband.

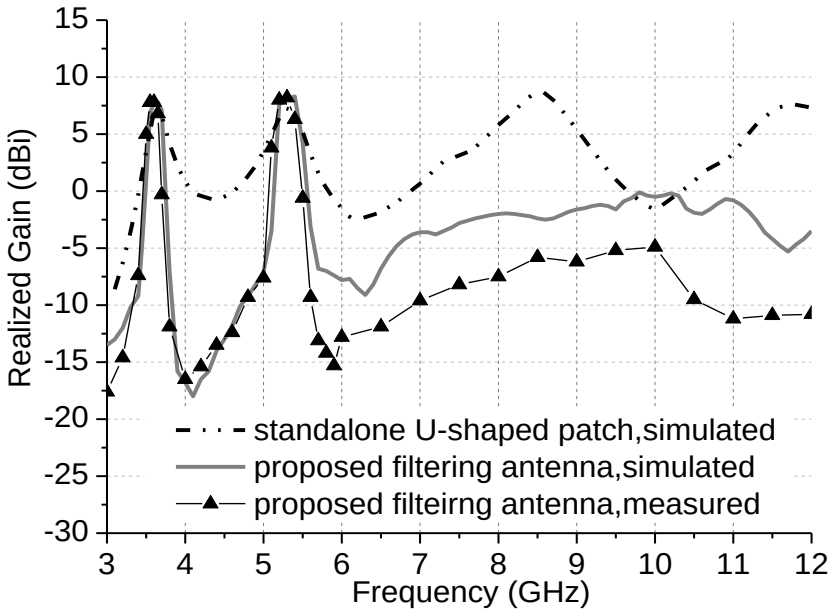

Figure 3.26 Simulated and measured gain of the proposed dual-band filtering antenna.

Table 3.6 compares the proposed dual-band filtering antenna with the other two reported dual-band filtering antennas in [133] and [134]. The comparison focuses on the harmonic suppression, polarization, gain and XPD at the two bands. The comparison shows that the proposed antenna has the improved gain and XPD at the two operation bands. The works in [133] and [134] did not investigate the harmonic and the gains are relatively lower. In addition, the work in [133] has the different polarizations at the two operation bands.

Table 3.6 Comparison with Other Dual-Band Patch Antennas

Types of antennas	Harmonics suppression	Polarization at two bands	Gain (dBi) (f_L/f_H)	XPD (dB) (f_L/f_H)
Ref. [133]	No	different	-1.8/1.1	-10/-22
Ref. [134]	No	consistent	-4.0/3.8	NA
This work	Yes	consistent	7.5/8.0	-40/-30

3.5 Summary

In this chapter, several filtering antennas with different functions are proposed. In the first design, a broadband filtering antenna is realized by using a multi-mode resonator to feed a patch. Then, the harmonic suppression function is investigated by detuning the resonators and the patches at the high-band. Finally, a novel dual-band filtering antenna with improved bandwidth and broadband harmonic suppression is presented. By these studies, we can observe the frequency responses of the filtering antennas are significantly improved as compared with traditional antennas. These improvements are beneficial to wireless communication systems.

Chapter 4. Integrated Microstrip Filtering Array Antennas

4.1 Introduction

In many wireless communication applications, such as satellite communications and mobile communication at base-stations, an antenna with high gain is always required. Microstrip array antenna, due to its merits of low profile, light weight and low cost, has been widely used in wireless systems. To achieve a large array antenna, power dividing networks are usually required to maintain a given magnitude and phase for each element. Besides, the quarter wavelength transmission lines and matching stubs are needed to realize the impedance matching. On the other hand, owing to the resonant characteristics and relatively high Q-values of microstrip antennas, they have the major drawback of narrow bandwidth. To enhance the bandwidth, techniques such as adding air gaps, increasing the thickness of the substrates are usually used at the expense of increased thickness and complexity [135]-[136].

For some applications, the array antenna with dual-band or multi-band capacities is highly demanded. Dual-band operations could effectively increase the versatility of the systems. In multifunction radar/spaceborne satellite applications, different frequency operations are also required to share the same aperture to reduce the cost and weight of the RF frontend. In general, high frequency operation provides images with higher resolution, whereas low frequency can penetrate bulky obstacles, giving some information relating to properties of targets. However, when antenna array works at different frequency bands, large and complicated feeding networks will be incurred. In traditional, dual-band operations of an antenna can be implemented by using two single-band elements or using one dual-band element. Employment of two single-band elements is always regarded more flexible for designing the dual-band antennas with high frequency ratios. In [137]-[141], perforated patches are used to design the dual-band arrays while sharing the same aperture. In [142]-[146], the radiating elements with different resonant frequencies are interlaced for dual-band operations. One of the challenges in these array designs is the congestion of the feeding networks since each band and each polarization is usually excited separately. This would be more challenging as the frequency ratio decreases (much smaller than 2). To date, very few works have been reported dealing with the dual-band dual-polarized (DBDP) array with low frequency ratio.

Polarization diversity is also very desirable in wireless communication or radar applications as it could enhance the information content as well as combat the multi-path fading [147]. To maintain a good performance, the isolation between the two polarizations should be high enough. Normally, the dual-polarization character is realized by exciting the two orthogonal modes of the antenna. This, however, brings about some serious problems in the designing. One of the challenges is that the number of the feeding networks are doubled when the antenna works at dual polarizations. Therefore, it is very challenging to accommodating the feeding networks of a dual-polarized antenna array, especially for the dual-band or multi-band array antenna.

To overcome these problems while maintaining a compact front-end, the methods of designing the filtering antennas in Chapter 3 are employed in this chapter to design the integrated filtering array antennas. The integration of filters, power dividers, antennas and other passive components provides a promising solution to solve these challenges. By the virtue of the resonant nature, the radiating elements can serve as the last resonators of the power dividing/filtering networks. Thus, the antennas can contribute to the poles of the filter and therefore the bandwidth and frequency selectivity. In [83], a microstrip filtering antenna array was proposed by using coupled resonators to design the feeding network. In this chapter, three array antennas with integrated filtering performance are explored. These works respectively exhibits the advantages of the filtering antenna arrays over the traditional array antennas.

4.2 Microstrip Filtering Antenna Array with Improved Selectivity and Harmonics Suppression

Usually, in traditional wireless communication systems, filters are cascaded with antennas for eliminating the unwanted interferences, which however leads to a complicated and bulky system. In this section, we will explore a method to integrate the passive components such as filters, power dividers and radiating elements. Here, a novel 2 × 2 antenna array using an all-resonator network is proposed. The filters and power dividing networks in traditional RF frontends are replaced by a group of coupled resonators. The array of patches serve not only as the radiating elements but also the last resonator of the filter. A resonator-based four-way out-of-phase power divider is designed to couple with a patch array. In this way, the bandwidth, frequency selectivity and harmonics suppression are significantly improved. The harmonics of the integrated design are suppressed by the use of three types of resonators with different harmonics characteristics, which will be detailed later.

4.2.1 Topology and Synthesis

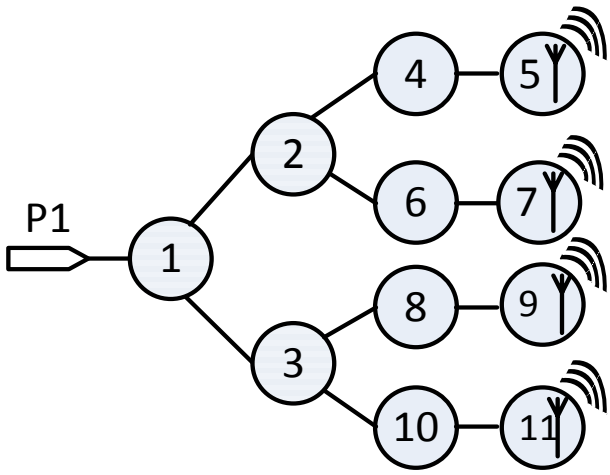

Figure 4.1 The topology of coupled resonators for the fourth-order filtering array proposed in this paper.

The multiple functions - filtering, power division and radiation - are integrated into a single network of coupled resonators. It is essentially a four-way all-resonator based topology as proposed and shown in Figure 4.1. The circles represent resonators or resonant antenna elements, whereas the lines between them represent the coupling. It should be noted that the resonators 5, 7, 9 and 11 work as resonators and radiators simultaneously. The resonators 1, 2 and 3 act as the power distribution elements, which are traditionally realized by transmission-line T-junctions. Such a network has the fourth-order filtering characteristics. A single coupling matrix *M* can be used to represent the topology in Figure 4.1. Due to its high symmetry, such a matrix can be directly synthesized. Basically, the coupling coefficients *mij* of the multi-port network can be related to those of a fourth-order two-port Chebyshev filter, as denoted by *m'ij*, using the following equations,

$$m_{12} = m'_{12} \Big/ \sqrt{2},\ m_{24} = m'_{24} \Big/ \sqrt{2},\ m_{45} = m'_{45},\ m_{13} = m_{12},$$
$$m_{24} = m_{26} = m_{38} = m_{3,10},\ m_{45} = m_{67} = m_{89} = m_{10,11}. \qquad \text{(Eq.4.1)}$$

The specifications in this design are given as follows: Centre frequency f_0 = 2.39 GHz, bandwidth BW = 130 MHz, return loss RL = 10 dB, and order N = 4. The coupling coefficients and external quality factors can be derived as Q_{ex} = 29.9, $m_{12} = m_{13}$ = 0.0275, $m_{24} = m_{26} = m_{38} = m_{3,10}$ = 0.0230, $m_{45} = m_{67} = m_{89} = m_{10,11}$ = 0.0389. $m_{i,j}$ is the coupling coefficient between the resonator *i* and *j*. All resonators are synchronously tuned, i.e. $m_{i,i}$ = 0. It should be noted that no source-load coupling is considered in the synthesis. Figure 4.2 shows the theoretical frequency response corresponding to the coupling matrix.

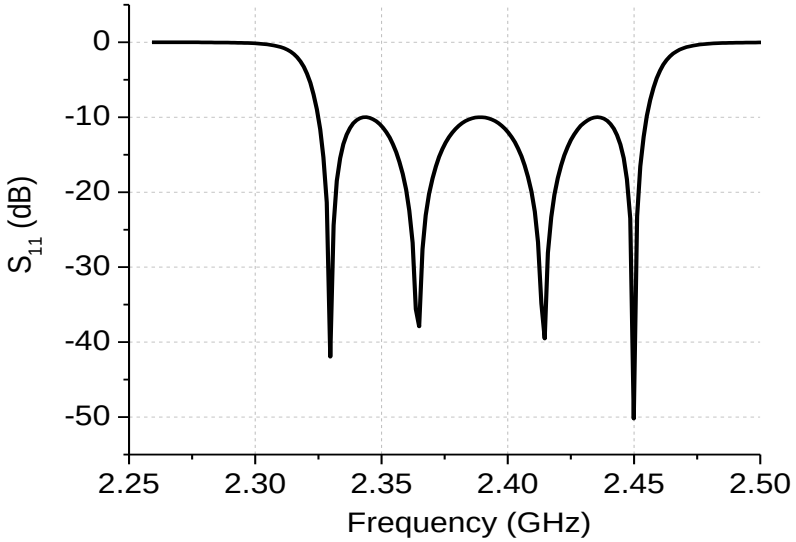

Figure 4.2 Theoretical S-parameters of the proposed topology corresponding to the synthesized coupling matrix.

4.2.2 Implementation Approaches

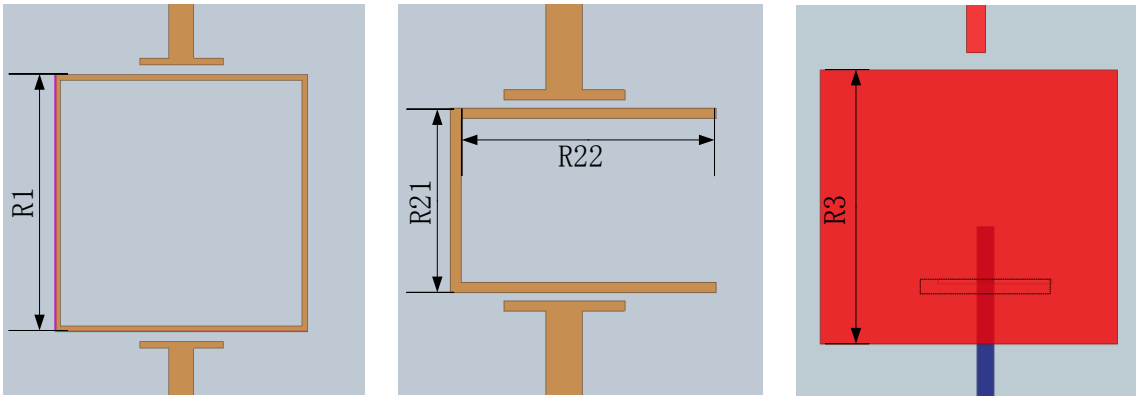

(a) **(b)** **(c)**

Figure 4.3 Configurations of three types of resonators with weak coupling to the input and output ports: (a) ring strip resonator, (b) hairpin resonator and (c) square patch resonator. R1 = 23.6 mm, R21 = 12 mm, R22 = 17.5 mm, R3 = 31.5 mm.

To implement the topology in Figure 4.1, microstrip resonators are employed here. In order to serve as the power dividing devices, the resonator 1, 2 and 3 are required to be symmetrical in geometry. In this work, the ring strip resonators are chosen due to their compactness and high Q-value, as shown in Figure 4.3(a). The total length of the resonator is about a wavelength at the resonant frequency. As for resonator 4, 6, 8 and 10, hairpin resonators, as shown in Figure 4.3(b), are adopted to couple power from the ring strip resonator and to feed the antenna again. The hairpin is a half-wavelength resonator. Resonators 5, 7,

9 and 11 are square patches, as shown in Figure 4.3(c). They not only act as the radiating elements but also the last resonators of the filtering network. Therefore, they contribute to one pole in the frequency response. The length of the square patch is approximate a half of a guided wavelength. It is worth mentioning that the patch antenna is treated as a two-port component as a first-order approximation to illustrate its resonance and harmonic performance. The different structures and therefore different resonant characteristics of the three types of resonators have the added benefit of having distinct harmonic frequencies. As shown in Figure 4.4, when the fundamental modes of the resonators are tuned to the same frequency at 2.4 GHz, their second-order harmonics vary widely with each other. This property has been used to suppress the harmonics in the higher band.

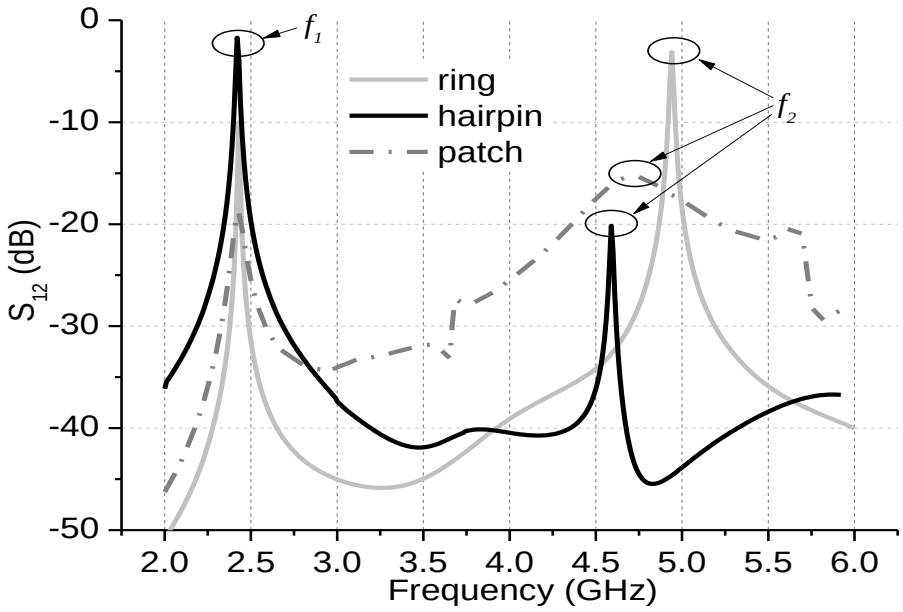

Figure 4.4 Simulated $|S_{21}|$ of the three resonators in Figure 4.3.

The couplings between the resonators are evaluated through simulations. The coupling strength between the two ring resonators and between the ring resonator and hairpin resonator can be adjusted by changing the spaces (S_1, S_2) between them. The coupling between the hairpin and the patch can be realized through a slot in the ground and the coupling strength is controlled by tuning the length and width of the slot. All the coupling coefficients are extracted using (1) [147],

$$M_{ij} = \frac{f_j^2 - f_i^2}{f_j^2 + f_i^2} \qquad \text{(Eq.4.2)}$$

where f_i and f_j are the resonant frequencies from the two coupled resonators. Using full-wave simulation, f_i and f_j can be obtained and coupling coefficients can be calculated.

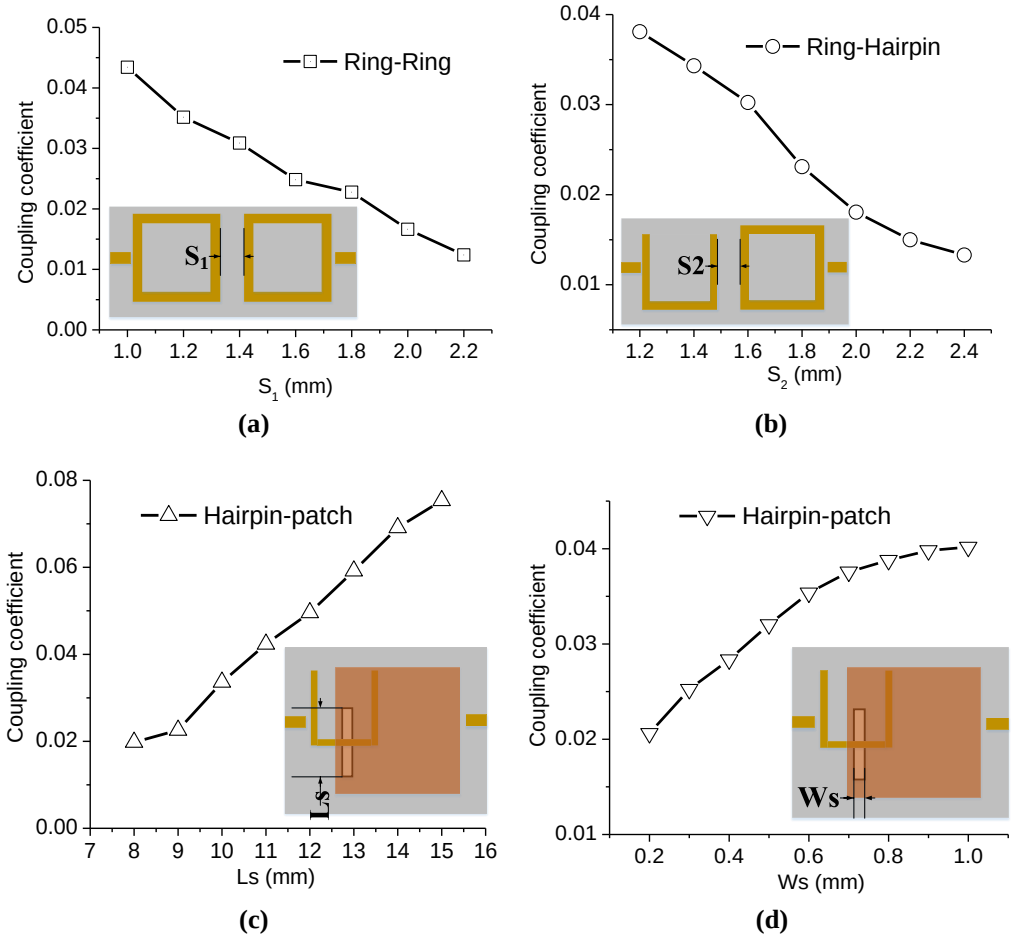

Figure 4.5 Coupling coefficients between resonators: (a) two ring strip resonators with S_1 (b) ring strip resonator and hairpin resonator with S_2, (c) hairpin resonator and the patch resonator with length of slot Ls and (d) hairpin resonator and the patch resonator with width of slot Ws.

Figure 4.5 shows the coupling coefficients between the resonators as a function of geometry parameters. During these simulations, the couplings to the input and output ports are kept weak so as to ensure the revealed coupling characteristics are from the two interacting resonators. Figure 4.5(a) shows the coupling between two ring strip resonators and Figure 4.5(b) shows the coupling between the ring strip and the hairpin resonator. As for the coupling between hairpin resonator and patch resonator, which are located on different circuit layers, the coupling is realized by slitting a slot in the ground plane. By increasing the length or the width of the slot, the coupling coefficient increases, as presented in Figure 4.5(c) and (d). To realize the required coupling coefficients, the initial values of the parameters have been found to be S_1 = 1.5 mm, S_2 = 1.6 mm, L_S = 11 mm and W_S = 0.8 mm.

4.2.3 Resonator-Based Out-of-Phase Power Divider

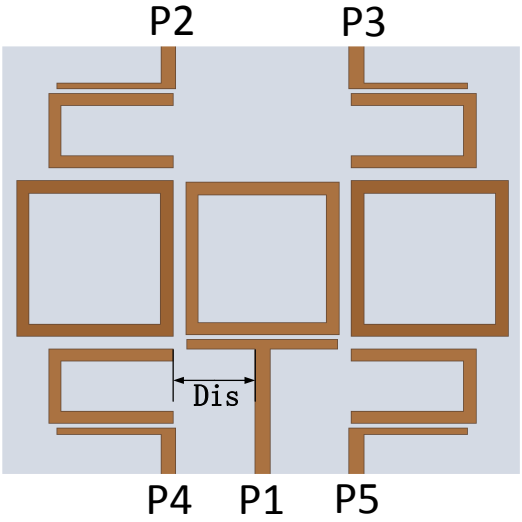

Figure 4.6 Configuration of the proposed four-way third-order power divider

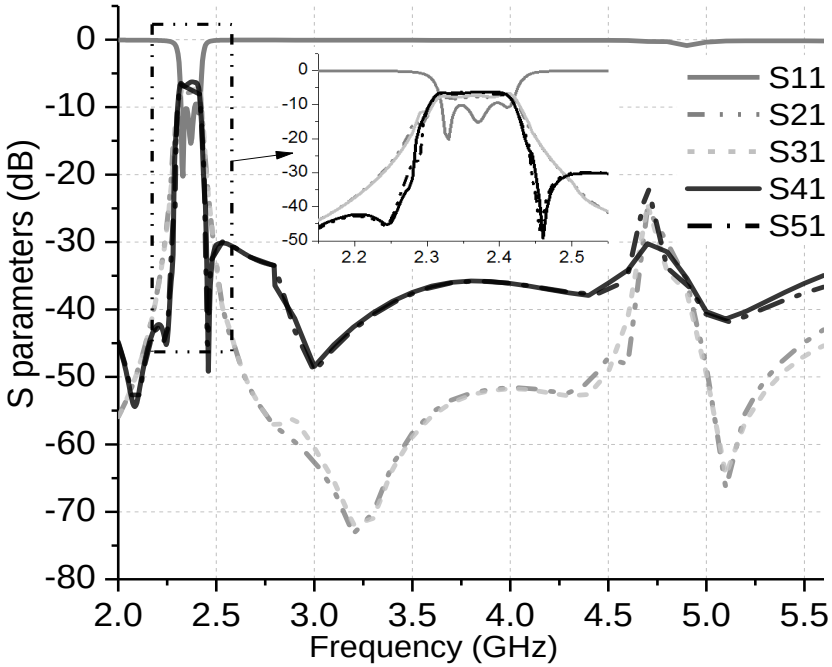

Figure 4.7 Simulated S-parameters of the proposed resonator-based four-way power divider.

By utilizing the resonators in the Figure 4.3 and their resonant characteristics, a resonator-based power divider with integrated filtering function is conceived, as shown in Figure 4.6. The power divider has the 3rd-order filtering responses. The power fed from the center ring strip resonator is divided and coupled to the other two ring resonators at both sides. This is then coupled to the hairpin resonator. The S-parameter in Figure 4.7(a) shows the S-parameters of the power divider. As can be seen, a filtering performance with three poles in the band is produced. These poles are introduced by the coupled resonators. At the harmonic

frequencies (4.5 to 5 GHz), due to the different second-order harmonics among the three types of resonators, the filtering divider is detuned. As a result, the harmonics at the high-band are suppressed.

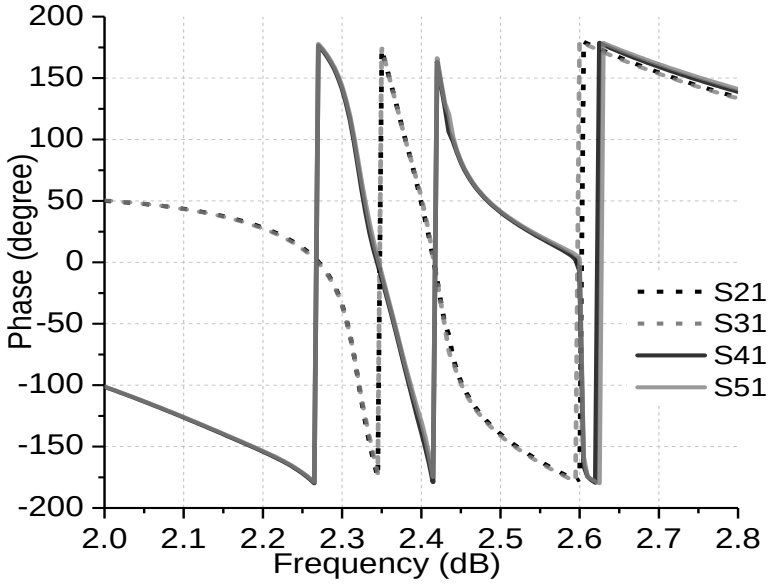

Figure 4.8 Simulated phase response of the resonator-based four-way power divider.

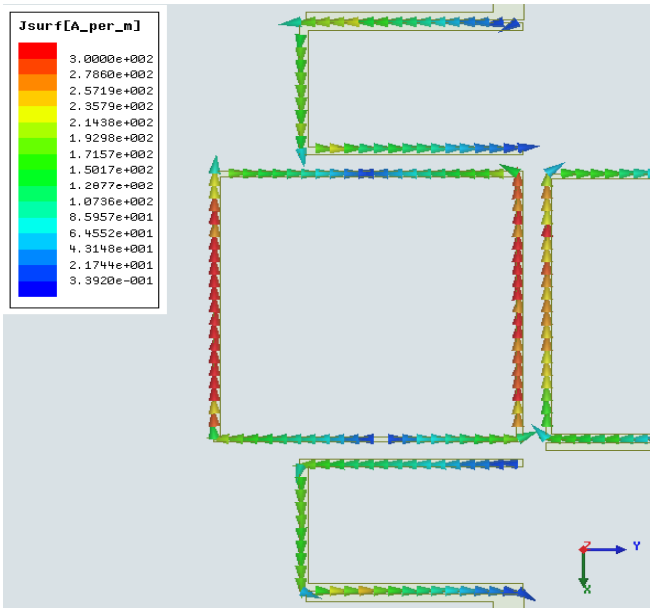

Figure 4.9 Simulated current distribution at 2.4 GHz.

Figure 4.8 shows the phase responses of the power divider. Due to the symmetrical configuration, the port 2 and 3 have consistent phase responses, so do the port 4 and 5. However, when we compare the port 2 and 4, or port 3 and 5, a 180º phase difference can be observed. This can be visualized in the current density distribution at 2.4 GHz as presented in Figure 4.9. The current reverses at the two coupling locations with the hairpin

resonators. The electrical length between the two locations is about half of a wavelength, which causes the 180º phase difference. The out-of-phase output not only makes the design more compact, but also improves the cross polarization discrimination [149].

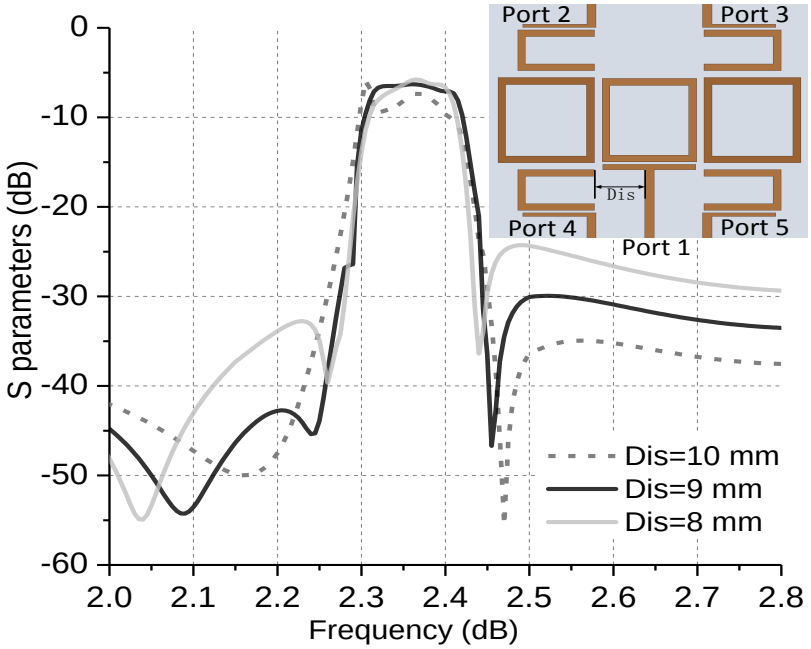

Figure 4.10 Simulated |S41| (|S51|) with different *Dis*.

It is worth noting that the |S41| (|S51|) response in Figure 4.7 is quite different from that of the |S21| (|S31|) response out of the band. As for |S41| (|S51|), three transmission zeros at 2.1, 2.25 and 2.45 GHz are visible, with the first two located at the lower band and the third one located at the higher band. These transmission zeros can be attributed to the source-load coupling between the port 1 and Port 4 (5) which are on the same side of the circuit and in proximity, as well as the cross coupling between the non-adjacent ring and the hairpin. These couplings were not considered in the synthesis of the coupling matrix. However, the resultant transmission zeros significantly improve the frequency selectivity of the filtering divider. Parameter studies have been performed to investigate the relationship between the couplings and the transmission zeros. As shown in Figure 4.10, the coupling between the source (Port-1) and load (Port-4 and 5) is varied by tuning the distance *Dis* between the hairpin and the feedline at Port-1. This should also affect the cross coupling between the non-adjacent ring and the hairpin. When *Dis* is over 10 mm, only one transmission zero is observable at the lower band and the other at the higher band. When *Dis* decreases, two transmission zeros appear at the lower band, whereas the third one shifts closer to the pass-band. This mechanism of creating and controlling the transmission zero can be used to design filter-antennas with further improved frequency selectivity without increasing the order of the filters.

4.2.4 Filtering Antenna Array Implementation

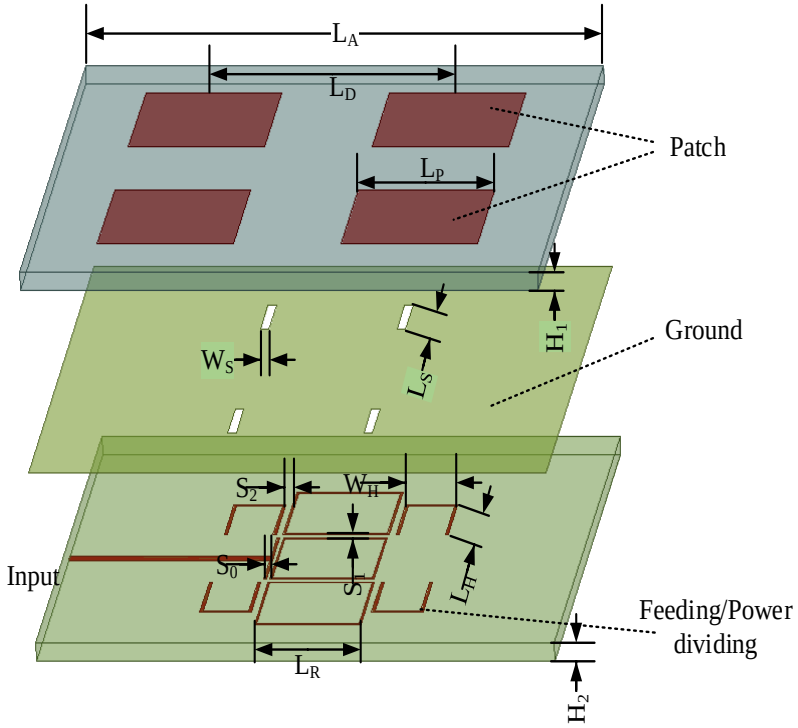

Figure 4.11 Configuration of the proposed 2 × 2 filtering antenna array. L_A = 120 mm, L_P = 31.5 mm, L_D = 60 mm, Ls= 11.6 mm, W_S = 0.9 mm, L_R = 24.6 mm, L_H = 16.7 mm, W_H =12 mm, S_0 = 0.25 mm, S_1 = 1.7 mm, S_2 = 1.6 mm, H_1 = 1.525 mm, H_2 = 0.787 mm.

Based on the topology in Figure 4.1 and studies of the filtering power dividing network, an antenna array with integrated filtering characteristics is achieved by replacing the outputs of the third-order filtering power divider with the radiating patches. Figure 4.11 shows the configuration of the proposed 2 × 2 filtering antenna array. The radiating patches are printed on the top layer of the upper substrate (Rogers 4003 with a dielectric constant of 3.55). The filtering power dividing network is printed on the bottom layer of the lower substrate (Rogers 5880 with a dielectric constant of 2.2). The power dividing network and the patches share a common ground plane in the middle layer. The patches on the top layer act as the last resonators and coupled to the hairpin resonators through the slots in the ground plane. The space between the patches L_D is 60 mm, i.e. 0.48 λ at the center frequency of 2.4 GHz. It should be noted that in this all-resonator based design the traditionally separated filter and the interfaces between the filter and antenna are eliminated, which results in a compact and highly integrated structure. The design and simulation were performed using High Frequency Simulation Software (HFSS 15), and the optimized parameters are given in the caption of Figure 4.11.

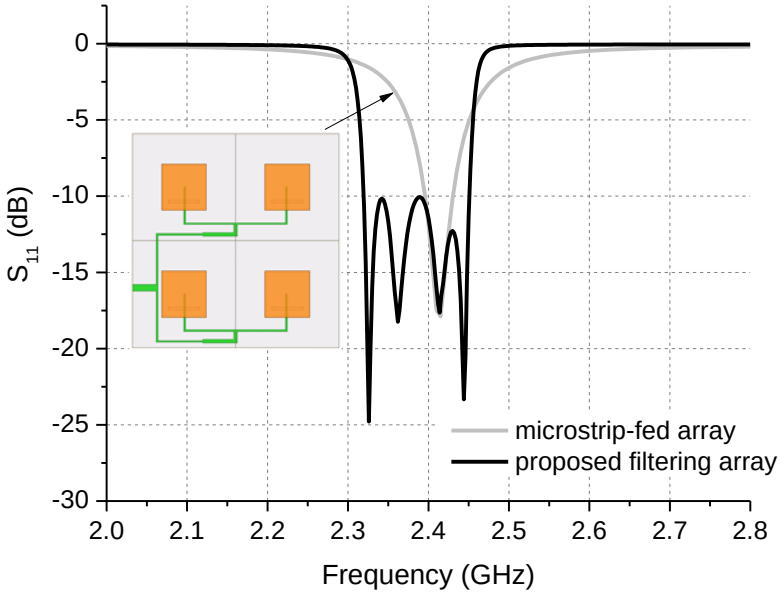

Figure 4.12 Comparison of the simulated $|S_{11}|$ between the proposed filtering antenna array and an antenna array with the traditional feed.

Figure 4.12 compares the simulated S-parameters of the proposed filtering antenna array with a microstrip array with a traditional feed. For the traditional array, the patches are fed by a microstrip-line power divider through the slots. The other parameters of the two patch array are kept identical. It can be seen from Figure 4.12 that the integrated antenna array has four clearly visible reflection zeros at 2.33, 2.36, 2.41 and 2.45 GHz, demonstrating the expected fourth-order filtering characteristics. A -10 dB impedance bandwidth of 5.6% is obtained. In contrast, only one resonant mode can be observed for the traditional patch array and the fractional bandwidth is only 1.6%. Thus, the integrated design approach in this work could significantly improve the bandwidth of the microstrip array antenna. The other apparent improvement of this work is that the frequency selectivity of the proposed antenna is largely enhanced due to the high-order resonant features of the feeding networks. To better quantify the frequency selectivity, the ratio of the -10 dB bandwidth (BW_{-10dB}) and the -3 dB bandwidth (BW_{-3dB}) is evaluated to be 30% and 87% respectively for the traditional antenna array and the integrated antenna array.

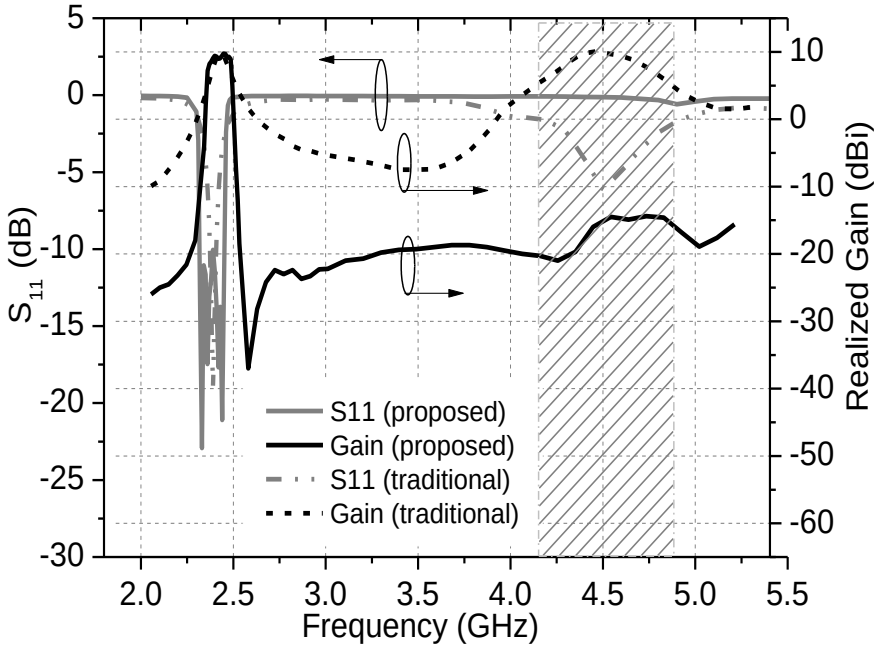

Figure 4.13 Simulated $|S_{11}|$ and antenna gains of the filtering antenna array in comparison with a traditional patch array over a broadband.

The other important issue is the high-order harmonics, which could deteriorate the quality of the wireless communication system. Higher order harmonics are commonly distributed in microstrip antenna, which are usually suppressed by cascading a filter. In this work, due to the integration of the three types of resonators with different harmonics, the harmonics could be suppressed effectively without integrating the extra bandpass filters. Figure 4.13 shows the simulated S_{11} and realized gains of the proposed filtering antenna array and a traditional patch antenna array over a broadband. For the traditional antenna, due to influence of the second order harmonics, a spurious band occurs at around 4.5 GHz with a S11 of -6.2 dB. This spurious band leads to a high antenna gain of 10 dBi at around 4.5 GHz. The proposed antenna array, however, the harmonic is almost eliminated with the return loss of below 0.7 dB. The gain of the proposed filtering array is reduced to below 15 dBi at the harmonic band. In the operation band, the traditional array has a peak gain of 9.9 dBi and which slowly decreases when the frequency offsets the center frequency 2.4 GHz. In contrast, the integrated array antenna has a flat gain of 9.7 dBi in the working frequency band. It then drops rapidly to below -20 dBi when the frequency moves to below 2.24 GHz or above 2.53 GHz.

Table 4.1 summaries the parameter comparison with the traditional antenna in terms of the resonant poles, bandwidth, frequency selectivity, harmonic level and gain in band as well as gain at the harmonic.

Table 4.1 Parameter Comparison with a Traditional Array Antenna

Antenna Type	Traditional Array	Proposed Array
Number of Resonant Poles	1	4
Fractional Bandwidth	1.60%	5.60%
Frequency Selectivity (BW_{-10dB}/BW_{-3dB})	30%	87%
Harmonic Level ($\|S_{11}\|$)	-6 dB	-0.7 dB
Gain (In band)	9.9 dBi	9.7 dBi
Gain (Harmonic)	10.1 dBi	-15 dBi

4.2.5 Results and Discussion

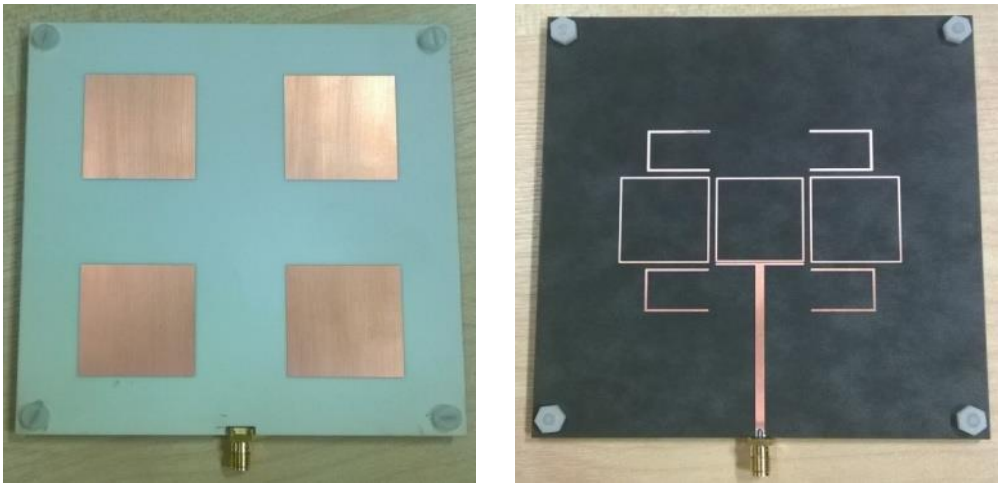

(a) **(b)**

Figure 4.14 Photograph of the 2×2 filtering antenna array: (a) front view, (b) back view.

Figure 4.14 shows the front and back views of the proposed 2 × 2 filtering antenna array prototype. The antenna is measured using a ZVL vector network analyzer and the results are shown in Figure 4.15. For comparison, the simulated, measured and the theoretical S-parameters are presented. As can be seen, the measured result agrees very well with the simulated and theoretical results with an impedance bandwidth from 2.31 GHz to 2.46 GHz achieved. There is an unexpected dip between 2.2 and 2.3 GHz, which may be caused by the cables and connectors used in the measurement.

Figure 4.16 shows the normalized simulated and measured co- and cross-polarization radiation patterns of the filtering antenna array in E and H plane, respectively. The patterns exhibit the expected radiation performance with maximum antenna gain in the broadside direction. The cross polarization discrimination (XPD) in the E and H plane are better than -36 dB and -28 dB, respectively, which is attributed to the slot coupling and the out-of-phase power divider.

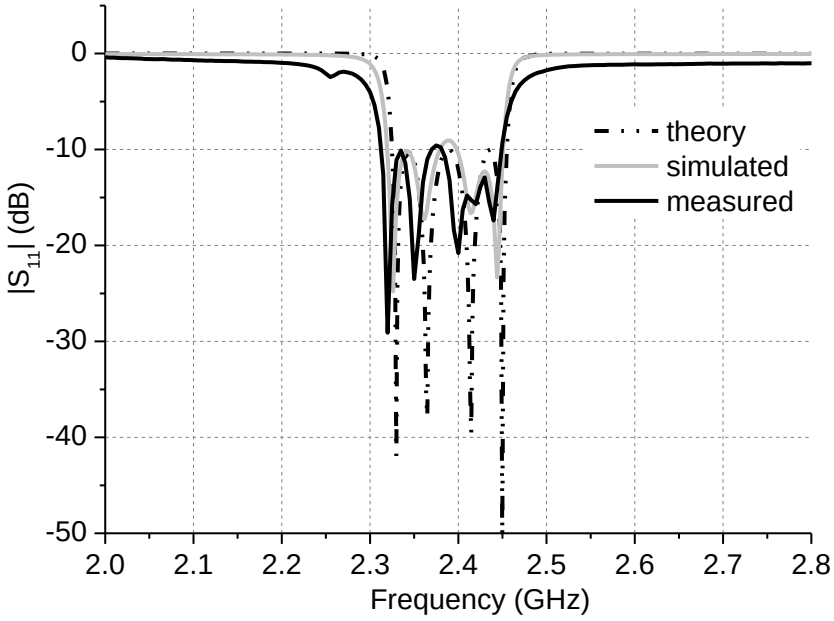

Figure 4.15 Theoretical, simulated and measured $|S_{11}|$ of the filtering antenna array.

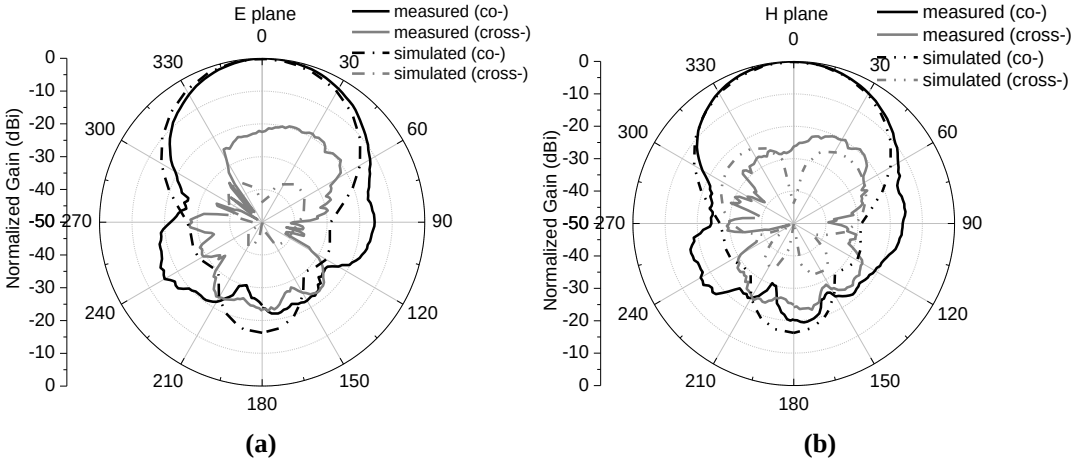

Figure 4.16 Normalized measured co- and cross-polarization radiation patterns at 2.4 GHz: (a) E plane, (b) H plane.

Figure 4.17 presents the measured and simulated realized antenna gains of the proposed filtering antenna array over a wide frequency range from 2 to 5.4 GHz. The simulated gain of the traditional antenna array is also included for comparison. It is observed that the simulated and measured results agree well with each other. The filtering antenna array has a flat gain response of 9 dBi from 2.30 to 2.45 GHz. For the measured gain, there are two nulls at the both sides of the operation band, resulting in a rapid drop of the gain out of the band. The gain reduces to -25 dBi below 2.24 GHz and above 2.53 GHz. These nulls are attributed to the source-load coupling and the cross coupling as discussed in Section III-C, which could significantly improve the frequency selectivity of the array antenna.

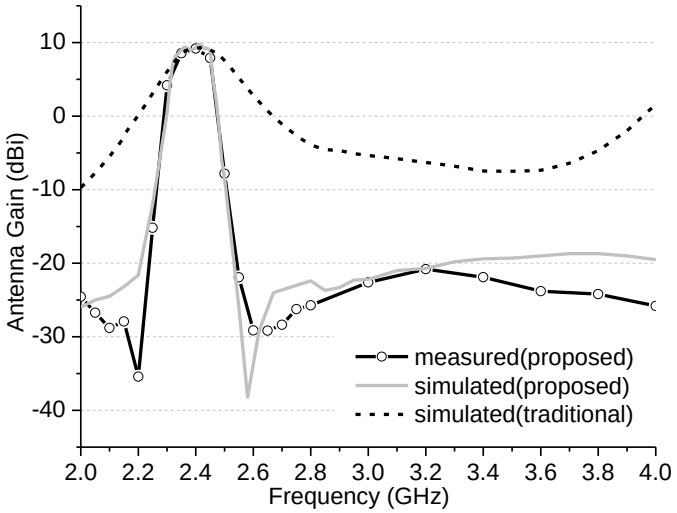

Figure 4.17 Measured gain of the filtering antenna array as a function of frequency.

One of the other obvious features is that the antenna gains at the high-band are significantly reduced by 22 dB as compared with the traditional patch antenna. This verifies the capability of harmonic suppression of the integrated design. There are some small discrepancies between the simulated and the measured gain curves especially outside the operation band. This is due to the reduced measurement sensitivity at these rejection bands where the power level is very low. For the traditional antenna array, the gain decreases slowly when the frequency deviates from the center frequency. The comparison of the gains between the two antenna arrays demonstrates that the integrated filtering antenna array has a much improved performance of frequency selectivity and harmonic suppression.

Table 4.2 Comparison with other Filteirng Antennas

Antennas	[83]	[45]	This work
Order of filtering	3rd	2nd	4th
Antenna Size	1.06 λ×1.06 λ	0.86 λ×1.16 λ	0.96 λ×0.96 λ
In-band Gain	9.6 dBi	6.1 dBi	9.7 dBi
Gain at Harmonic	-	-5 dBi	-15 dBi

Table 4.2 compares the filtering antenna in this paper with the other reported filtering array in the literature [83] and [45]. The comparison mainly focuses on order of the filtering, antenna size, in-band gain and gain at the harmonic. This comparison shows that this work exhibits a better filtering performance with the 4th filtering features than that in [83] and an improved harmonic suppression than that in [45]. These enhancements are attributed to the mixed use of different types of resonators and the out-of-phase divider.

4.3 Dual-Polarized Filtering Array Antenna with Improved Bandwidth and Selectivity

In many wireless applications, such as radars and satellite communications, the microstrip antennas with dual-polarization and high-gain characteristics are usually desired. The other issues to be concerned are impedance bandwidth of the antenna and the capability of combating interferences. Broadband features can be realized by adopting stacked parasitic patches with a large air gap between them [150]-[153]. In this section, the method of designing broadband filtering antenna in Chapter 3.2 is developed to achieve a dual-polarized microstrip antenna array with a low profile and improved bandwidth. Due to the seamless integration of filter and antenna is employed, the antenna array also exhibits a good filtering performance.

4.3.1 Dual-Polarized Antenna Element

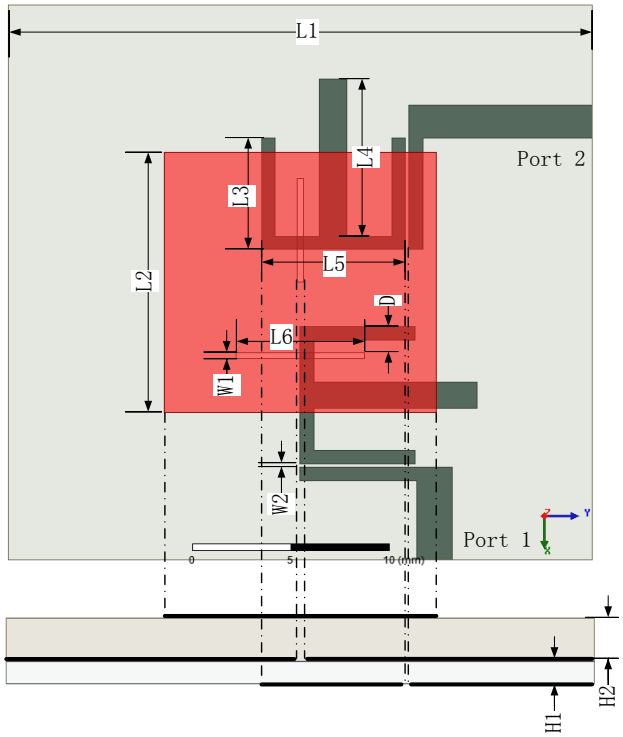

Figure 4.18 Configuration of proposed dual-polarized microstrip antenna element. *L1* = 30 mm, *L2* = 14 mm, *L3* = 5.9 mm, *L4* = 8.4 mm, *L5* = 7.4 mm, *L6* = 6.8 mm, *W1* = 0.3 mm, *W2* = 0.2 mm, *D* = 1.4 mm, *H1* = 0.813 mm, *H2* = 1.525 mm.

Figure 4.18 shows the configuration of the proposed integrated dual-polarized microstrip antenna element. The antenna has two substrates, which are stacked together. The square patch is printed on the top layer of the upper substrate, which is fed by two group of

stub loaded resonator (SLR) in the bottom layer through the slot lines in the ground. RO4003C substrate is used in the designing. The thicknesses of the lower and upper boards are 0.813 mm and 1.525 mm, respectively. The two slots in the ground plane are placed perpendicular to each other to reduce the coupling between the two polarizations. Different from the traditional aperture coupled microstrip antenna, the patch in this work is coupled and fed by a resonator. The SLR is perpendicular relative to the slot so as to achieve a strong magnetic coupling between them. To realize a broad impedance bandwidth, the odd- and even-mode of the SLR are placed at both sides of the resonant frequency of the patch. The study and methods of controlling the dimension of the SLR were presented in Chapter 3.2. The simulations are performed using HFSS v15 and the optimized parameters are presented in the caption of Figure 4.18.

4.3.2 Implementation approaches

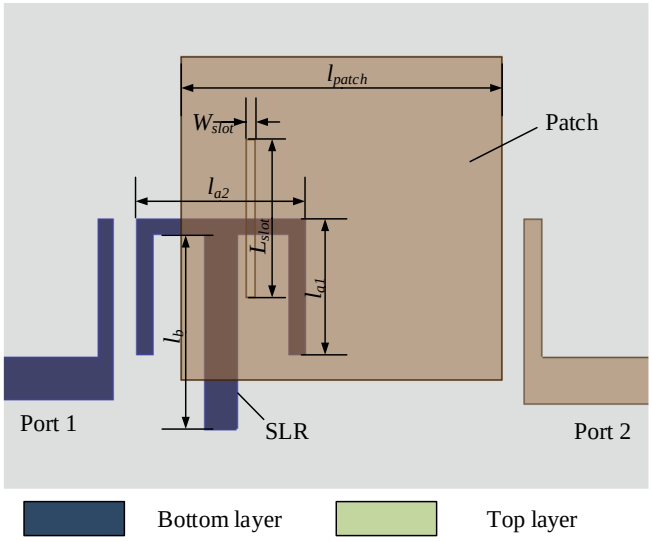

Figure 4.19 Configuration of a two-port component with a SLR and a patch at different layers.

In order to illustrate the mechanism, a two-port component with a SLR and a patch at different layers is investigated to study the resonant characteristics of each polarization of the antenna, as shown in Figure 4.19. The SLR is printed on the bottom layer of the lower substrate and the patch is printed on the top layer of the upper substrate. A slot is etched in the ground plane to enable the coupling between them. It should be noted that, weak coupling is conceived between them so as to examine the resonant characteristics of the component. By adjusting the dimensions and the coupling between the SLR and patch, a pass-band with three resonances can be obtained, forming a broad impedance bandwidth, as

shown in Figure 4.20. The odd- and even-mode resonant frequencies f_1 and f_2 of the SLR are situated at both sides of the patch's resonant frequency f_0 at the center. As can be seen, the f_0 increases to higher band when L_{patch} decreases from 15.6 mm to 15.2 mm.

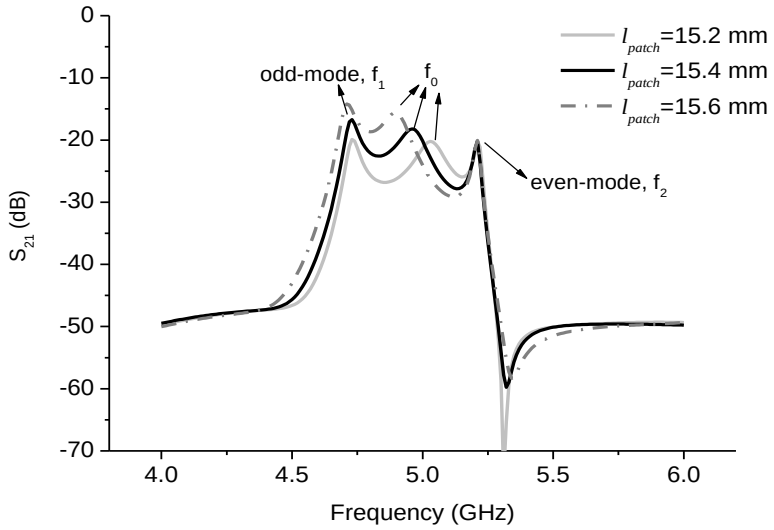

Figure 4.20 Simulated S21 of the two-port component with different l_{patch}.

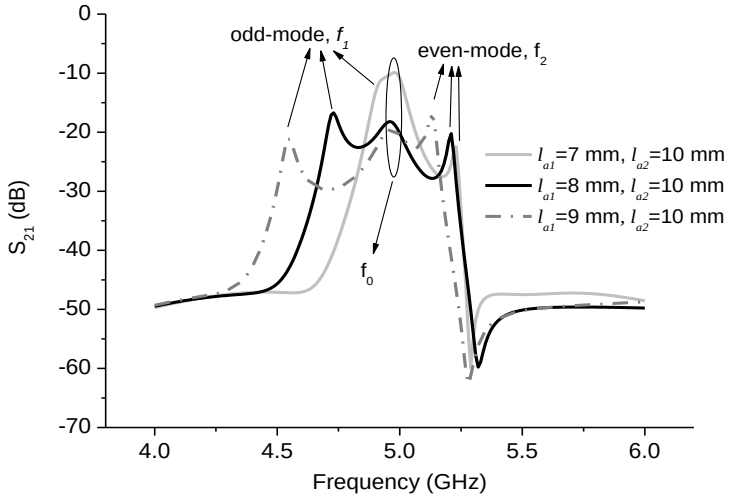

Figure 4.21 Simulated S21 of the two-port component with different l_{a1}.

Figure 4.21 shows the simulated S21 of the two-port component with different l_{a1}. As can be seen, the length of l_{a1} has an influence on the first and the third modes of the component, and the first one is much significant than the third one. Figure 4.22 shows the resonant modes vary with the l_b. In contrast, the third resonant frequency moves to lower band when l_b increases, whereas the other two resonant frequencies keep unchanged. Therefore, the

operation frequency band of the antenna can be controlled intentionally by adjusting the dimensions of the patch and SLR.

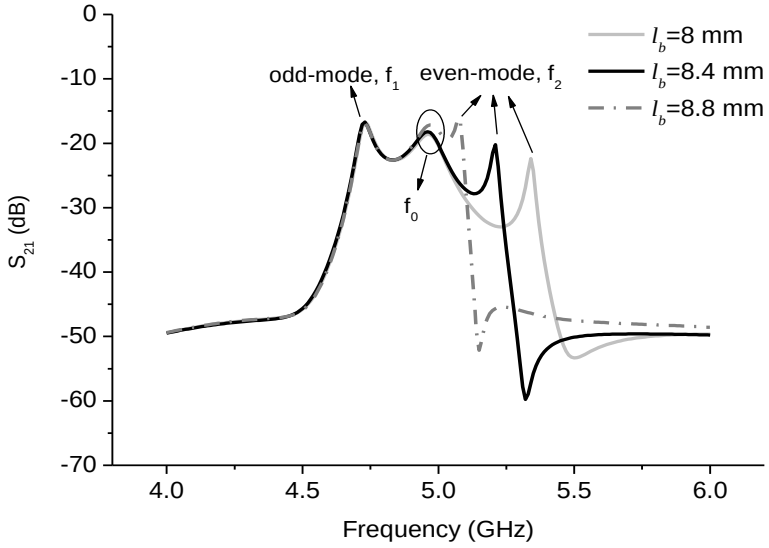

Figure 4.22 Simulated S21 of the two-port component with different l_b.

4.3.3 Dual-Polarized Filtering Array Antenna

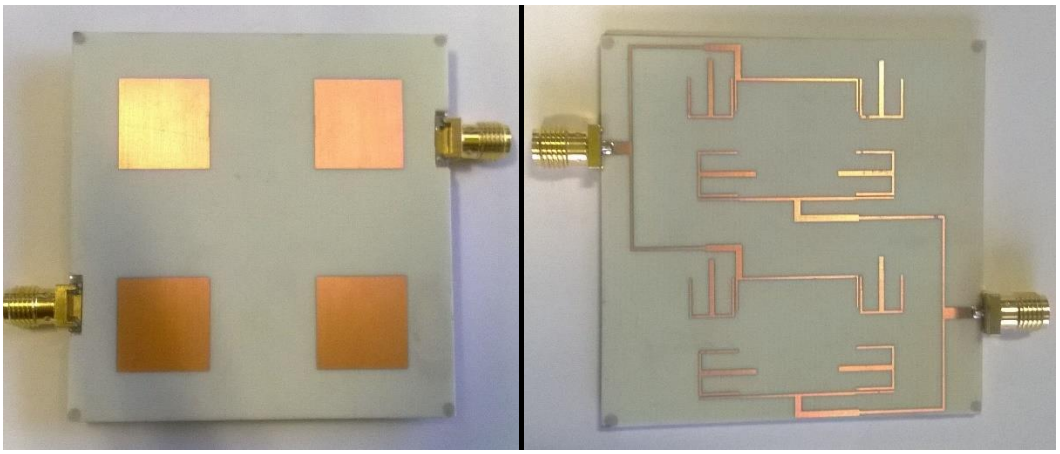

(a) **(b)**

Figure 4.23 Prototype of the 2 × 2 dual-polarized SLR-fed array: (a) top layer, (b) bottom layer.

The antenna element in Figure 4.18 can be extended to form a dual-polarized filtering array, as shown in Figure 4.23. The spacing between the elements is set as 30 mm (0.53 λ_0). For one polarization, a four-way in-phase T-shaped power divider is used to feed the four SLR. For the other polarization, an out-of-phase T-shaped power divider is utilized. The 180^o phase difference is achieved by extending one branch of transmission lines by half of

a guided wavelength (i.e. 17.8 mm). The out-of-phase power divider here is used to improve the cross polarization discrimination (XPD).

To illustrate the merits of the proposed filtering array antenna over the traditional patch antenna arrays and the cascaded filter and patch antenna, the S-parameters of these antennas are compared and discussed. Figure 4.24 shows the configuration of a traditional cascaded filter-antenna, which includes a bandpass filter and a traditional patch array. The bandpass filter and the patch array are designed independently and then cascaded with the 50 Ω interface. The bandpass filter is composed of the dual-mode SLR. The four-element patch array is directly fed by a T-shape four-way power divider via coupling slots.

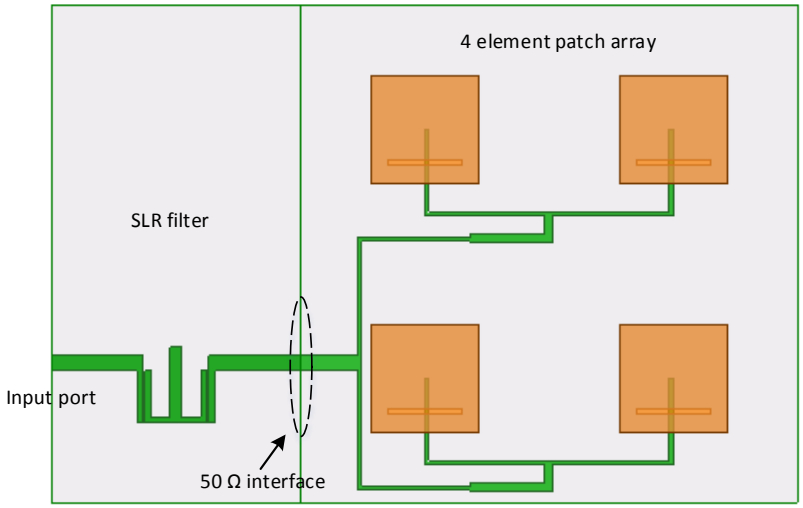

Figure 4.24 Configuration of the conventional cascaded filter and antenna.

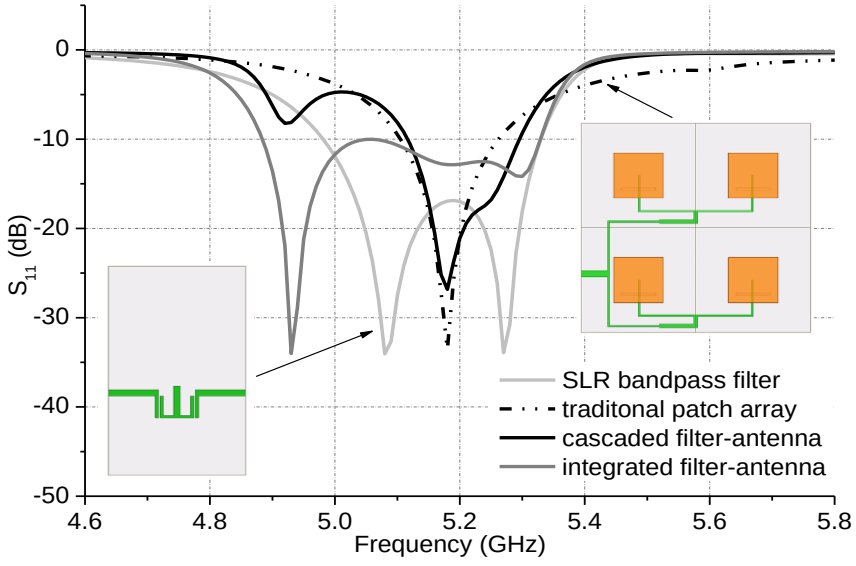

Figure 4.25 Comparison of the S-parameters among the antennas.

Figure 4.25 compares the impedance bandwidths of the SLR filter, the standalone patch array, the cascaded filter-antenna and the proposed integrated filter-antenna. As can be seen, the traditional patch array has a narrow -10 dB bandwidth of about 150 MHz, due to the narrowband nature of the patch. The standalone SLR filter can achieve a bandwidth of 350 MHz with the 2nd-order characteristics. For the traditional cascaded filter-antenna, the bandwidth is mainly limited by the narrowband component which is the patch array in the design. The Figure 4.25 shows that a bandwidth of only 170 MHz could be achieved for the cascaded filter-antenna, which is much narrower than the proposed integrated filter-antenna. Using the proposed design methods, the bandwidth of the patch antenna is enhanced to 470 MHz without changing the thickness of the antenna. On the other hand, as can be observe in the figure, the non-uniform bandwidths between the patch array and the filter leads to an unexpected performance degradation at around 4.95 GHz due to the multiple reflections. Thanks to the integrated design methods used in this work, not only the size of filter-antenna subsystem is reduced but also the bandwidth and frequency selectivity are significantly improved. The integrated filter-antenna also shows the rapid transition at both edges of the operation band and excellent out-of-band rejection.

4.3.4 Results and Discussion

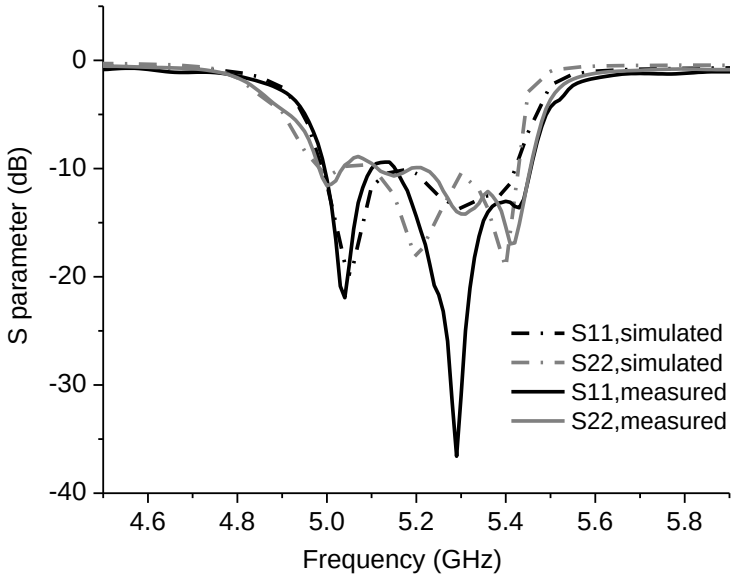

Figure 4.26 Simulated and measured S-parameters of the proposed filtering microstrip array.

The simulated and measured S-parameters of the 2 × 2 filtering array are presented in Figure 4.26. The measured results agree well with the simulations, showing a broadband performance from 4.96 GHz to 5.48 GHz (FBW = 10%).Three reflection zeros located at 5,

5.25 and 5.45 GHz can be identified in S11 and S22. The antenna also exhibits the excellent frequency selectivity and out-of-band rejection performance from Figure 4.26. The small difference between the simulation and measurement is attributed to the fabrication sensitivity. Figure 4.27 shows the simulated and measured isolation between the two ports. A very good isolation of over 32 dB is achieved between the two ports/polarizations.

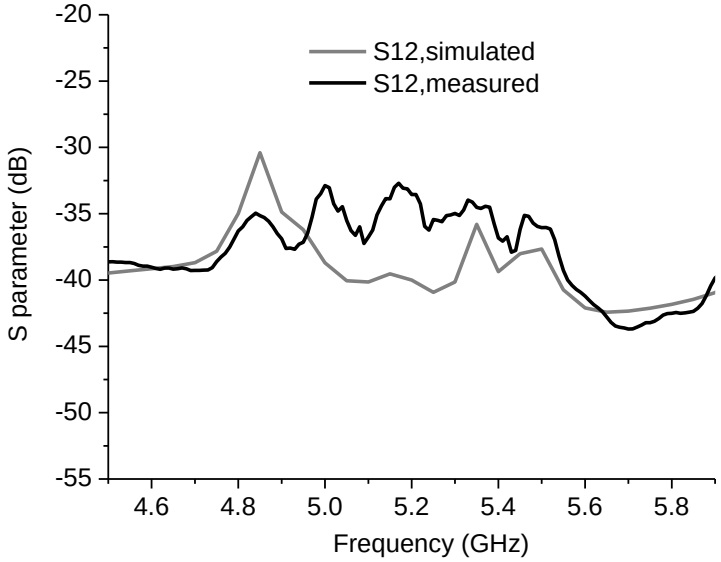

Figure 4.27 Simulated and measured isolation between the two ports.

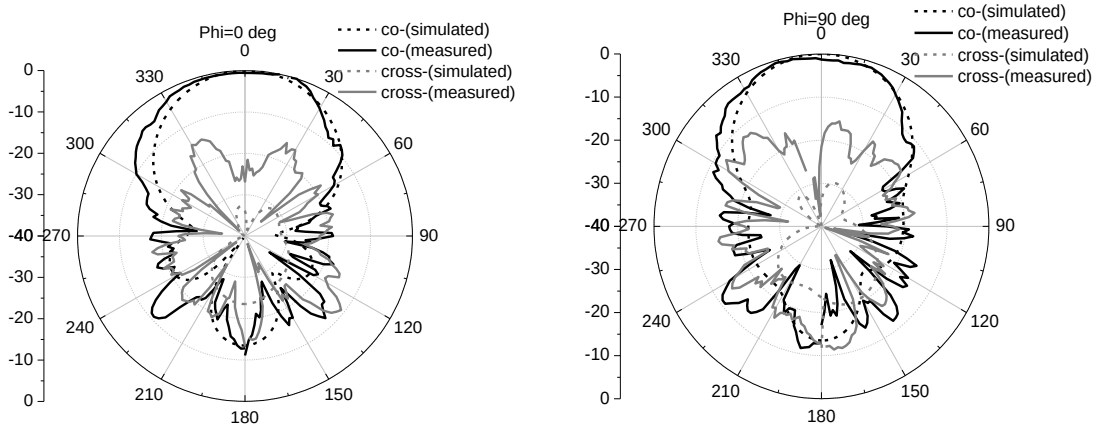

(a) **(b)**

Figure 4.28 Normalized simulated and measured co- and cross-polarization radiation patterns at 5.2 GHz when port 1 is excited: (a) $\varphi = 0^0$, (b) $\varphi = 90^0$.

Figure 4.28 shows the normalized simulated and measured co- and cross-polarization radiation patterns of the array at 5.2 GHz. During the measurement, port 1 is excited and the port 2 is terminated with a 50 Ω load. It is observed that the simulated and measured results

agree well with each other, exhibiting the maximum radiation in the broadside direction. The cross polarization discrimination is over 20 dB in XOZ plane (φ =0°) and YOZ plane (φ =90°).

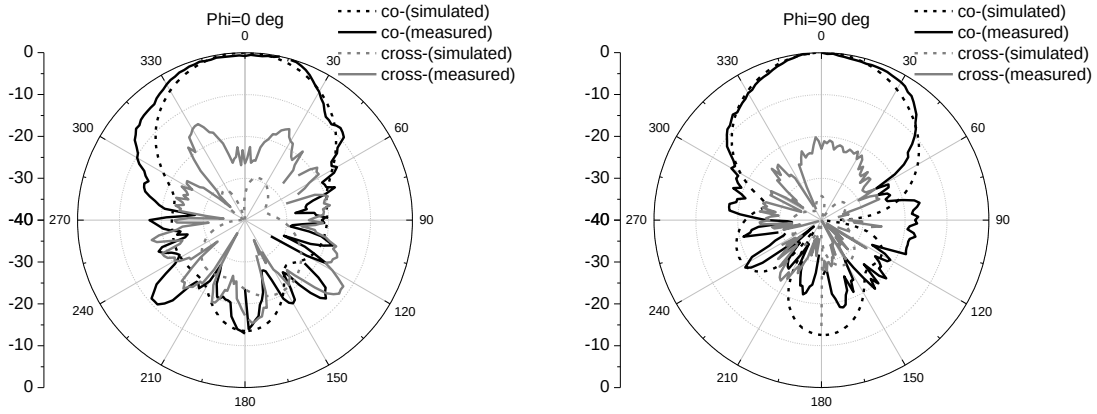

(a) **(b)**

Figure 4.29 Normalized simulated and measured co- and cross-polarization radiation patterns at 5.2 GHz when port 2 is excited: (a) φ = 0⁰, (b) φ = 90⁰.

Figure 4.29 shows the simulated and measured normalized radiation patterns of the array at 5.2 GHz when port 2 is excited and the port 1 is terminated with a 50 Ω load. In both φ = 0° and φ = 90° planes, the antenna exhibits a similarly radiation patterns as port 1. The cross polarization discrimination is over 22 dB in both orthogonal planes. It is worth mentioning that the discrepancy of the backward radiation patterns is caused by the blockage of the test instruments.

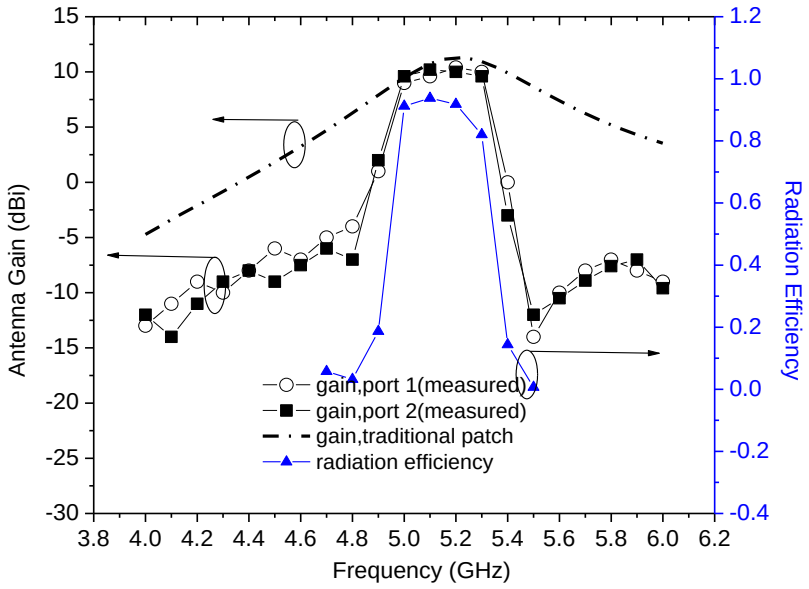

Figure 4.30 Measured antenna gains and radiation efficiency of the proposed antenna array.

The antenna gains of the array antenna are measured when two ports are excited independently. Figure 4.30 shows the measured gains with comparison with the gain characteristics of a traditional patch array. It is observed that the gain of the traditional patch array slowly reduces as the frequency deviates from the center frequency. In contrast, the proposed antenna array has a flat antenna gain of about 10.5 dBi from 4.9 to 5.3 GHz, but which dramatically drop to below -7 dBi at 4.6 and 5.7 GHz, exhibiting the much improved frequency selectivity and out-of-band rejection performances. The radiation efficiency is around 80% in the operating band. Out of the band, the efficiency drops sharply to 10% or below.

4.4 Dual-Band Dual-Polarized Filtering Array Antenna with Shared Aperture

The dual-band dual-polarized (DBDP) antenna has been intensively adopted in multi-functional radars and satellite communications. It is known that polarization diversity is desirable for enhancing the information content and combating the multi-path fading, whereas the dual-band operations could increase the versatility of the systems. Moreover, to reduce the cost and weight of the RF frontend, the antennas working at different bands are usually required to share a same aperture. Traditionally, DBDP antennas with shared apertures are implemented by employing the perforated layouts or the interlaced layouts. Both configurations are suitable for designing the DBDP array antennas with a high frequency ratio. However, as the frequency ratio decreases (much less than 2), it is very challenging to accommodate the multiple feeding networks of the array antenna at different bands and polarizations. To the best of the authors' knowledge, very few works have been reported focusing on the DBDP array with low frequency ratio.

To overcome the problems in designing an array antenna with a low frequency ratio, a novel highly integrated approach is proposed in this section by employing the highly integrated filtering antenna design methods. In [100], a method of using a multi-mode resonator as a feed of a patch antenna is further developed to achieve the DBDP antenna with a low frequency ratio. Using this method, not only the RF frontend is simplified but also the frequency responses of the antenna can be improved. In this work, two nested patches are coupled and tuned with a dual-mode stub-loaded resonator (SLR), generating two operation bands with 2^{nd}-order filtering characteristics simultaneously. The bandwidths as well as the out-of-band rejection performance can be improved. As a proof-of-concept, a 2 × 2 array is

conceived, prototyped and measured. Such an array antenna can be extended to a massive array or used as the feed of a reflector antenna.

4.4.1 Configuration and Topology

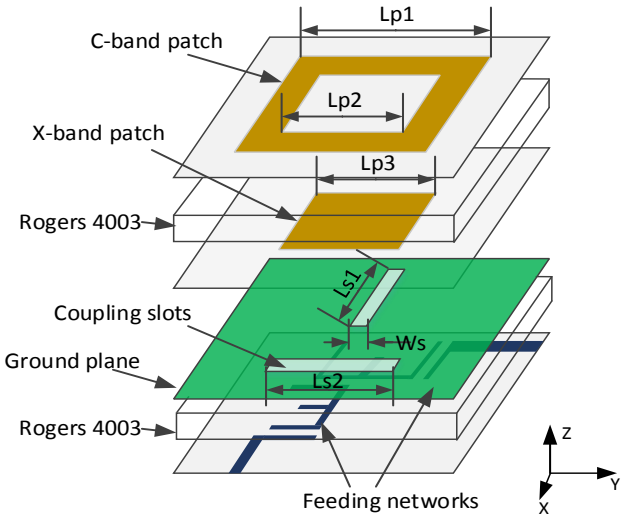

(a)

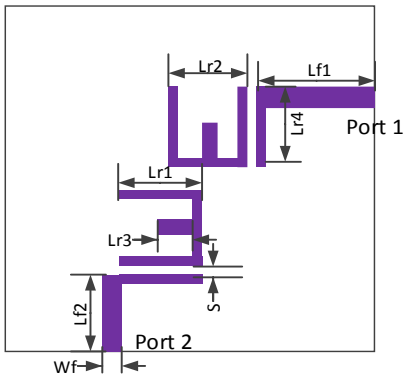

(b)

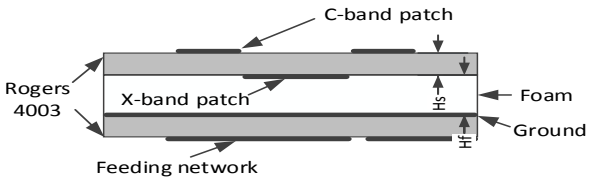

(c)

Figure 4.31 Configuration of the proposed DBDP element: (a) exploded view, (b) bottom view, (c) side view.

Figure 4.31 shows the configuration of the proposed DBDP antenna element, which is composed of two stacked substrates and a foam layer between them. The low and high band radiating elements are printed on the top- and bottom-layer of the upper substrate, respectively. As shown in Figure 4.31(a), the low-band antenna is a perforated patch with the

perforation large enough for allowing the radiation of the high band square patch. The length of the square patch is approximately a half-wavelength of the high frequency band operation, whereas the perimeter of the perforated patch is about one wavelength at the low-band center frequency. The two patches are nested and each polarization of the two patches are simultaneously fed by a folded SLR through a slot. To improve the isolations while reducing the cross polarization level, the two coupling slots for the two orthogonal polarizations are placed perpendicularly with each other.

Figure 4.31(b) shows the configuration of the feeding networks printed on the bottom layer of the lower substrate. Because of its flexibility in controlling the antenna resonant frequencies, the dual-mode SLR is used here so that it can be tuned with the two patches. The two resonant modes of the SLR can be derived using the odd- and even-mode method. Because the two bands of each polarization are fed using a single SLR, the number of the feeding networks as well as the input ports can be reduced by a half. The stacked configuration of the antenna is shown in Figure 4.31(c). Rohacell 51HF foam with a thickness of 2 mm is inserted between the two substrates as a spacer to improve the antenna impedance matching and bandwidths. RT/Duriod 4003C substrate with a relatively dielectric constant of 3.55 and loss tangent of 0.0027 is used in the design. High Frequency Simulation Software (HFSS 15) is employed to perform the simulations and the optimized parameters are listed in Table 4.3.

Table 4.3 Parameters of the Proposed Antenna (mm)

Lp1	*Lp2*	*Lp3*	*Lp4*	*Ls1*	*Ls2*	*Ws*	*Lf1*	*Lf2*
14.5	9	7.8	3	7.2	10	0.5	11.8	8.4
Wf	*Lr1*	*Lr2*	*Lr3*	*Lr4*	*S*	*Hs*	*Hf*	
1.8	5.5	6	2	5.5	0.3	0.813	2	

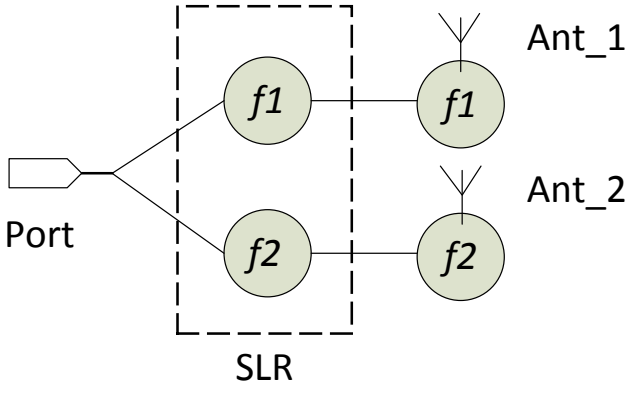

Figure 4.32 Equivalent resonator-based topology of the proposed dual-band filtering antenna at each polarization.

The proposed dual-band element for each polarization can be represented and synthesized using a coupled resonator-based topology, as shown in Figure 4.32. The two patches can be regarded as two single-mode resonators or a dual-mode resonator with corresponding resonant frequencies of f_1 and f_2, respectively. The odd- and even-mode of the SLR are also tuned to resonate at f_1 and f_2. Then the SLR and the two patches are electromagnetically coupled, two separate passbands with 2nd-order filtering response are produced. The two passbands of each polarization are excited simultaneously. The lines between the resonators in the topology represent the coupling between the resonators. As an example to implement a DBDP antenna with low frequency ratio (less than 2), the specifications of the dual-band antenna are given as follows,

Low band: f_1 = 5.2 GHz, BW = 200 MHz

High band: f_2 = 10 GHz, BW = 500 MHz

The coupling coefficients and the external quality factors can be derived,

Low band: $m_{1,2}$ = 0.031, Q_{ext} = 45.1

High band: $m_{1,2}$ = 0.051, Q_{ext} = 27.2

where $m_{i,j}$ is the coupling coefficient between the resonator i and j.

4.4.2 Design Methodology

In this integrated design, the two patches can be fed by the SLR through electromagnetic coupling only if the two patches are tuned with the dual modes of the SLR, respectively. Figure 4.33 shows the simulated tangential magnetic-field distribution of an unfolded SLR corresponding to the odd- and even-mode resonance. As can be observed in Figure 4.33(a), the SLR has the strongest magnetic-field distribution at its central part (denoted as point A) when the odd-mode is excited (low-band operation). It is noted that the dashed rectangle indicates the location of the coupling slot where the power is transferred to the patches through a coupling. When the even-mode is excited (high-band operation), there are two magnetic-field maxima, as the point B and C indicated in Figure 4.33(b). On the contrary, point A becomes the minima. By positioning the slot between A and C, the electromagnetic energy can be coupled to the two patches simultaneously.

The coupling strengths at the two operation bands can be tuned by adjusting the relative coupling positions (d) and the dimension of the coupling slot. According to experimental studies, the approximate equations for evaluating coupling strengths can be derived,

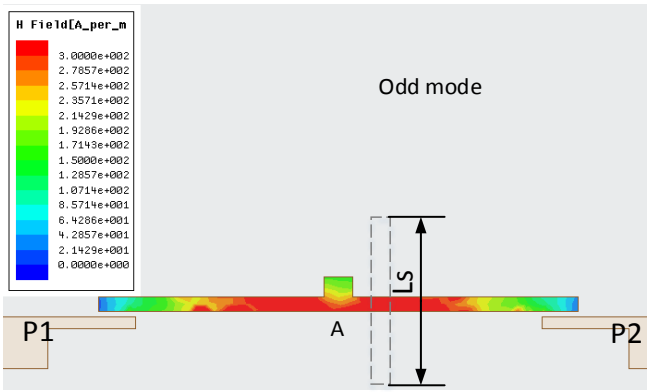

(a)

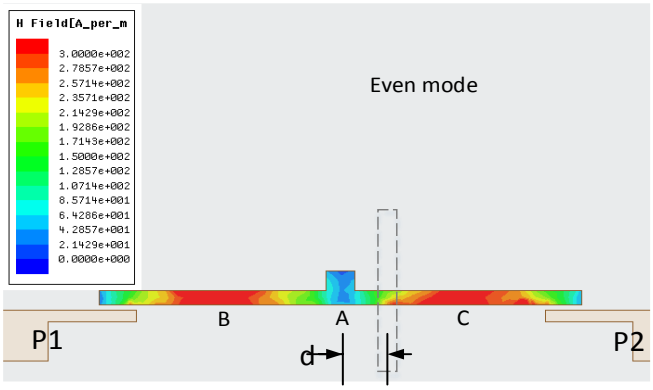

(b)

Figure 4.33 Tangential magnetic-field distribution on the surface of an unfolded SLR: (a) the odd-mode resonance at 5.2 GHz and (b) the even-mode resonance at 10 GHz.

$$M_{f1} \approx \frac{A_1 \cdot Ls \cdot Ws}{d} \qquad \text{(Eq.4.3)}$$

$$M_{f2} \approx A_2 \cdot Ls \cdot Ws \cdot d, \qquad A < d < C, \qquad \text{(Eq.4.4)}$$

where, M_{f1} and M_{f2} are the mutual couplings between the SLR and the patch at f_1 and f_2; Ls is the length of the coupling slot; Ws is the width of the coupling slot; d is coupling position, which is situated between the point A and C. A_1 and A_2 are the corresponding coefficients. As can be observed, the mutual couplings are proportional to the length and width of the coupling slot. At the low-band (f_1), M_{f1} is inversely proportional to the d. At the high-band (f_2), M_{f2} is proportional to the d.

By using full-wave simulations, the corresponding coupling coefficients between the SLR and the patches can be evaluated. Figure 4.34 presents the coupling coefficients between the SLR and the two patches corresponding to different lengths of the slot (denoted

as *Ls*) and the locations of the slot (denoted as *d* in Figure 4.33). As can be seen, the dimension of the slot has a similar influence on the coupling strength at both bands. But the variation of the coupling coefficients between the SLR and the square patch (high band operation) is more significant than that of the low-band. In contrast, changing the locations of the coupling slot has a reverse effect on the two bands, as shown in Figure 4.34(b). This disparate relationship provides another degree of freedom to obtain the coupling coefficients required for the two bands.

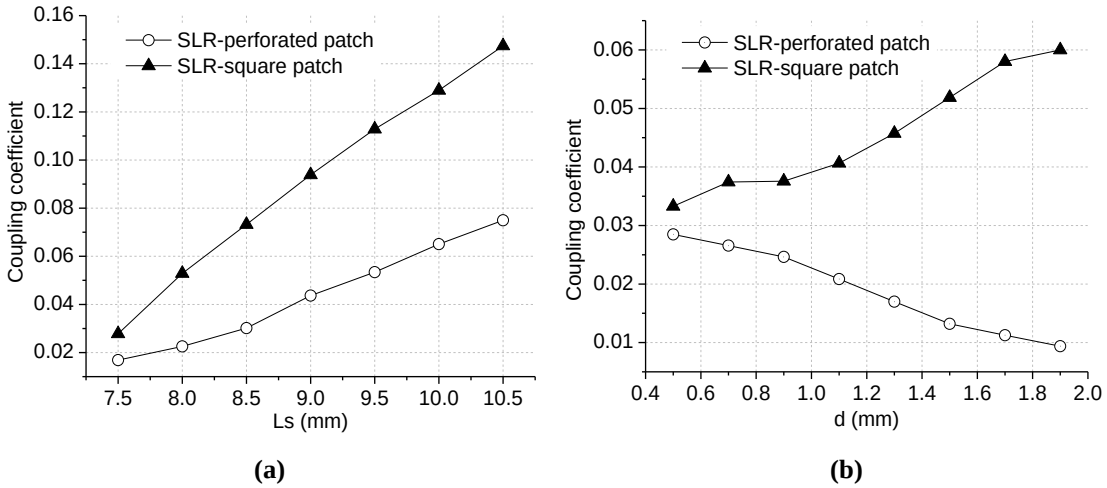

Figure 4.34 Coupling coefficients between the SLR and the two patches with different: (a) length of slot *Ls*, (b) location of the slot *d*.

4.4.3 Improved Frequency responses

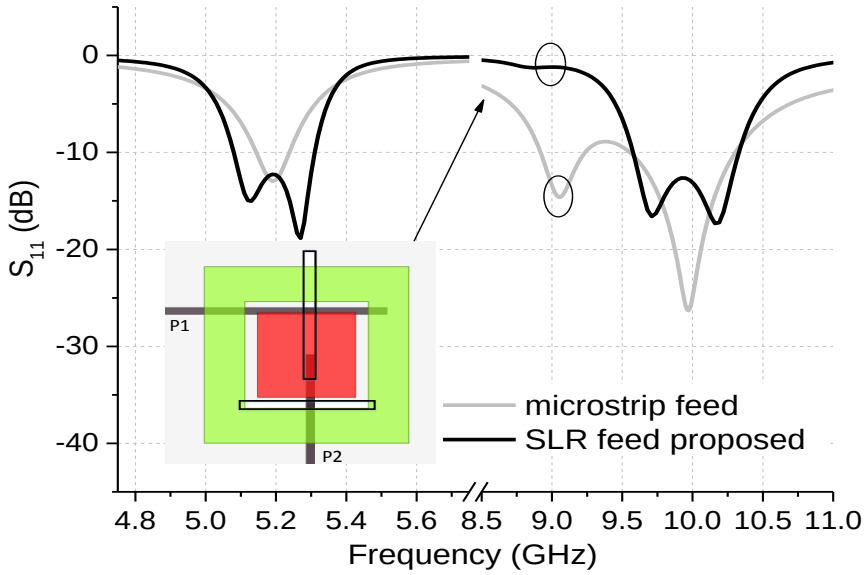

Figure 4.35 S-parameters comparison between the SLR-feed dual-band antenna and a microstrip feed dual-band antenna.

As the dual-mode SLR is coupled and tuned with two single-mode patches, 2nd-order filtering features at the both bands are achieved. The advantages of this coupling structure can be appreciated by the comparison with the case that is fed by a microstrip line. Figure 4.35 compares the simulated S-parameters of the proposed SLR-coupled antenna with a counterpart fed by microstrip. It is observed that the proposed antenna exhibits a 2nd-order filtering characteristic with improved bandwidth and out-of-band rejection as compared with the counterpart. For the microstrip-fed antenna, only one resonant frequency is produced in the low-band and fractional bandwidth (FBW) is only 1.9%. In contrast, when the patches are fed by the resonator, two resonant frequencies are generated at both bands, resulting in wider bandwidth (FBW = 4.6%).

The other function of the proposed SLR-fed antenna is harmonic suppression. As shown in Figure 4.35, a 2nd-order harmonic emerges at around 9 GHz for the microstrip-fed antenna, causing channel interference. When the patches are fed by the resonator, the harmonic can be significantly suppressed with the return loss suppressed from 15 to 2 dB. This harmonic suppression is attributed to the filter-antenna integration that only the signal at the given frequencies could be transmitted/received. Such a filtering function is useful for reducing the interferences from unwanted channels.

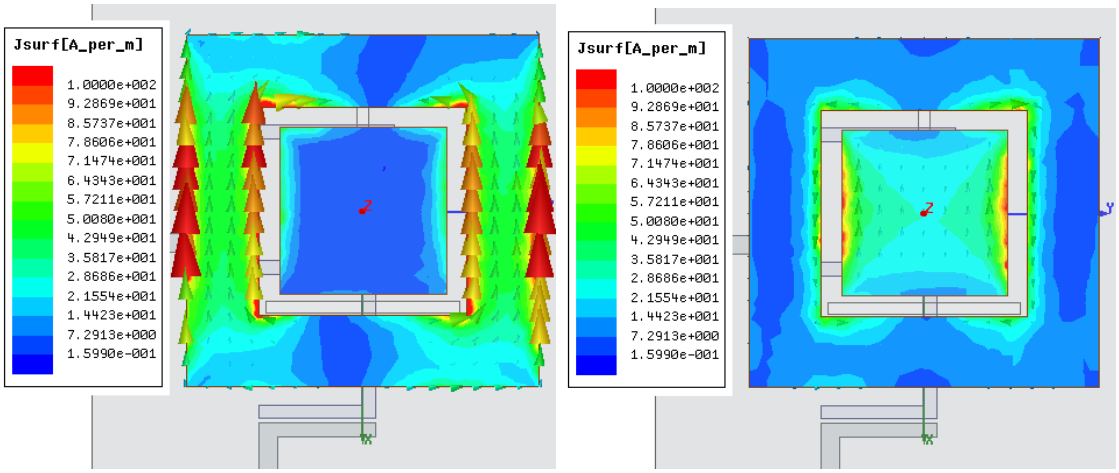

(a) **(b)**

Figure 4.36 Current distribution of the antenna at two bands: (a) 5.2 GHz, (b) 10 GHz.

The current distribution at the two operation bands is shown in Figure 4.36. A strong current flows along the perforated patch at the low band operation, as shown in Figure 4.36(a). In contrast, the current on the inner square patch is very weak. At high band (10 GHz), however, the square patch is excited with intensive current distribution. The current distribution demonstrates that the perforated patch operates at low band whereas the inner

square patch works at the high band. Besides, the mutual coupling between the two patches is considerable weak.

Another interesting feature of the proposed SLR-fed antenna is that the bandwidths of the low- and high-band operations can be easily adjusted by tuning the coupling coefficients between the SLR and patches. Using the results presented in Figure 4.34, the coupling coefficients and therefore the bandwidths can be adjusted by changing the dimensions of the coupling slot. Figure 4.37 shows the S-parameters at both bands with different lengths of the coupling slot. As can be observed, when the *Ls1* is less than 7 mm, the two reflection zeros in each band are merged together. When the length increases from 7 to 8 mm, the two reflection zeros emerge and the bandwidths are increased from 150 to 250 MHz (500 to 800 MHz) for the low band (high band) operations.

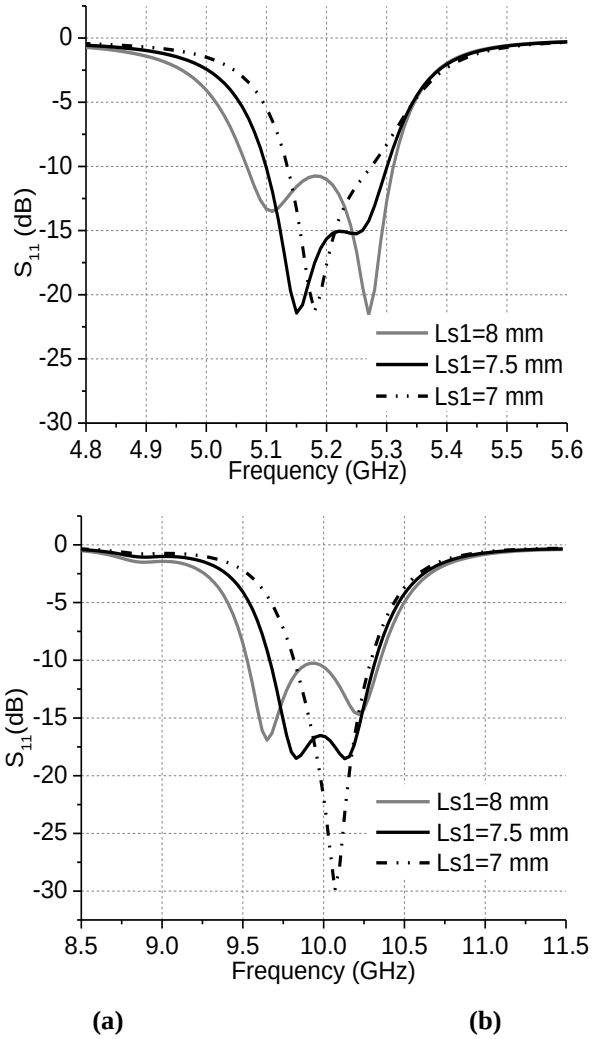

Figure 4.37 Simulated bandwidths with different lengths of the slot *Ls1*: (a) low band, (b) high band.

4.4.4 SLR-Fed DBDP Filtering Array Antenna

The proposed DBDP filtering antenna element can be extended to large antenna arrays. To verify this, a 2 × 2 array is designed, as the configuration shown in Figure 4.38. The two operation bands of each polarization are combined using an SLR and fed by a power divider, resulting in the reduction of the coupling slots, feed networks and input ports. Thus, only two feed networks are employed to feed the DBDP array. This reduction is very useful for simplifying the complexity of the designs of the dual-band antenna arrays with dual polarizations, especially for the shared-aperture DBDP array with a low frequency ratio.

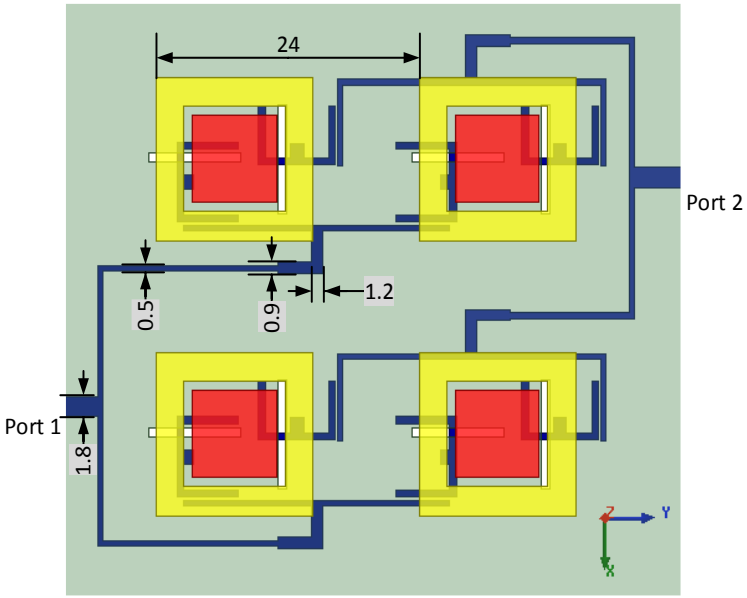

Figure 4.38 Layout of the proposed 2 × 2 DBDP filtering antenna array: (unit: mm).

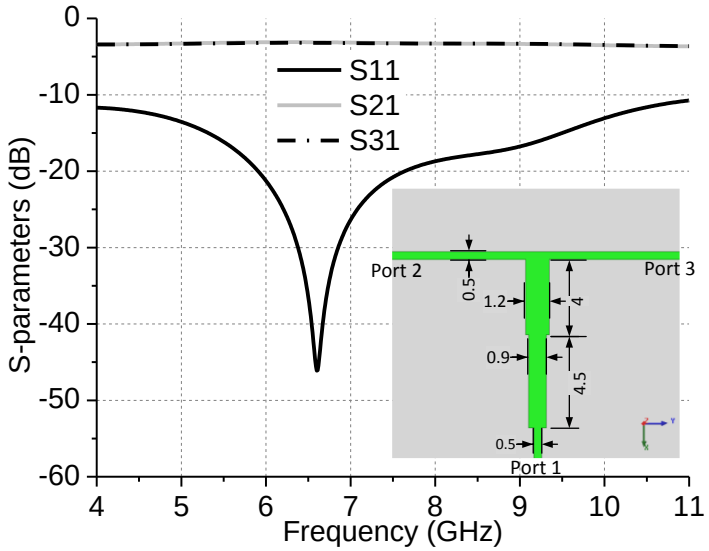

Figure 4.39 Simulated S-parameters of the stepped two-way power divider: (unit: mm).

One of the problems to be solved in this DBDP array is that a wideband dividing network is required to evenly feed the radiating elements. To broaden the bandwidth, a 2-way stepped quarter-wavelength impedance transformer is adopted. Figure 4.39 shows the configuration of the power divider and the corresponding S-parameters. As can be observed, the power divider has a very wide bandwidth, covering the C- and X-band simultaneously. The insertion loss is about 3.4 dB at the both two operation bands, including the 3 dB power division loss.

4.4.5 Results and Discussion

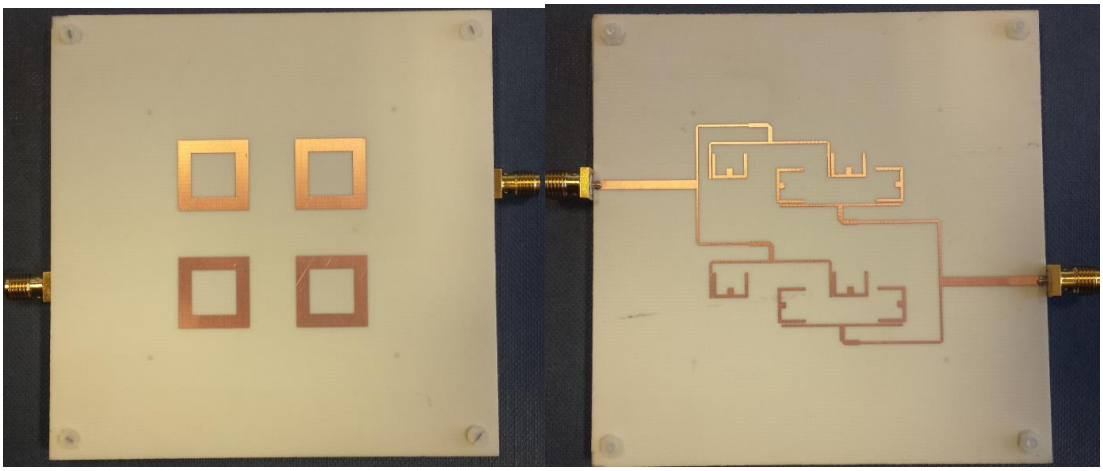

(a) (b)

Figure 4.40 Prototype of the proposed DBDP filtering antenna: (a) front-view, (b) back-view.

Both the element and array of the proposed DBDP filtering antenna were prototyped and measured. Figure 4.40 shows the front- and back-view of the prototype. Figure 4.41 presents the simulated and measured S-parameters of the element. It is observed that the measured results agree well with the simulations over a broadband. For each polarization/port, two operation bands are achieved. The impedance bandwidth at low band is from 5.1 to 5.3 GHz for the two polarizations. At the high band, the operation bandwidth is measured from 9.6 to 10.2 GHz. The antenna element exhibits the 2^{nd}-order filtering features with two reflection zeros are produced at both bands. These reflection zeros are beneficial to increasing the bandwidths and shaping the sharp roll-off at both edges of the two bands. Out of the bands, the antenna exhibits good harmonic suppression. The antenna also shows a good isolation between the two polarizations/ports with the measured $|S_{21}|$ is lower than -20 dB and -24 dB at the low- and high-band, respectively. The discrepancy between the simulated and measured results is caused by misalignment between the substrates when the prototype was assembled.

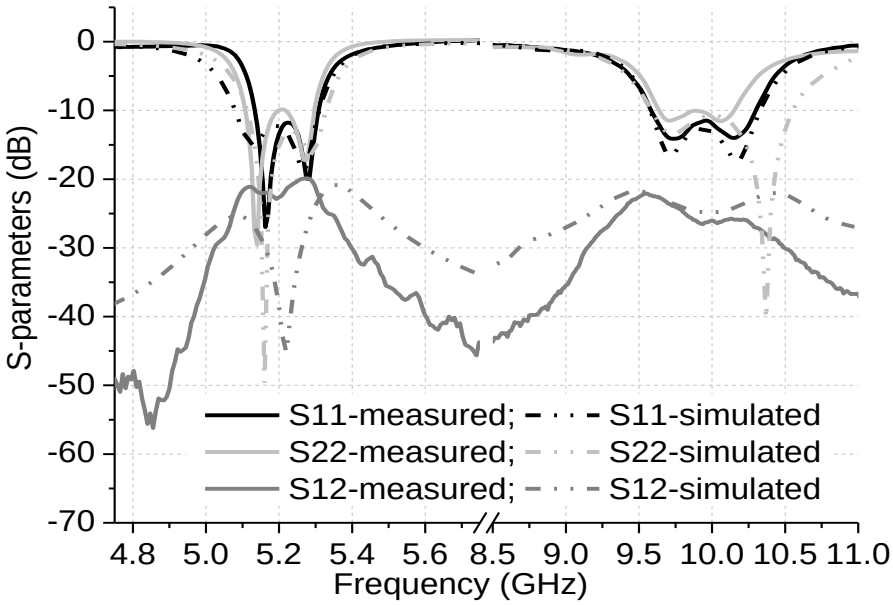

Figure 4.41 Measured and simulated S-parameters of the DBDP element.

Figure 4.42 shows the simulated and measured S-parameters of the 2 × 2 DBDP array. The measured results agree reasonably well with the simulations. Both the two polarizations of the array show two operation bands from 5.05 to 5.3 GHz and from 9.6 to 10.3 GHz, respectively. At low- and high-band, the measured isolations between the two polarizations are over 25 dB and 23 dB, respectively. Compared with the results in Figure 4.42, the array shows the wider bandwidths than the element at both bands, which may be caused by the influence of the power dividing networks.

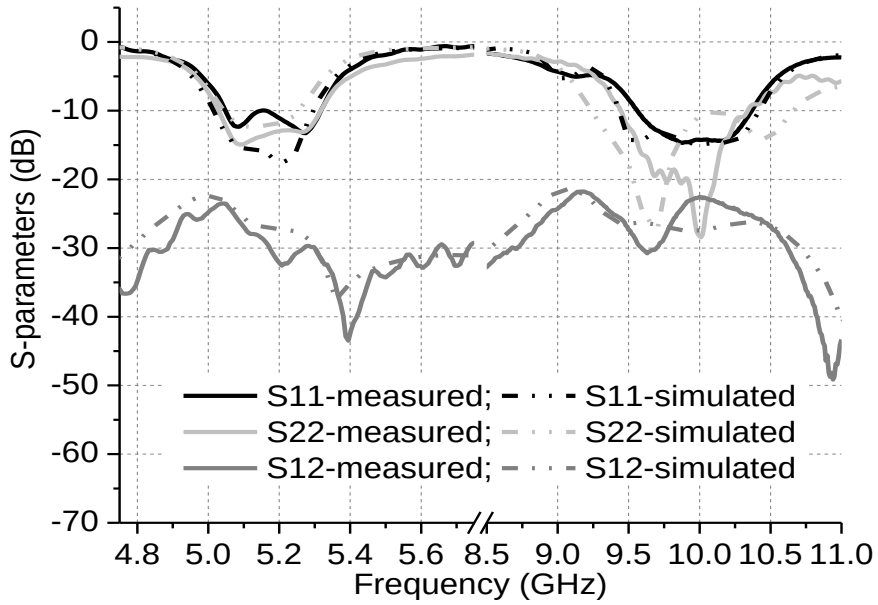

Figure 4.42 Measured and simulated S-parameters of the DBDP filtering antenna array.

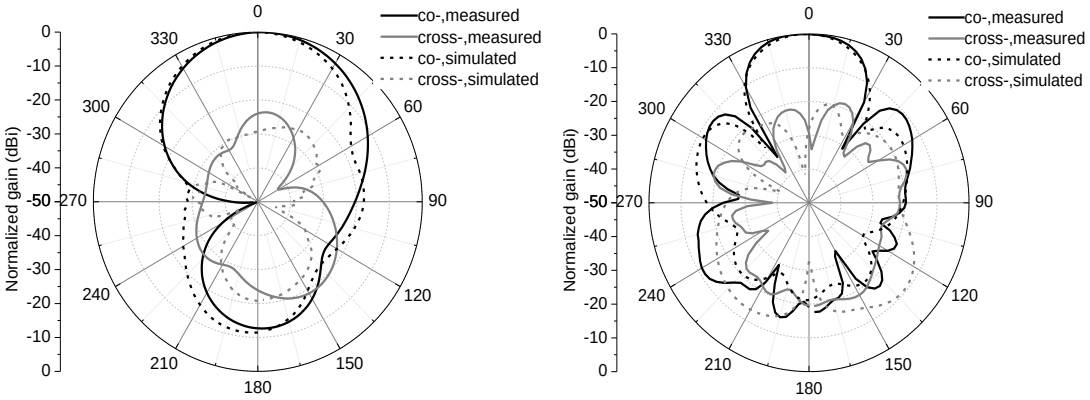

Figure 4.43 Simulated and measured normalized radiation patterns of the 2 × 2 DBDP array antenna: (a) 5.2 GHz, (b) 10 GHz.

The radiation patterns of the 2 × 2 DBDP array were measured. Figure 4.43 shows the simulated and measured normalized co-polarization and cross-polarization radiation patterns. As can be observed, measured results agree well with the simulated ones, showing the main beam in the broadside direction. The measured cross polarizations are lower than -24 and -26 dB at 5.2 GHz and 10 GHz, respectively.

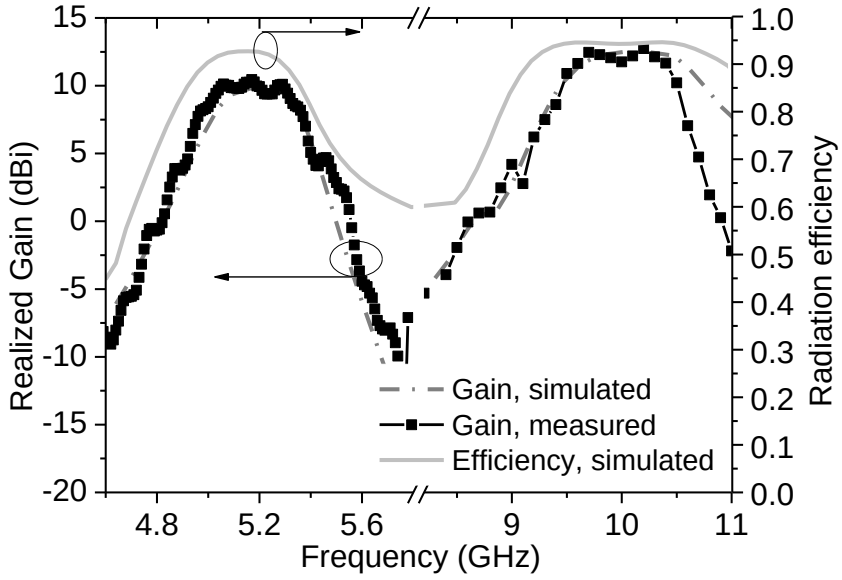

Figure 4.44 Simulated and measured realized gains and the simulated radiation efficiency of the proposed 2 × 2 C/X-band filtering array.

Figure 4.44 shows the simulated and measured realized gains and the simulated radiation efficiency of the 2 × 2 antenna array. It is observed that the measured and simulated gains agree very well with each other. The antenna exhibits a flat gain of 10 dBi and 12 dBi at the low- and high-band, respectively. Out of the bands, the gains rapidly decrease to below

0 dBi as the frequency is below 4.7 GHz (8.8 GHz) and above 5.6 GHz (10.9 GHz) for the low band (high band) operation. This rapid decrease of the gain demonstrates that the antenna has the good filtering characteristics. In the two operation bands, the simulated radiation efficiencies are above 90%.

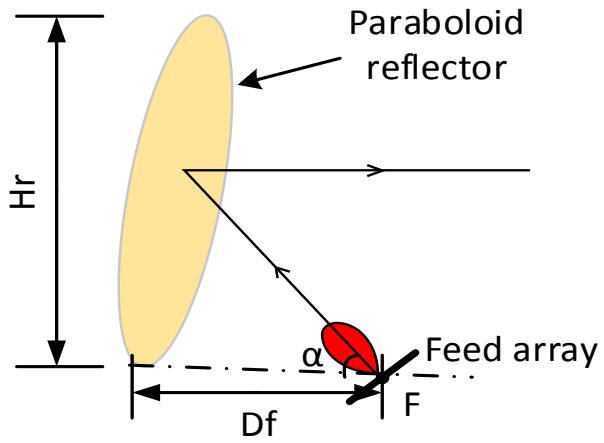

Figure 4.45 Geometry of the offset paraboloid reflector antenna system. *Hr* = 300 mm, *Df* = 300 mm.

The proposed integrated filtering array antenna is also suitable for serving as a dual-band dual-polarized feed of a reflector antenna due to its high integration. Figure 4.45 shows the geometry of a paraboloid reflector. The paraboloid reflector is illuminated using the proposed 2 × 2 DBDP array, which is placed at the focal point with its aperture facing the center section of the reflector. The reflector has a diameter (*Hr*) of 300 mm and the focal length (*Df)* of 300 mm which is about 5 and 10 wavelengths at 5.2 and 10 GHz, respectively. The reflector antenna system under measurement is shown in Figure 4.46.

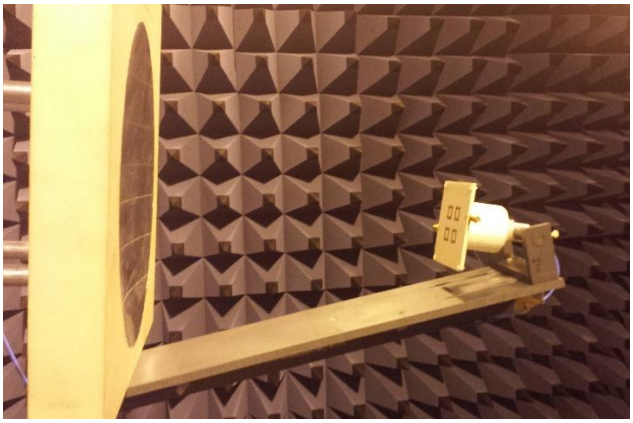

Figure 4.46 Proposed feed array with a paraboloid reflector antenna under measurement.

Figure 4.47 shows the measured normalized co- and cross- polarization patterns of the reflector antenna at 5.2 GHz. The antenna shows a good radiation performance with the main beam in the broadside. When port 1 is excited (X-polarization), the antenna has a half-

power beam width (HPBW) of 10.4 degrees and the directivity of the antenna can be calculated as 24.7 dBi. The side lobe is below -15 dB and the cross polarization discrimination (XPD) is over 29 dB in broadside. For the Y-polarization, an HPBW of 10.6 degrees is achieved and the calculated directivity is 24.6 dBi. The side lobe is lower than -14 dB and the XPD is over 23 dB. Compared with the X-polarization, the radiation performance is slightly deteriorated, which is caused by the misalignment between the reflector and feed.

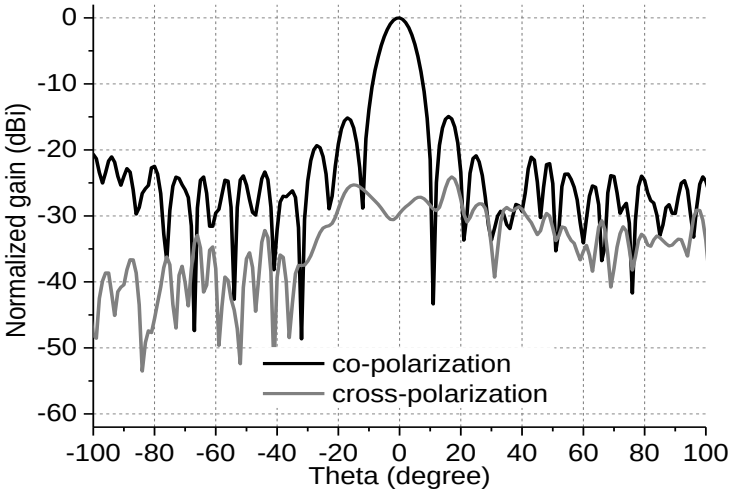

(a)

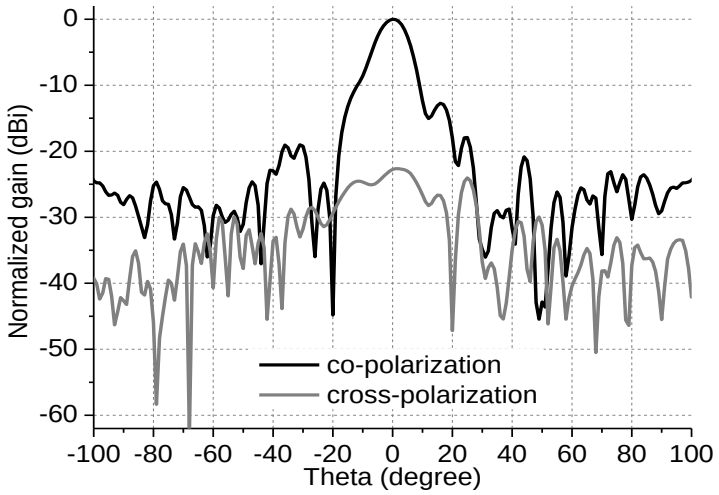

(b)

Figure 4.47 Measured normalized co- and cross-polarization radiation patterns of the paraboloid reflector antenna at 5.2 GHz: (a) Port-1 excitation, (b) Port-2 excitation.

Figure 4.48 shows the measured normalized co- and cross-polarization radiation patterns of the reflector antenna at 10 GHz. Due to the increase of the electrical size at the higher hand, the antenna exhibits a narrower HPBW and higher directivity. When port 1 is

excited (X-polarization), the HPBW of the antenna is 6.7 degrees and the directivity is calculated as 28.6 dBi. The side-lobe is below to -24 dB and the XPD is over 25 dB. For Y-polarization, the HPBW is about 6.2 degrees and the calculated directivity is 29.2 dBi. The side lobe is below -20 dB and the XPD is over 33 dB.

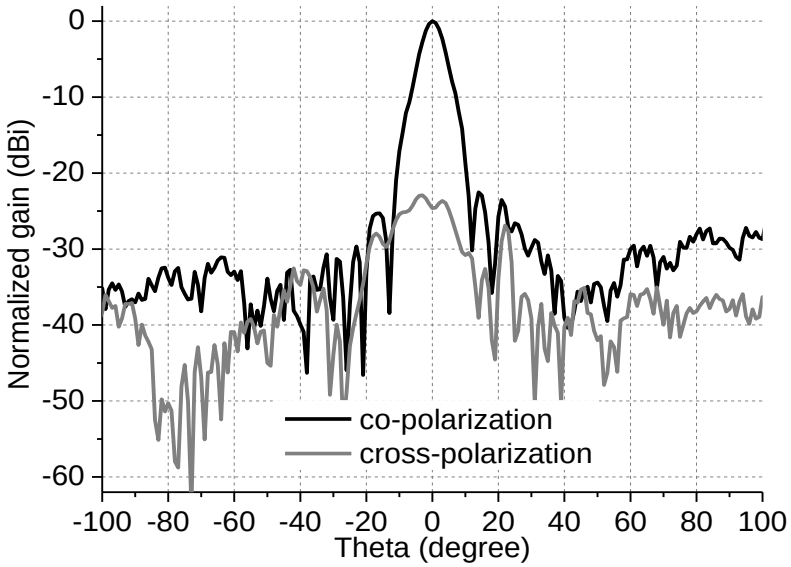

(a)

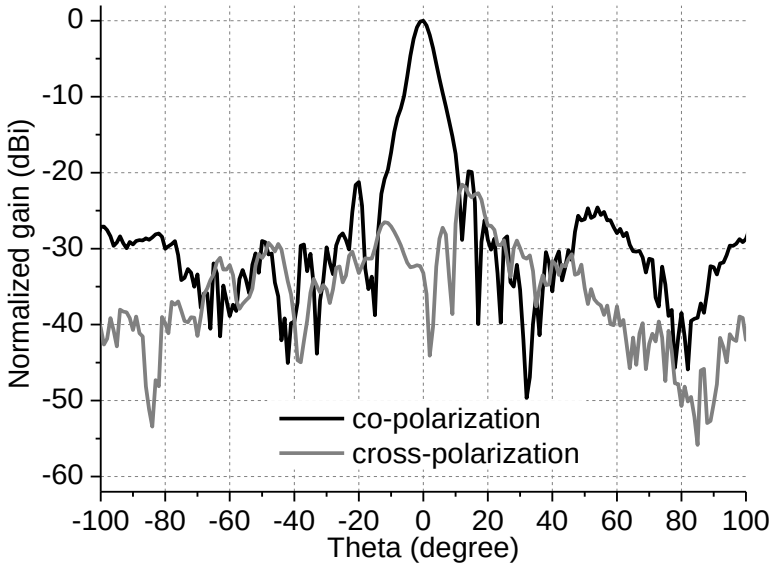

(b)

Figure 4.48 Measured normalized co- and cross-polarization radiation patterns of the paraboloid reflector antenna at 10 GHz: (a) Port-1 excitation, (b) Port-2 excitation.

4.5 Broadband High-Gain Filtering Antenna Array for Millimeter-Wave Applications

4.5.1 Introduction

One of the most important potential applications of the high-integration filtering antenna is millimeter wave (mm-Wave) communications. Thanks to the huge advantages in mm-Wave such as high data rate and significant reduction of digital traffic, the fifth-generation (5G) mobile communication has attracted intensive research interests in academia and industry [154]-[155]. In the 5G era, lots of things such as electronic devices, vehicles and the equipment in the offices and homes will be wirelessly connected through the Internet. Users will be able to access ultra-high-definition (UHD) multimedia streaming and services such as Virtual Reality (VR) and Augmented Reality (AR). All these potential services will inevitably demand a broadband to support the extremely high data rate in 5G wireless communications.

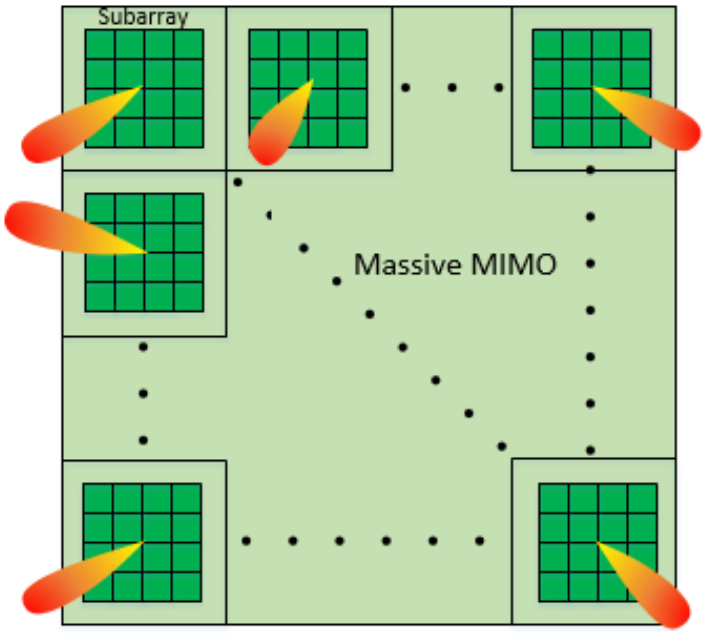

Figure 4.49 Architecture of the massive MIMO base-station antenna array.

The mm-Wave frequency band is widely believed to be a good candidate to realize a wideband operation. The other problems to be concerned are the higher transmission loss and link stability, which require an enhancement of the gain and adaptive directional beam [155]. Massive multiple-input multiple-output (MIMO) base station is a promising technique for improving the capacity and service quality by accurately concentrating the transmitted energy to the mobile users [156]-[158], as the architecture shown in Figure 4.49.

The massive MIMO antenna has multiple antenna subarrays in two dimensions and each can adaptively direct the beams to the users in azimuth and elevation directions. Thanks to each subarray is composed of $n \times n$ radiating elements, high antenna gain and steerable beam can be achieved. Due to the short wavelength at mm-waves and limited coverage of each 5G cellular, the mm-wave base-station antennas with low cost, low profile and light weight will be in huge demand in urban areas. The integration of filter and antenna could significantly reduce the potential cost of the wireless communication systems due to the removal of the traditional expensive mm-Wave filters and interfaces.

To date, several mm-wave antennas have been reported for 5G communications. However, the research on mm-Wave antenna arrays with filtering functions is insufficient. In [159], a stacked patch is proposed to achieve a broadband antenna at 28 GHz. But this antenna suffers from poor radiation pattern that some radiation nulls emerged in the main-lobe. In [160], a tilted antenna was designed by combining a patch and a waveguide aperture, but this is not suitable for integration. Dual-band (28/38 GHz) antenna element with circular polarization is reported in [161]. However, the bandwidths are considered too narrow (less than 3%). Usually, bandwidth can be enhanced by adding parasitic patches, but it will lead to the high profile and cost [162]-[163]. In [164]-[165], mm-Wave antenna arrays using substrate integrated waveguide (SIW) and low temperature co-fired ceramic (LTCC) technologies were achieved. In [166]-[167], massive MIMO arrays for 5G wireless communications were reported. However, these works cannot fulfill the requirements of broad bandwidth, high gain, low profile and low cost, simultaneously.

In this section, a broadband, high gain microstrip array antenna with low profile is proposed for the first time. The antenna is achieved by employing a novel vertically coupled resonant structure, which could not only effectively broaden the bandwidth of a microstrip antenna without increasing the thickness of the antenna but also produce the required filtering function. These features could lead to the removal of the mm-wave band-pass filters and 50 Ω interfaces, and therefore the complexity and the potential cost could be significantly reduced. To demonstrate the operation schemes, a 4 × 4 antenna array with broadside radiation and a 4 × 4 beam scanning array are respectively implemented in this chapter.

4.5.2 Antenna Implementation

Figure 4.50(a) shows the configuration of the proposed antenna element working at mm-Wave. The patch is printed on the top layer of the upper substrate whereas the microstrip line and hairpin resonator are printed on the bottom layer of the lower substrate. The patch

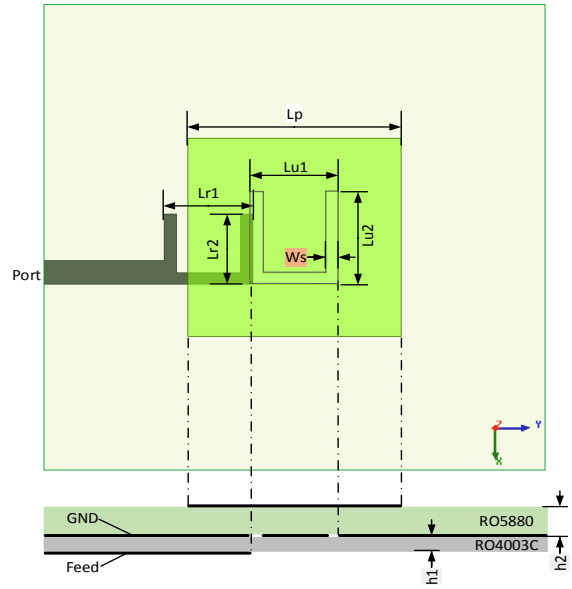

(a)

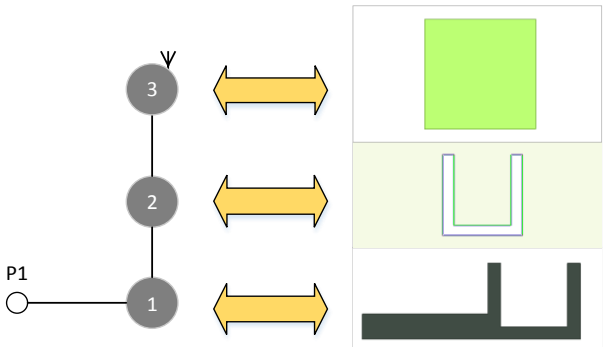

(b)

Figure 4.50 (a) Configurations of the proposed antenna element, (b) equivalent circuit. *Lp* = 3.05 mm, *h1* = 0.2 mm, *h2* = 0.787 mm, *Lr1* = 1.3 mm, *Lr2* = 1.15 mm, *Lu1* = 1.2 mm, *Lu2* = 1.4 mm, *Ws* = 0.2mm.

and the feeding network share the same ground plane, which is placed on the top layer of the lower substrate. In the ground plane, a U-shaped slot is etched to form a slot resonator. The patch, U-slot resonator and the hairpin resonator are stacked and vertically coupled, leading to a strong coupling between them [168]. Therefore, a high-order filtering antenna is achieved. RO 4003C substrate with a permittivity of 3.55 and loss tangent of 0.0027 is used for the lower substrate. To reduce the antenna loss, RO 5880 substrate with a permittivity of 2.2 and loss tangent of 0.0009 is used for the upper substrate. The thicknesses of the RO 4003C and the RO 5880 are 0.2 mm and 0.787 mm, and thus the total thickness of the antenna is less than 1 mm. The optimization was performed using high frequency structural simulator (HFSS 15) and the optimized parameters are presented in the caption.

To illustrate the design approaches, the antenna element is decomposed by each layer and shown in Figure 4.50(b). The hairpin resonator on the bottom layer is connected by a 50

Ω microstrip line, which serves as the 1st-order resonator. The U-shaped slot in the ground plane is served as the 2nd-order resonator. The U-slot is a half-wavelength resonator and its resonance can be controlled by adjusting the length and the width of the slot. The square patch on the top layer, not only works the radiating element but also the last order resonator of the antenna. The patch, U-slot resonator, and hairpin resonator are stacked and coupled in vertical, forming a 3rd-order filtering antenna. All of them have the same resonant frequency at around 27 GHz. The dimensions of the U-slot and hairpin resonators can be approximately evaluated using the expressions below,

$$Lu1 + 2 \cdot Lu2 \approx \frac{c}{2 f_0 \sqrt{\varepsilon_{eff1}}} \quad \text{(Eq.5.1)}$$

$$Lr1 + 2 \cdot Lr2 \approx \frac{c}{2 f_0 \sqrt{\varepsilon_{eff2}}} \quad \text{(Eq.5.2)}$$

where, f_0 is the resonant frequency. ε_{eff1} and ε_{eff2} are the effective dielectric constants of the slot-line in the ground and the microstrip, respectively. c is the speed of light in free space.

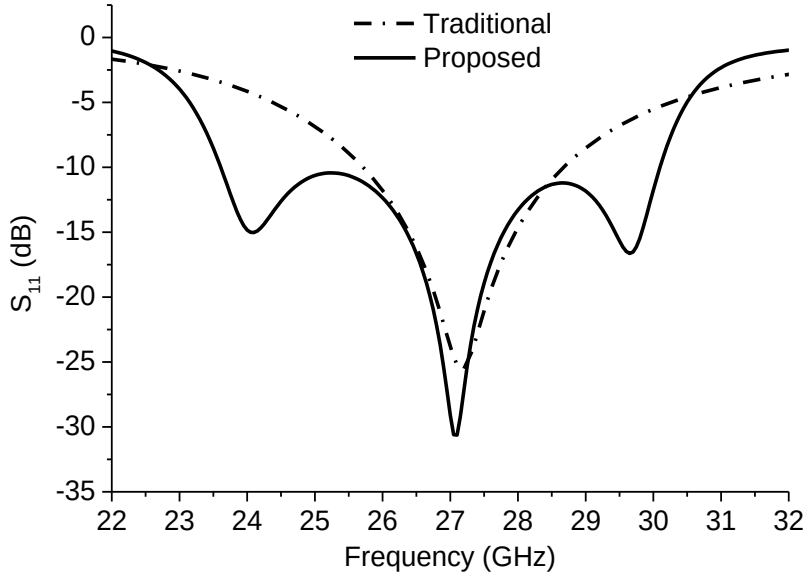

Figure 4.51 Comparison of the simulated S_{11} between the proposed antenna element and a traditional microstrip fed patch antenna.

To illustrate the advantages of the proposed antenna, the simulated S_{11} of the proposed antenna and a traditional counterpart patch antenna with the same thickness are compared in Figure 4.51. As can be seen, the proposed vertically coupled antenna has a significantly wider the impedance bandwidth than the traditional patch antenna. The traditional patch has only one resonant frequency at 27.2 GHz, shaping a bandwidth from 26 to 28.5 GHz (FBW = 9.3%). In contrast, the proposed antenna has three matching points at around 24, 27 and

30 GHz, respectively, generating a broad bandwidth from 23.5 to 30.5 GHz (FBW = 26%). In addition, the proposed antenna exhibits a 3rd-order filtering characteristic.

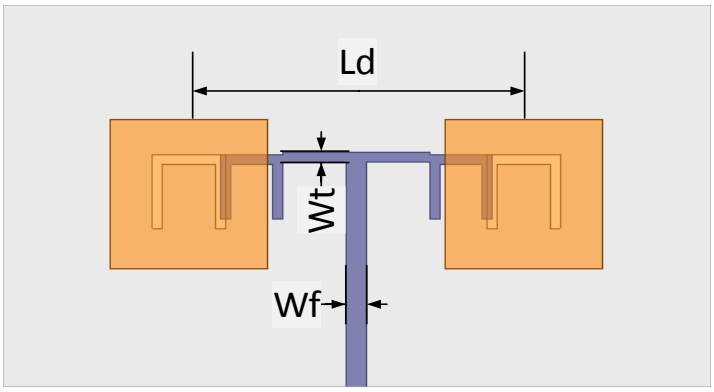

Figure 4.52 Configurations of the 1 × 2 subarray, subarray-I. *Wf* = 0.4 mm, *Wt* = 0.24 mm, *Ld* = 6 mm.

To meet the requirements of high gain in mm-Wave applications while providing the beam scanning ability, the antenna elements are combined to form antenna subarrays. Figure 4.52 shows the configurations of the proposed 1 × 2 subarray (denoted as subarray-I). The distance between the elements is set to be 6 mm, 0.54 wavelength at 27 GHz. In this work, due to the symmetry of the design, the elements can be excited from both sides while maintaining a consistent phase, as shown in the figure. Such a layout is beneficial to reduce the size and complexity of the feeds.

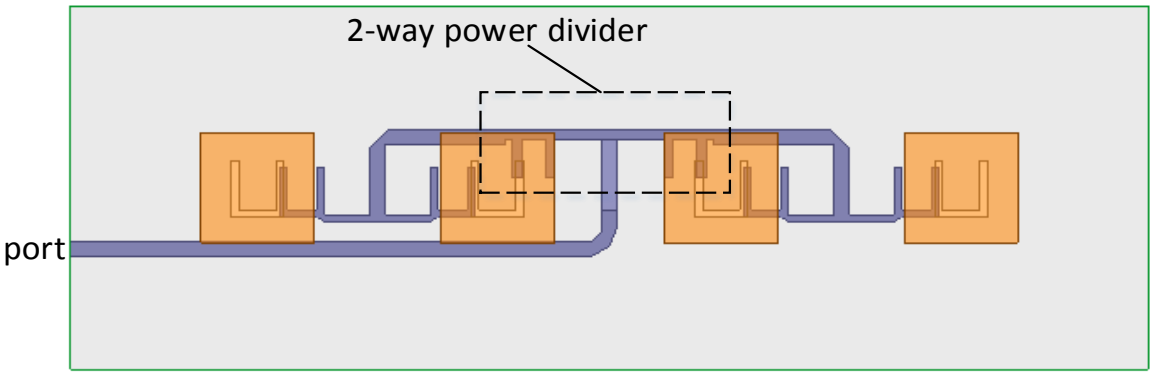

Figure 4.53 Configurations of the proposed 1 × 4 subarray, subarray-II.

Figure 4.53 shows the configuration of the 1 × 4 subarray (denoted as subarray-II), which is combined by two 1 × 2 subarrays. The subarray is fed by a two-way power divider. Different from traditional power dividers, the adopted divider integrates two resonant structures at its two outputs, which could be used to further enhance the impedance bandwidth of

the antenna. Figure 4.54 shows the simulated S-parameters of the power divider. The results show that it has a good power divider performance over a very wide bandwidth with two reflection nulls emerged at around 22 and 32 GHz, respectively.

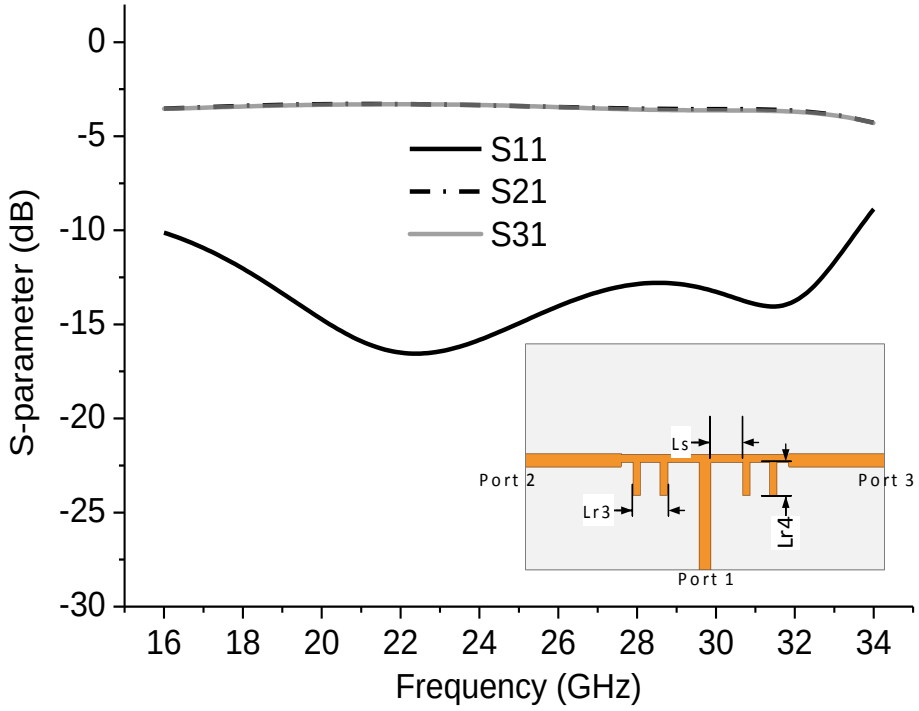

Figure 4.54 Configuration and simulated S-parameters of the two-way power divider. Ls = 1.5 mm, L3 = 1.1 mm, L4 = 1.2 mm.

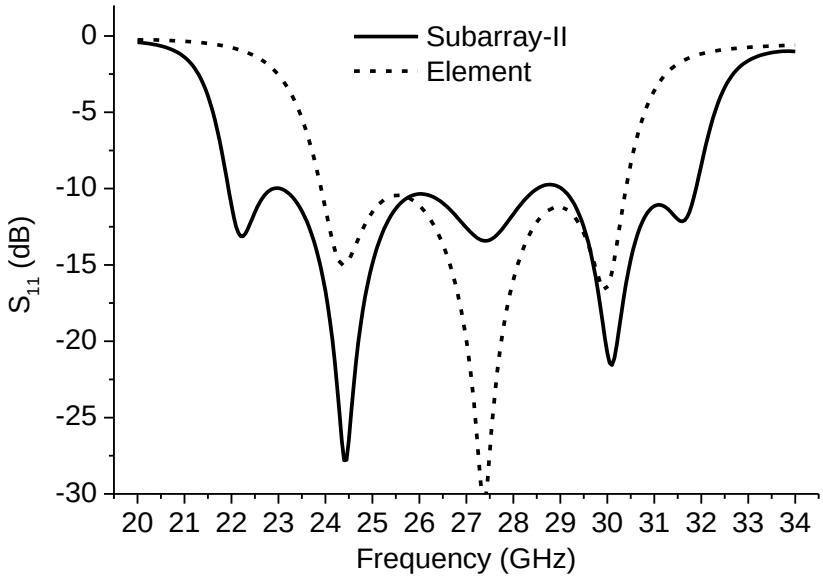

(a)

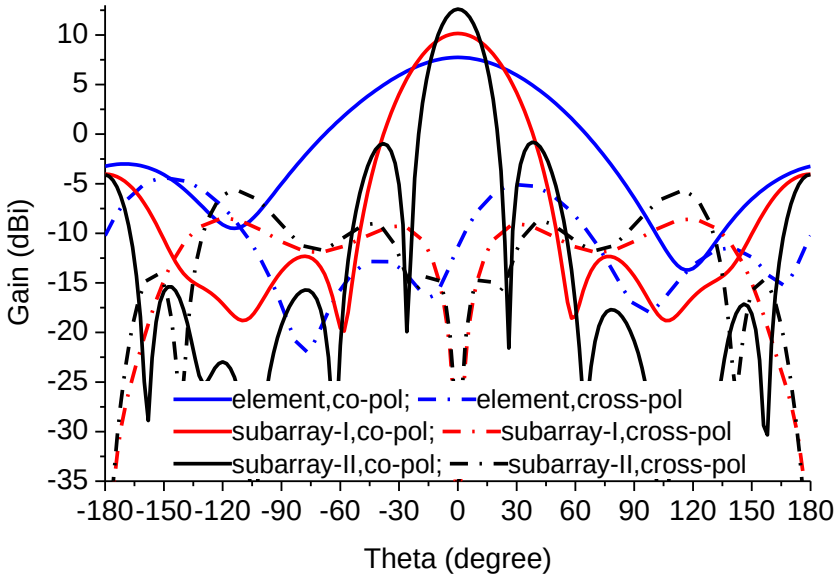

(b)

Figure 4.55 Comparisons of the radiation patterns at 27 GHz between the element and the subarrays: (a) S-parameters, (b) radiation patterns.

Figure 4.55 compares the simulated S-parameters and radiation patterns at 27GHz of the proposed element and the two subarrays. As can be seen from Figure 4.55(a), there are totally three resonant frequencies for the element but five resonant frequencies for the subarray-II. These two additional resonant frequencies result from the power divider presented in Figure 4.53, which results in a wider impedance bandwidth from 22 to 32 GHz (FBW = 37%). The radiation patterns of the antenna element, subarray-I and II in Figure 4.55(b) show that the three antennas have the maximum radiation in the broadside direction. The gains of the three antennas are 7.5 dBi, 10 dBi and 12.5 dBi, respectively.

4.5.3 Filtering Array Antennas and Results

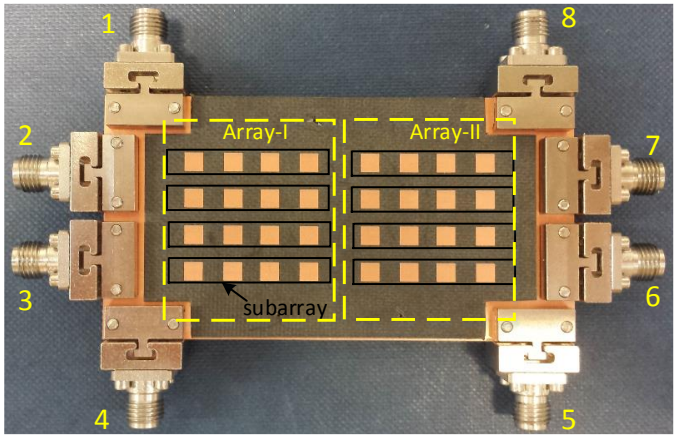

(a)

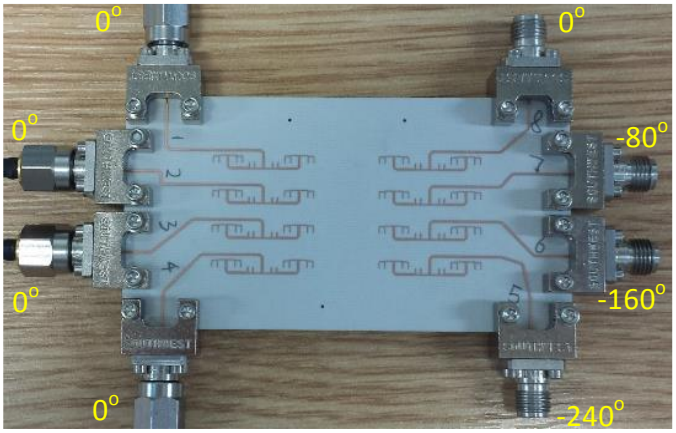

(b)

Figure 4.56 Prototype of the two arrays: (a) front view, (b) bottom view.

Based on the 1 × 4 subarray, two 4 × 4 array antennas were conceived to demonstrate the operation schemes in Figure 5.1, as the prototypes shown in Figure 4.56. The first one is an array with the maximum radiation in the broadside direction, denoted as Array-I. The Array-I has the identical input phase and amplitude for each subarray. The second one is a beam scanning array, which has the gradient input phases for the four subarrays, denoted Array-II. Both arrays were fabricated on the same board. To facilitate the measurement, a 4-way power divider was used to feed the subarrays.

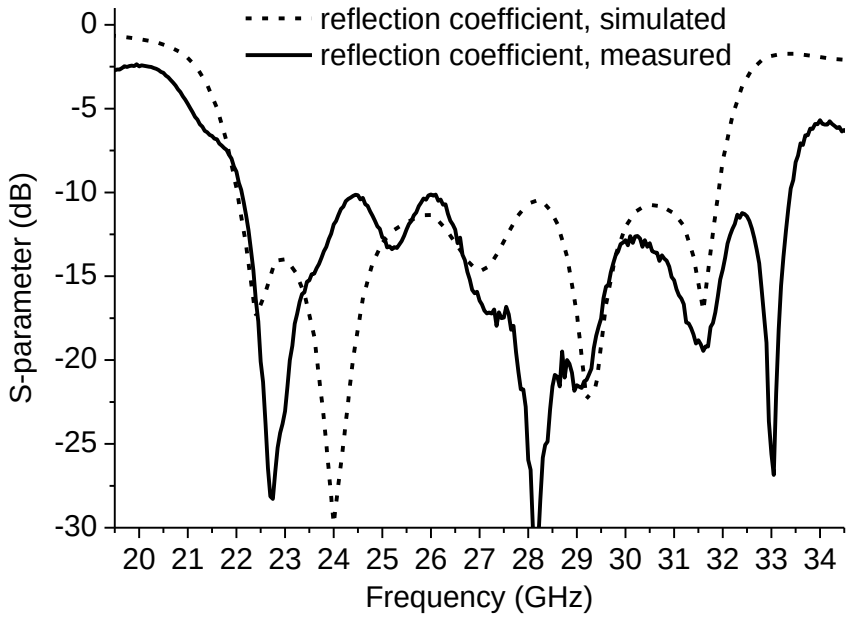

Figure 4.57 Simulated and measured reflection coefficients of the subarrays.

Figure 4.57 shows the simulated and measured reflection coefficients of the subarray. The measured results agree reasonably well with the simulations, showing a very wide impedance bandwidth from 22 to 33.5 GHz (FBW = 41.8%). Such a broad bandwidth is

attributed to the proposed vertically coupled structure and the broadband power divider. The discrepancy between the simulations and measurements, especially the additional matching point at 33 GHz, may be caused by the unknown harmonics and fabrication tolerance.

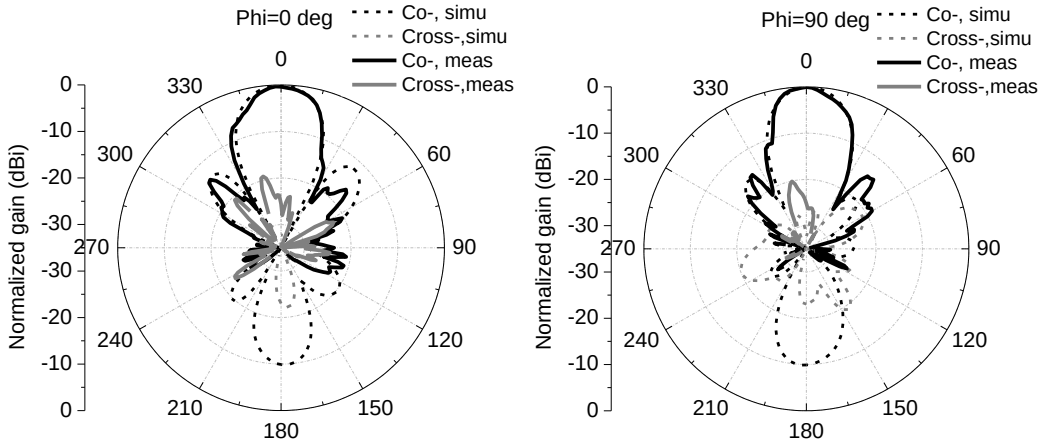

(a)

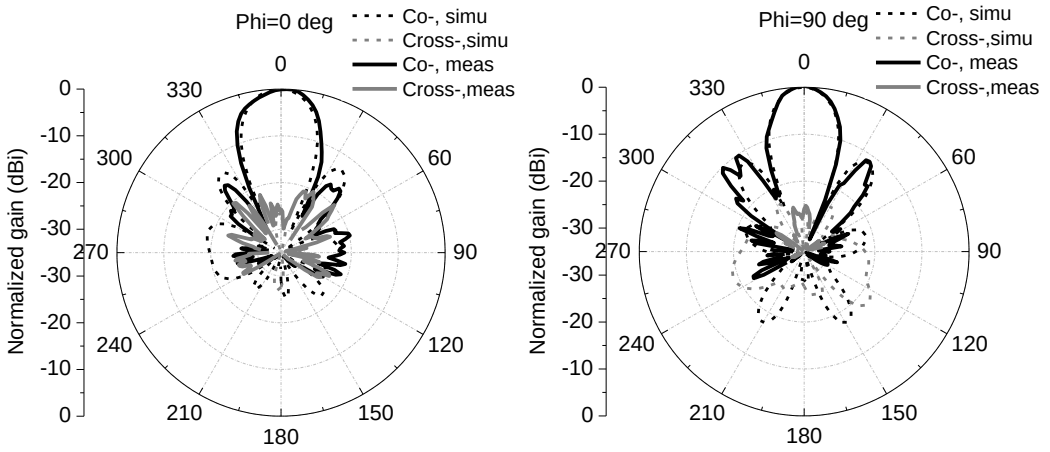

(b)

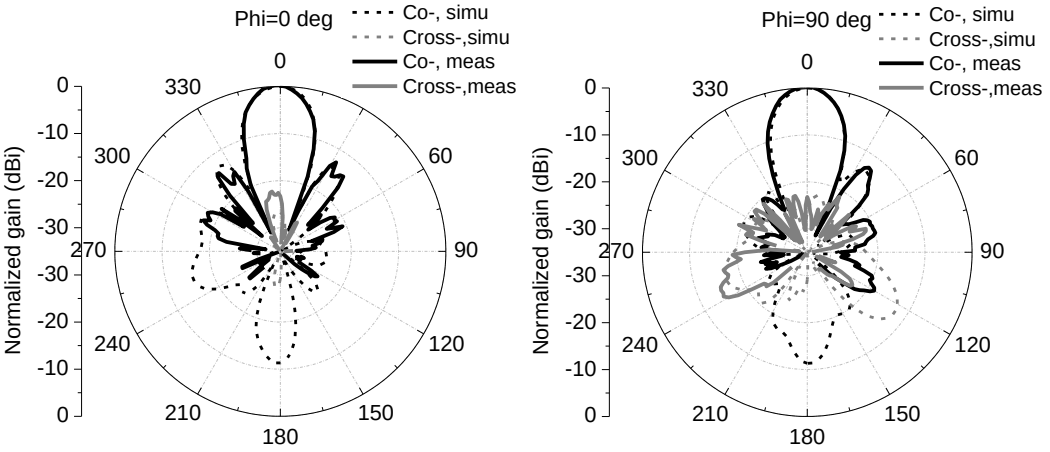

(c)

Figure 4.58 Simulated and measured normalized E-plane and H-plane radiation patterns of the Array-I: (a) 23.5 GHz, (b) 27 GHz and (c) 30.5 GHz.

Figure 4.58 shows the simulated and measured normalized E- and H-plane radiation patterns of the Array-I at 23.5, 27 and 30.5 GHz, respectively. As can be seen, good agreement between the measurements and simulations is achieved. The Array-I exhibits an almost consistent broadside radiation over a broad bandwidth. The measured XPD in broadside direction is over 25 dB. The minor discrepancy between the simulated and measured results is attributed to the measurement tolerance.

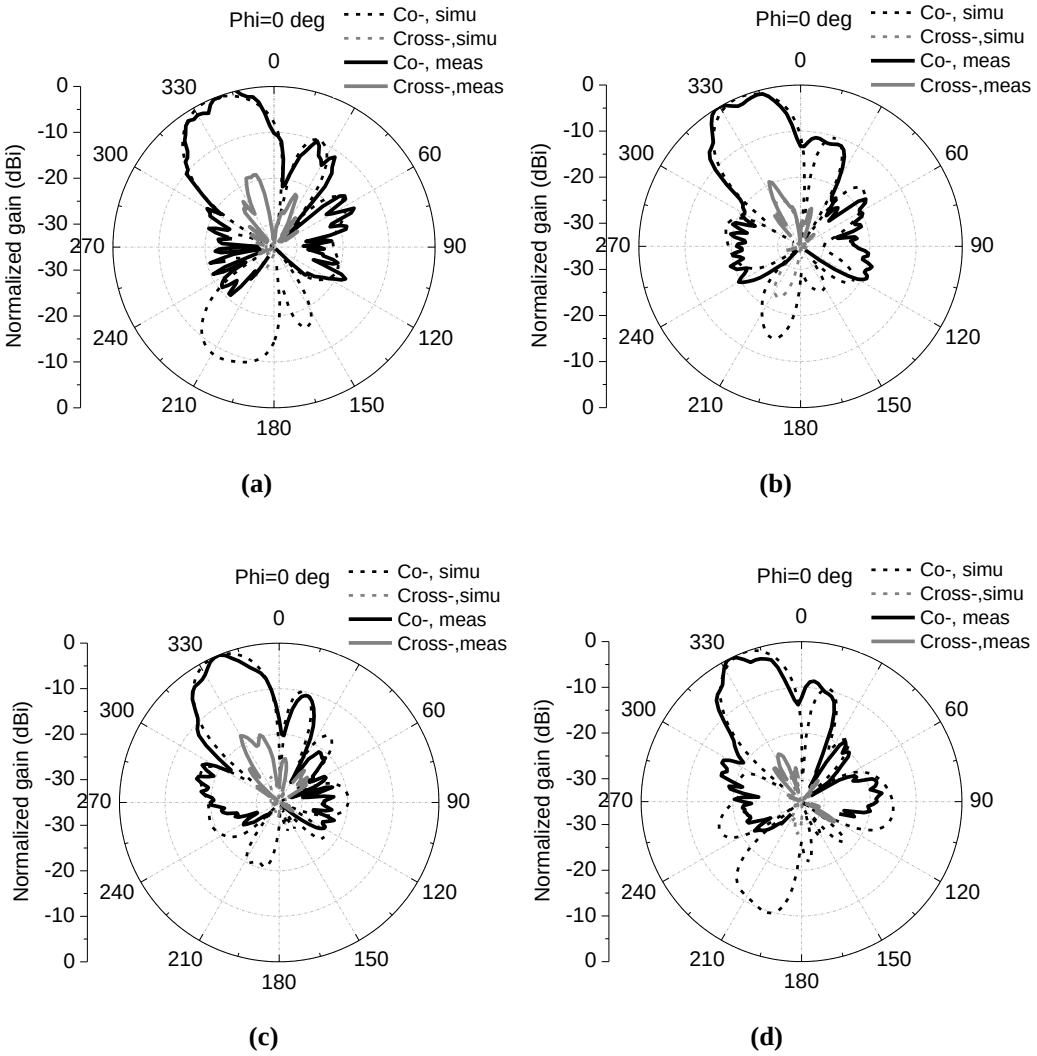

Figure 4.59 Simulated and measured normalized radiation patterns of the Array-II: (a) 22.5 GHz, (b) 25.5 GHz, (c) 28.5 GHz and (d) 31.5 GHz.

Figure 4.59 shows the simulated and measured E-plane normalized radiation patterns of the Array-II at 22.5, 25.5, 28.5 and 31.5 GHz, respectively. The measured results of the Array-II agree reasonably well with the simulations, showing a scanned beam of over 25 degrees over a broadband. The measured side-lobes are below to -10 dB and the XPD in the main beam are over 20 dB.

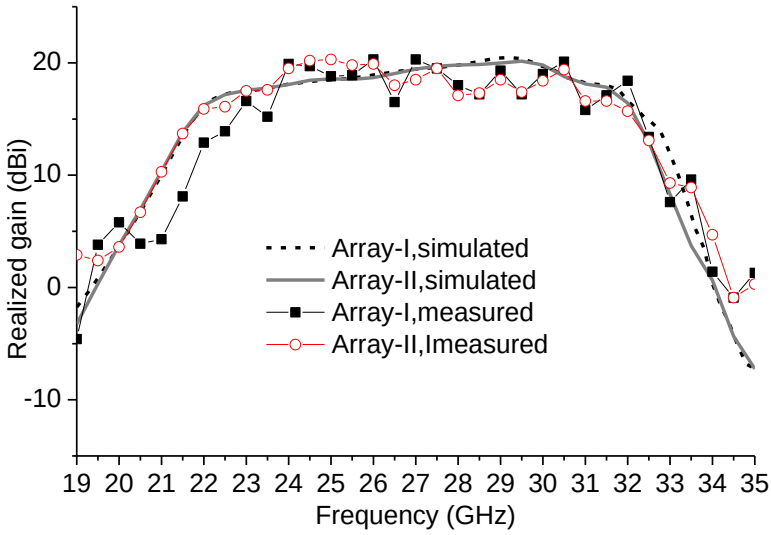

Figure 4.60 Simulated and measured antenna gains of the Array-I and II.

Figure 4.60 shows the simulated and measured realized gains of the Array-I and Array-II, respectively. As can be observed, both arrays exhibit a flat gain response of around 19 dBi from 23 to 32 GHz. The measured results agree reasonably well with the simulations, except for some fluctuation of the measurements. Beyond the operation band, the gain dramatically drops to below 0 dBi, exhibiting a good out-of-band rejection performance.

4.6 Summary

In this chapter, the methods of designing integrated filtering antennas in Chapter 3 are further developed and four planar array antennas with integrated filtering features are proposed. At first, a highly integrated filtering power dividing network is proposed and coupled with the radiating elements, resulting in a filtering array antenna with improved bandwidth, frequency selectivity and out-of-band rejection. Then, the resonator-fed broadband technique is adopted in dual-polarized array application to achieve the broadband low-profile array antenna with filtering functions. The dual-mode SLR in filtering antennas is further developed to achieve a low frequency ratio dual-band dual-polarized array antenna. Thanks to the filtering antenna integration techniques, the feeding networks, coupling structures and inputs are largely reduced, contributing to the simplified configuration but improved frequency responses. Finally, the filtering antenna techniques are employed in mm-Wave array antenna designs. According to the requirements of the 5G mobile communications, a highly integrated, low profile microstrip array antenna with the broadband filtering characteristics is proposed. The techniques presented can effectively increase the bandwidth of a low-profile microstrip antenna in mm-Wave. In addition, the integrated multiple functions could

remove the separate filters and the interfaces and therefore could significantly reduce the cost of the wireless communication systems. Measurement results have verified the validity of the presented integrated filtering antenna arrays.

Chapter 5. High-Integration Duplexing Filtering Antennas

5.1 Introduction

The rapid development of wireless communications in the past decades requires the components of the systems with compact size, high integration and low cost. Traditionally, the frequency division duplex (FDD) communication uses the uplink and downlink channels of a communication system occupy two separate frequency bands for high isolation. As a result, a separate duplexer/diplexer is usually required between the transmitting/receiving channels and a shared broadband antenna. One of the disadvantages of this configuration is its bulk as separate antennas, duplexers, filters and interfaces are required to be designed individually and cascaded in series. This inevitably leads to a high weight, low efficiency and high cost system. The integrated filtering antennas presented in Chapter 3, 4 and 5 provide a feasible and efficient way to reduce the volume, weight and cost of the wireless communication systems.

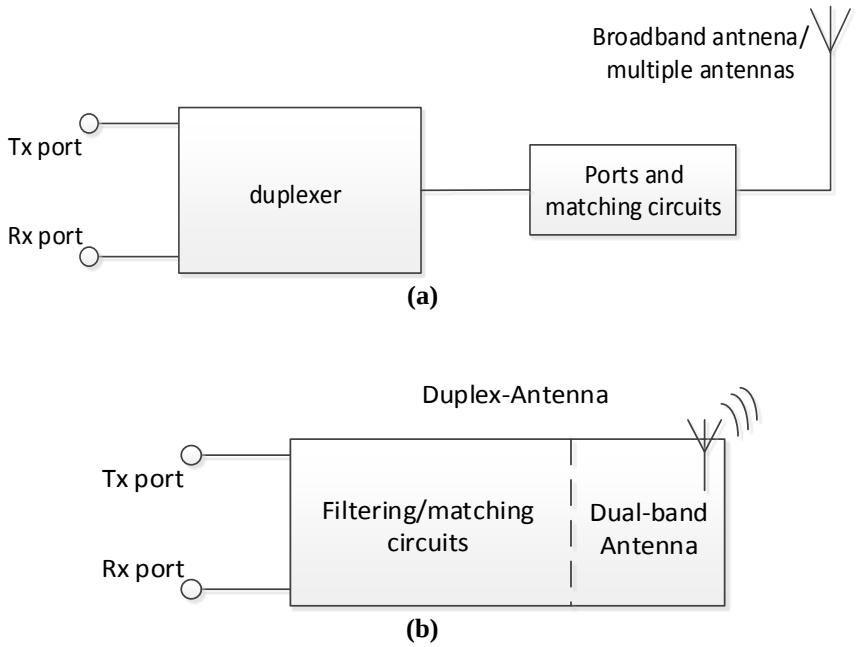

Figure 5.1 The block diagrams of (a) traditional cascaded subsystem; (b) integrated duplex-antenna subsystem.

In this chapter, a highly integrated multi-functional device based on integrated filtering antennas is investigated. The device has the functions of duplexing, filtering and radiation simultaneously. Figure 5.1 presents the block diagrams of a traditional cascaded wireless subsystem and the proposed integrated duplexing antenna subsystem. For the traditional cascaded subsystem, a duplexer with high isolation between the Tx and Rx ports is required

for reducing the channel interference and protecting the receiver module [170]-[171]. To date, many duplexers with high isolation over 30 dB have been reported, but they have a complicated configuration or 3-D structure, which make them are not very suitable for integration with other components. As for the radiation section, multiple antennas can be used to cover the uplink and downlink bands independently. However, to save the space, a broadband antenna with a duplexer is always preferable.

The concept of integration of the passive components provides a feasible method to achieve a dual- or triple-port antenna with integrated filtering and duplexing/triplexing functions. In [172], a triplex-antenna has been reported by exciting multiple modes of the antenna. However, the three bands of the triplex-antenna are widely separated in frequency, and the polarizations are different at the different bands, which is undesirable in practical applications. It is worthwhile to investigate the integration of the duplexer and antenna with the closely located frequency bands and uniform polarization. In this chapter, a novel highly integrated duplexing antenna system is proposed. Based on filtering antenna design methods presented, the antenna, duplexer and filters can be integrated seamlessly by electromagnetic coupling directly without the use of 50 Ω inter-connections and matching networks, as shown in Figure 6.1(b). Different with the conventional cascaded duplexer-antenna, the proposed duplexing antenna not only makes the RF frontend more compact and integrated, but also improves the frequency responses of system due to removal of the matching circuits and interfaces.

Another important applications of the integrated duplexing antenna is in intelligent transportation systems (ITS), which will significantly influence our future daily life as it could provide lots of applications associated with traffic safety and traffic efficiency. As the key area in vehicular communication systems, highly integrated duplexing antennas play an important role in realizing the direct information exchange between vehicles. Since the RF frontends will support the transmission and reception of the signals between vehicles and the requirements of the vehicular-based communications are usually different from the traditional wireless communications, it is worthwhile to pay more attention to the research on the vehicular-based RF frontends [173].

In this chapter, the duplexing filtering antenna elements and arrays are proposed based on different applications. Due to the high integration design methods, the antennas shows the improved frequency responses in terms of frequency selectivity, bandwidth, and radiation characteristics. Such a multifunctional component could significantly reduce the volume and potential cost of the RF front end systems.

5.2 Planar Duplexing Antenna for Wireless Communications

Highly integrated RF modules with a compact size and multiple functions are increasingly demanded in modern wireless communication applications for the purpose of reducing the size, mass and cost of the RF systems. The integration of passive components such as filters, power dividers, duplexers and antennas in the RF front-end has attracted intensive research interests in the past several years and lots of filtering antennas with compact size, enhanced bandwidth and excellent frequency selectivity have been reported. In this section, an integrated design by using the 2nd-order resonant characteristics of a junction resonator and the coupled hairpin-patch antenna is investigated. Such a design results in a higher order (4th-order) filtering performances for each channel with only two single-mode resonators in each filtering path. This integrated design provides a feasible way to achieve an improved duplex-antenna with a compact size.

5.2.1 Topology and Integration Approaches

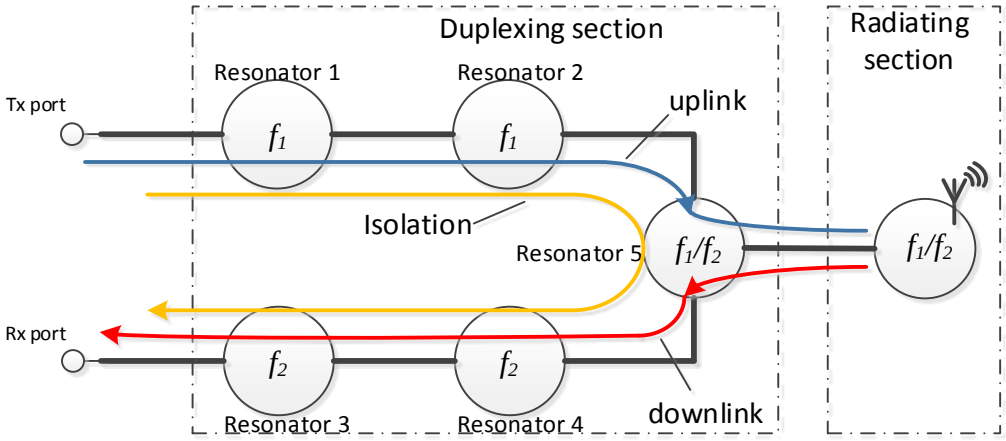

Figure 5.2 Topology of the all-resonator based integrated duplex-antenna.

Based on the architecture in Figure 5.1(b), a two-port all-resonator based highly integrated duplexing antenna is proposed. Such a device combine multiple functions such as filtering, duplexing and radiation. Figure 5.2 shows the topology of the duplexing antenna. The duplexing function is realized by two sets of single-mode resonators as the channel filters, which are combined using a dual-mode resonator at the junction between the channel filters and the dual-band antenna. The junction resonator as well as the antenna exhibit dual-mode resonant characteristics at f_1 and f_2. So the duplex-antenna is essentially formed of 4th-order filters for each channel and merged at Resonator 5 and radiating section. The transmitting path contains the Resonator 1 and 2, the f_1 mode of the dual-mode Resonator 5 and

the f_1 band of the antenna. The receiving path contains the rest of the resonators, the second mode f_2 mode of the junction resonator and antenna. A unique feature of this design is that the duplex-antenna is formed exclusively of coupled resonators without the use of separated duplexers, antennas and inter-connections matching networks between them. This effectively forms a multi-port filtering network with all of the resonators and radiating elements contributing to the bandwidth and frequency selectivity.

The isolation between the transmitting and receiving ports is realized by the path of resonators as shown in Figure 5.2. The isolation can be further improved as the orders of the two filtering channels are increased, namely more resonators are used in the uplink and downlink paths. It is also noted that the isolation will be deteriorated as the two channels much closely located. This problem can be overcome by introducing transmission zeros between the two bands.

In this design, the uplink and downlink frequencies of 2.58 and 2.88 GHz are chosen as a demonstrator for potential wireless communication applications. It should be noted that the operating frequencies can be changed according to the requirements of applications. To assist with the synthesis and design, such a filtering network can be represented by two coupling matrices. For the 4^{th}-order transmitting channel with the central frequency f_1 = 2.58 GHz, bandwidth BW = 120 MHz and return loss RL = 10 dB, the coupling matrix for a Chebyshev response is obtained as M_{12} = M_{34} = 0.0332, and M_{23} = 0.0278. The external quality factor is Q_{ex1} = 34.9. As for the receiving channel with the central frequency f_2 = 2.88 GHz, bandwidth BW = 110 MHz and return loss RL = 10 dB, the coupling matrix is M_{12} = M_{34} = 0.0273, M_{23} = 0.0228 and Q_{ex2} = 42.6.

5.2.2 Planar Duplexer

Figure 5.3 shows the configuration of the proposed duplexer, which is composed of two sets of split ring resonators and a SLR. The method of using a dual-band split ring resonator as the junction section of the duplexer has been proposed in [174]. Such design can reduce the size of the duplexer. In this design, the SLR is used as the junction section which is fed by a common port (Port 3). The port 1 is assumed for transmitting and the port 2 for receiving. The split ring resonator is a half wavelength resonator and the SLR can be analyzed using odd- and even-mode method [175]. The T-shape folded stub is adopted for compactness. Such a SLR offers more degrees of freedom in tuning its two resonant frequencies to match with the two groups of split ring resonators. The duplexer is printed on the Rogers 4003 substrate with a dielectric constant of 3.55 and dielectric loss tangent of 0.0027. All

the simulations were performed using HFSS 15 and the geometry parameters of the duplexer are listed in Table 5.1.

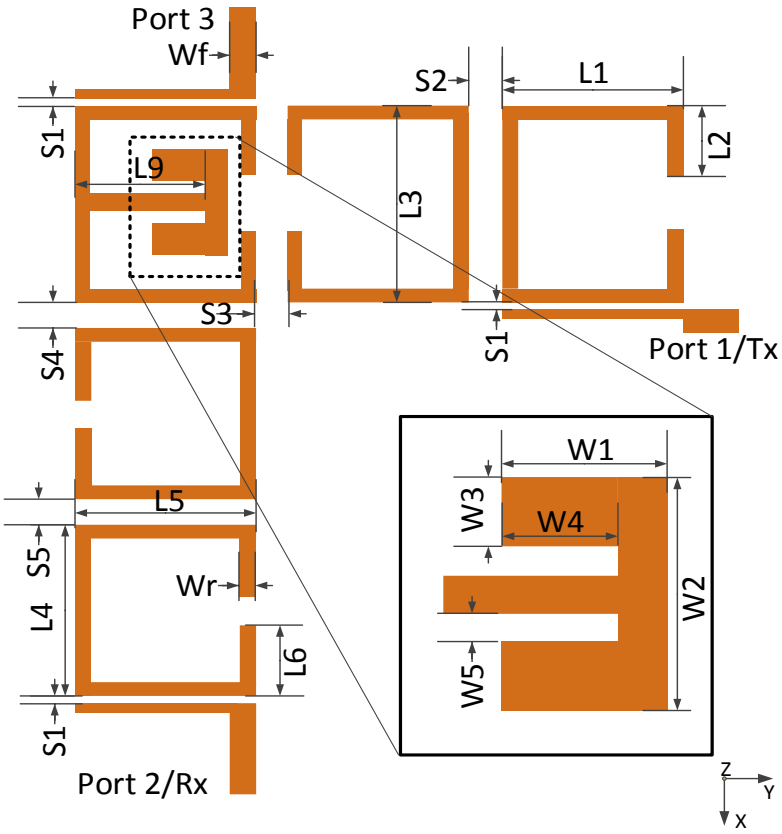

Figure 5.3 The layout of the all-resonator based duplexer with a dual-band SLR resonant junction.

Table 5.1 Parameters of The Proposed Antenna: (MM)

L1	*L2*	*L3*	*L4*	*L5*	*L6*	*L7*	*L8*	*L9*
10	3.5	11.4	9.4	10	3	10	8.4	6.5
S_L	*Wf*	*Wr*	*W1*	*W2*	*W3*	*W4*	*W5*	*Ws*
13.5	1.8	1	4	6	2	2.5	0.5	1
S1	*S2*	*S3*	*S4*	*S5*	*S6*	*Patch_L*	*H1*	*H2*
0.25	1.6	1.15	1.3	1.45	0.9	26.6	0.813	2.34

As the duplexer is an intermediate design towards the duplex-antenna, it was not fully optimized. Figure 5.4 shows the simulated S-parameters of the duplexer. It is observed that the duplexer has a passband of 2.48-2.63 GHz between port 1 and port 3 and a passband of 2.8-2.9 GHz between port 2 and port 3. The isolations between the port 1 and 2 in the two bands are over 32 dB and 35 dB, respectively.

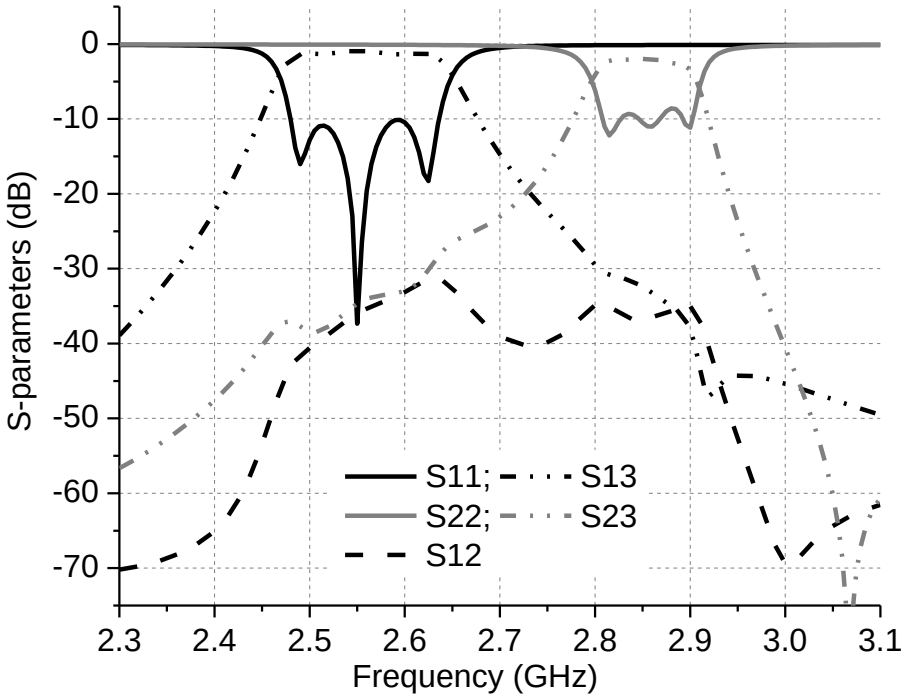

Figure 5.4 The simulated S-parameters of the proposed duplexer.

5.2.3 Dual-Band Patch Antenna

To facilitate the radiation at two closely located frequency bands, traditional broadband or multi-band antennas are usually used to cover the two frequency bands of the duplexer simultaneously. Multiple-band antennas have been achieved by adopting multiple patches or splitting slots in the patches. However, these antennas are less favorable for the purpose of integrating the antenna with the duplexer. In addition, it is difficult to maintain a uniform radiation direction and polarization at the two bands. The isolation between the two operation bands is another challenging task.

To achieve the dual-band unidirectional antenna with consistent polarization at the two frequency bands using a single patch, a novel antenna is proposed based on a coupled resonator and patch. Figure 5.5(a) shows the configuration of the proposed hairpin-fed patch antenna, which has a stacked configuration. The patch is printed on the top layer of the upper substrate, while the hairpin resonator is printed on the bottom layer of the lower substrate. The patch and the resonator share the same ground plane in the middle layer, where a slot is cut to enable coupling between them. Due to the high-Q value and resonant characteristics, the patch can be treated as the last-order half-wavelength resonator. As a result, this coupled hairpin-patch can be equivalent as a 2^{nd}-order resonant circuit, as shown in Figure 5.5(b).

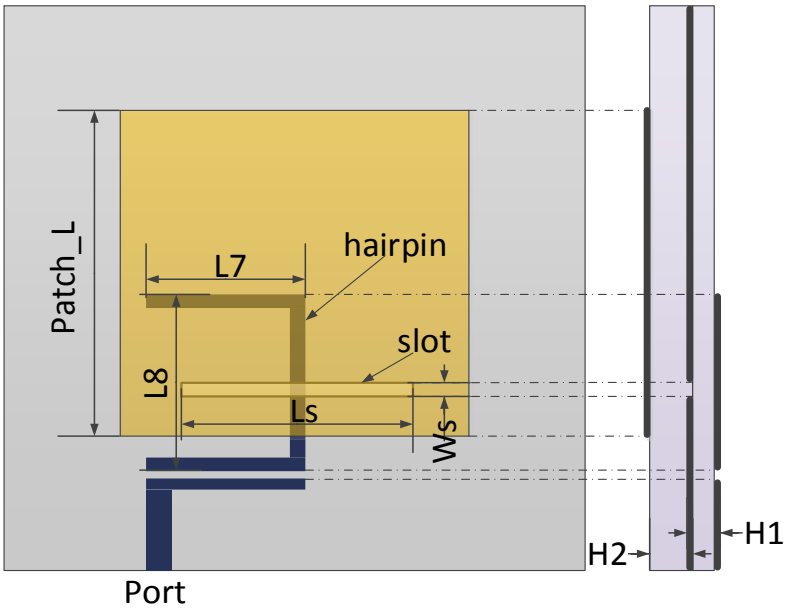

(a)

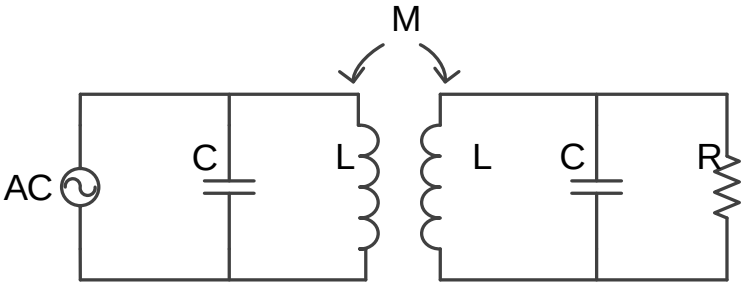

(b)

Figure 5.5 The dual-band hairpin-patch antenna: (a) configuration, (b) equivalent circuit diagram.

The operation mechanism of the dual-band hairpin-patch antenna can be explained based on the 2nd-order resonant circuit. The hairpin resonator is a half wavelength resonator, which is equivalent to a shunt *LC* resonant circuit. The patch antenna, however, is modelled using a shunt *RLC* resonant circuit, where *R* represents the radiation resistance. The resonant frequencies of the *LC* circuit and the *RLC* circuit can be controlled by tuning the dimensions of the hairpin and the patch. The slot in the ground plane provides the coupling *M* between the hairpin and the patch. When the patch and the hairpin resonator are synchronously tuned at the same frequency, the 2nd-order resonant characteristics with two poles at different frequencies can be achieved. By properly adjusting the coupling strength between the hairpin and the patch, these two resonant frequencies can be controlled. Different from the traditional patch antenna with the single-mode characteristics, the proposed hairpin-fed patch antenna has the dual-band operations.

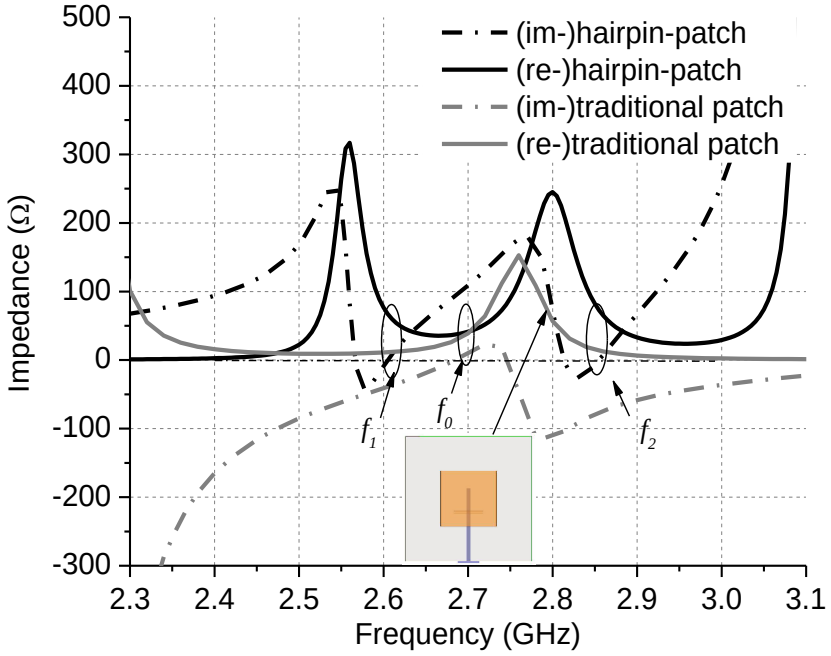

Figure 5.6 Simulated input impedance of the hairpin-patch antenna in comparison with a traditional patch.

Figure 5.6 shows the simulated imaginary and real part of the input impedance of the dual-band hairpin-patch antenna in comparison with a traditional patch antenna. It is observed that the traditional patch has only one resonant frequency f_0 at 2.7 GHz. However when the patch is fed using a hairpin resonator, two resonant frequencies f_1 and f_2 can be achieved at 2.6 and 2.88 GHz. The 2nd-order resonant characteristics of the coupled hairpin-patch enable a single patch to radiate at two distinct frequency bands while maintaining the uniform radiation characteristics. This dual-resonant feature make it possible to couple the hairpin-patch with the two channels of the duplexer.

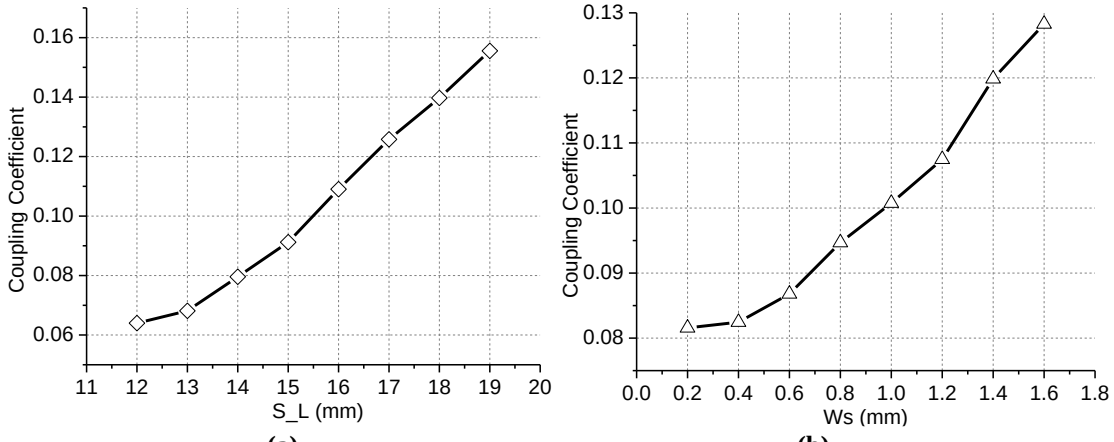

(a) **(b)**

Figure 5.7 Coupling coefficients as a function of the dimension of the slot: (a) length, (b) width.

The coupling slot in the ground is placed perpendicularly near the center of the hairpin resonator, where the current peaks and magnetic coupling is dominant [148]. The dimensions of the slot play an important role in controlling the coupling strength between the patch and the hairpin resonator. The coupling coefficient m_{ij} can be derived from [148]. Using full-wave simulations, the coupling coefficient m_{ij} can be obtained. Figure 5.7 shows the coupling coefficients as a function of the length and width of the coupling slot. As can be observed, the coupling coefficient increases as the length or the width of the slot increase.

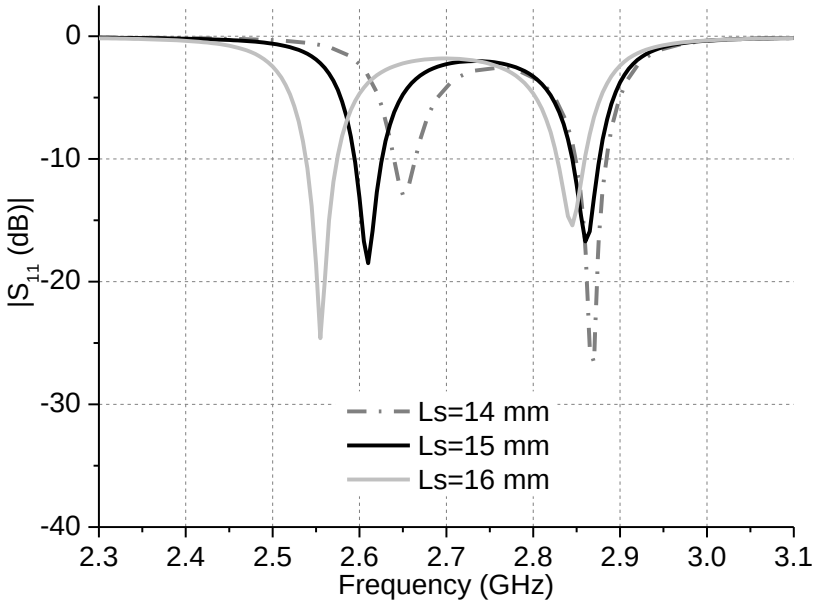

Figure 5.8 The variation of simulated S_{11} of the hairpin-patch with different lengths of the slot.

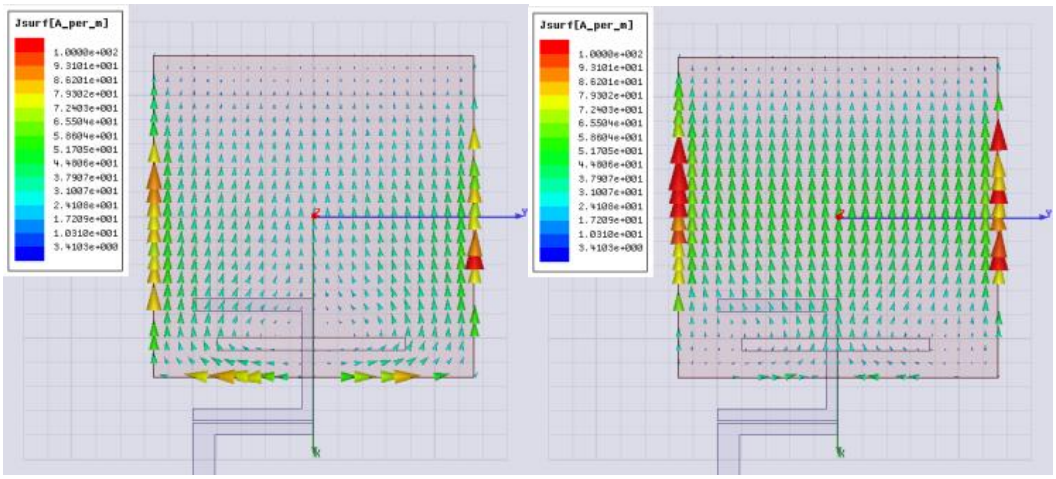

(a) **(b)**

Figure 5.9 The simulated current distribution: (a) 2.6 GHz, (b) 2.88 GHz.

It is observed from Figure 5.8 that the spacing between the two resonant frequencies increases when the length of the slot increases from 14 mm to 16 mm. It is also noted but not shown here that the width of the slot has a similarly effect. Figure 5.9 shows the current

distributions of the dual-band patch antenna at 2.6 and 2.88 GHz, respectively. It is observed that the patch operates in the fundamental mode (TM_{01}) at both resonant frequencies. The current at the two frequencies distributes along the same direction with the maximum at the central part of the patch. The current distribution on the patch determines a uniform polarization when the antenna operates in uplink and downlink modes.

5.2.4 Integrated Duplexing Antenna

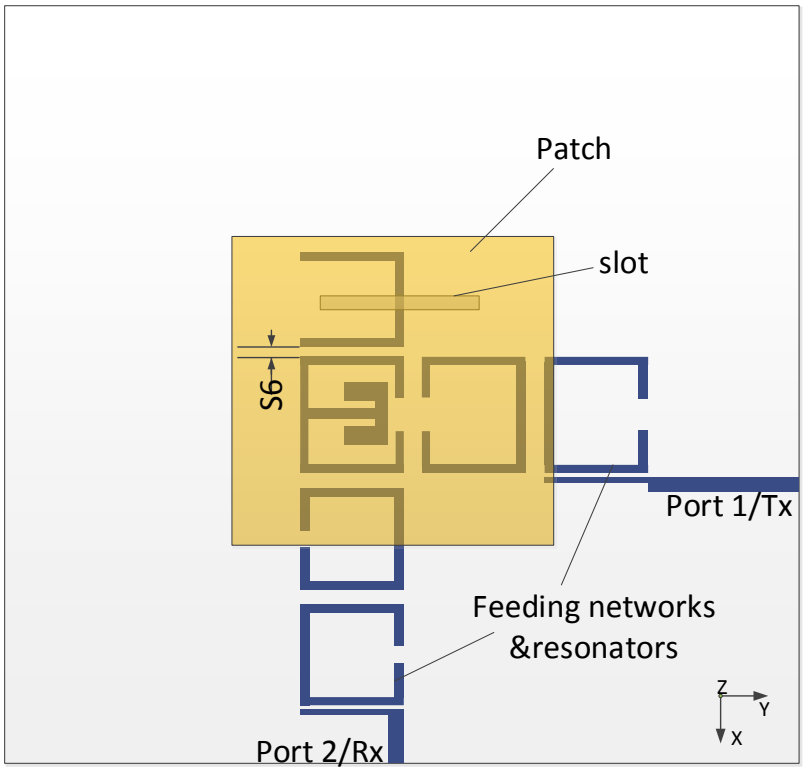

Figure 5.10 Configuration of the proposed integrated duplexing filtering antenna.

Figure 5.10 shows the configuration of the proposed duplexing filtering antenna. The antenna is achieved by removing the ports and the transmission lines between the duplexer and the hairpin-fed dual-band patch antenna and coupling them together through electromagnetic. This results in a high integration that the duplexing and the radiating components are seamlessly combined together. To obtain the impedance matching performance at both bands, the center frequencies of the two channels of the duplexer and the dual-band antenna must be matched well. Then, by tuning the coupling strength between the SLR and the hairpin at its optimal, good impedance matching performance can be achieved.

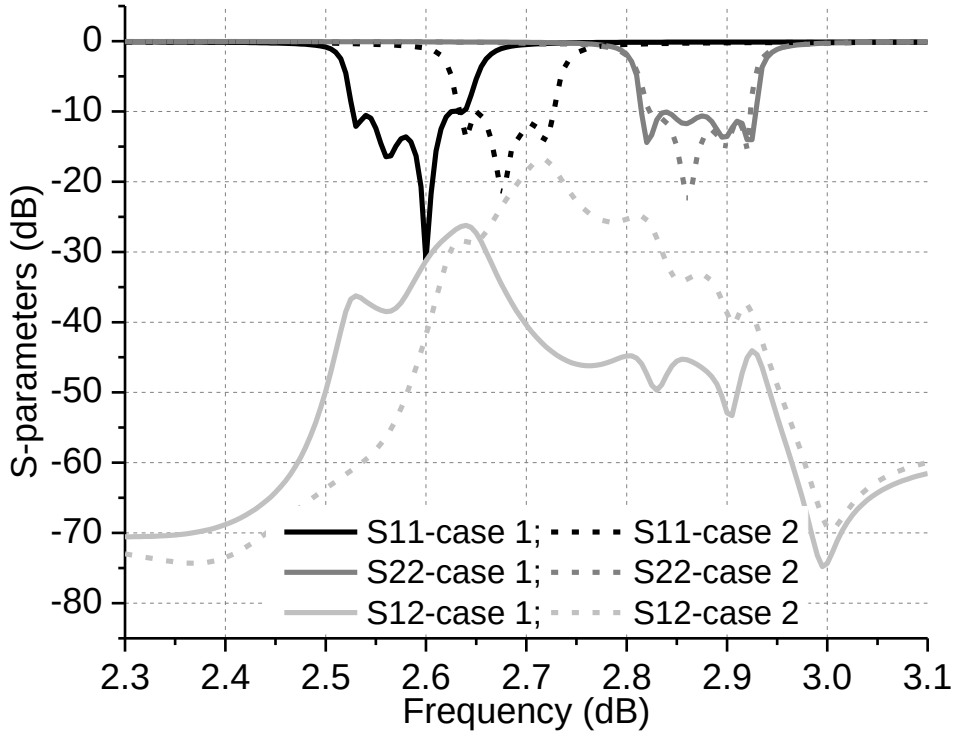

Figure 5.11 Comparison of simulated S-parameter between the two duplexing antenna Case 1 and Case 2.

It should be noted that the isolation between the two ports will be deteriorated as the two bands closely located as the isolation is achieved by using the different resonant frequencies of the two filtering channels. To illustrate these issues, two examples with different bandgaps were investigated: Case 1, the center frequencies of the low-band and high-band are 2.58 GHz and 2.88 GHz respectively with the bandgap of 180 MHz; Case 2, the center frequencies are 2.68 and 2.88 GHz and the bandgap is only 90 MHz. By tuning the resonant frequencies of the resonators and the coupling strengths between them, the duplex-antenna with different channels (the two cases) were achieved, as shown in Figure 5.11. It can be seen that the duplexing filtering antenna with a narrower bandgap (Case 2) exhibits a worse isolation performance (-17 dB vs -27 dB).

5.2.5 Results and Discussion

The proposed duplexing filtering antenna was prototyped to verify the design concept. Figure 5.12 shows the top and bottom layers of the duplexing antenna prototype. The antenna has a network as the feed on the bottom, which is composed of six coupled resonators. On the front side, a normal square patch is printed on the top. These resonators and patch form an eight-pole filtering network. In each channel, multiple poles can be realized, which

is confirmed by the simulation and measurement results in Figure 5.13. In this integrated design, the stub-loaded resonator not only combines the transmitting and receiving channels, but also couples to the hairpin-patch antenna.

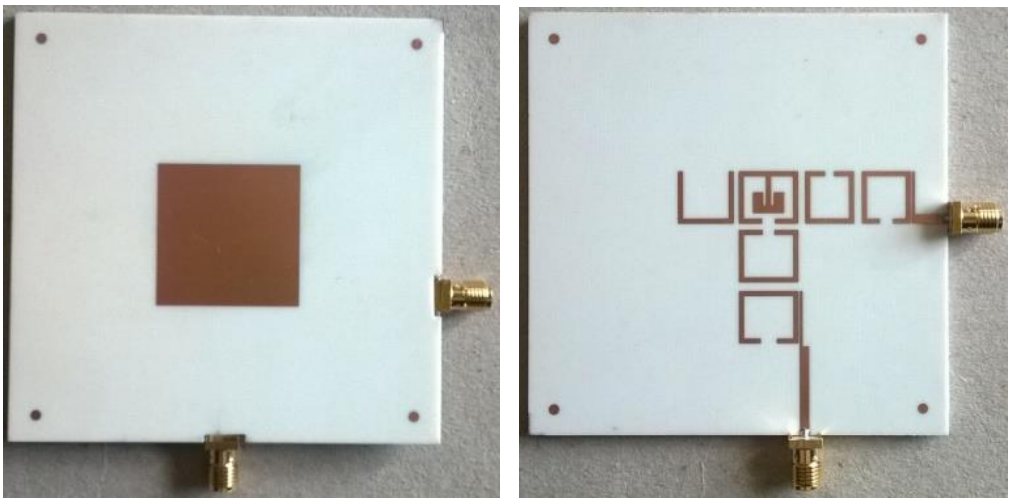

(a) **(b)**

Figure 5.12 The prototype of the proposed highly integrated duplexing filtering antenna: (a) top layer, (b) bottom layer.

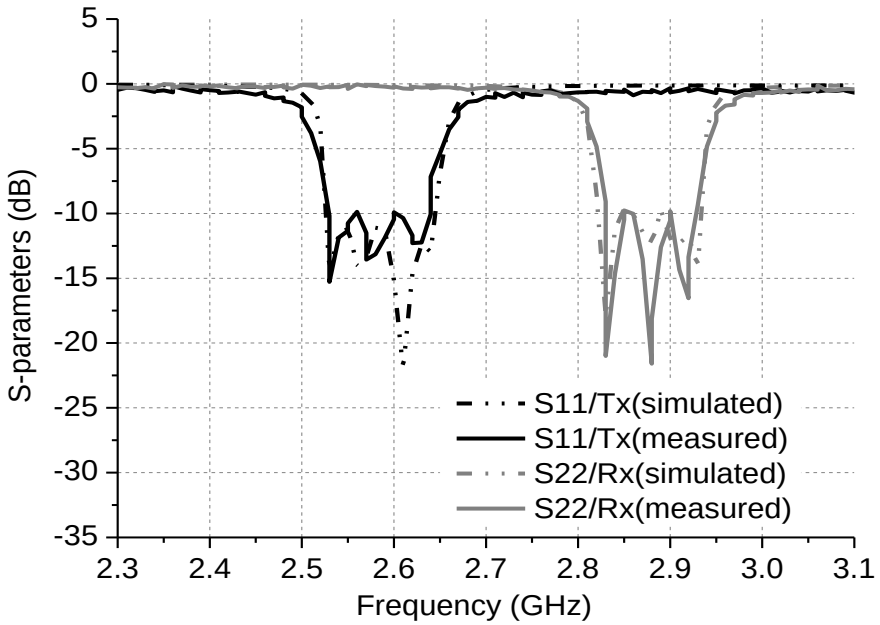

Figure 5.13 The simulated and measured S-parameter of the duplexing antenna.

The simulated and the measured reflection coefficients are shown in Figure 5.13. As can be observed, the measured results agree well with the simulated ones, showing an uplink operating band from 2.52 to 2.65 GHz (FBW = 5%) and a downlink band from 2.82 to 2.93 GHz (FBW = 4.2%). It is also observed that four poles can be identifiable in both bands. Compared with the two bands of the standalone antenna in Figure 6.8, the bandwidths are

significantly increased from 1.2% to 4.2%. The duplexing antenna also exhibits a good filtering performance with a sharp skirt from out-of-band to in-band and a guard band between the two channels. These improved features are attributed to the integrated design that all resonators and the patch contribute to the bandwidth enhancement and the filtering improvement. Besides, this co-design is also beneficial to reduce the footprint of the system. The small difference between the simulated and measured results is attributed to the fabrication and test errors.

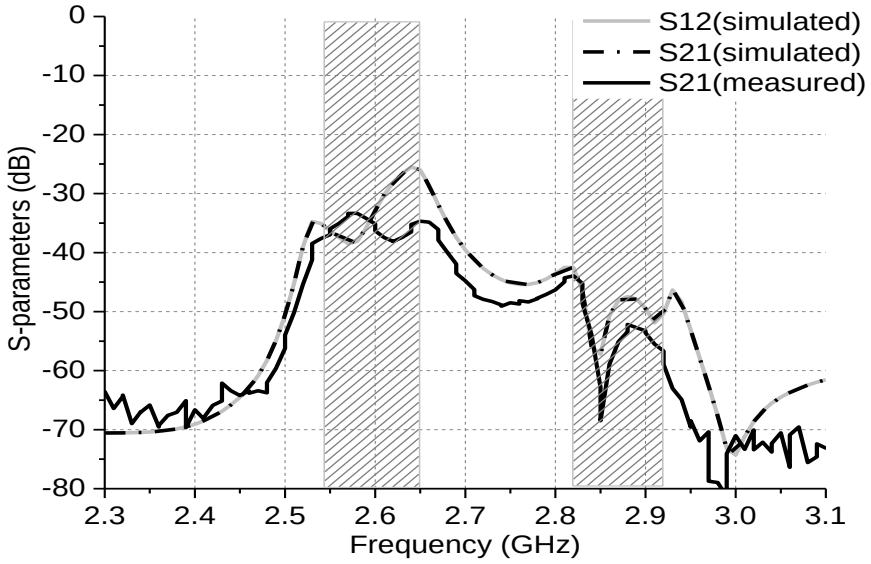

Figure 5.14 Simulated and measured isolation of the duplex-antenna.

The simulated and measured inter-channel isolation S_{21} of the duplexing antenna are presented in Figure 5.14. The measured results agree well with the simulated one, showing a good isolation of over 32 dB in the uplink channel (2.52 to 2.65 GHz) and over 42 dB in the downlink frequency band (2.82 to 2.93 GHz).

Figure 5.15 shows the simulated and measured 2.6 GHz normalized radiation patterns in two orthogonal planes when the port 1 was excited and the port 2 was terminated with a 50 Ω load. The measured results agree well with the simulated ones. The duplexing antenna exhibits a maximum radiation in the broadside direction with the polarization in X-axis. The measurements show that the cross polarization discrimination (XPD) is over 20 and 25 dB in $\varphi = 0^o$ and $\varphi = 90^o$ planes, respectively. Figure 5.16 shows the normalized simulated and measured radiation patterns at 2.88 GHz when the port 2 was excited and the port 1 was terminated with a 50 Ω load. The radiation patterns also exhibit a maximum radiation in broadside direction. The measured XPD is over 30 dB and 28 dB in in $\varphi = 0^o$ and $\varphi = 90^o$ planes, respectively. The small discrepancy between the simulated and measured patterns may be attributed to the setting tolerance of the rotator and the influences of the cables.

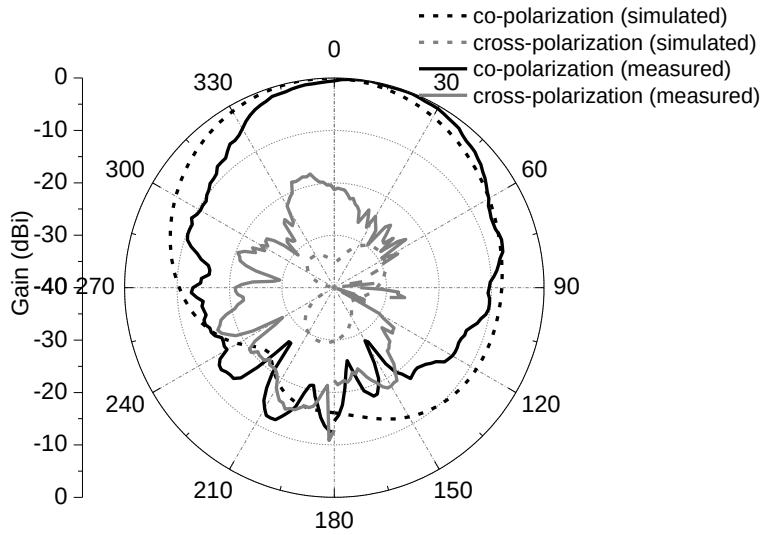

(a)

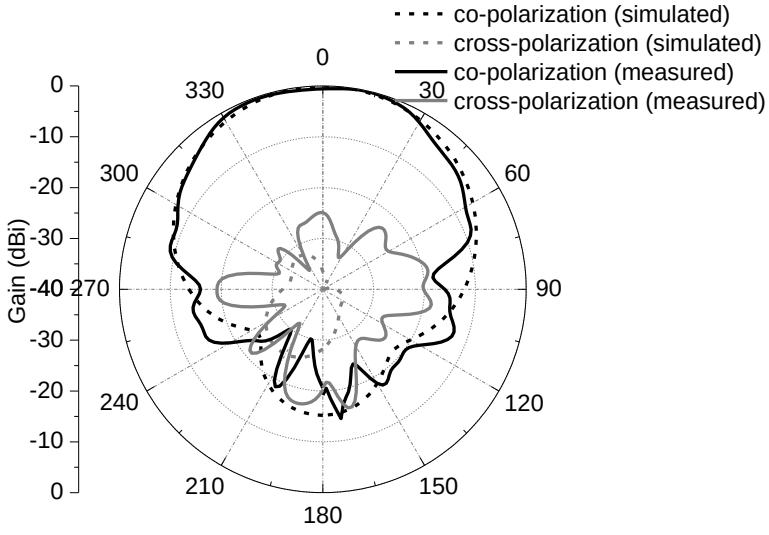

(b)

Figure 5.15 The normalized radiation patterns at 2.6 GHz when port 1 is excited: (a) $\varphi=0^0$, (b) $\varphi=90^0$.

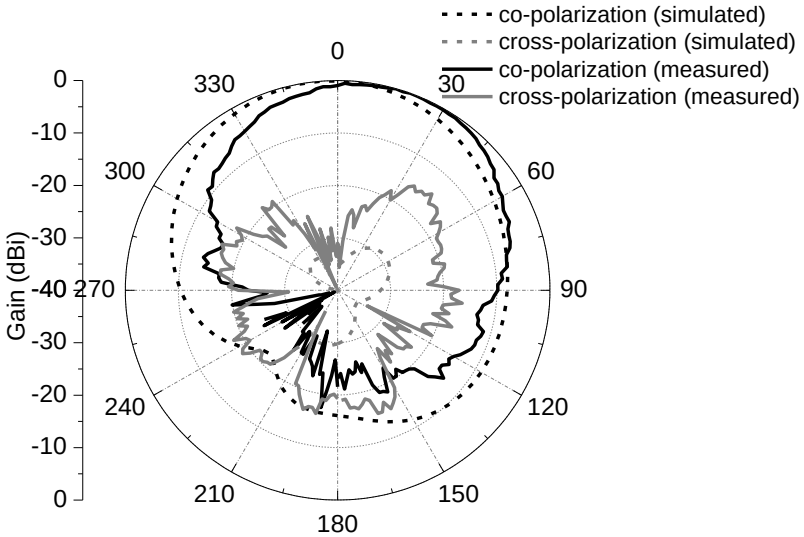

(a)

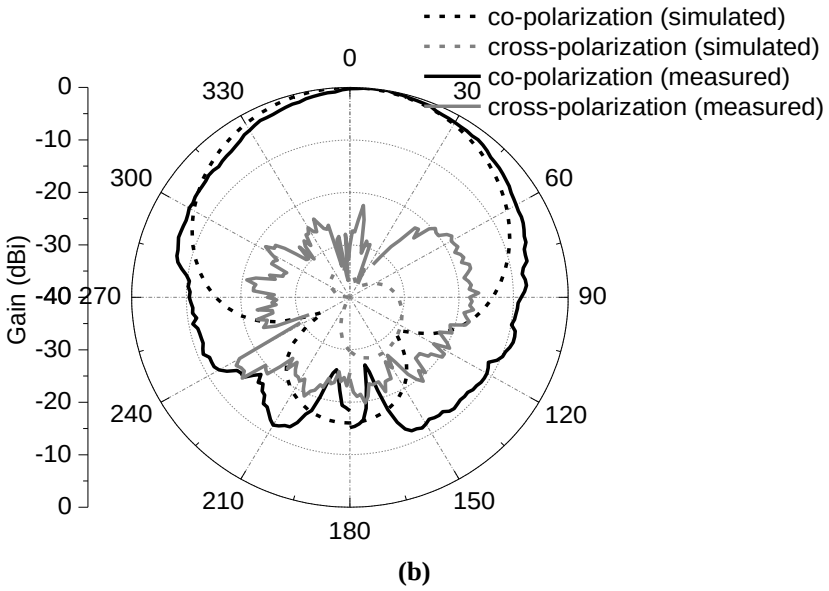

(b)

Figure 5.16 Normalized radiation patterns at 2.88 GHz when port 2 is excited: (a) φ=0⁰, (b) φ=90⁰.

Figure 5.17 shows the simulated and measured antenna gains when the two ports of the antenna are respectively excited. As can be observed, the proposed duplexing antenna has a flat gain response of about 5 dBi from 2.52 to 2.64 GHz (uplink) when port 1 is excited. The gain sharply drops to below -20 dBi as the frequency shifts to below 2.5 GHz or above 2.7 GHz. This gain is suppressed to below -22 dBi in the band of downlink. When port 2 is excited (downlink), the antenna has a stable gain about 4.5 dBi from 2.82 to 2.93 GHz. The gain is suppressed to below -19 dBi in the uplink operation band. These results reveal a good isolation is achieved between the uplink and downlink channels.

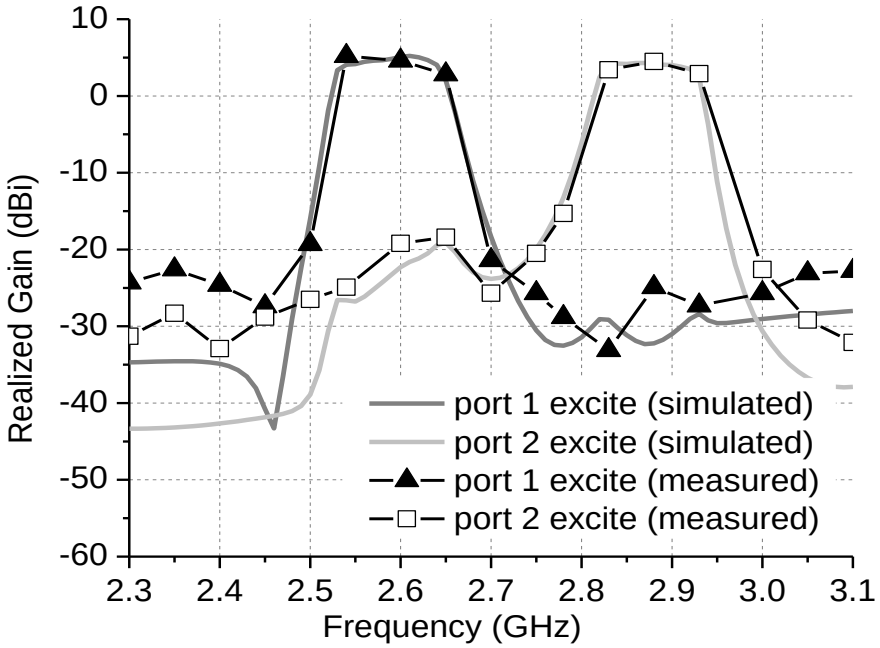

Figure 5.17 Simulated and measured antenna gains of the proposed duplexing antenna.

5.3 High-Integration Full-Duplex Tx/Rx Array Antennas

The integration of the passive RF components can be utilized to effectively reduce the complexity of the RF frontends while providing an improved frequency response. However, these reported works did not fully consider the requirements of full-duplex operation and compactness in the future vehicular communication. The proposed duplexing antenna element in Chapter 5.2 has a considerable large footprint, and it is not suitable for array antenna applications in ITS. In this section, the work in Chapter 5.2 is further developed and a novel compact high-integrated full-duplex Tx/Rx antenna with improved frequency selectivity, channel isolation and out-of-band rejection is proposed. To improve the gain, two antenna arrays are also conceived and investigated.

5.3.1 RF Frontend Architectures and Specifications

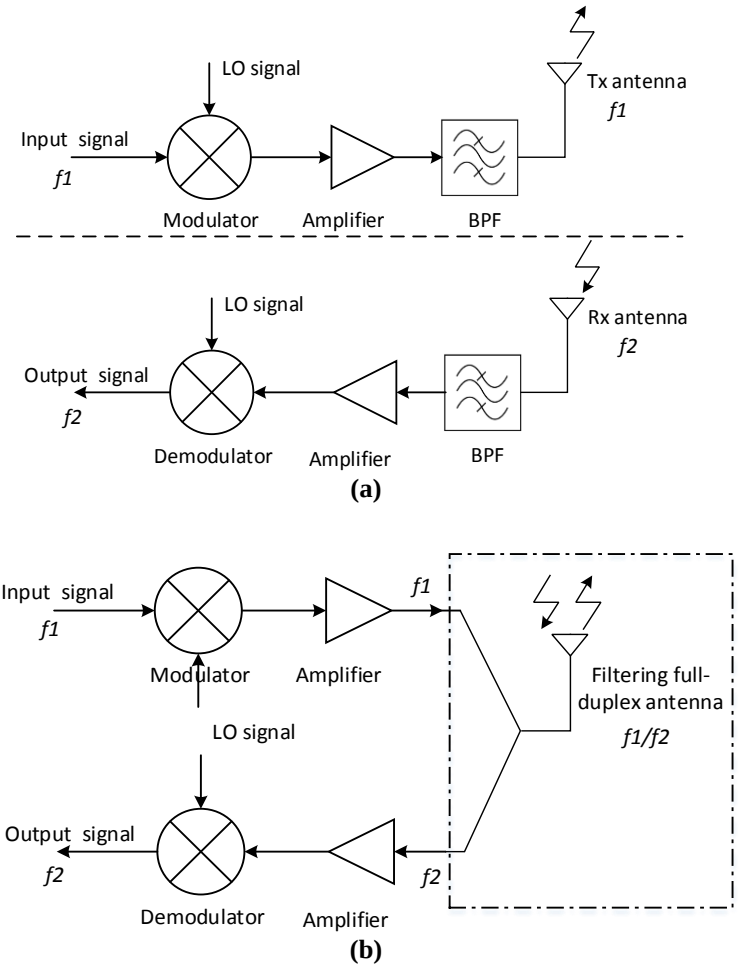

Figure 5.18 Block diagrams of (a) traditional separated Rx/Tx systems, (b) proposed integrated Rx/Tx system.

To support the full-duplex Rx/Tx operations in vehicular communications while reducing the interferences between the Rx/Tx channels, two different frequency bands are usually used in receiving and transmitting modules. Figure 5.18 compares the block diagrams of a conventional separated Rx/Tx systems with the proposed integrated Rx/Tx system. For the conventional system, as shown in Figure 5.18(a), the Rx and Tx system have two independent processing blocks at different frequencies. The input signal is modulated, amplified, filtered and then transmitted out; at the receiving module, the received signal is first filtered, amplified, demodulated and then output for processing. One of the disadvantages is that two groups of antennas and bandpass filters are required to facilitate the full-duplex operation, which leads to a bulky and complicated RF frontend at both vehicle and infrastructure sides.

Looking at the proposed block diagram in Figure 5.18(b), the Tx antenna and the Rx antenna are replaced by one novel dual-port full-duplex antenna, which can operate at f_1 and f_2 simultaneously while providing a high channel isolation between them. Furthermore, the separate bandpass filters and corresponding interfaces are removed due to the integrated filtering functions in the full-duplex antenna, as compared with the Figure 5.18(a). As a result, the weight, complexity and therefore the cost of the system can be significantly reduced. Such a full-duplex antenna is suitable for the applications in vehicular communications.

Table 5.2 Specifications of the full-duplex Antenna

Frequency bands	Uplink: *f1*=4.7 GHz; Downlink: *f2*=6 GHz
Fractional bandwidths	Low-band: 5.0%; high-band: 5.0%
Polarization characteristics	Vertical polarization
Isolation between bands	30 dB
Cross-polarization level	-30 dB
Gain fluctuation in-bands	± 0.5 dB
Inter-channel gain suppression	20 dB
Antenna element size	0.5λ × 0.5λ

The given specifications for the full duplex filtering antenna are listed in Table 5.2. The antenna works at C-band and the central frequencies for the uplink and downlink operations are 4.7 and 6.0 GHz, respectively. The fractional bandwidths (FBW) for both bands are required to be above 5%. The two operation bands are expected to have the consistent vertical polarization characteristics. An inter-channel isolation of 30 dB between the uplink and downlink is demanded. The antenna is also required to have a very polarization purity with the cross-polarization level lower than -30 dB at both operations. Additionally, flat gain

response (± 0.5 dB) in the passbands and high inter-channel gain suppression (20 dB) are required in this work. Moreover, in order to further conceive an array antenna, the duplex antenna element, including the two feeding/filtering channels should be confined in an area of 0.5 λ × 0.5 λ. These stringent specifications lead to a big challenge in the design.

5.3.2 Implementation of Dual-Port Full-Duplex Antenna Element

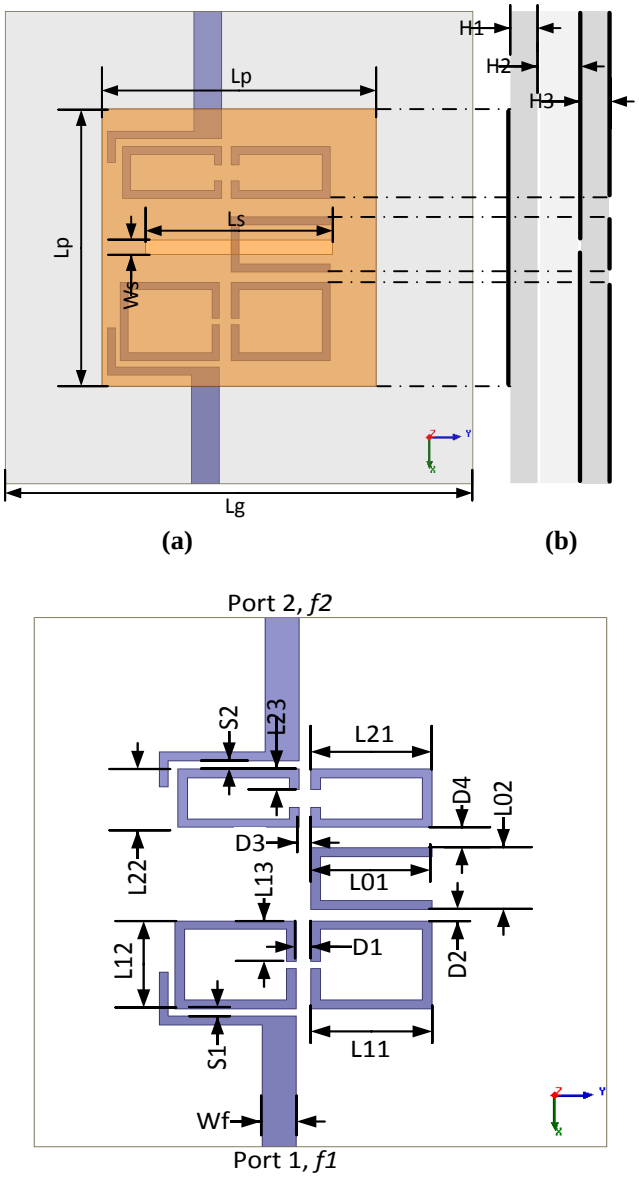

Figure 5.19 Configurations of the proposed dual-port full-duplex antenna element: (a) front view, (b) side view and (c) back view.

Figure 5.19 shows the configurations of the proposed dual-port full-duplex filtering antenna element. It has a stacked structure, which composes of two substrates and a thin Rohacell foam between them. Viewing from the front, the radiating element is a normal

square patch printed on the top layer of the upper substrate, as shown in Figure 5.19(a). The feeding networks and the resonators of the two channels are placed on the bottom layer of the lower substrate, as shown in Figure 5.19(c). There are two sets of open-loop resonators with different resonant frequencies (f_1 and f_2) adopted as the channel filters for the uplink and downlink operations. They are joined together by a hairpin resonator in the middle, which is coupled with the patch through a straight coupling slot in the ground. It should be noted that the hairpin and the patch are synchronically tuned to f_0 = 5.4 GHz, which is different from the f_1 and f_2 of the two filtering channels. The patch and the feeding structures/resonators share the same ground plane, which is printed on the top layer of the bottom substrate. Such configuration not only makes the design more integrated but also reduce the adverse interference between the radiation unit and the feeding structures/resonators.

In this work, half wavelength resonators (open-loop and hairpin) are used for realizing the filtering channels. The relationship between the lengths of the resonators and the resonant frequencies can be approximately calculated using the following equations,

$$2 \cdot (L_{11} + L_{13}) + L_{12} \approx \frac{c}{2 \cdot f_1 \sqrt{\varepsilon_r}} \qquad \text{(Eq.6.1)}$$

$$2 \cdot (L_{21} + L_{23}) + L_{22} \approx \frac{c}{2 \cdot f_2 \sqrt{\varepsilon_r}} \qquad \text{(Eq.6.2)}$$

$$2 \cdot L_{01} + L_{02} \approx \frac{c}{2 \cdot f_0 \sqrt{\varepsilon_r}} \approx L_p \qquad \text{(Eq.6.3)}$$

where c is the speed of the light in free space, ε_r is the effective permittivity. f_1 = 4.7 GHz and f_2 = 6 GHz are the central frequencies of the two operations, respectively. f_0 = 5.4 GHz is the resonant frequency of the hairpin and the patch. Simulations and optimizations were performed using High Frequency Structural Simulator (HFSS) and the optimized dimensions are presented in Table 5.3.

Table 5.3 Parameters of the Proposed Antenna: (MM)

Lp	*Lg*	*Ls*	*Ws*	H_1	H_2	H_3	*Wf*	L_{01}
17.6	50	12	0.9	0.813	1	0.813	1.8	6.35
L_{02}	L_{11}	L_{12}	L_{13}	L_{21}	L_{22}	L_{23}	S_1	S_2
3.5	6.35	5	2.3	6.35	3.3	1.15	0.4	0.4
D_1	D_2	D_3	D_4					
0.75	0.65	1.15	0.6					

5.3.3 Topology and Coupling Matrix

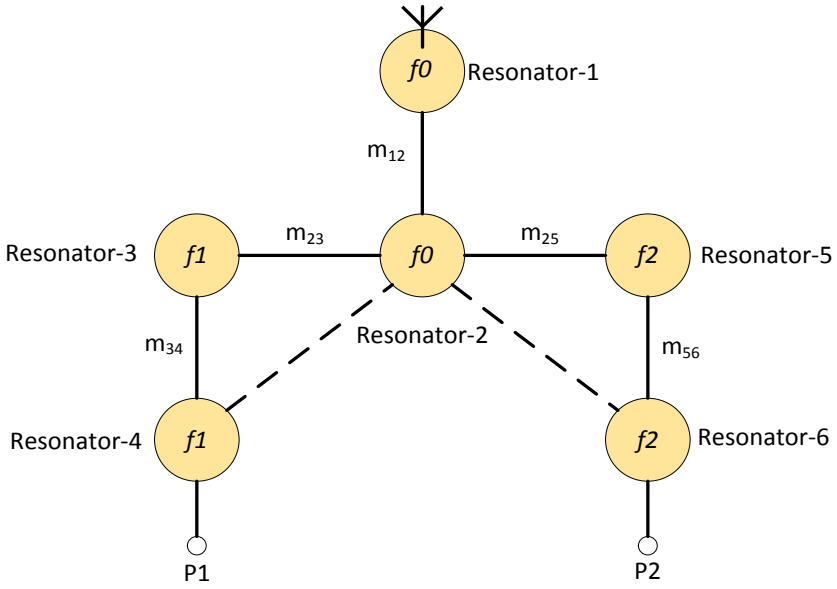

Figure 5.20 Topology of the proposed dual-port full-duplex antenna.

The full-duplex antenna in Figure 5.19 can be represented using a coupled-resonator network, as shown in Figure 5.20. The circles represent single-mode resonators whereas the lines represent the coupling between them. It should be noted that the radiating patch (Resonator-1) also serves as the last order single-mode resonator of the network. The proposed duplexing antenna is essentially an all-resonator based duplexer with its common port is a radiator. The hairpin, as the junction resonator, joins the two sets of resonators as the channel filters. The patch and the hairpin both resonate at around f_0. The coupled hairpin-patch can generate two separate resonant frequencies (f_1 and f_2) and both of them are coupled to the two filtering channels simultaneously. As a result, the duplexing antenna is formed and each channel presents 3rd-order filtering characteristics. It should be noted that cross-couplings are introduced between the resonator-2 and the resonator-4 (resonator-6), as indicated by the dash line in Figure 5.20. The cross-couplings are elaborately introduced to produce transmission zeros for improving the isolation between the two channels and out-of-band rejection, which will be discussed later. In this topology, three types of resonators with different resonant frequencies (f_0, f_1 and f_2) are highly integrated together, leading to a very compact device.

To guide the initial design, the coupling matrix is synthesized based on the topology in Figure 5.20. For simplicity, the weak cross couplings are ignored here. The optimization based synthesis method is used. For the 5% low-band centered at f_1 = 4.7 GHz, 5% high-

band centered at 6 GHz and the return loss of 10 dB, the following coupling matrix M is found [176]-[177],

$$M=\begin{bmatrix} 0 & 0.2546 & 0 & 0 & 0 & 0 \\ 0.2546 & 0 & 0.0586 & 0 & 0.0603 & 0 \\ 0 & 0.0586 & -0.2377 & 0.0405 & 0 & 0 \\ 0 & 0 & 0.0405 & -0.2466 & 0 & 0 \\ 0 & 0.0603 & 0 & 0 & 0.2356 & 0.0411 \\ 0 & 0 & 0 & 0 & 0.0411 & 0.2476 \end{bmatrix} \quad \text{(Eq.6.3)}$$

where m_{ij} represents the coupling coefficient between the resonator i and resonator j.

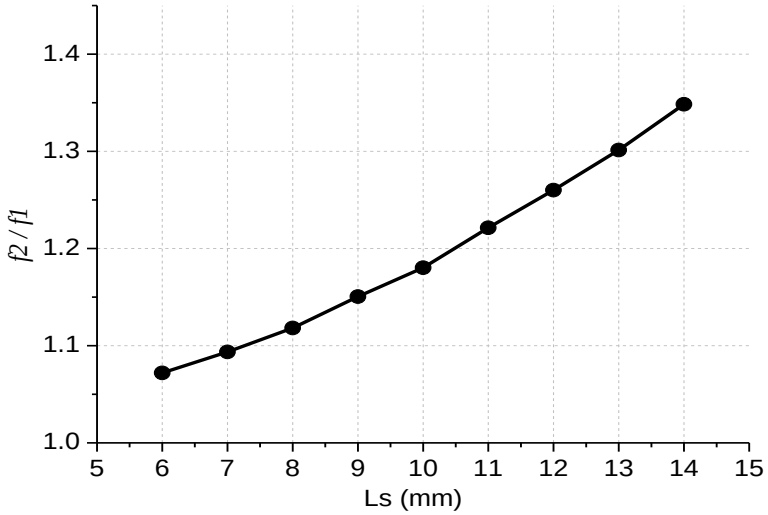

Figure 5.21 The frequency ratio (f_2 / f_1) of the dual-band antenna as a function of the lengths of the slot, *Ls*.

As can be observed in the coupling matrix, strong coupling exists between the patch and the hairpin resonator (m_{12} = 0.2546). This strong coupling helps to achieve dual-band impedance matching at the two designated operation bands while maintaining a consistent radiation polarization. Using full-wave simulation, the ratio of the two bands (f_2 / f_1) as the function of the length of the slot (*Ls*) is obtained and presented in Figure 5.21. By adjusting *Ls* and therefore the coupling strength between the patch and the resonator, the frequency ratio (f_2 / f_1) of the dual-band patch antenna can be tuned accordingly. When *Ls* is 6 mm, the two resonant frequencies are very close to each other (f_2 / f_1 = 1.07). The frequency ratio increases to more than 1.35 as *Ls* increases to 14 mm. It should be noted that the width of the slot has a similar effect on the two resonant frequencies, which is not presented here for brevity. To achieve the two frequency bands of 4.7 and 6 GHz in this design (frequency ratio is 1.28), *Ls* is determined to be 12 mm.

5.3.4 Cross-Coupling Study

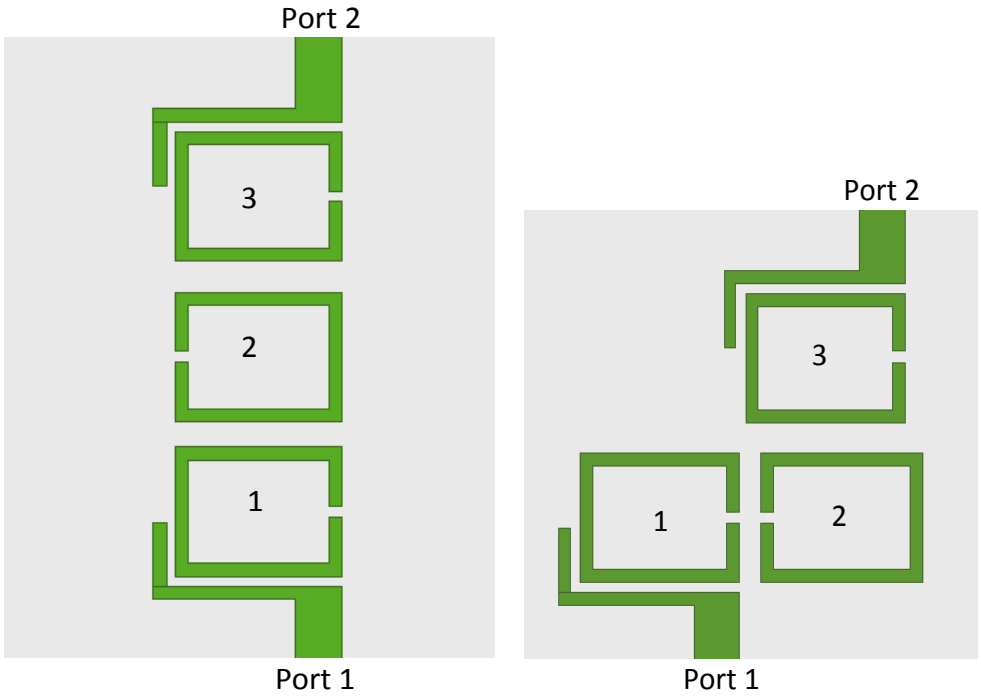

Figure 5.22 The configurations of two 3rd-order band-pass filters with different layouts: (a) cascaded, Type-I, (b) proposed, Type-II.

Traditionally, the isolation between the two input ports can be enhanced by using the higher order filtering channels, but this will inevitably increase the volume and insertion loss of the component. To keep a compact size, the 2nd-order filtering channels are adopted in this work, as shown in Figure 5.19. To further improve the isolation and out-of-band rejection of the duplexing filtering antenna while maintaining a compact size, cross couplings are resorted in this work to generate additional transmission zeros. To illustrate this concept, two configurations of 3rd-order bandpass filters with different layouts are investigated. As shown in Figure 5.22(a), the first one is a cascaded layout, denoted Type-I. Figure 5.22(b) shows the adopted resonator layout in this work (denoted as Type-II), where the cross coupling is introduced between resonator-1 and resonator-3.

Figure 5.23 compares the simulated S_{21} between the two bandpass filters prototypes in Figure 5.22. As can be observed, the Type-II filter has two transmission zeros at 4.18 and 5.22 GHz, which contributes to the improved frequency selectivity and out-of-band rejection. Compared with the Type-I filter, the attenuation at 4.2 GHz (5.2 GHz) is increased from 35 dB (26 dB) to 50 dB (42 dB). When the cross coupling configuration is used in the duplexing antenna design, the isolation between the two channels can be improved without

increasing its footprint. Figure 5.24 shows the simulated S_{21} of the proposed duplexing antenna as a function of the locations of the hairpin resonator, donated as *Ld* in the inset of Figure 5.24. The locations of the hairpin can be used to tune the cross coupling. It can be seen that the transmission zeros move to lower frequency as *Ld* increases.

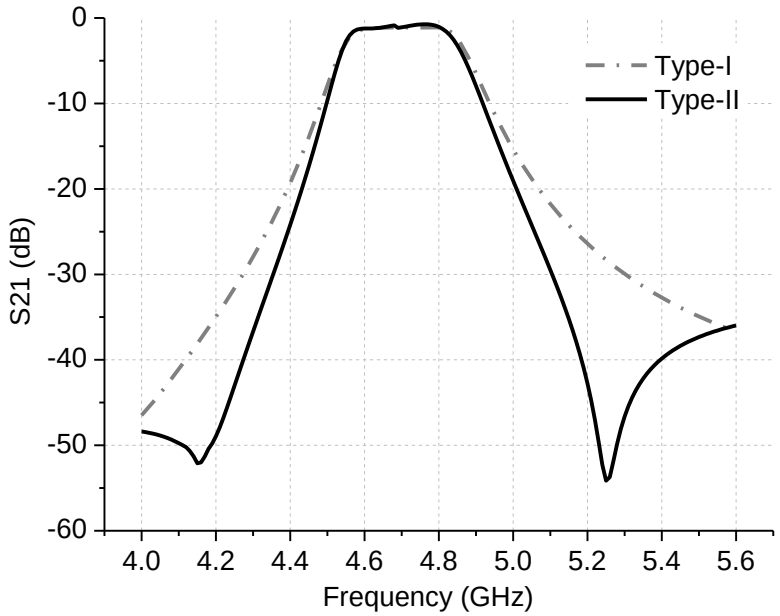

Figure 5.23 Comparison of transmission responses between the two bandpass filters prototypes.

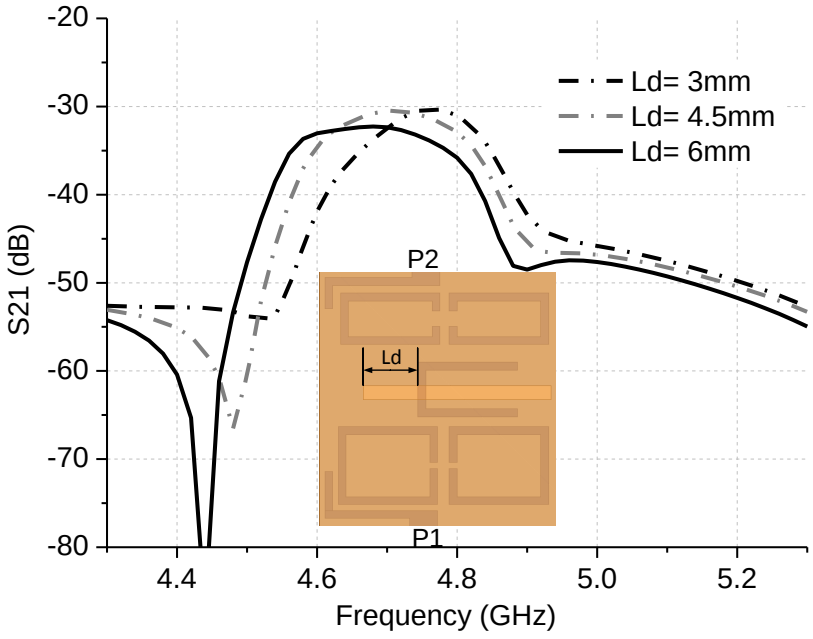

Figure 5.24 Simulated S_{21} of the proposed duplexing antenna (inset) as a function of the locations of the hairpin, *Ld*.

5.3.5 Operation Mode and Current Distribution

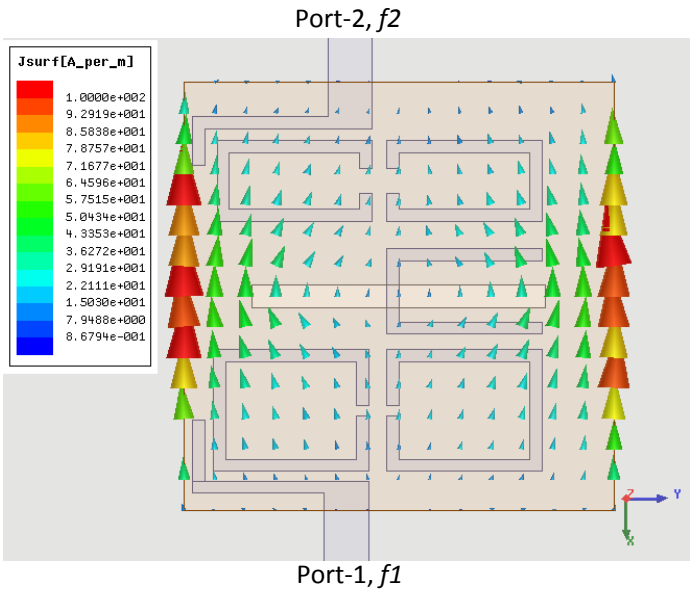

(a)

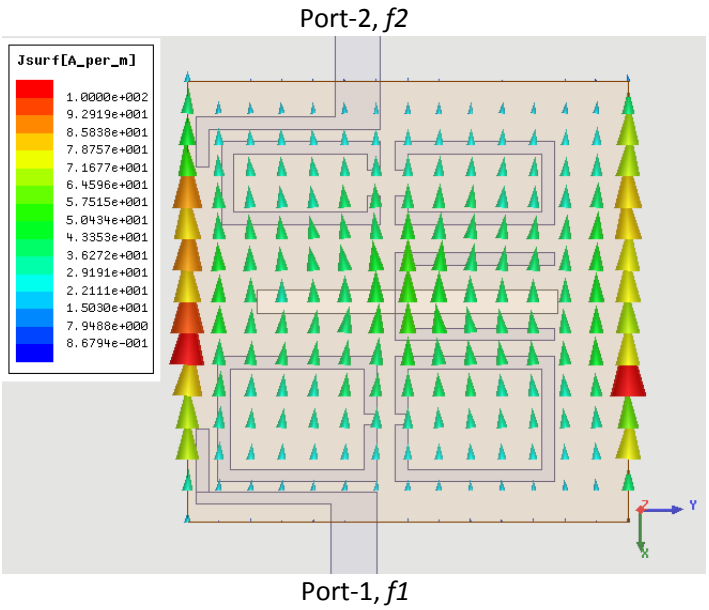

(b)

Figure 5.25 The simulated current distribution: (a) Port 1 excitation, 4.7 GHz, (b) Port 2 excitation, 6 GHz.

One of the features of this work is that the two operation bands of the duplexing antenna have the consistent radiation characteristics. Here, the antenna works at its fundamental mode (TM10-mode) when it works at downlink or uplink. This, contributes to uniform polarization characteristics at the far-field. Due to the far-field electric distribution is resulted from the current distribution on the antenna, it is essential to investigate the current distribution on the radiating element. Figure 5.25 shows the simulated current distribution on the

patch of the dual-port full-duplex antenna. When Port 1 is excited at 4.7 GHz, as shown in Figure 5.25(a), the current on the patch is symmetric but its path is slightly bent around the slot line. The extended current path leads to an operation frequency lower than the patch's intrinsic resonance. When the Port 2 is excited at 6 GHz, as shown in Figure 5.25(b), similar current distribution but with a shorter path can be seen. It is evident that the antenna works at its fundamental mode (TM10) for both frequency bands (channels). As a result, the full-duplex antenna has the consistent radiation and polarization characteristics at the two operation bands.

5.3.6 Full-Duplex Array Antennas

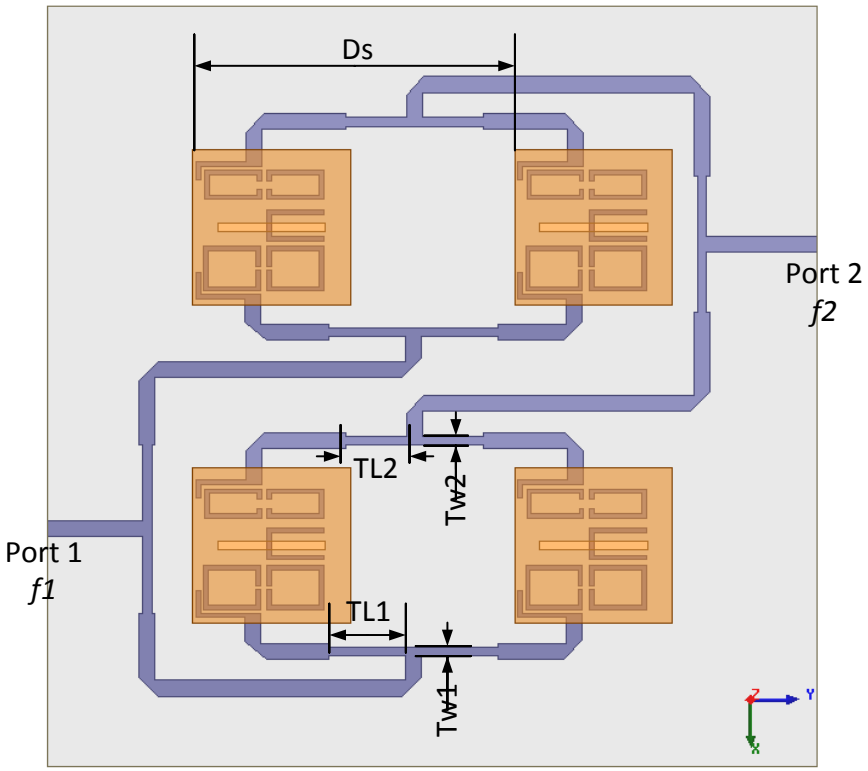

Figure 5.26 Configurations of the 2 × 2 full-duplex antenna array (Array-I), with a 3rd-order filtering response and a traditional quarter-wavelength transformer feeding network. *Ds* = 36 mm, *TL1* = 8.6 mm, *TL2* = 6.8 mm, *Tw1* = 1 mm, *Tw2* = 1mm.

To increase the channel capacities of the Tx/Rx devices and reduce the losses in the transmission paths, especially for the RSUs, array antennas with a high gain are usually adopted in the applications. Thanks to the compact size of the proposed full-duplex element in Figure 5.20 (less than 0.5 λ), it is very suitable to extend to an array antenna. In this section, two full-duplex 2 × 2 arrays with different feeds and orders will be presented and discussed. Figure 5.26 shows the configurations and feeding networks of the first dual-port

full-duplex antenna array, donated as Array-I. It is conceived based on the full-duplex antenna element presented in Figure 5.19. Because the two channels share the same aperture (patch), the spacing between the radiating elements is a trade-off between the efficiency and side-lobe level at the two operation bands. The spacing is finally chosen to be *Ds* = 36 mm.

Again due to the shared aperture, the feeding networks for the two operation bands are designed separately. Port 1 is assigned to feed the low-band operation, whereas Port 2 is used for the high-band. Here, the conventional 4-way power dividers with quarter wavelength transformers are used in the design. The width of the 50 Ω feed lines is 1.8 mm. For the low-band operation, the length and width of the transformer are *TL1* = 8.6 mm and *Tw1* = 1 mm, respectively. For the high-band operation, the length and width are *TL2* = 6.8 mm and *Tw2* = 1 mm.

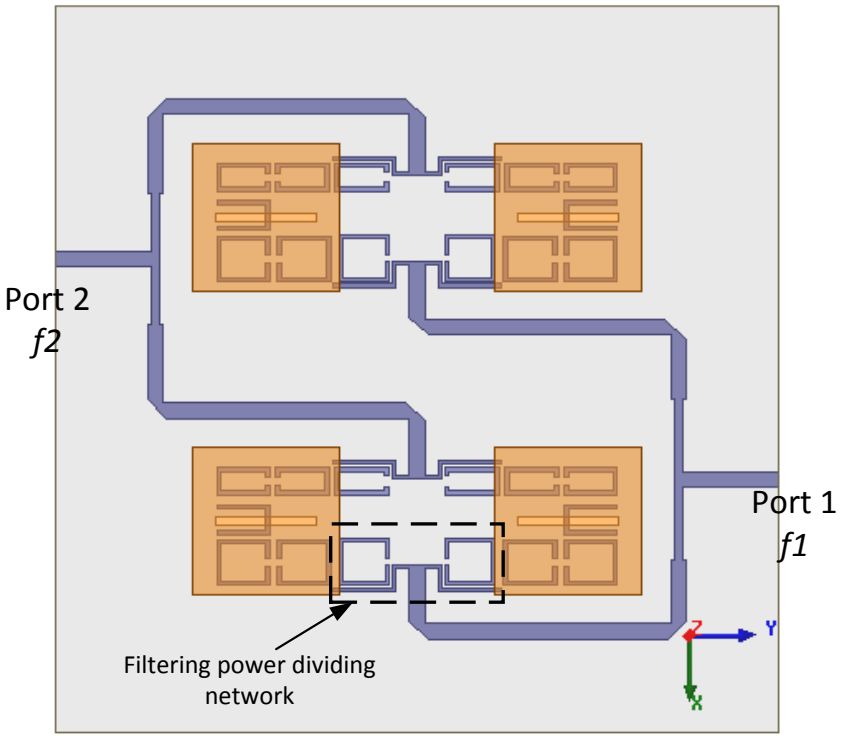

Figure 5.27 Configurations of the other 2 × 2 full-duplex antenna arrays (Array-II), with a 4th-order filtering response and a novel filtering power dividing network.

To further increase the order of the channels and therefore the frequency selectivity of the full-duplex array, another new design of array is proposed based on a filtering power-dividing network, as the configuration shown in Figure 5.27. Different from the Array-I, the quarter wavelength transformers are replaced with a resonator-based power dividing network, as zoomed in and replotted in Figure 5.28. The input power is coupled directly from the feed line to two open loop resonators. The resonant frequencies of the resonators for the low-band and the high-band operation are *f1* and *f2* respectively. Each of these resonators is

then coupled to a channel of the duplexing antenna element without any extra circuits. Such an integrated design increases the orders of the filtering channels from 3 to 4 without increasing the size of the circuit. As a result, the frequency responses such as frequency selectivity, bandwidths, isolations and out-of-band rejection can be improved.

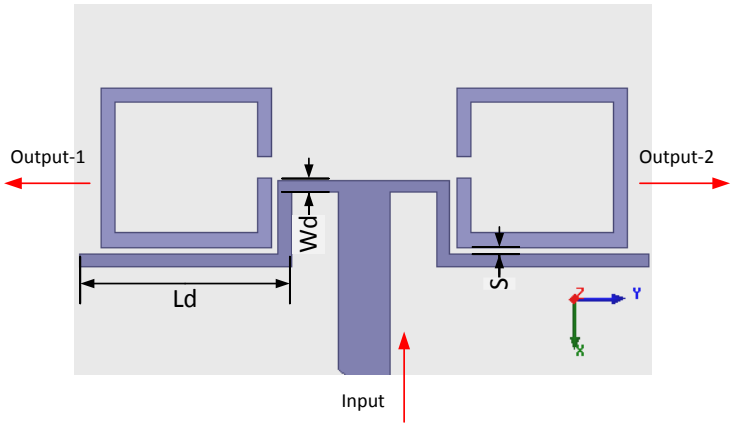

Figure 5.28 The configuration of the 2-way filtering power dividing network in Array-II. *Ld* = 6.8 mm, *Wd* = 0.45 mm, *S* = 0.35 mm.

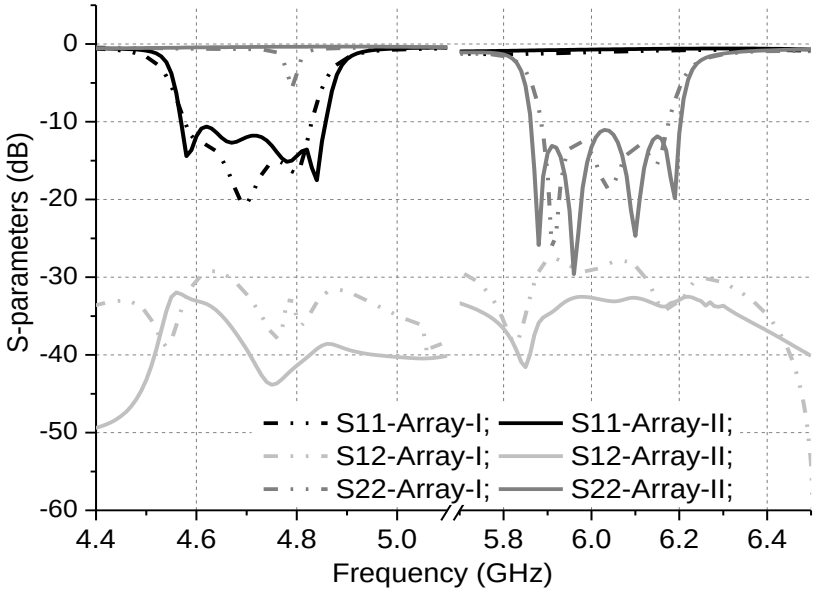

Figure 5.29 The comparison of simulated S-parameters between the two array antennas.

Figure 5.29 compares the simulated S-parameters of the two proposed full-duplex filtering array antennas. As can be observed, both array antennas have a good impedance matching and isolation performance at the two frequency bands. For Array-I, there are three reflection zeros at each band, contributing to a 3rd-order filtering function. The bandwidths of the low-band and the high-band are 250 MHz and 300 MHz, respectively. The isolations for the low-band and high-band operations are 30 dB and 28 dB. As for Array-II, there are

four reflection zeros can be identified at each operation channel. The additional reflection zero results from the integrated filtering power dividing networks. Therefore, a 4th-order filtering response is achieved for each frequency band. Compared with that of Array-I, the bandwidths, frequency selectivity and the isolations of the Array-II are all improved. The bandwidths of the low- and high-band operations are increased to 280 MHz and 350 MHz. The isolations at the low- and high-band are improved by 6 dB and 4 dB, respectively. It should also be noted that the Array-II exhibits a sharper roll-off at both edges of the two bands, which is beneficial to improve frequency selectivity and remove the separate band-pass filters.

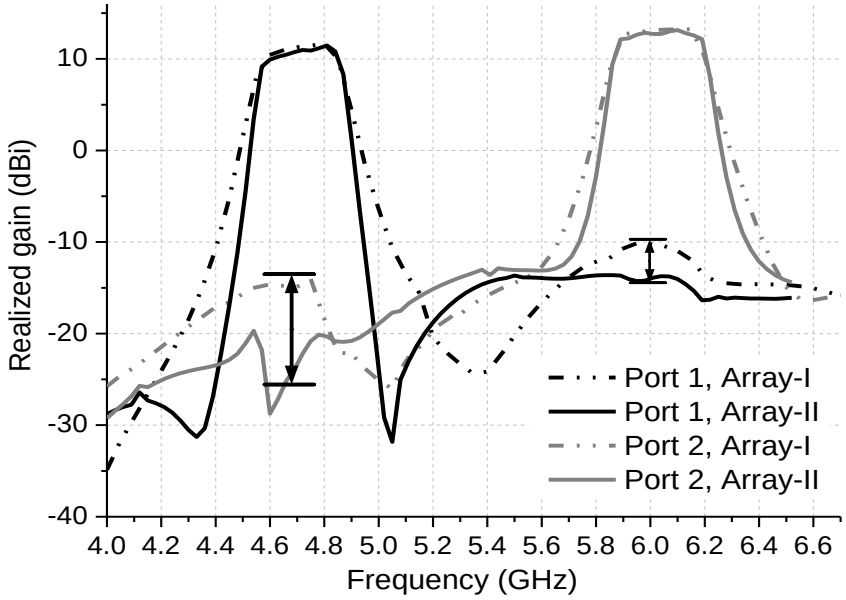

Figure 5.30 Comparison of the simulated gains between Array-I and Array-II.

Figure 5.30 compares the simulated gain responses of the two array antennas at both operation bands. It is observed that the two antennas show a similar and flat gain curve within the passbands, but different out-of-band responses. The Array-II with the higher order filtering performance shows a sharper roll-off at the band edges and higher out-of-band rejection than that of the Array-I. For Array-II, there are two clear nulls just outside the passbands, resulting in a rapid reduction of the gain, especially for the low-band operation. At 4.4 and 5.0 GHz, 6% beyond the central frequency, the gain of Array-II is reduced by more than 15 dBi. Furthermore, the inter-channel rejections of the Array-II have been improved by 10 dB (low-band) and 4 dB (high-band) as compared with Array-I.

Another noticeable feature of the proposed full-duplex antenna arrays is the broadband harmonics suppression. Figure 5.31 shows the simulated gains curves of the Array-II over a broadband when the two ports are excited, respectively. As can be observed, the antenna has

an excellent out-of-band rejection performance with the higher order harmonics significantly suppressed over a wideband up to 13 GHz. For the low-band operation (port 1 excitation), the gains at the harmonics are suppressed by more than 22 dB. When the port 2 is excited, the gains at the harmonics are reduced by over 25 dB.

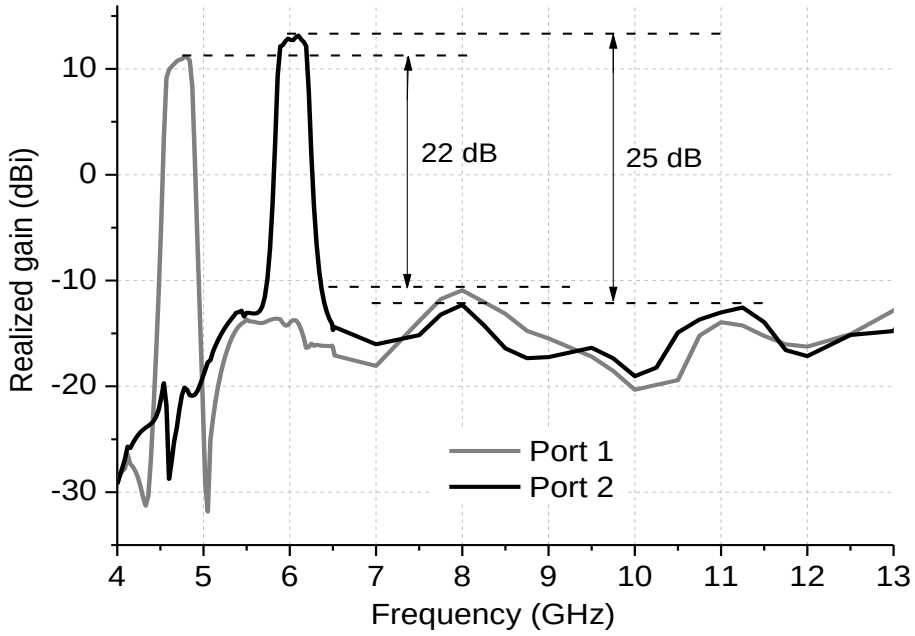

Figure 5.31 The simulated antenna gains of Array-II over a broadband.

5.3.7 Prototypes and Measurement results

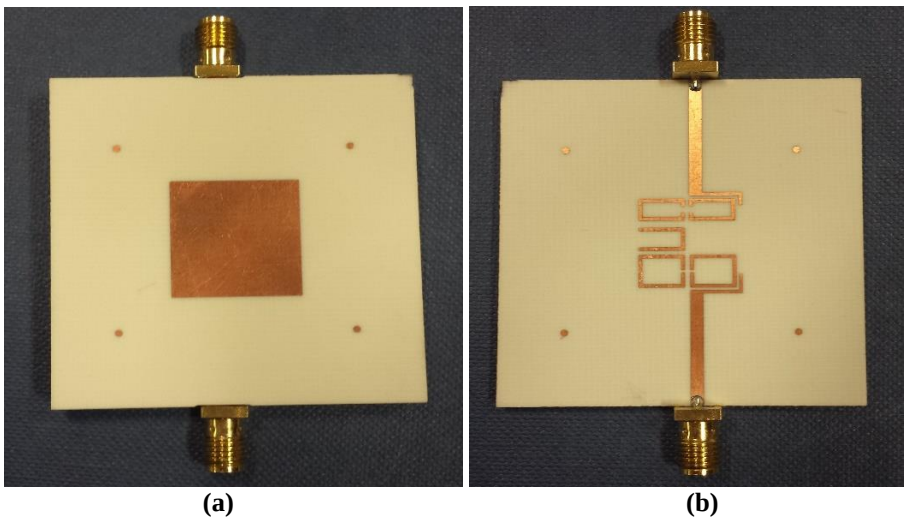

(a) **(b)**

Figure 5.32 Prototype of the proposed dual-port full-duplex element: (a) front-view, (b) back-view.

The proposed full-duplex antenna element and the two array antennas (Array-I and II) were prototyped and measured to verify the design concepts. Figure 5.32 shows the front and back view of the dual-port full-duplex antenna element prototype. The reflection coefficients at the two ports and the isolation between them are measured and presented in Figure

5.33. The measured results match very well with the simulations, showing two operation bands from 4.58 to 4.82 GHz (FBW = 5.1%) and 5.87 to 6.2 GHz (FBW = 5.8%) for uplink and downlink communications. At both bands, the antenna exhibits a 3rd-order filtering characteristics with a good frequency selectivity. Out of the bands, the antenna exhibits a favorable rejection performance with the return loss close to 0. The antenna element has an excellent isolation of over 30 dB at both bands as indicated by S_{12}.

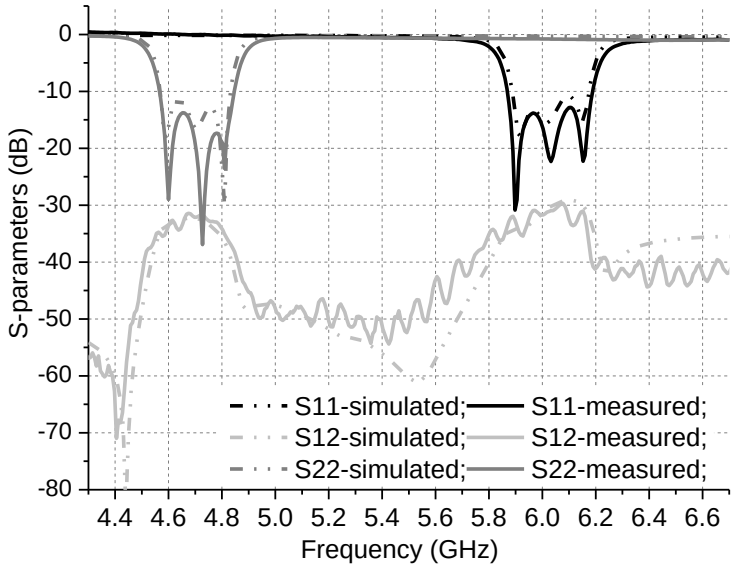

Figure 5.33 Simulated and measured S-parameters of the proposed dual-port full-duplex element.

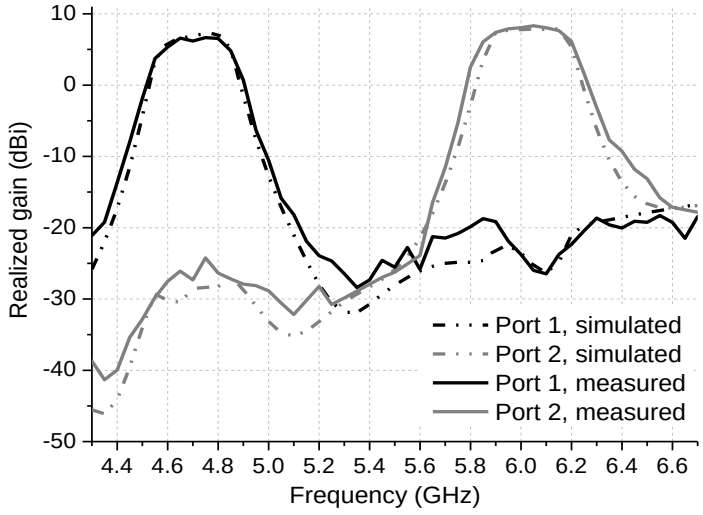

Figure 5.34 Simulated and measured gain of the full-duplex antenna element.

Figure 5.34 shows the simulated and measured realized gains of the dual-port full-duplex antenna element when the two ports are excited, respectively. As can be observed, the measured gains agree well with the simulations. When port 1 is excited (low-band operation), the antenna has a flat gain of about 6.7 dBi from 4.6 to 4.8 GHz. The antenna also

exhibits excellent frequency selectivity with the gains rapidly reduced to below -20 dB as the frequency decreases to 4.38 GHz or increases to 5.08 GHz. The gain is suppressed by more than 30 dB at the high-band (6 GHz). When the port 2 is excited (high-band operation), the antenna has a flat gain of about 8 dBi from 5.88 to 6.18 GHz. The gain is significantly suppressed to below -25 dBi at around 6 GHz, which is 33 dB lower than that in-band. The minor discrepancies between the simulations and measurements are attributed to the measurement sensitivity.

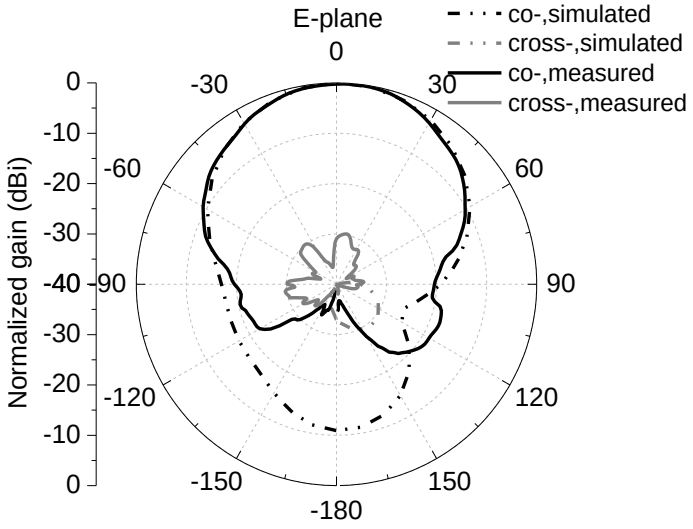

(a)

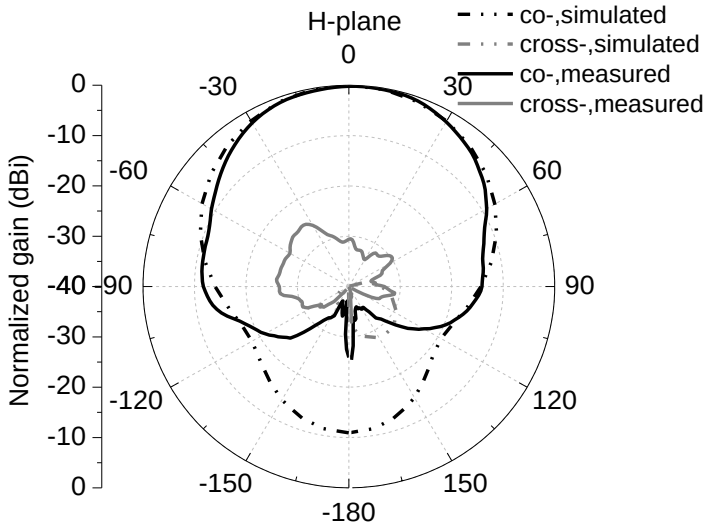

(b)

Figure 5.35 Simulated and measured normalized radiation patterns of the full-duplex antenna element at 4.7 GHz (port 1 is excited): (a) $\varphi=0^0$, (b) $\varphi=90^0$.

The simulated and measured normalized radiation patterns of the full-duplex antenna element at 4.7 GHz are presented in Figure 5.35. The measurements and simulations agree very well with each other, showing the maximum radiation in the broadside direction. The

antenna also exhibits a very pure polarization performance with the measured cross polarization discrimination (XPD) over 30 dB in $\varphi = 0^o$ (E-plane) and $\varphi = 90^o$ (H-plane) planes, respectively. Figure 5.36 shows the normalized simulated and measured radiation patterns of the full-duplex element at 6 GHz when the port 2 is excited and the port 1 is terminated with 50 Ω load. As can be seen, the antenna has similar radiation patterns as those in the low-band operation. The measured XPD are over 30 dB in $\varphi = 0^0$ and $\varphi = 90^0$ planes. It should be noted that the discrepancies in the backward radiation are caused by the absorber used to mount the antenna in the chamber.

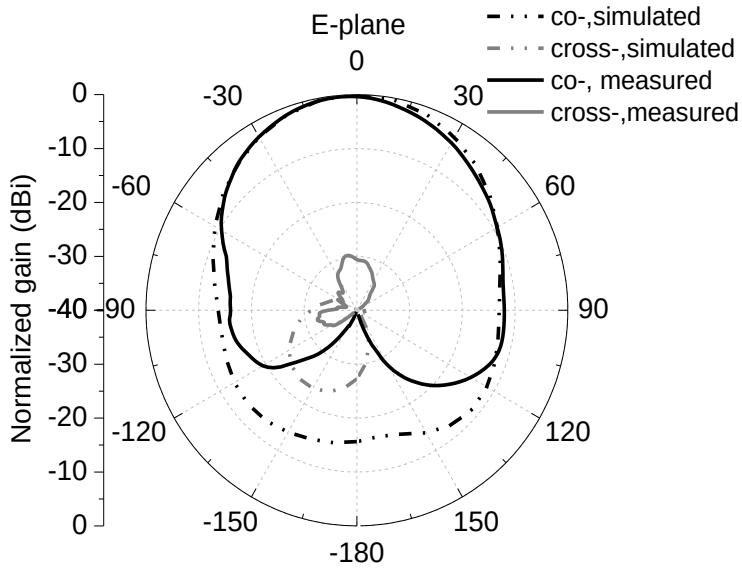

(a)

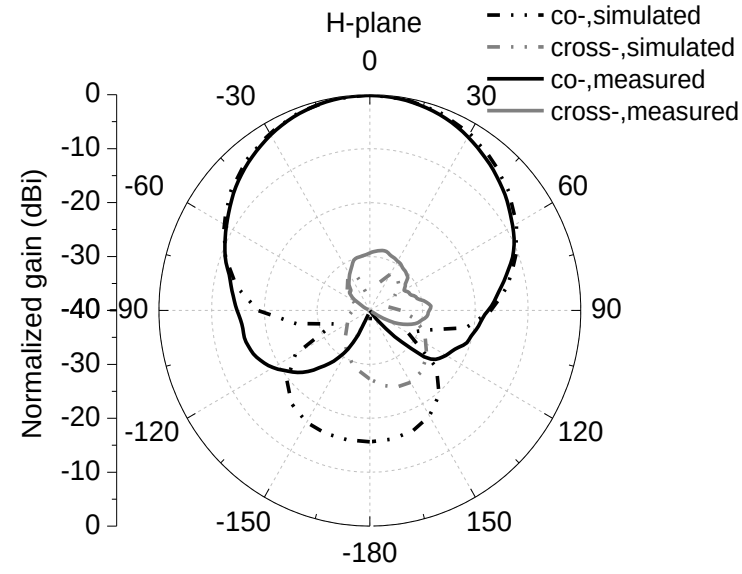

(b)

Figure 5.36 Simulated and measured normalized radiation patterns of the full-duplex antenna element at 6 GHz (port 2 is excited): (a) $\varphi=0^0$, (b) $\varphi=90^0$.

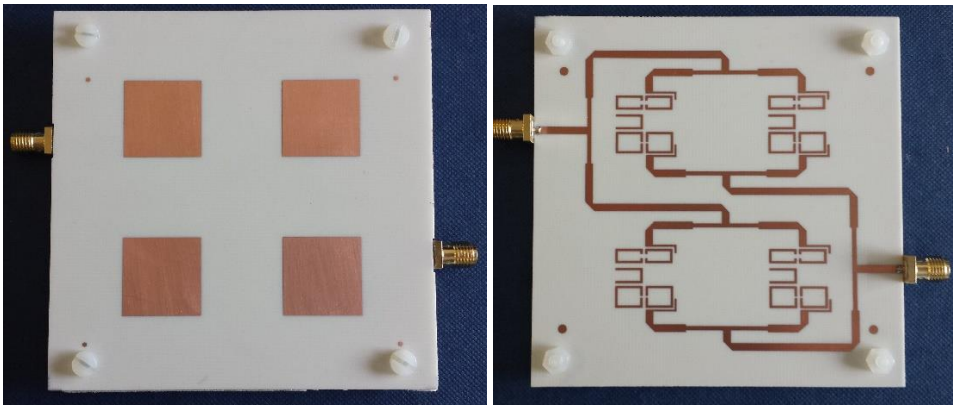

(a)

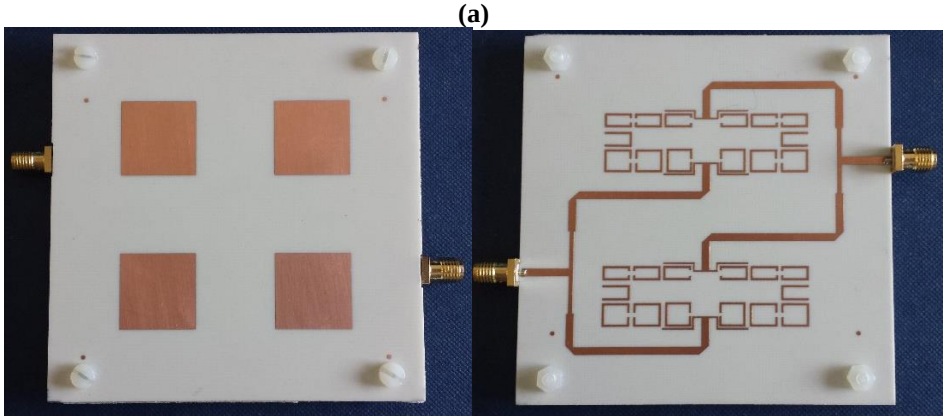

(b)

Figure 5.37 The front- and back-view of the full-duplex antenna arrays: (a) Array-I, (b) Array-II.

The two dual-port full-duplex antenna arrays (Array-I and II) were also prototyped and displayed in Figure 5.37. The two arrays have the same top layer but different layouts on the bottom layer. Figure 5.38 shows the simulated and measured S-parameters of the Array-I. As can be seen, the simulated and measured S-parameters agree well with each other with three identifiable poles in both operation bands. For the low-band operation, the antenna has a bandwidth from 4.57 to 4.82 GHz. When port 2 is excited, the antenna works at high-band with a bandwidth from 5.86 to 6.2 GHz. Between the two operation bands (ports), the antenna achieves a high isolation with the measured S_{21} lower than -30 and -28.5 dB at the low- and high-band, respectively.

Figure 5.39 shows the simulated and measured S-parameters of the Array-II. As expected and different from Array-I, Array-II exhibits 4^{th}-order filtering characteristics for both operations with four reflection zeros in each band. The increased order results in wider bandwidths, higher isolation and sharper roll-off at the edges of the bands. For the low-band operation, a bandwidth from 4.58 to 4.86 GHz is achieved. The isolation in the low-band is over 33 dB for the measurement. When the antenna works at the high-band, a frequency bandwidth from 5.85 to 6.22 GHz is obtained. The isolation of the measurement in this band is higher than 32 dB.

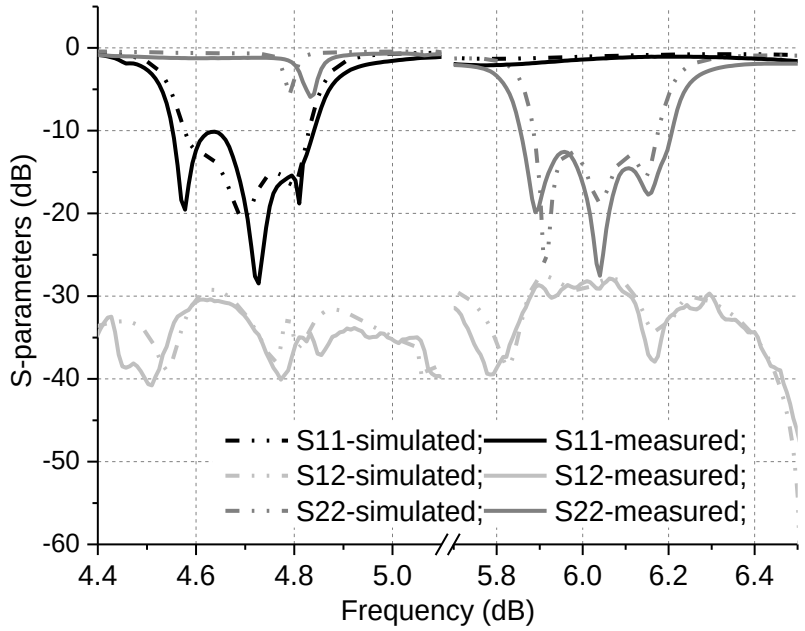

Figure 5.38 Simulated and measured S-parameters of the proposed Array-I.

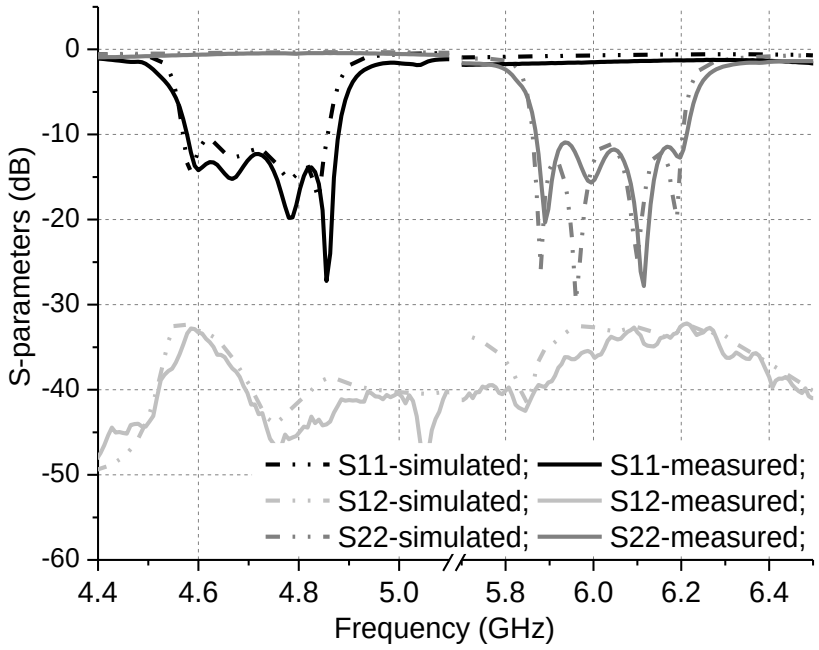

Figure 5.39 Simulated and measured S-parameters of the proposed Array-II.

Figure 5.40 shows the simulated and measured realized gains of the proposed duplexing Array-II. (For brevity, the gains and the radiation patterns of Array-I are not presented in this paper.) The measured results agree reasonably well with the simulations. For the low-band operation, the antenna exhibits a flat gain about 10.2 dBi from 4.6 to 4.82 GHz. At around 6 GHz (high-band operation), the gain is reduced to below -15 dBi, which is more than 25 dB lower than that in-band. For the high-band operation, the antenna has a flat gain

of 12.5 dBi from 5.88 to 6.2 GHz. The gain is suppressed to below -22 dB at around 4.7 GHz. It should also be noted that there are two nulls at both sides of each passbands, which lead to sharp roll-off at the edges of the two bands and therefore the improved frequency selectivity.

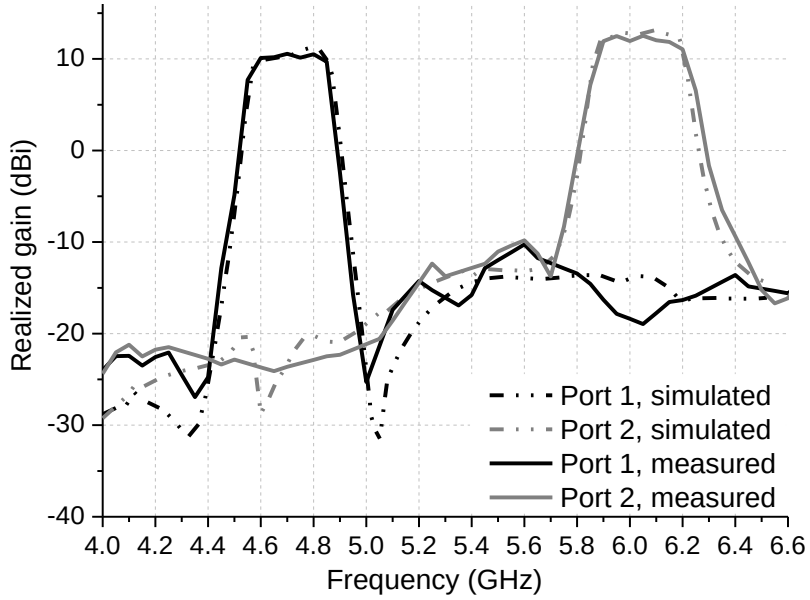

Figure 5.40 The simulated and measured antenna gain of Array-II.

The simulated and measured normalized radiation patterns of the other full-duplex antenna array (Array-II) at the low-band are presented in Figure 5.41. The measurements and simulations agree well with each other. The antenna shows a good radiation characteristics in $\varphi = 0^0$ and $\varphi = 90^0$ planes. The measured cross polarization discrimination (XPD) is over 28 and 27dB in E-plane ($\varphi = 0^0$) and H-plane ($\varphi = 90^0$), respectively.

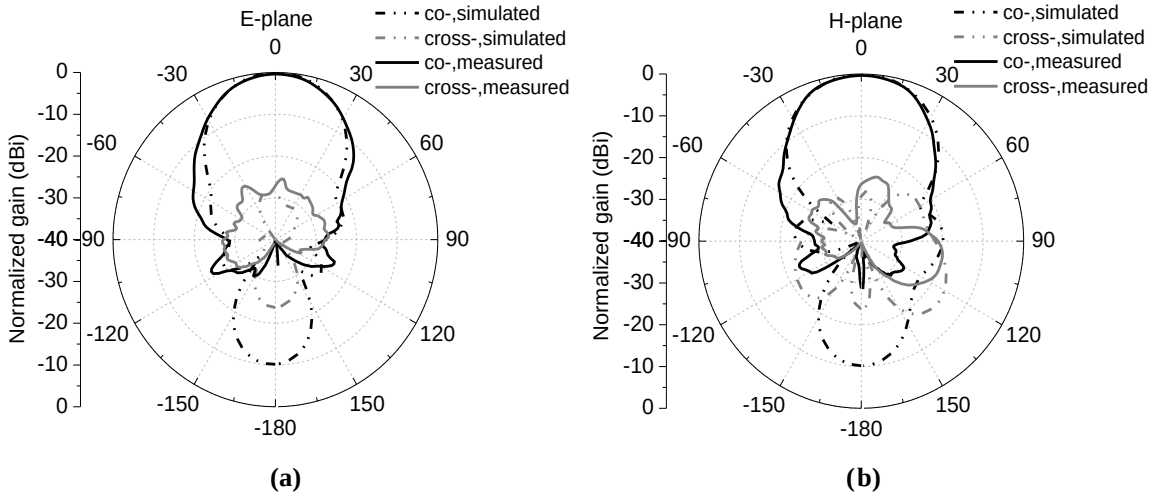

Figure 5.41 Simulated and measured normalized radiation patterns of the proposed Array-II at 4.7 GHz (port 1 is excited): (a) $\varphi=0^0$, (b) $\varphi=90^0$.

Figure 5.42 presents the normalized radiation patterns of the Array-II at 6 GHz (high-band operation) when port 2 is excited and port 1 is terminated with a 50 Ω load. As can be observed, the antenna shows the expected radiation patterns with the maximum radiation also in the broadside. However, the main beam is narrower than that of the low-band operation due to the larger electrical size of the aperture at the higher frequency. The measured XPD of the array are over 29 dB and 32 dB in $\varphi = 0^0$ and $\varphi = 90^0$ planes, respectively.

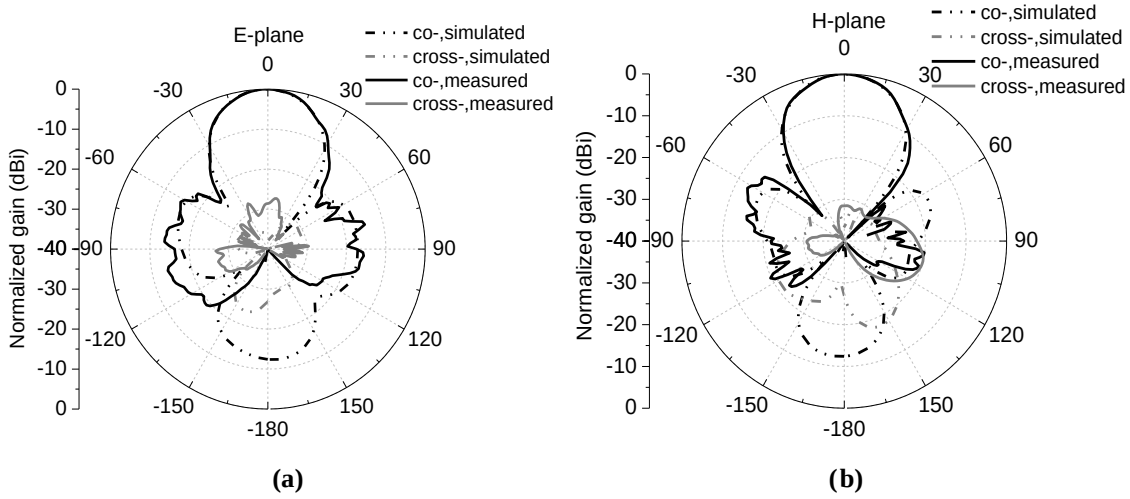

Figure 5.42 Simulated and measured normalized radiation patterns of the proposed Array-II at 6.0 GHz (port 2 is excited): (a) $\varphi=0^0$, (b) $\varphi=90^0$.

The results of the three dual-port full-duplex antennas are summarized in Table 5.4 for comparison. The comparison is mainly focused on the filtering orders of the channel, bandwidths, isolation and inter-channel gain suppression. As can be seen, the element and Array-I have the similar bandwidths whereas the bandwidths of the Array-II is slightly increased due to the higher order filtering channels (4^{th}-order versus 3^{rd}-order). The isolation of the Array-II at the low- and high-band are 35 and 33 dB, which is an increase of 5 dB compared with the Array-I. The results achieved have met the specifications in Table 5.4.

Table 5.4 Comparison of the Proposed Full-Duplex Antennas

Antennas proposed	Order of channel	Bandwidth (low-/high-band)	Isolation (low-/high-band)	Inter-channel gain suppression (low-/high-band)
Element	3^{rd}-oder	5.1% /5.4%	32dB /30dB	30dB /36dB
Array-I	3^{rd}-oder	5.3% /5.7%	30dB /28dB	- /-
Array-II	4^{th}-order	6.0% /6.1%	35dB /33dB	26dB /38dB

5.4 Summary

In this chapter, a novel high-integration duplexing antenna is proposed for the first time based on filtering antenna design methods. This multi-functional device integrates multiple functions such as radiation, duplexing and filtering within a compact size. Such a highly-integrated component could find potential applications in wireless communications and intelligent transport systems. Compared with the traditional cascaded system with multiple single-function components connected, this novel device can significantly reduce the size, insertion loss, weight and cost of the systems. All results have demonstrated that the proposed duplexing antennas have the excellent frequency selectivity performance and isolation between the ports/operations.

Chapter 6. Conclusion and Future Work

6.1 Conclusion

The rapid development of the wireless communication technologies nowadays has been stimulating research on highly integrated, miniaturized and low-cost RF/microwave passive components. To reduce the volume and complexity of the systems, one promising method is to conceive one single device which possesses multiple functions but without increasing the size of the system. The integration of the filter and antenna, also called 'filtering antenna', is believed one of the feasible techniques to reduce the size and complexity of the future wireless communications systems. In the past several years, the research on filtering antenna has attracted significant interest in academia and industries all over the world. The integrated filtering antenna could also considerably reduce the cost of the RF front-ends, especially for the mm-Wave applications, such as the fifth-generation (5G) communications.

The integrated design of filter, antenna and other passive components has many advantages as compared with traditional cascaded systems which consist of multiple single-functional components successively. One of the obvious advantages is that the number of components in the system is reduced and the interfaces between the components are removed. This results in the reduction of the system's volume/size, insertion losses, and the cost. The other important merit is that the frequency responses of the system, such as frequency bandwidth, out-of-band rejection and the frequency selectivity, could be improved significantly. The integrated filtering antenna could also bring about all-new devices, such as the multi-port full-duplex antennas, which has been demonstrated in this thesis.

The purpose of this thesis is to investigate the methods to realize the required filtering antennas and apply them in wireless applications and solve the existing the problems. We have fully studied the filtering antenna based on the fact that the radiating element itself has the resonant characteristics. By serving the radiator of antenna as the last resonator of a filtering/feeding networks and properly controlling the coupling between the antenna element and the inserted resonator, the antenna with integrated filtering features can be achieved without assorting the separate filters.

To achieve the filtering antennas according to the requirements, other aspects such as antenna complexity, substrate layers, fabrication cost have been taken into consideration. According to the potential application scenarios, different filtering antennas with different functions have been proposed in this thesis. We have also exploited the filtering antennas in array antenna applications for improving the antenna gains. To meet the requirements of 5G

applications and reduce the potential cost, a broadband high-gain highly integrated filtering antenna/array with tilted beam have studied. Furthermore, the filtering antenna has been further developed and a dual-port duplexing antenna has been proposed for wireless applications with uplink/downlink operations required.

In this thesis, the design methods are first studied and then based on its potential applications in wireless communications, several kinds filtering antennas/arrays are discussed. In Chapter 3, the techniques of achieving filtering antennas with different functions are introduced first. We proposed a broadband filtering antenna by employing dual-mode stub-loaded resonator (SLR) to feed the radiating element. Then, the methods for suppressing the high-order harmonics are introduced by utilizing the different resonant characteristics of the patch and feed, which is designed based on the planar inverted-F antenna (PIFA). In addition, we proposed a dual-band filtering antenna with broadband harmonic suppression for wireless communication systems for the first time. Through these original studies, the advantages of the integrated filtering antenna over the traditional antennas are fully exhibited and highlighted. Based on these methods, several filtering antenna arrays are proposed and demonstrated in Chapter 4. We first exploited a highly integrated filtering antenna array, which integrates the functions of filtering, power dividing and radiation in the design. Due to the introduced cross coupling, the antenna has excellent frequency selectivity. Furthermore, the different high-order harmonics of the resonators are purposely used to eliminate the harmonics of the antenna. Then, the broadband filtering antenna methods are employed in the design of dual-polarization array antennas. This method is then further developed to conceive a dual-band dual-polarized filtering antenna array. Owing to the adoption of the SLR as the feed, the feeding networks and ports are significantly reduced. This filtering antenna technique can be used to solve the congestion challenges in dual-band dual-polarized array designs. The filtering antenna technique is further developed to design the mm-wave filtering antenna by integrating a U-shaped slot resonator in the ground plane. This configuration results in a strong coupling between them and therefore a very wide impedance bandwidth is achieved. Thanks to the resonant characteristics of these resonator/patch, a very good wideband filtering feature is achieved. Such a highly integrated antenna is benefit to reduce the cost of the RF frontend subsystems significantly.

Apart from the design of filtering antennas/arrays, we further investigated a novel dual-port component with the functions of duplexing, filtering and radiation integrated in Chapter 5. This dual-port device could effectively reduce the complexity of the RF frontend system and thus the potential cost. This dual-port device also exhibits an excellent isolation between

the two operation bands, and thus it could be served as the uplink/downlink Tx/Rx of the wireless communication systems. This technique is further developed and improved to achieve a much integrated and compact full-duplex antenna/array for intelligent transport systems. Figure 6.1 summaries the features of technical contribution of the proposed filtering antennas in this thesis.

Table 6.1 Summary of the proposed filtering antennas in this thesis

Antenna types	Locations in the thesis	Features and technical contribution
Filtering antenna element	Chapter 3.2	Dual-mode resonator is used to feed a patch to improve the bandwidth and frequency selectivity in parallel
	Chapter 3.3	PIFA antenna is adopted to feed a dipole for wideband harmonic suppression
	Chapter 3.4	Dual-mode SLR is adopted to couple to a U-slot patch to produce the dual-band filtering performance
Filtering Antenna array	Chapter 4.2	A filtering power splitting network is proposed to couple with a patch array; wide bandwidth with 4th-order filtering features and wideband harmonic suppression achieved.
	Chapter 4.3	Broadband filtering antenna technique is first used in dual-polarized antenna array design
	Chapter 4.4	For the first time, dual-band dual-polarized filtering antenna array is achieved; largely reduce the complexity of the feeding network.
	Chapter 4.5	Filtering antenna technique is firstly used in mm-wave to achieve a broadband high-gain filtering antenna array
Duplexing filtering antenna	Chapter 5.2	For the first time dual-port dual-band duplexing filtering antenna with consistent polarization is achieved by using the filtering antenna technique.
	Chapter 5.3	A highly integrated, compact dual-port dual-band duplexing antenna is proposed and used in array antenna design.

6.2 Future Work

Although much work has been done in researching filtering antenna/array and duplexing antennas, filtering antennas have other important applications in wireless communications. One potential applications is to use the filtering antenna techniques to design circularly polarization antennas/arrays. The other useful application of filtering antenna is to design the reconfigurable antennas, including the polarization reconfigurable antennas and frequency reconfigurable antennas. Besides, it is important to design the duplexing filtering antenna with a closer uplink/downlink frequency bands to meet the applications of wireless communications.

To design a novel circularly-polarized antenna based on filtering antenna design methods, one important requirement is how to excite the two orthogonal modes of the patch with a 90 degree phase difference. Other challenges such as broad 3-dB axial ratio (AR) bandwidth and radiation efficiency to be overcome. Then, other work of how to apply the circularly-polarized filtering antenna in satellite/radar applications could be investigated.

To achieve the frequency reconfigurable filtering antenna, one main problem is how to easily adjust the resonant frequencies of the resonators and antennas. Besides, the coupling between the resonator and antenna will change as the frequency moves. Thus, much work need to be done in the future to achieve a frequency-reconfigurable antenna with the filtering features.

It is a challenge to design the duplexing filtering antenna with two operation bands close to each other as it is usually very difficult to guarantee a very good isolation between two such bands. Higher order filtering of the channels can improve the isolation, but this will also lead to a higher insertion loss and larger volume. Other types of design method need to be investigated. In addition, the back-lobe needs to be considered more carefully in future work.

References

[1] H. F. Puse and A. V. Capelle, "An impedance-matching technique for increasing the bandwidth of microstrip" *IEEE Transactions on Antennas and Propagation*, vol. 37, pp. 1345-1354, 1989.

[2] T. L. Nadan, J. P. Coupez, S. Toutain, and C. Person, "Optimization and miniaturization of a filter/antenna multi-function module using a composite ceramic-foam substrate," in I*EEE MTT-S Int. Microw. Symp. Dig.*, Jun. 1999, pp. 219–222.

[3] T. Le Nadan, J. P. Coupez, S. Toutain, C. Person, "Integration of an antenna/filter device using a multi-layer, multi-technology process", in *Proc. 28th EuMC*, Amsterdam, vol. 1, pp. 672-77, Oct. 1998.

[4] C. T. Chuang, and S. J. Chung, "Synthesis and Design of a New Printed Filtering Antenna," *IEEE Trans. Antennas Propag.*, vol. 59, no. 3, pp. 1036–1042, Mar. 2011.

[5] J.-S. Hong and M. J. Lancaster, *Microstrip Filters for RF/Microwave Applications:* Wiley, 2001.

[6] R. J. Cameron, C. M.Kudsia, and R. R. Mansour, *Microwave Filters for Communication Systems: Fundamentals, Design, and Applications*. New York: Wiley, 2007, ch. 11.

[7] N. Yang, C. Caloz, and K.Wu, "Co-designed CPS UWB filter-antenna system," in *Proc. IEEE AP-S Int. Symp.*, Jun. 2007, pp. 1433–1436.

[8] C.-H. Wu, C.-H. Wang, S.-Y. Chen, and C. H. Chen, "Balanced-tounbalanced bandpass filters and the antenna applications," *IEEE Trans. Microw. Theory Tech.*, vol. 56, no. 11, pp. 2474–2482, Nov. 2008.

[9] G. Q. Luo,W. Hong, H. J. Tang, J. X. Chen, X. X. Yin, Z. Q. Kuai, and K. Wu, "Filtenna consisting of horn antenna and substrate integrated waveguide cavity FSS," *IEEE Trans. Antennas Propag.*, vol. 55, no. 1, pp. 92–98, Jan. 2007.

[10] Y. Chen, W. Hong, Z. Kuai, and H. Wang, "Ku-band linearly polarized omnidirectional planar filtenna," *IEEE Antennas Wireless Propag. Lett.*, vol. 11, pp. 310–313, Mar. 2012.

[11] Y. C. Lin and K. J. Hung, "Compact ultra-wideband rectangular aperture antenna and band-notched designs," *IEEE Trans. Antennas Propag.*, vol. 54, no. 11, pp. 3075–3081, Nov. 2006.

[12] Y. J. Cho, K. H. Kim, D. H. Choi, S. S. Lee, and S. O. Park, "A miniature UWB planar monopole antenna with 5-GHz band-rejection filter and the time-domain characteristics," *IEEE Trans. Antennas Propag.*, vol. 54, no. 5, pp. 1453–1460, May 2006.

[13] Q. X. Chu and Y. Y. Yang, "A compact ultra wideband antenna with 3.4/5.5 GHz dual band-notched characteristics," *IEEE Trans. Antennas Propag.*, vol. 56, no. 12, pp. 3637–3644, Dec. 2008.

[14] Y. Zhang, W. Hong, C. Yu, Z. Q. Kuai, Y. D. Don, and J. Y. Zhou, "Planar ultra wideband antennas with multiple notched bands based on etched slots on the patch and/or split ring resonators on the feed line," *IEEE Trans. Antennas Propag.*, vol. 56, no. 9, pp. 3063–3068, Sep. 2008.

[15] W. J. Lui, C. H. Cheng, and H. B. Zhu, "Improved frequency notched ultra wideband slot antenna using square ring resonator," *IEEE Trans. Antennas Propag.*, vol. 55, no. 9, pp. 2445–2450, Sep. 2008.

[16] Z. L. Zhou, L. Li, and J. S. Hong, "Compact UWB printed monopole antenna with dual narrow band notches for WiMAX/WLAN bands," *Electron. Lett.*, vol. 47, no. 20, pp. 1111–1112, Sep. 2011.

[17] F. Zhu, S. Gao, A. Ho, R. Abd-Alhameed, C. See, T. Brown, J. Li, G. Wei, J. Xu, " Multiple Band-Notched UWB Antenna with Band-Rejected Elements Integrated in the Feed Line," *IEEE Trans. Antennas Propag.*, vol. 61, no. 8, pp. 3952–3960, Aug. 2013.

[18] Yin Qin; S. Gao; A. Sambell, "Broadband high-efficiency circularly polarized active antenna and array for RF front-end application," *IEEE Trans Microw. Theory Tech*., vol. 54, no. 7, pp. 2910–2916, Jul. 2006.

[19] A. Abbaspour-Tamijani, J. Rizk, and G. Rebeiz, "Integration of filters and microstrip antennas," *in Proc. IEEE AP-S Int. Symp.*, Jun. 2002, pp. 874–877.

[20] F. Queudet, I. Pele, B. Froppier, Y. Mahe, and S. Toutain, "Integration of Pass-Band Filters in Patch Antennas," *in Proc. 32nd Eur. Microw. Conf.*, 2002, pp. 685–688.

[21] C. K. Lin and S. J. Chung, "A Compact Filtering Microstrip Antenna With Quasi-Elliptic Broadside Antenna Gain Response" *Antenna Wireless Propag. Lett.*, vol. 10, 2011, pp. 381–384.

[22] Y. Yusuf and X. Gong, "Compact low-loss integration of high-Q 3-D filters and highly efficient slot antennas," *IEEE Trans Microw. Theory Tech*., vol. 59, no. 4, pp. 857–865, Apr. 2011.

[23] Y. Yusuf, H. T. Cheng, and X. Gong, "A seamless integration of 3-D vertical filters with highly efficient slot antennas," *IEEE Trans. Antennas Propag.*, vol. 59, no. 11, pp. 4016–4022, Nov. 2011.

[24] Y. Yusuf, H. T. Cheng, and X. Gong, "Co-designed substrate-integrated waveguide filters with patch antennas," *IET Microwaves, Antennas and Propagation*, vol. 7, no. 7, pp. 493–501, 2013.

[25] C. K. Lin and S. J. Chung, "A Filtering Microstrip Antenna Array," *IEEE Trans. Microw. Theory Techn., vol.* 59, no. 11, pp. 2856-2863, Mar. 2011.

[26] C. K. Lin and S. J. Chung, "A Compact Filtering Microstrip Antenna with Quasi-Elliptic Broadside Antenna Gain Response" *Antenna Wireless Propag. Lett.*, vol. 10, pp. 381–384, 2011.

[27] O. A Nova, J. C Bohorquez, N. M Pena, G. E Bridges, L. Shafai and C. Shafai, "Filter-Antenna Module Using Substrate Integrated Waveguide Cavities," *Antenna Wireless Propag. Lett.*, vol. 10, pp. 59–62, 2011.

[28] C. T. Chuang and S. J. Chung, "Synthesis and Design of a New Printed Filtering Antenna," *IEEE Trans. Antennas and Propag.*, vol. 59, no. 3, pp. 1036-1042, Mar. 2011.

[29] X. W. Chen, F. X. Zhao, L. Y. Yan and W. M. Zhang, "Compact Filtering Antenna With Flat Gain Response Within the Passband," *Antenna Wireless Propag. Lett.*, vol. 12, pp. 857–860, 2013.

[30] W. J. Wu, Y. Z. Yin, S. L. Zuo, Z. Y. Zhang and J. J. Xie, "A New Compact Filter-Antenna for Modern Wireless Communication Systems," *IEEE Antenna Wireless Propag. Lett.*, vol. 10, 2011, pp. 1131–1134.

[31] X. P. Chen, W. Hong, T. J. Cui, Z. C. Hao, and K. Wu, "Substrate integrated waveguide elliptic filter with transmission line inserted inverter," *Electron. Lett*., vol. 41, no. 15, pp. 581–582, July 2005.

[32] L. Yan andW. Hong, "Investigation on the propagation characteristics of the substrate integrated waveguide based on the method of lines," *Inst. Elect. Eng. Proc. Microw. Antennas Propag.*, vol. 152, no. 1, pp. 35–42, Feb. 2005.

[33] N. Yang, C. Caloz, and K.Wu, "Co-designed CPS UWB filter-antenna system," in *Proc. IEEE AP-S Int. Symp*., Jun. 2007, pp. 1433–1436.

[34] C. T. Chuang, and S. J. Chung, "A compact printed filtering antenna using a ground-intruded coupled line resonator," *IEEE Trans. Antennas Propag.*, vol. 59, no. 10, pp. 3630–3637, Oct. 2011.

[35] C. T. Chuang, and S. J. Chung, "New printed filtering antenna with selectivity enhancement," in *Proc. 39th European Microwave Conference*, Sep. 2007, pp. 747–750.

[36] W. J. Wu, R. Fan, C. Wang and J. Wang, "A Compact and Anti-interference Filter-antenna for modern wireless communication systems," in *Proc. IEEE 6th International Symposium on Microwave, Antenna, Propagation, and EMC Technologies (MAPE)*, 2015, pp. 60–62.

[37] W. J. Wu, C. Wang, C. Wang, X. Wang and Q. Liu, "Design of A Compact Filter-Antenna using DGS structure for modern wireless communication systems," in *Proc. IEEE 5th IEEE International Symposium on Microwave, Antenna, Propagation and EMC Technologies for Wireless Communications*, 2013, pp. 355–358.

[38] X. Chen, F. Zhao, L. Yan, W. Zhang, "A Compact Filtering Antenna With Flat Gain response within the passband," *IEEE Antenna Wireless Propag. Lett.*, vol. 12, 2013, pp. 857–860.

[39] H. Chu, C. Jin, J. X. Chen, and Y. X. Guo, "A 3-D Millimeter-Wave Filtering Antenna With High Selectivity and Low Cross-Polarization," *IEEE Transactions on Antennas and Propagation*, vol. 63, pp. 2375-2380, 2015.

[40] F. J. Paoloni, "A Cavity-Backed Resonant Slot Array-Theory and measurement," *IEEE Transactions on Antennas and Propagation*, vol. 28, pp. 259-263, 1980.

[41] H. Cheng, S. Ebadi, X. Ren, Y. Yusuf, and X. Gong, "A Compact Wireless Passive Sensing Mechanism based on a seamlessly integrated resonator antenna," *2011 IEEE International Symposium on Antennas and Propagation (APSURSI)*, pp. 1350-1353, 2011.

[42] H. Chu and Y. X. Guo, "A filtering dual-polarized antenna subarray targeting for base stations in millimeter-wave 5G wireless communications," *IEEE Transactions on Components, Packaging and Manufacturing Technology*, vol. 7, pp. 964-973, 2017.

[43] H. Chu, J. X. Chen, S. Luo, Y. X. Guo, "A Millimeter-Wave Filtering Monopulse Antenna Array based on substrate integrated waveguide technology," *IEEE Transactions on Antennas and Propagation*, vol. 64, pp. 316-321, 2016.

[44] Y. Yusuf and X. Gong, "A new class of 3-D filterantenna integration with high quality factor and high efficiency," *2010 IEEE MTT-S International Microwave Symposium*, pp. 892-895, 2010.

[45] H. Chu, Y. X. Guo, "A Novel Approach for Millimeter-Wave Dielectric Resonator Antenna Array designs by using the substrate integrated technology," *IEEE Transactions on Antennas and Propagation*, vol. 65, pp. 909-914, 2007.

[46] Y. Yusuf, H. T. Cheng and X. Gong, "A Seamless Integration of 3-D Vertical Filters with Highly Efficient Slot Antennas," *IEEE Transactions on Antennas and Propagation*, vol. 59, pp. 4016-4022, 2011.

[47] R. Lovato, and X. Gong, "A Third-Order High-Q SIW Filter antenna with Two cavities and one integrated slot antenna," *2016 IEEE International Symposium on Antennas and Propagation (APSURSI)*, pp. 1219-1220, 2016.

[48] Y. Yusuf, and X. Gong, "A Vertical Integration of High-Q Filters with Patch Antennas with enhanced bandwidth and high efficiency," *2011 IEEE MTT-S International Microwave Symposium*, pp. 1-4, 2011.

[49] O. A. Nova, J. C. Bohorquez, N. M. Pena, "An approach to filter-antenna integration in SIW technology," *2011 IEEE Second Latin American Symposium on Circuits and Systems (LASCAS),* pp. 1-4, 2011.

[50] A. A. Melcon, J. R. Mosig, F. E. Gardiol, "An efficient procedure for the optimization of cavity backed printed antennas for broadband communications," *1998 28th European Microwave Conference*, pp. 666-671, 1998.

[51] T. Li, K. Karnati, X. Gong, "Approach to Realize Wide-Sean-Angle Phased Array with Enhanced bandwidth and filtering function by using integrated filter patch," *2014 IEEE MTT-S International Microwave Symposium (IMS2014),* pp. 1-3, 2014.

[52] Y. Yusuf, H. Cheng, and X. Gong, "Co-designed substrate-integrated waveguide filters with patch antennas," *IET Microwaves, Antennas & Propagation*, vol. 7, pp. 493-501, 2013.

[53] Y. Yusuf, and X. Gong, " Compact Low-Loss Integration of High- Q 3-D Filters With Highly Efficient Antennas," *IEEE Transactions on Microwave Theory and Techniques,* vol. 59, pp. 857-865, 2011.

[54] O. A. Nova; J. C. Bohorquez; N. M. Pena; G. E. Bridges; L. Shafai; C. Shafai, "Filter-antenna module using substrate integrated waveguide," *IEEE Antennas and Wireless Propagation Letters,* vol. 10, pp. 59-62, 2011.

[55] Y. Yusuf, and X. Gong, "Integrated Filter Antennas with High Efficiency and Increased Bandwidth," *WAMICON 2011 Conference Proceedings,* pp. 1-4, 2011.

[56] T. Li, H. Cheng, and X. Gong, "Integrated Single-Fed Circularly-Polarized Patch antenna with high-Q caveity filters," *2014 IEEE Antennas and Propagation Society International Symposium (APSURSI),* pp. 1873-1874, 2014.

[57] T. Li, and X. Gong, "Integration of Slot Antenna with Evanescent-Mode filter for tunable frontend applications," *2013 IEEE Antennas and Propagation Society International Symposium (APSURSI),* pp. 580-581, 2013.

[58] Y. Yusuf, and X. Gong, "Integration of three-dimensional high-Q filters with aperture antennas and bandwidth enhancement utilizing surface wave," *IET Microwaves, Antennas & Propagation,* vol. 7, pp. 468-475, 2013.

[59] H. Chu, C. Jin, W. J. Sun, J. X. Chen, Y. X. Guo, "Substrate-Integrated Millimeter-Wave Short Backfire antenna by a novel quad-slot cavity-backed feed," *IEEE Transactions on Components, Packaging and Manufacturing Technology*, vol. 5, pp. 1694-1699, 2015.

[60] H. Cheng, Y. Yusuf, X. Gong, " Vertically Integrated Three-Pole Filter Antennas for array applications," *IEEE Antennas and Wireless Propagation Letters*, vol. 10, pp. 278-271, 2011.

[61] K. C. Huang, D. J. Edwards (2008). Millimetre wave antennas for gigabit wireless communications: a practical guide to design and analysis in a system context. *USA: John Wiley & Sons.* pp. 115–121.

[62] P. F. Hu, Y. M. Pan, X. Y. Zhang, S. Y. Zheng, "Broadband filtering dielectric resonator antenna with wide stopband," *IEEE Transactions on Antennas and Propagation,* vol. 65, pp. 2079-2084, 2017.

[63] P. F. Hu, Y. M. Pan, X. Y. Zhang, S. Y. Zheng, "A compact filtering dielectric resonator antenna with wide bandwidth and high gain," *IEEE Transactions on Antennas and Propagation,* vol. 64, pp. 3645-3651, 2016.

[64] E. H. Lim, K. W. Leung, "Use of the dielectric resonator antenna as a filter element," *IEEE Transactions on Antennas and Propagation,* vol. 56, pp. 5-10, 2008.

[65] B. Sahu, P. Tripathi, S. Singh, M. K. Meshram, S. P. Singh, " A simple structured filtering dielectric resonator antenna," *2016 IEEE Uttar Pradesh Section*

International Conference on Electrical, Computer and Electronics Engineering (UPCON), pp. 543-545, 2016.

[66] B. J. Xiang, S. Y. Zheng, Y. M. Pan, Y. X. Li, "Wideband Circularly Polarized Dielectric Resonator Antenna With Bandpass Filtering and Wide Harmonics Suppression Response," *IEEE Transactions on Antennas and Propagation*, vol. 65, pp. 2096-2101, 2017.

[67] Y. M. Pan, S. Y. Zheng, "A Low-Profile Stacked Dielectric Resonator Antenna with high-gain and wide bandwidth," *IEEE Antennas and Wireless Propagation Letters*, vol. 15, pp. 68-71, 2016.

[68] X. Y. Zhang, W. Duan, and Y. M. Pan, "Single/dual polarized filtering patch antennas without using extra circuits," in *2016 IEEE 5th Asia-Pacific Conference on Antennas and Propagation (APCAP)*, 2016, pp. 311-312.

[69] X. Y. Zhang, D. Xue, L. H. Ye, Y. M. Pan and Y. Zhang, "Compact dual-band dual-polarized interleaved two-beam array with stable radiation pattern based on filtering elements," *IEEE Transactions on Antennas and Propagation*, vol. 65, 2017.

[70] X. Y. Zhang, Y. Zhang, Y. M. Pan and, W. Duan, " Low-profile dual-band filtering patch antenna and its application to LTE MIMO system," *IEEE Transactions on Antennas and Propagation*, vol. 65, pp. 103-113, 2017.

[71] Y. M. Pan, P. F. Hu, X. Y. Zhang, "Parasitic Patch Antenna with Filtering Response," in *2016 IEEE 5th Asia-Pacific Conference on Antennas and Propagation (APCAP)*, pp. 315-316, 2016.

[72] R. Z. Li, C. Z. Hua, Y. L. Lu, Z. M. Wu, Y. Wang, "Dual-polarized aperture-coupled filtering antenna," in *2017 International Workshop on Electromagnetics: Applications and Student Innovation Competition*, pp. 152-153, 2017.

[73] Y. Zhang, X. Y. Zhang, and Y. M. Pan, "Compact single- and dual-band filtering patch antenna arrays using novel feeding scheme," *IEEE Transactions on Antennas and Propagation*, vol. 65, pp. 4057-4066, 2017.

[74] C. Eswarappa, R. Anderson, F. Kolak, "Periodic filters for performance enhancement of millimeter-wave microstrip antenna arrays," *2004 IEEE MTT-S International Microwave Symposium Digest (IEEE Cat. No.04CH37535)*, pp. 353-356, 2004.

[75] A. I. Abunjaileh, I. C. Hunter, A. H. Kemp, "Application of dual-mode filter techniques to the broadband matching of microstrip patch antennas," *IET Microwaves, Antennas & Propagation*, vol. 1, pp. 273-276, 2007.

[76] C. K. Lin, S. J. Chung, "A Compact Edge-Fed Filtering Microstrip Antenna with 0.2 dB Equal-Ripple response," in *2009 European Microwave Conference (EuMC)*, pp. 378-380, 2009.

[77] H. M. Hizan, I. C. Hunter, A. I. Abunjaileh, "Integrated SIW filter and microstrip antenna," in *40th European Microwave Conference*, pp. 184-187, 2010.

[78] Y. J. Lee, G. W. Gao, S. J. Chung, "A compact dual-band filtering microstrip antenna with the same polarization planes," in *2012 Asia Pacific Microwave Conference Proceedings*, pp. 1178-1180, 2012.

[79] M. Ohira, Z. W. Ma, "An efficient design method of microstrip filtering antenna suitable for circuit synthesis theory of microwave bandpass filters," in *2015 International Symposium on Antennas and Propagation (ISAP)*, pp. 1-4, 2015.

[80] L. Li, G. Liu, "A differential microstrip antenna with filtering response," *IEEE Antennas and Wireless Propagation Letters*, vol. 15, pp. 1983-1986, 2016.

[81] F. C. Chen, H. T. Hu, R. S. Li, Q. X. Chu, M. J. Lancaster, "Design of Filtering Microstrip Antenna Array With Reduced Sidelobe Level," *IEEE Transactions on Antennas and Propagation*, vol. 65, pp. 903-908, 2017.

[82] T. L. Wu, Y. M. Pan, P. F. Hu, S. Y. Zheng, "Design of a low profile and compact omnidirectional filtering patch antenna," *IEEE Access,* vol. 5, pp. 1083-1089, 2017.

[83] C. K. Lin, S. J. Chung, "A filtering microstrip antenna array," *IEEE Transactions on Microwave Theory and Techniques,* vol. 59, pp. 2856-2863, 2011.

[84] F. Queudet, I. Pele, B. Froppier, Y. Mahe, S. Toutain, " Integration of Pass-Band Filters in Patch Antennas," in *32nd European Microwave Conference,* pp. 685-688, 2002.

[85] A. Abbaspour-Tamijani, J. Rizk, G. Rebeiz, "Integration of filters and microstrip antennas," in *IEEE Antennas and Propagation Society International Symposium (IEEE Cat. No.02CH37313),* pp. 874-877, 2002.

[86] J. H. Zuo, X. W. Chen, G. R. Han, L. Li, W. M. Zhang, "An Integrated Approach to RF Antenna-Filter co-design," *IEEE Antennas and Wireless Propagation Letters,* vol. 8, pp. 141-144, 2009.

[87] C. K. Lin, S. J. Chung, "A Compact Filtering Microstrip Antenna With Quasi-ellipitic broadside antenna gain response," IEEE Antennas and Wireless Propagation Letters, vol. 10, pp. 381-384, 2011.

[88] W. Duan, X. Y. Zhang, Q. Xue, "Dual-polarized high-selectivity filtering antennas without extra circuits," *2016 IEEE International Conference on Microwave and Millimeter Wave Technology (ICMMT),* pp. 501-503, 2016.

[89] X. Y. Zhang, W. Duan, and Y. M. Pan, "High-Gain Filtering Patch Antenna Without Extra Circuit," *IEEE Transactions on Antennas and Propagation,* vol. 63, pp. 5883-5888, 2015.

[90] W. Duan, X. Y. Zhang, and Y. M. Pan, "Compact differential-fed antenna with filtering response," in *2015 IEEE International Conference on Computational Electromagnetics,* pp. 278-280, 2015.

[91] W. Duan, X. Y. Zhang, Y. M. Pan, J. X. Xu, Q. Xue, "Dual-Polarized Filtering Antenna With High Selectivity and Low Cross Polarization," *IEEE Transactions on Antennas and Propagation,* vol. 64, pp. 4188-4196, 2016.

[92] Y. Zhang, X. Y. Zhang, L. H. Ye, Y. M. Pan, "Miniaturized Dual-Band Base-Station Array Using filtering antenna element," in *2016 IEEE 5th Asia-Pacific Conference on Antennas and Propagation (APCAP),* pp. 95-96, 2016.

[93] Y. Zhang, X. Y. Zhang, B. Li, "Dual-band Filtering Antenna with Controllable frequencies and bandwidths," in *2016 IEEE 5th Asia-Pacific Conference on Antennas and Propagation (APCAP),* pp. 185-186, 2016.

[94] C. X. Mao, S. Gao, Y. Wang, F. Qin, and Q. X. Chu, "Compact Highly Integrated Planar Duplex Antenna for Wireless Communications," *IEEE Transactions on Microwave Theory and Techniques,* vol. 64, pp. 2006-2013, 2016.

[95] C. X. Mao, S. Gao, Y. Wang, Q. Luo, and Q. X. Chu,, "A Shared-Aperture Dual-Band Dual-Polarized Filtering-Antenna-Array With Improved Frequency Response," *IEEE Transactions on Antennas and Propagation,* vol. 65, pp. 1836-1844, 2017.

[96] C. X. Mao, S. Gao, Y. Wang, *et al.*, "Dual-Band Patch Antenna With Filtering Performance and Harmonic Suppression," *IEEE Transactions on Antennas and Propagation,* vol. 64, pp. 4074-4077, 2016.

[97] C. X. Mao, S. Gao, Y. Wang, Z. Q. Cheng, "Filtering Antenna With Two-Octave Harmonic Suppression," *IEEE Antennas and Wireless Propagation Letters,* vol. 16, pp. 1361-1364, 2017.

[98] C. X. Mao, S. Gao, Z. P. Wang, Y. Wang, F. Qin, B. Sanz, Q. X. Chu, "Integrated filtering-antenna with controllable frequency bandwidth," *2015 9th European Conference on Antennas and Propagation (EuCAP),* pp. 1-4, 2015.

[99] C. X. Mao, S. Gao, Y. Wang, F. Qin, and Q. X. Chu, "Multimode Resonator-Fed Dual-Polarized Antenna Array With Enhanced Bandwidth and Selectivity," *IEEE Transactions on Antennas and Propagation,* vol. 63, pp. 5492-5499, 2015.

[100] C. X. Mao, S. Gao, Y. Wang, B. Sanz-Izquierdo, "A Novel Multiband Directional Antenna for Wireless Communications," *IEEE Antennas and Wireless Propagation Letters,* vol. 16, pp. 1217-1220, 2017.

[101] C. X. Mao, S. Gao, Y. Wang, Z. P. Wang, F. Qin, B. Sanze-Izquierdo, and Q. X. Chu, "Multimode Resonator-Fed Dual-Polarized Antenna Array With Enhanced Bandwidth and Selectivity," *IEEE Transactions on Microwave Theory and Techniques,* vol. 64, pp. 1798-1805, 2016.

[102] Z. H. Jiang, D. H. Werner, "A Compact, Wideband Circularly Polarized Co-designed Filtering Antenna and Its Application for Wearable Devices With Low SAR," *IEEE Transactions on Antennas and Propagation,* vol. 63, pp. 3808-3818, 2015.

[103] Z. H. Jiang, D. H. Werner, "A Compact, Wideband Circularly Polarized Co-designed Filtering Antenna and Its Application for Wearable Devices With Low SAR," *IEEE Antennas and Wireless Propagation Letters,* vol. 8, pp. 1087-1090, 2009.

[104] H. Kaouach, A. Kabashi, " Antenna-filter-antenna based frequency selective surfaces for quasi-optical applications in Q-band," *2015 9th European Conference on Antennas and Propagation (EuCAP),* pp. 1-4, 2015.

[105] D. Zayniyev and D. Budimir, "An Integrated Antenna-Filter with Harmonic Rejection," *3rd European Conf. on Antennas and Propag.*, pp. 393-394, 2009.

[106] L. Inclan, J. L. Wazquez and E. Rajo, "Proximity coupled microstrip patch antenna with reduced harmonic radiation," *IEEE Transactions on Antennas and Propagation,* vol. 57, no. 1, pp. 27–32, Jan. 2009.

[107] Y. Qin, S. Gao and A. Sambell, "Broadband high-efficiency linearly and circularly-polarized active integrated antennas," I*EEE Trans. on Microwave Theory and Techniques,* Vol. 54, No. 6, June 2006, pp. 2723-2732.

[108] Y. Qin, S. Gao and A. Sambell, "Broadband high-efficiency circularly-polarized active antennas and arrays," *IEEE Trans. on Microwave Theory and Techniques,* Vol. 54, No. 7, July 2006, pp. 2910-2916.

[109] D.Li, P. F. Guo, Q. Dai and Y. Q. Fu, "Broadband Capacitively Coupled Stacked Patch Antenna for GNSS Applications," *IEEE Antenna Wireless Propag. Lett.*,vol. 11, pp. 701-704, 2012.

[110] R. Caso, A. A. Serra, M. R. Pino, P. Nepa and G. Manara, "A Wideband Slot-Coupled Stacked-Patch Array for Wireless Communications," *IEEE Antenna Wireless Propag. Lett.,* vol. 9, pp. 986–989, 2010.

[111] W. H. Hsu, K. L. Wong, "Broad-Band Probe-Fed Patch Antenna With a U-shaped Ground Plane for Cross-Polarization Reduction," *IEEE Transactions on Antennas and Propagation*, vol. 50, no. 3, pp. 352-355, March 2002.

[112] X. Y. Zhang, J. X. Chen, Q. Xue and S. M. Li, "Dual-band Bandpass Filters Using Stub-Loaded Resonators," *IEEE Microw. Wireless Components Lett.,* vol. 17, No. 8, pp. 583-585, Aug. 2007.

[113] X. Y. Zhang, C. H. Chan, Q. Xue and B. J. Hu, "Dual-Band Bandpass Filter with Controllable Bandwidths Using Two Coupling Patchs," *IEEE Microw. Wireless Compon. Lett.,* vol. 20, no. 11, pp. 616-618, Nov. 2010.

[114] S. Kwon, B. M. Lee, Y. J. Yoon, W. Y. Song and J. G. Yook, "A harmonic suppression antenna for an active integrated antenna," *IEEE Antenna Wireless Propag. Lett.,* vol. 13, no. 2, pp. 54–56, 2003.

[115] F. J. Huang, T. C. Yo, C. M. Lee and C. H. Luo, "Design of circular polarization antenna with harmonic suppression for rectenna application," *IEEE Antenna Wireless Propag. Lett.*, vol. 11, no. 2, pp. 592–595, 2012.

[116] H. Liu, Z. Li, X. Sun and J. Mao, "Harmonic suppression with photonic bandgap and defected ground structure for a microstrip patch antenna," *IEEE Antenna Wireless Propag. Lett.*, vol. 15, no. 2, pp. 55–56, 2005.

[117] Q. X. Chu, C. X. Mao and H. Zhu, "A compact notched band UWB slot antenna with sharp selectivity and controllable bandwidth," *IEEE Trans. Antennas and Propag*., vol. 61, no. 8, pp. 3961–3966, Aug. 2013..

[118] Y. Xu, S. Gong and Y. Guan, "Coaxially fed microstrip antenna for harmonic suppression," Electron. Lett., vol. 48, no. 15, pp. 895-896, 2012.

[119] S. Biswas, D. Guha and C. Kumar, "Control of higher harmonics and their radiations in microstrip antennas using compact defected ground structures," *IEEE Transactions on Antennas and Propagation*, vol. 61, no. 6, pp. 3349–3353, Jun. 2013.

[120] C. Y. D. Sim, M. H. Chang and B. Y. Chen, "Microstrip-fed ring slot antenna with wideband harmonic suppression," *IEEE Transactions on Antennas and Propagation*, vol. 62, no. 9, pp. 4828–4832, Sep. 2014.

[121] L. Inclan, J. L. Wazquez and E. Rajo, "Proximity coupled microstrip patch antenna with reduced harmonic radiation," *IEEE Transactions on Antennas and Propagation*, vol. 57, no. 1, pp. 27–32, Jan. 2009.

[122] H. Liu, Z. Li, X. Sun and J. Mao, "Harmonic suppression with photonic bandgap and defected ground structure for a microstrip patch antenna," *IEEE Antenna Wireless Propag. Lett*., vol. 15, no. 2, pp. 55–56, 2005.

[123] K. F. Lee, K. F. Tong, "Microstrip Patch antennas – Basic Characteristics and Some Recent Advances," *IEEE Proceedings*, vol. 100, no. 7, pp. 2169-2180, Jul. 2012.

[124] K. F. Lee, S. L. S. Yang, A. Kishk and K. M. Luk, "The Versatile U-slot Patch Antenna," *IEEE Antennas and Propag. Magazine*, vol. 52, no. 1, pp. 71-88, Feb. 2010.

[125] W. C. Mok, S. H. Woong, K. M. Luk, K. F. Lee, "Single-Layer Single Patch Dual-Band and Tri-Band Patch Antenna," *IEEE Transactions on Antennas and Propagation*, vol. 61, no. 8, pp. 4341-4344, Aug. 2013.

[126] I. Yeom, J. M. Kim and C. W. Jung, "Dual-Band Slot-Coupled Patch Antenna with Broad Bandwidth and High Directivity for WLAN Access Point," Electron. Lett., vol. 50, no. 10, pp. 726-728, 2014.

[127] Y. X. Guo, K. M. Luk and K. F. Lee, "Dual-Band Slot-Loaded Short-Circuited Patch Antenna," Electron. Lett., vol. 36, no. 4, pp. 289-291, 2000.

[128] M. Al-Joumayly, S. Aguilar, N. Behdad and S. Hagness, "Dual-Band Miniaturized Patch Antennas for Microwave Breast Imaging," *IEEE Antenna Wireless Propag. Lett.*, vol. 9, pp. 268–271, 2010.

[129] C. Y. Hsieh, C. H. Wu and T. G. Ma, "A Compact Dual-Band Filtering Patch Antenna Using Step Impedance Resonators," *IEEE Antenna Wireless Propag. Lett*., vol. 14, pp. 1056–1059, 2015.

[130] Y. J. Lee, G. W. Cao and S. J. Chung, "A Compact Dual-Band Filtering Microstrip Antenna with the Same Polarization Planes," *in Proc. Asia-Pacific Microw. Conf.*, pp. 1178-1180, 2012.

[131] Y. J. Ren, M. Farooqui and K. Chang, "A compact dual-frequency rectifying antenna with high-orders harmonic-rejection," *IEEE Trans. Antennas and Propag.*, vol. 55, no. 7, pp. 2110–2113, Jul. 2007.

[132] L. Yang, P. Cheong, L. Han, W. W. Choi, K. W. Tam and K. Wu, "Miniaturized Parallel Coupled-Line Filter-Antenna With Spurious Response Suppression," in *IEEE Antennas and Wireless Propag. Lett.*, vol. 10, no. , pp. 726-729, 2011.

[133] C. Y. Hsieh, C. H. Wu and T. G. Ma, "A Compact Dual-Band Filtering Patch Antenna Using Step Impedance Resonators," *IEEE Antenna Wireless Propag. Lett*., vol. 14, pp. 1056–1059, 2015.

[134] D. Pozar and S. Targonski, "A shared-Aperture Dual-Band Dual-Polarized Microstrip array," *IEEE Transactions on Antennas and Propagation*, vol. 49, no. 2, pp. 150-157, Feb. 2001.

[135] S. Gao and A. Sambell, "Low-Cost Dual-Polarized Printed Array with Broad Bandwidth," *IEEE Transactions on Antennas and Propagation*, vol. 52, no. 12, pp. 3394-3397, Dec. 2004.

[136] S. Gao and A. Sambell, "Dual-Polarized Broad-Band Microstrip Antenna Fed by Proximity Coupling," *IEEE Transactions on Antennas and Propagation*, vol. 53, no. 1, pp. 526-530, Jan. 2005.

[137] L. Shafai, W. Chamma, M. Barakat, P. Strickland and G. Seguin, "Dual- Band Dual-Polarized Perforated Microstrip Antennas for SAR Application," *IEEE Transactions on Antennas and Propagation*, vol. 48, no. 1, pp. 58-66, Jan. 2000.

[138] D. M. Pozar, S. D. Targonski, "A Shared-Aperture Dual-Band Dual Polarized Microstrip Array," *IEEE Transactions on Antennas and Propagation*, vol. 49, no. 2, pp. 150-157, Feb. 2001.

[139] T. W. Chiou and K. L. Wong, "A Compact Dual-Band Dual-Polarized Patch Antenna for 900/1800-MHz Cellular Systems," *IEEE Transactions on Antennas and Propagation*, vol. 51, no. 8, pp. 1936-1940, Jan. 2003.

[140] G. Vetharatnam, C. B. Kuan and C. H. Teik, "Combined Feed Network for a Shared-Aperture Dual-Band Dual-Polarized Array," *IEEE Micro. and Wireless Components Lett*., vol. 4, pp. 297-299, 2005.

[141] S. Soodmand, "A novel circular shaped dual-band Dual-polarized Patch antenna and introducing a new approach for designing combined feed networks", *in 2009 Loughborough Antennas & Propagation Conference, LAPC 2009*, pp. 401-404.

[142] R. Pokuls, J. Uher and D. M. Pozar, "Dual-Frequency and Dual-Polarization Microstrip Antennas for SAR Application," *IEEE Transactions on Antennas and Propagation*, vol. 46, no. 9, pp. 1289-1296, Sep. 1998.

[143] Z. Yang and K. Warnick, "Multiband dual-polarization high-efficiency array feed for Ku/reverse-band Satellite communications," *IEEE Antennas Wireless Propag*., vol. 13, pp. 1325-1328, 2014.

[144] H. Moghadas, M. Daneshmand and P. Mousavi, "A dual-band high-gain resonant cavity antenna with orthogonal polarizations," *IEEE Antennas Wireless Propag*., vol. 10, pp. 1220-1223, 2011.

[145] K. Naishadham, R. Li, L. Yang, T. Wu, W. Hunsicker, M. Tentzeris, "A shared-aperture dual-band planar array with self-similar printed folded dipoles," *IEEE Transactions on Antennas and Propagation*, vol. 61, no. 2, pp. 606-613, Feb. 2013.

[146] S. S. Zhon, Z. Sun, L. B. Kong, C. Gao, W. Wang and M. P. Jin, "Tri-band dual-polarization shared-aperture microstrip array for SAR application," *IEEE Transactions on Antennas and Propagation*, vol. 60, no. 9, pp. 4157-4165, Sep. 2012.

[147] S. Gao, L. W. Li, M. S. Leong and T. S. Yeo, "Dual-polarized slot-coupled microstrip antenna with wide bandwidth," *IEEE Transactions on Antennas and Propagation*, vol. 51, no. 3, pp. 441-448, Mar. 2003.

[148] J. S. Hong and M. J. Lancaster, Microwave Filger for RF/Microwave Application. New York: Wiley, 2001.

[149] J. Granholm and K. Woelders, "Dual Polarization Stacked Microstrip Patch Antenna Array With Very Low Cross-Polarization," *IEEE Transactions on Antennas and Propagation*, vol. 49, no. 10, pp. 1393-1402, Oct. 2001.

[150] S. S. Zhong, Z. Sun, L. B. Kong, C. Gao, W. Wang and M. P. Jin, "Tri-Band Dual – Polarization Shared-Aperture Microstrip Array for SAR Applications," *IEEE Transactions on Antennas and Propagation*, vol. 60, no. 9, pp. 4157-4165, Sep. 2012.

[151] R. Caso, A. A. Serra, M. R. Pino, P. Nepa and G. Manara, "A Wideband Slot-Coupled Stacked-Patch Array for Wireless Communications," *IEEE Antenna Wireless Propag. Lett.*, vol. 9, pp. 986–989, 2010.

[152] K. L. Wong, H. C. Tung, and T. W. Chiou, "Broadband dual-polarized aperture-coupled patch antennas with modified H-shaped coupling slots," *IEEE Transactions on Antennas and Propagation*, vol. AP-50, no. 2, pp. 188–191, Feb. 2002.

[153] K. L.Wong and T.W. Chiou, "Broadband dual-polarized patch antennas fed by capacitively coupled feed and slot-coupled feed," *IEEE Transactions on Antennas and Propagation*, vol. AP-50, no. 3, pp. 346–351, Mar. 2002.

[154] T. Rappaport, S. Sun, R. Mayzus, H. Zhao, Y. Azar, K. Wang, G. Wong, J. Schulz, M. Samimi and F. Gutierrez, "Millimeter wave mobile communications for 5G cellular: It will work!," *IEEE Access*, vol. 1, pp. 335-349, 2013.

[155] Samsung. (2015, Aug.). Samsung demo: 5G vision, Korea. Available: http://www.samsung.com/global/business/networks/insights/news/samsung-electronics-sets-5g-speed-record-at-7-5gbpsover-30-times-faster-than-4g-lte.

[156] F. Rusek, D. Persson, B. Lau, E. Larsson, T. Marzetta, O. Edfors and F. Tufvesson, "Scaling up MIMO: Opportunities and challenges with very large arrays," *IEEE Signal Process. Mag.*, vol. 30, no. 1, pp. 40-60, Jan. 2013.

[157] F. Rusek, D. Persson, B. K. Lau, E. G. Larsson, T. L. Marzetta, O. Edfors, and F. Tufvesson, "Scaling up mimo: Opportunities and challenges with very large arrays," *IEEE Signal Process. Mag.*, vol. 30, no. 1, pp. 40–60, Jan. 2013.

[158] E. Larsson, O. Edfors, F. Tufvesson, and T. Marzetta, "Massive mimo for next generation wireless systems," *IEEE Commun. Mag.*, vol. 52, no. 2, pp. 186–195, Feb. 2014.

[159] S. Ershadi, A. Keshtkar, A. Abdelrahman, X. Yu and H. Xin, "Design of wideband unit-cell element for 5G antenna arrays," *2015 Asia-Pacific Microwave Conference (APMC)*, pp. 1-3, 2015.

[160] J. S. Park, J. B. Ko, H. K. Kwon, B. S. Kang, B. Park and D. Kim, "A tilted combined beam antenna for 5G communications using a 28-GHz Band," *IEEE Antennas Wireless Propog. Lett*, vol. 15, pp. 1685-1688, 2016.

[161] H. Aliakbari, A. Abdipour, R. Mirzavand, A. Costanzo and P. Mousavi, "A single feed dual-band circularly polarized millimeter-wave antenna for 5G communication," *2016 10th European Conference on Antennas and Propag. (EuCAP)*, pp. 1-5, 2016.

[162] S. Gao and A. Sambell, "Low-Cost Dual-Polarized Printed Array with Broad Bandwidth," *IEEE Transactions on Antennas and Propagation*, vol. 52, no. 12, pp. 3394-3397, Dec. 2004.

[163] Y. X. Guo, K. M. Luk, and K. F. Lee, "Broadband dual-polarization patch element for cellular-phone base stations," *IEEE Transactions on Antennas and Propagation*, vol. 50, no. 2, pp. 251–253, Feb. 2002.

[164] W. Zhai, V. Miraftab, M. Repeta, D. Wessel and W. Tong, "Dual-band millimeter-wave interleaved antenna array exploiting low-cost PCB technology for high speed 5G communication," *2016 IEEE MTT-S International Microw. Symposium (IMS)*, pp. 1-4, 2016.

[165] F. F. Manzillo, M. Ettorre, M. Lahti, K. Kautio, D. Lelaidier, E. Seguenot, R. Sauleau, "A multilayer LTCC solution for integrating 5G access point antenna modules," *IEEE Trans. on Microwave Theory and Techniques*, vol. 64, no. 7, pp. 2272-2283, 2016.

[166] J. Hirokawa, "Millimeter-wave antenna technologies for 5G mobile communication systems," *in 2016 IEEE International Workshop on Electromagnetics: Applications and Student Innovation Competition (iWEM)*, pp. 1-3, 2016.

[167] M. M. Ali, A. R. Sebak, "Design of compact millimeter wave massive MIMO dual-band (28/38 GHz) antenna array for future 5G communication systems," *in 2016 17th International Symposium on Antenna Technology and Applied Electromagnetics (ANTEM)*, pp. 1-2, 2016.

[168] Kin-Fai Tong; Kwai-Man Luk; Kai-Fong Lee; R. Q. Lee, "A broad-band U-slot rectangular patch antenna on a microwave substrate," *IEEE Transactions on Antennas and Propagation*, vol. 48, pp. 954-960, 2000.

[169] Y. Gao, R. Ma, Y. Wang, Q. Zhang and C. Parini, "Stacked patch antenna with dual-polarization and low mutual coupling for massive MIMO," *IEEE Transactions on Antennas and Propagation*, vol. 64, pp. 4544-4549, 2016.

[170] T. Kodera, C. Caloz, "Integrated Leaky-Wave Antenna–Duplexer/ Diplexer Using CRLH Uniform Ferrite-Loaded Open Waveguide," *IEEE Transactions on Antennas and Propagation*, vol. 58, no. 8, pp. 2508-2514, Aug. 2010.

[171] M. Hikita, K. Sakiyama, O. Hikino, M. Kijima, "New Low-Distortion Band-Switching Techniques for SAW Antenna Duplexers Used in Ultro-Wide-Band Cellular Phone," *IEEE Transactions on Microwave Theory and Techniques*, vol. 52, no. 1, pp. 38-45, Jan. 2004.

[172] P. Choeng, K. F. Chang, W. W. Choi, K. W. Tam, "A Highly Integrated Antenna-Triplexer With Simultaneous Three-Port Isolation Based on Multimode Excitation," *IEEE Trans. Antennas and Propag.*, vol. 63, no. 1, pp. 363-386, Jan. 2015.

[173] T. Varum, J. Natos, P. Pinho and R. Abreu, "Nonuniform broadband circularly polarized antenna array for vehicular communications," *IEEE Trans. Veh. Technol*., vol. 65, no. 9, pp. 7219-7227, Sep. 2016.

[174] A. Garcia-Lamperez, R. Gomez-Garcia and M. Salazar-Palma, "Compact diplexer with edge-coupled and nonbianisotropic split-ring resonators," in 2012 IEEE MTT-S Int. Microw. Symp., Montréal, QC, 2012, pp. 1-3.

[175] X. Y. Zhang, J. X. Chen, Q. Xue and S. M. Li, "Dual-band Bandpass Filters Using Stub-Loaded Resonators," IEEE Micro. and Wireless Components Lett., vol. 17, No. 8, pp. 583-585, Aug. 2007.

[176] X. Shang, Y. Wang, W. Xia, M. J. Lancaster, "Novel multiplexer topologies based on all-resonator structure," *IEEE Transactions on Microwave Theory and Techniques*, vol. 61, no. 11, pp. 3838-3845, Nov. 2013.

[177] A. M. Mohammed, Y. Wang, "Four-way waveguide power dividers with integrated filtering function," *2015 European Microwave Conference (EuMC)*, pp. 486-489, 2015.